EXAMINING THE IMPACT OF PAD FLEXIBILITY ON THE ROTORDYNAMIC COEFFICIENTS OF ROCKER-PIVOT-PAD TILTING-PAD JOURNAL BEARINGS

A Thesis

by

JENNIFER ELIZABETH GAINES

Submitted to the Office of Graduate and Professional Studies of
Texas A&M University
in partial fulfillment of the requirements for the degree of

MASTER OF SCIENCE

Chair of Committee,	Dara W. Childs
Committee Members,	Luis San Andrés
	Gary T. Fry
Head of Department,	Andreas A. Polycarpou

December 2014

Major Subject: Mechanical Engineering

ABSTRACT

Measured and predicted static and dynamic load characteristics are provided for a three-pad, rocker-pivot, tilting-pad journal bearing in the load-between-pad orientation. The bearing has the following characteristics: 3 pads, .50 pad pivot offset, 0.6 L/D ratio, 60.69 mm (2.4 in) pad axial length, and 0.0762 mm (0.003 in) radial clearance. Three interchangeable pad configurations were tested with pad thicknesses of 8.5 mm (0.33 in), 10 mm (0.39 in), and 11.5 mm (.45 in). Tests were performed on a test bearing floating about a rigid rotor design with unit loads ranging from 172 to 1,724 kPa (25 to 250 psi) and speeds from 6 to 12 krpm.

Cold and hot clearances were taken to measure the nominal and operating, respectively, radial bearing clearance. The cold clearance was taken at room temperature while the hot clearance was taken for each operating speed immediately after the rig was shut down. The hot bearing clearance shows a 23 – 34% decrease in radial bearing clearance. As the operating speed increased, the operating temperature in the bearing increased. The increase in operating temperatures caused the bearing and pads to expand and reduced the radial bearing clearance.

Static load tests were performed once the test rig reached steady-state conditions. The maximum measured eccentricity ratio was over one for each pad configuration. As pad flexibility increased, the static eccentricity ratio decreased. The eccentricity ratio predictions agreed well with the measured results in the loaded direction. The measured attitude angles were as high as approximately 10°. The attitude angles remained fairly constant at low rotational speeds for t_p = 8.5 mm and t_p = 10 mm and decreased as unit load increased for t_p = 11.5 mm. XL_TPJB© predicted attitude angles that had a smaller magnitude than the measured results for all rotational speed and unit load conditions and were negative.

The temperatures did not vary greatly across pad configurations. The predictions agreed well with the measured values at low speeds and low unit loads. As the operating speed and unit load increased, the predictions were lower than the measured values.

Pad flexibility was characterized as the change in the pad's bending stiffness or the change in pad thickness. A finite-element model (FEM) was created in SolidWorks® to predict the structural bending stiffness of each pad configuration. Once the pivot was fixed in the FEM, a uniform pressure distribution was applied to the rotor-side surface of the pad. Results from the finite-element analysis (FEA) show an increase in pad flexibility as the thickness of the pad decreased.

Dynamic load tests were performed for all nominal test conditions over a range of excitation frequencies to obtain complex dynamic-stiffness coefficients as a function of excitation frequency. The real and imaginary parts of dynamic-stiffness were fitted with quadratic and linear models, respectively, with respect to excitation frequency. A constant coefficient [K][C][M] model produced frequency-independent rotordynamic coefficients. For the load-between-pad configuration, the dynamic-stiffness coefficients show significant bearing orthotropy, especially as the unit load increased. In general, the dynamic-stiffness was larger in the non-loading direction than it was in the loading direction. Negative virtual mass coefficients were commonly obtained for all pad configuration.

To examine the effect of pad flexibility on the rotordynamic coefficients, the measured results were compared across each pad configuration. The measured results show that the increase in pad flexibility decreased the direct damping coefficients by 12-20% and, on average, decreased the cross-coupled damping coefficients by approximately 10%. On average, the measured results show a slight increase in the stiffness coefficients as pad flexibility increased. The direct stiffness coefficients varied from an increase of 12% at low unit loads and a decrease of 3% at high unit loads. The cross-coupled stiffness coefficients change by 0 to 12% as pad flexibility increased. In general, the direct virtual mass coefficients decreased by approximately 29% as pad flexibility increased. The average change for the cross-coupled coefficients is an increase in M_{xy} and M_{yx} by 2% as pad flexibility increased.

XL_TPJB© was used to predict the performance of the tilting-pad bearing tested in this work. XL_TPJB© accounts for pad and pivot flexibility. The predictions using

XL_TPJB© agreed well with the measured values for direct stiffness coefficients. For a given pad set, the predictions agreed well with the measured results for one operating speed case and were either lower or higher than the measured results for the remaining speed cases for C_{xx}. The predicted values were generally higher than the measured values for C_{yy} at low unit loads and were lower than measured values at high unit loads. The measured values had a smaller magnitude than the predictions for the direct virtual-mass coefficients at lower speeds. At higher speeds, the predictions had a lower magnitude than the measured direct virtual-mass coefficients. All cross-coupled-coefficient predictions were nearly zero and, the measured values were typically non-zero and negative.

A non-dimensional pad flexibility parameter α_{flex} was used to relate the pad flexibility of multiple bearings of different sizes. The parameter related the average deflection across the pad surface to the pad's arc length. XL_TPJB© was used to predict the percent change in direct damping coefficients for a rigid pad, flexible pivot and flexible pad, flexible pivot for a surface speed of 54 m/s and a unit load of 783 kPa. The results show the pads tested in this thesis are extremely flexible compared to pads used in industry.

Results show that the pad's structural bending stiffness or flexibility is important when predicting the bearing's dynamic performance. Damping is consistently over-predicting when excluding pad flexibility, and this could have a significant impact in predicting the bearing's stability characteristics. In general, all codes should account for pad flexibility, as well as pivot flexibility, to properly predict the performance of a tilting-pad journal bearing.

DEDICATION

To my family,

Chuck, Nancy, and Alex Gaines and Patricia Courtois

For their unending guidance, support, and encouragement.

“When everything goes to hell, the people who stand by you without flinching -- they are your family.”

— Jim Butcher

ACKNOWLEDGEMENTS

I would like extend my deepest thanks to Dr. Dara Childs for giving me the opportunity to work at the Turbomachinery Laboratory. I was unsure of the path I wanted to follow when I started graduate school. Through my work at the turbo lab, I developed an interest in rotordynamics that I hope to continue to develop once I graduate.

I wish to thank Dr. Luis San Andrés and Dr. Gary Fry for their insight and support through my undergraduate career and for serving on my committee.

My sincere thanks to Michael Murphey and David Coghlan for teaching me all the tricks to running the test rig and their continued advice. I wish to thank Yingkun Li for her work on modifying XL_TPJB© so that I could use it in my thesis. I would also like to extend my thanks to the remaining members at the turbo lab. Thank you for all your help, support, opinions, and for always putting a smile on my face. I would like to thank the previous students of the turbo lab for their work on developing the test rig and computer programs for testing.

Lastly, I wish to thank my parents, Chuck and Nancy Gaines, for their love and support and for always being on the sidelines to cheer for me. Everything I have accomplished in life is due to your encouragement to never given up. I wish to thank my brother, Alex, for being an amazing, imaginative, and creative older brother. We will make your space elevator happen one day. I wish to thank my aunt, Patti, for teaching me the sky is the limit and to never give up on my dreams.

TABLE OF CONTENTS

LIST OF FIGURES

Page

LIST OF TABLES

Page

NOMENCLATURE

$\mathbf{A_{ij}}$	Fourier transforms for the measured stator acceleration. (e.g. A_{ij} is the acceleration in the "j" direction, due to an excitation force in the "i" direction) [L/t^2]
C_{ij}	Direct and cross-coupled damping coefficients [F.t/L]
ΔC_{ij}	Uncertainty of direct and cross-coupled damping coefficients [F.t/L]
C_b	Radial bearing clearance [L]
C_{hb}	Radial "hot" bearing clearance [L]
C_p	Radial pad clearance [L]
C_{po}	Undeflected radial pad clearance [L]
D	Bearing diameter [L]
$\mathbf{D_{ij}}$	Fourier transforms for the measured stator relative motion [L]
$\mathbf{F_{ij}}$	Fourier transforms for the measured stator force [F]
E_p	Pad Elastic modulus [F/L^2]
$f_{bx}\ f_{by}$	Bearing reaction force component in the x, y directions [F]
$f_x\ f_y$	Measured excitation force component in the x, y directions [F]
F_s	Static force applied by pneumatic loader [F]
$\mathbf{H_{ij}}$	Direct and cross-coupled dynamic-stiffness [F/L]
j	Imaginary unit, $\sqrt{-1}$ [-]
k_p	Pad's structural bending stiffness [F]
K_{ij}	Direct and cross-coupled stiffness coefficients [F/L]
ΔK_{ij}	Uncertainty of direct and cross-coupled stiffness coefficients [F/L]
L	Pad length [L]
L_{arc}	Pad arc length [L]
$\bar{M}_{c_p}$	Average applied fluid-film moment [FL]
M_p	Pad preload [-]
M_s	Mass of the stator [M]
M_{ij}	Direct and cross-coupled virtual-mass coefficients [M]

ΔM_{ij}	Uncertainty of virtual-mass coefficients [M]
O_p	Pad Center [L]
O_{po}	Undeflected Pad Center [L]
O_s	Rotor Center [L]
R_b	Bearing radius [L]
R_p	Pad radius [L]
R_{po}	Undeflected pad radius [L]
R_s	Rotor radius [L]
Re	Reynolds number, $Re = \frac{\rho C_b R \omega}{\mu}$ [-]
S	Sommerfeld number, $S = \frac{\mu N L D}{W}\left(\frac{R}{C_b}\right)^2$ [-]
t_p	Pad thickness [L]
T	Tempeature [T]
u	Linear displacement [L]
$\ddot{u}$	Linear acceleration [L/t^2]
x, y	Rotor's Position in the x, y directions [L]
x_o, y_o	Bearing's Position in the x, y directions [L]
$\ddot{x_s}$ $\ddot{y_s}$	Stator's Absolute acceleration in the x, y directions [L/t^2]]
Δx Δy	Relative motion between the rotor and the stator in the x, y directions [L]
$\Delta\dot{x}$ $\Delta\dot{y}$	Relative velocity between the rotor and the stator in the x, y directions [L]
$\Delta\ddot{x}$ $\Delta\ddot{y}$	Relative acceleration between the rotor and the stator in the x, y directions [L]
α	Thermal expansion coefficient [1/T]
α_{flex}	Non-dimensional pad flexibility [-]
δ	Linear deflection [L]
δ_{c_p}	Pad deflection [L]
δ_p	Pad deflection [L]
ε	Thermal expansion [-]
ε_o	Eccentricity ratio [-]

ε_{xo} ε_{yo}	Bearing equilibrium position in the x, y directions [L]
θ_{pad}	Pad arc angle [°]
θ_{pivot}	Pivot arc angle [°]
ϕ	Attitude angle [°]
Θ	Ratio of inner pad radius to outer pad radius [-]
Λ	Square of the excitation frequency, Ω^2 [$(1/t)^2$]
ρ	Lubricant density [M/L^3]
μ	Lubricant viscosity [$F.t/L^2$]
ω	Running speed of rotor [1/t]
Ω	Excitation frequency of stator [1/t]

Subscripts

x,y	x and y direction
i,j	x,y
k	Pad number

Abbreviations

DE, NDE	Drive end, non-drive end
LBP	Load-between-pad
LOP	Load-on-pad
rpm	Revolutions per minute
TPJB	Tilting-pad journal bearing
WFR	Whirl frequency ratio

INTRODUCTION

Tilting-pad journal bearings (TPJB) are typically used as flexible rotor supports in high-speed rotating machinery; the absence of cross-coupled destabilizing forces leads to inherent stability. Turbines, compressors, and turbo generators are frequently supported on TPJBs. A TPJB use multiple pads, typically four to six, and pivots, which allow the pad to tilt when a force is applied. Figure 1 shows a schematic view of a three-pad TPJB.

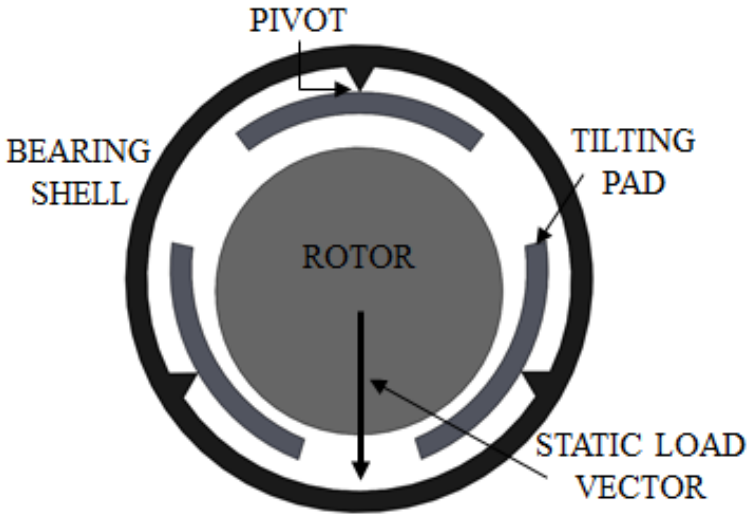

Figure 1. Schematic view of a tilting-pad journal bearing.

TPJBs provide support to the rotor though hydrodynamic fluid-film pressure. As the rotor spins, viscous fluid is dragged into a converging wedge, and hydrodynamic pressure is created between the rotor and tilting-pads. The hydrodynamic pressure provides a net reaction force that supports and lifts the rotor. Assuming small-amplitude vibrations about an equilibrium position, the fluid-film reaction forces between the TPJB

and rotor can be approximated as a linearized, two degree-of-freedom system of springs and dampers, as shown in Figure 2.

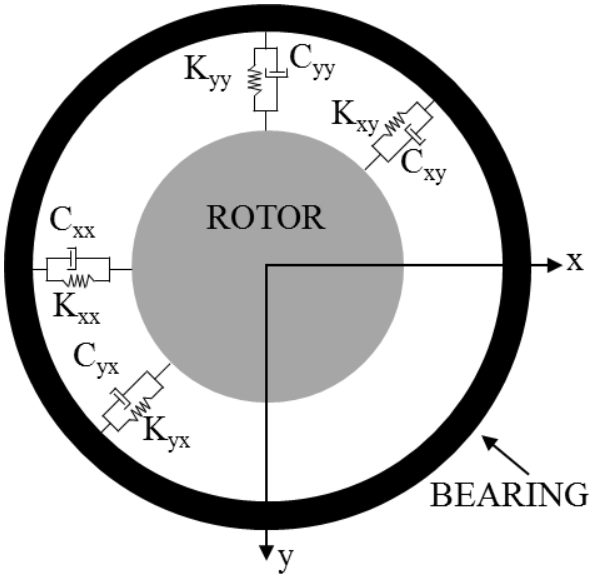

Figure 2. Linearized spring damper model for a fluid-film.

The symbols K_{ij} and C_{ij} represent the stiffness and damping coefficients, also known as the rotordynamic force coefficients. The bearing reaction forces can be written in terms of the rotordynamic force coefficients

$$-\begin{Bmatrix} f_{bx} \\ f_{by} \end{Bmatrix} = \begin{bmatrix} K_{xx} & K_{xy} \\ K_{yx} & K_{yy} \end{bmatrix} \begin{Bmatrix} \Delta x \\ \Delta y \end{Bmatrix} + \begin{bmatrix} C_{xx} & C_{xy} \\ C_{yx} & C_{yy} \end{bmatrix} \begin{Bmatrix} \Delta \dot{x} \\ \Delta \dot{y} \end{Bmatrix} \tag{1}$$

where Δx and Δy are the relative displacement between the rotor and bearing housing, $\Delta \dot{x}$ and $\Delta \dot{y}$ are the relative velocity between the rotor and bearing housing, and f_{bx} and f_{by} are the bearing reaction forces.

Identical subscripts (xx, yy) represent the direct coefficients, while different subscripts (xy, yx) represent the cross-coupled coefficients. The direct coefficients

produce reaction forces that are collinear to the displacement or velocity vectors. The cross-coupled coefficients produce reaction forces in the one direction due to displacement or velocity vectors in the orthogonal direction. Cross-coupled stiffness forces are frequently the cause of rotor instability.

The tilting nature of the pad and pivot allows the pad to rotate freely when a force or moment acts on the pad to maintain an oil-film. The pad reaches an equilibrium tilt angle once the net moment on the pad is zero. When this occurs, the resultant force vector generated by the hydrodynamic pressure on the pad passes directly through the center of the rotor and pivot, and causes a collinear displacement of the rotor. Since the resultant force and displacement are collinear, the cross-coupled forces are practically zero. For certain pivot types, TPJBs can have measureable cross-coupled forces. The resultant force and displacement are not collinear for fixed arc bearings. As a result, fixed arc bearings have larger cross-coupled forces that could lead to instability.

The three different types of pivots for TPJBs, shown in Figure 3, are the flexure-pivot, the rocker-pivot, and the spherical-pivot.

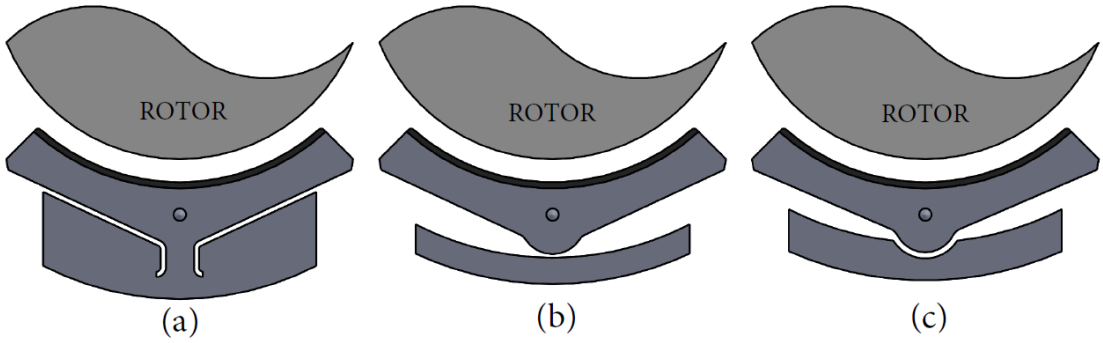

Figure 3. Three basic pivot types, (a) flexure-pivot, (b) rocker-pivot, and (c) spherical-pivot

For the flexure-pivot, the pad tilts on a flexible web that is machined using wire electric discharge machining (EDM). Flexure-pivot bearings are typically used for smaller diameter applications. The flexure pivot design eliminates tolerance stack-ups

and pivot contact wear, which can plague the other two designs. However, it introduces a rotational stiffness and consequent cross-coupled stiffness coefficients not generally present in the other pivot types.

Unlike the flexure-pivot pad, the rocker-pivot pads and spherical-pivot pads are separate from the bearing shell. The rocker-pivot has a cylindrical back with a radius that is smaller than the bearing shell's radius. The cylindrical back allows the pivot to rock on the surface of the bearing shell. Typically, the rocker-pivot has a line-to-line (no curvature) contact on the rocker surface. Some rocker-pivots have a slight axial curvature to correct for angular misalignment. The spherical-pivot, also known as "ball-in-socket", has approximately the same size radius as the pocket machined in the bearing shell that it rests in. The spherical-pivot adjusts for any axial misalignments. When compared to the rocker-pivot, the spherical-pivot has lower contact stresses due to the increase in contact area.

The geometric parameters of TPJBs, such as loading configuration, pad preload, pivot offset, and clearance etc., affect the bearing's static and dynamic performance. These parameters are defined in Table 1 and shown in Figure 4.

Table 1. Definitions of TPJB geometric parameters.

Symbol	Definition
$\mathbf{R_b}$	Bearing Radius
$\mathbf{R_p}$	Pad Radius
$\mathbf{R_s}$	Rotor Radius
$\boldsymbol{\theta_{pad}}$	Pad Arc Angle
$\boldsymbol{\theta_{pivot}}$	Pivot Arc Angle
L	Pad Axial Length
L/D	Length to Diameter Ratio
$\mathbf{C_b}$	Radial Bearing Clearance $C_b = R_b - R_s$
$\mathbf{C_p}$	Radial Pad Clearance $C_p = R_p - R_s$

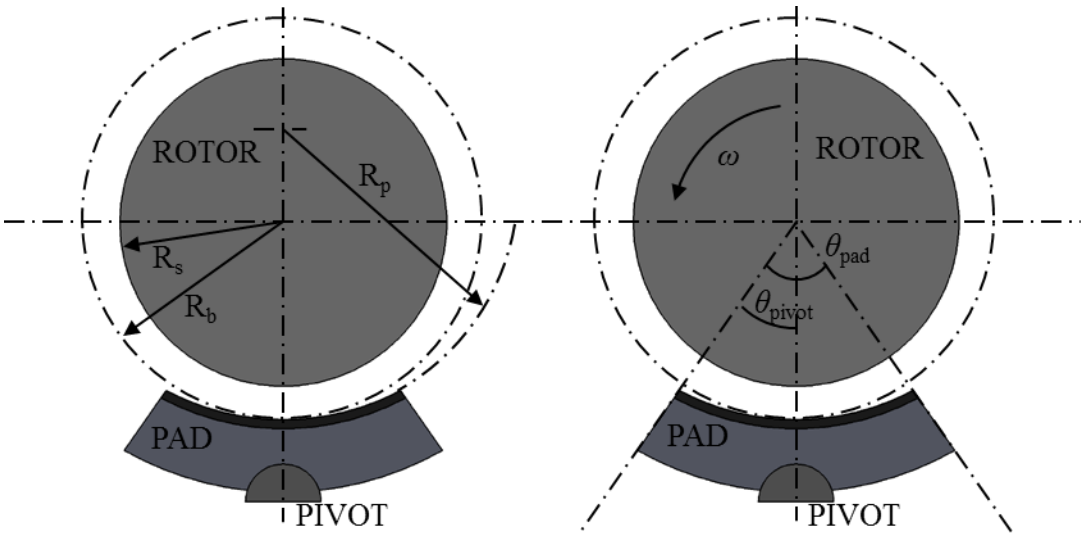

Figure 4. Geometric parameters for TPJBs.

Figure 4 shows the rotor's radius, bearing, and pad as well as the pivot's location relative to the pad's leading edge, i.e. pivot offset. The pivot offset is

$$PIVOT\ \ OFFSET = \frac{\theta_{pivot}}{\theta_{pad}}. \tag{2}$$

For a pad with the pivot located at the center of the pad, the pivot offset is 0.5 or 50%. Industrial applications typically use pivot offsets between 50% and 60%. Table 1 defines the radial bearing and pad clearance. The pad preload is defined in terms of the radial bearing clearance and pad clearance by

$$M_p = 1 - \frac{C_b}{C_p}. \tag{3}$$

A preload of zero implies that the bearing clearance and pad clearance are the same. A negative preload is typically avoided. A positive preload creates a converging wedge which is necessary to produce the reaction forces to support the rotor. Most bearings have a positive preload to ensure a converging wedge is created and to decrease the

likelihood of pad flutter [1]. Pad flutter and the lack of a converging wedge could lead to instabilities.

In general, an external static load is applied on a TPJB in either load-on-pad (LOP) or load-between-pad (LBP). Figure 1 depicts an LBP orientation. Generally, the LBP orientation can support heavier rotors and offers more symmetric ($K_{xx} = K_{yy}$) rotordynamic force coefficients. The LOP orientation provides stiffness orthotropy, causing the bearing to be stiffer in the loaded direction than in the non-loaded direction.

Knowledge of the geometrical parameters listed above is required to accurately predict the static and dynamic force performance of TPJBs. However, experience shows that there is sometimes poor correlation between predictions from computational codes and measured results; specifically, the TPJBs damping coefficients can be over predicted. As detailed below, researchers suggest the difference in numerical solutions and measured results can be attributed to the exclusion of pad and pivot flexibility in the computational bearing codes.

Pad flexibility refers to the pad's deflection relative to the pivot, while pivot flexibility refers to the pad's deflection relative to the bearing housing. Pad flexibility results in a change in curvature of the pad surface under load.

Few papers have made as large of an impact in rotordynamics as Lund's 1964 paper [2], in which he developed a method to calculate the rotordynamic coefficients of a TJPB. To predict the bearings' rotordynamic coefficients, Lund's pad assembly model predicted the stiffness and damping coefficients of a single pad, and summed the individual pad's coefficients to find the bearing's rotordynamic coefficients. He also presented non-dimensional stiffness and damping design curves versus "American" Sommerfeld number for various bearing configurations to be used by bearing designers. Lund's analysis includes pad-inertia effects yet neglects both pad and pivot flexibility.

In 1977, Varga [3] developed a code to predict the static characteristics of a 900 mm diameter three-pad TPJB and tested the bearing to determine the correlation between the measured results and predictions. Varga predicted the static characteristics of a TJPB with pads of increasing arc lengths (60°, 90°, 120°, and 150°). He found that the

bearing's predictions depended on the unit load, operating speed, and the bearing's pad clearance. He attributed the change in pad clearance as the rotor rotates to the pad's flexibility.

Varga's predictions show a larger change in pad clearance as the arc length of the pad increased. This change in pad clearance affected the minimum film thickness, maximum temperature, and power loss. In general, power loss increased as the pad clearance increased. As the pad arc length increased, the power loss trends became parabolic, and there was an optimum clearance to minimize the power loss. An optimum pad clearance was predicted for maximizing the minimum film thickness and minimizing the maximum temperature experienced in the pad. Predictions also show the operating clearance increased 50-100% relative to the design clearance. The pad can deflect due to thermal and mechanical deflections, which can be related to the speed and the bearing's load capacity.

Varga compared the measured results from the test on the 900 mm bearing with an in-house finite-element analysis (FEA) TJPB code. The bearing was equipped with sensors to measure the pad vibrations, oil-gap pressures, and Babbitt temperatures. These measurements were used as a baseline for comparing the results of the FEA TPJB code. Measured results show the finite-element model (FEM) could predict the measured increase in pad clearance. Varga noted that, "Pad deformation causes a distinct change in bearing behavior," and should be considered when designing a bearing.

In 1978, unlike Varga's work on the static performance of a TPJB, Nilsson [4] developed a computational code to examine the influence of bearing flexibility properties on the dynamic performance of radial oil-film bearings. He only included pad bending due to the pressure distribution and excluded pivot contact flexibility in his deflection analysis of the TP bearing. Nilsson modeled the pads in a TPJB as curved beams that deflect due to the hydrodynamic pressure applied to the pads from the oil-film. Nilsson simulated a single pad with three different pad arc lengths: 60°, 90°, and 120°. For the parametric study, pad flexibility had a minimal impact on the bearing's

static characteristics. However, the predicted rotordynamic coefficients changed markedly as the pad's flexibility increased. There was a decrease in stiffness coefficients and an even greater decrease in damping coefficients as the eccentricity ratio in the loaded direction increased. The decrease in dynamic coefficients was more pronounced as the pad's arc length increased. Predictions show a reduction in damping of approximately 60% of the value of the stiff pad due to bending deflections for the pad with an arc length of 90°.

In 1980, Ettles [5] predicted the rotordynamic coefficients by calculating the bearing's rotordynamic coefficients and pads together instead of Lund's pad assembly model. Unlike Lund, Ettles included the thermal and mechanical deflection effects on the TPJB's performance, but excluded the effect of contact flexibility. Ettles compared his model's predictions to the predictions from previous computational codes and measured results conducted by Malcher [6] and Klumpp [7]. With the inclusion of pad deflection, there was good agreement between Ettles' predictions and the measured results for the stiffness coefficients, but the damping coefficients were still slightly over predicted. This discrepancy could be attributed to the exclusion of pivot flexibility. Ettles, like Nilsson, observed a reduction in the predicted rotordynamic coefficients when considering pad deflections. Compared to predictions for a bearing with rigid pads, the predictions for a bearing with flexible pads at an eccentricity ratio of 0.9 show a reduction in stiffness and damping coefficients of approximately 16% and 44%, respectively. Ettles attributed the large reduction in system damping due to the "unwrapping" of the pad under thermal and mechanical deflection.

Hashimoto et al. [8] included pad deflection in their computational analysis of the effect of laminar and turbulent oil-flow on the performance of a large TPJB. They used a one-dimensional elastic beam equation to calculate the pad deflection solely in the circumferential direction and neglected pivot contact flexibility. The computational code predicted an overall decrease in the stiffness and damping coefficients for a large range of "American" Sommerfeld numbers, regardless if the flow was laminar or turbulent. The decrease in damping coefficients was up to approximately 30% while the

decrease in stiffness coefficients was approximately 15% for the laminar condition. For low Sommerfeld numbers, the eccentricity ratios were higher when considering pad deflection. As the Sommerfeld number increased, the predicted eccentricity ratio including pad deflection was smaller than the model neglecting pad deflection.

In 1987, Lund and Pederson [9] expanded the work of Nilsson, Ettles, and Hashimoto et al. to develop a computational model that included the effect of pad and pivot flexibility. They modeled the pad as a curved beam and approximated pad flexibility as the change in pad clearance caused by the hydrodynamic pressure distribution. For the simulated pad, pad flexibility affects the load-carrying capacity and the stiffness and damping coefficients. Increasing pad flexibility significantly decreased the damping coefficients as the non-dimensional expression of oil-film thickness at the pivot decreased. The load carrying capacity and direct stiffness coefficients slightly decreased as a non-dimensional expression of oil-film thickness at the pivot decreased. Lund and Pederson also show that the pad clearance increased as the flexibility increased, indicating that a flexible pad can bend more enabling larger film thicknesses. They concluded that pad and pivot flexibility could equally affect the rotordynamic coefficients and must be included to accurately predict the bearing's performance.

In 1989, Brugier and Pascal [10] expanded on Lund and Pederson's work to include axial and circumferential deflections by creating a three-dimensional FEM of the pad and pivot. They analyzed the effect of pad flexibility on both the static and dynamic load characteristics by introducing thermal and mechanical deflections in calculating the distribution of the oil-film thickness. They simulated a large turbo-generator with a diameter of 0.750 m, an L/D ratio of 0.75, for heavy unit-load conditions (1190 to 4762 kPa). They predicted that including the deflections had a small impact on the static characteristics; there is a small decrease in the minimum oil-film thickness and maximum pad temperature. The predictions that solely considered mechanical deflection have a larger minimum film thickness compared to the predictions with thermal and mechanical deflection.

Brugier and Pascal's predictions show the change in the stiffness coefficients depend on the static load. At lower static loads, the stiffness coefficients increase when pad flexibility is included in the model. At higher static loads, the stiffness coefficients decrease when the model includes pad flexibility, following the trend of previous prediction results. There is an overall decrease in the damping coefficients regardless of static load when pad flexibility is included in the model. The difference between the predictions of the computational model excluding and including the pad deflection increased as the load increase, indicating that pad flexibility has a greater effect as the load increases. The predicted damping coefficients are 10 to 25% smaller for all loads. Brugier and Pascal's article stressed the importance of including the effect of flexibility on the performance of a TPJB, especially on its dynamic performance.

Earles et al. [11]-[12] performed similar work as Brugier and Pascal in 1990 but modeled the pad with a two-dimensional FEM instead of the three-dimensional FEM pad model of Brugier and Pascal. They first modeled a single pad and then extended their work to a full bearing model. There was good agreement between their predictions and Lund and Pederson's predictions. They show the same decrease in bearing damping as the pad stiffness decreased. Their full rotor-bearing model shows that including pad and pivot flexibility decreased the predicted onset speed of instability. Earles et al. stressed that a two-dimensional finite-element model was superior to the curved beam model because the pad surface does not remain circular under very heavy loading. So, not only is it important to include pad flexibility in the analysis, but it is equally important to accurately model the pad, especially under heavy loading.

Also in 1990, Brockwell et al. [13] tested a 76.2 mm (3 in) nominal diameter, five-pad TPJB and developed a code to predict the bearing's performance. Their code included pad thermal and elastic deflections and pivot support flexibility. The pad's deflection due to the thermal and elastic effects was found using beam theory. There was good correlation between the predictions and the measured results with the inclusion of pad and pivot flexibility. Brockwell et al. were among the first to discuss the effect of bearing size on pad flexibility. They stated that while pad deflection did not have a

significant effect on the bearing coefficients, for their bearing size, and it would have a greater impact as the bearing's size increases.

Brockwell et al.'s measured results were used as a benchmark for several researchers' computational codes. The first was Kim et al. in 1995 [14], who developed a thermo-elastic-hydrodynamic (TEHD) approach to see the thermal and elastic effects on the dynamic coefficients predictions. They compared their predictions to the results of Brockwell et al. and found good agreement. Kim et al. modeled the pads using finite-elements to accurately capture the complex pad shapes. Much like their predecessors, Kim et al. concluded that the flexibility effects have a greater impact on the damping coefficients than the stiffness coefficients. Kim et al. stated that pad flexibility can be directly related to the pad's thickness. A decrease in pad thickness corresponds to an increase in pad flexibility. They modeled two different pad thicknesses and predicted a decrease in damping coefficients up to 25% as the pad's thickness decreased from 0.02 m to 0.01 m. The decrease in damping varied with speed. When the pad's thickness decreased, there was a slight decrease in stiffness coefficients at lower speeds and a slight increase in stiffness coefficients at higher speeds.

Several papers [15-19] in the 1990s investigated the effect of pad flexibility on the bearing's static performance, i.e., maximum hydrodynamic pressure, pad temperature, and minimum film thickness. Although the researchers used different models to approximate pad flexibility (two- and three-dimensional FEM) and different lubrication regimes – elastro-hydrodynamic (EHD), thermal-hydrodynamic (THD), and TEHD – they produced similar predictions.

Additionally, in 1999 El-Butch and Ashour [20], professors at Helwan University in Cairo, Egypt, performed a numerical study on the static performance of a three pad TPJB with rigid and elastic pads, and fixed rubber pad segments using a THD model. An FEM was used to approximate the thermal and mechanical deflection of the elastic and rubber pads. A linear two-dimensional model was used to approximate the mechanical pad deflections

$$[\mathrm{K}]\{\delta\} = \{\mathrm{F}\}. \tag{4}$$

They used the finite-element method for the rubber pads and the metal pads. They differentiated between the two FEMs by applying suitable boundary conditions and material specifications for each pad configuration.

Using the linear approximation of Eq. (4), predictions show increasing pad flexibility increased the minimum film thickness and in general decreased the maximum hydrodynamic pressure. However, the decrease in maximum pressure is often small as the flexibility increased and therefore does not have a large effect on the TPJB's load carrying capacity. An increase in minimum film thickness is contrary to the predictions by Brugier and Pascal.

In 2011, Cerda and Santos [21] performed a stability analysis on an industrial gas compressor under different lubrication regimes (EHD and THD). The pads were modeled using a three-dimensional finite-element method, the resultant model is

$$[M]\{\ddot{u}\}+[K]\{u\}=\{f\}. \tag{5}$$

Pad deflection is expressed as the linear combination of the pad's eigen modes. The first eigen mode corresponds to the pad's rigid-body mode while the higher modes correspond to pad elastic deflection. When compared to the rigid pads, the eccentricity ratio decreased and pad rotation angle increased for a flexible pad as the rotational speed increased. The effect of pad flexibility increased as the rotational speed increased, and this increase corresponded to a higher effective pad preload. Cerda and Santos, much like their predecessors, observed that pad flexibility alters the bearing clearance. According to Cerda and Santos, this alteration in bearing clearance resulted in a stiffening effect of the overall bearing system. This is contrary to prior researchers who predicted that direct stiffness coefficients decrease with the inclusion of pad deflection.

Cerda and Santos also analyzed the effect of pad flexibility on the dynamic coefficients. Their model predicted an increase in direct stiffness in the loaded direction and a significant reduction in damping coefficients, especially as the rotational speed increased. There was no change in onset speed of instability for a rotor supported by a flexible pad when compared to a rigid pad. For the rotor modeled, and the specific operating conditions, pad flexibility was not relevant when analyzing the rotor's

stability. This does not imply that pad flexibility should be excluded when analyzing the stability of a rotor system, but that it should be considered on a case-by-case basis.

Cerda and Santos [22] extended this research in 2012 using a TEHD model where the thermal deflection is approximated using the expansion coefficient

$$\varepsilon = \alpha \Delta T \, . \tag{6}$$

The predictions from their model were compared to the measured results from Brockwell et al. The model did not include pivot support flexibility and over predicted the damping coefficients. The model created by Cerda et al. [23] that same year included pivot and pad flexibility and show excellent agreement with Brockwell et al.'s measured results. Recall that Brockwell et al.'s bearing did not show significant pad flexibility due to the bearing's size (76.2 mm).

Branagan and Barrett [24] modeled pad flexibility as the change in pad curvature due to an applied moment at the pad's leading and trailing edge due to the fluid-film pressure, as seen in Figure 5.

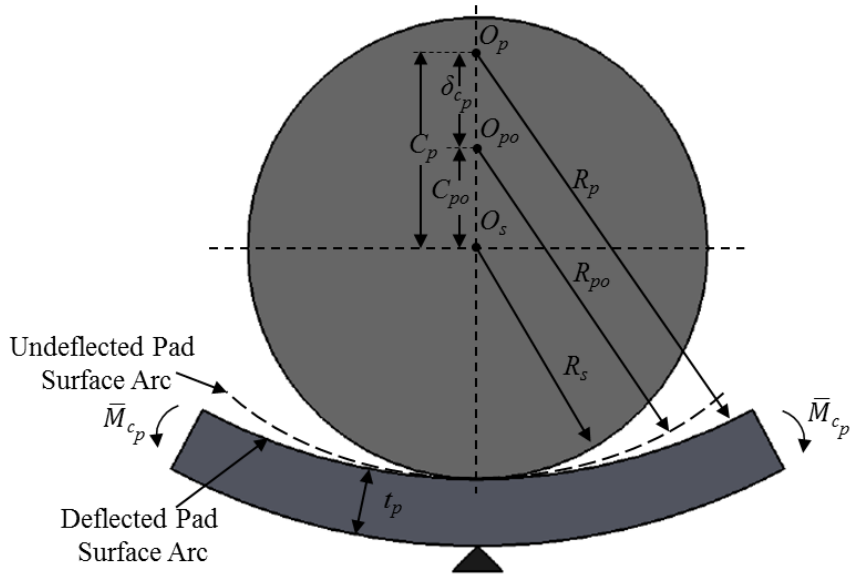

Figure 5. Change in pad curvature due to applied moments at the leading and trailing edge of the pad.

where O_j and O_p represent the centers of the rotor and bearing, respectively, and δ_{c_p} is the change in pad radius resulting from the applied fluid pressure field. Branagan and Barrett compared several analytic bending stiffness formulas, and concluded that the bending stiffness formula by Deutschman et al. [25] was the most accurate when predicting the change in pad curvature

$$\bar{k}_{p,k} = \frac{E_{p,k} L_{p,k} t_{p,k}}{\Theta_k - 1} \frac{\left(\Theta_k^2 - 1\right)^2 - \left[2\Theta_k \ln\left(\Theta_k\right)\right]^2}{4\left\{1 - \Theta_k^2\left[1 - 2\ln\left(\Theta_k\right)\right]\right\}} \tag{7}$$

where $\Theta_k = \left(1 + t_{p,k} / r_{p,k}\right)$ is the ratio of the outer to inner pad radii and t_p is the pad's thickness.

In 2012, Wilkes [26] analyzed the importance of including pad and pivot flexibility in predicting TPJB's dynamic-stiffness coefficients. Wilkes tested a five-pad, rocker-pivot TPJB, 50% pivot offset, 0.44 pad preload, in the LOP orientation. Wilkes' pads had a removable pivot insert that was bolted into the bearing side of the pad, unlike other pads that have the pivot rigidly attached to the pad. Figure 6 shows an illustration of the pads tested in Wilkes' dissertation.

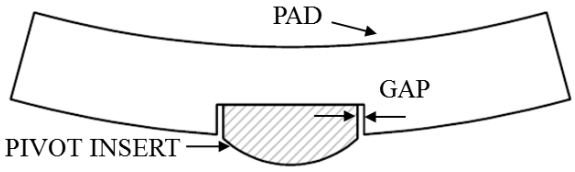

Figure 6. Schematic of a pad with a pivot insert.

Wilkes obtained the following model for pad stiffness similar to the model from Branagan and Barrett

$$\delta_{c_p} = \frac{\bar{M}_{c_p}}{k_p} \tag{8}$$

where $\bar{M}_{c_p}$ is the average applied fluid-film moment and k_p is the pad's structural bending stiffness. Wilkes developed an FEM of the pad in ANSYS to correlate the bending stiffness predictions from Deutschman et al. with the bending stiffness predictions results from the FEA.

In addition to testing the TPJB, Wilkes developed a predictive code, incorporating the effect of both pad and pivot flexibility, to predict the bearing's performance. The code over predicted direct stiffness and damping coefficients when pad and pivot flexibility were neglected. Table 2 lists the results of Wilkes' experimental tests showing the overestimation of direct stiffness and, more importantly, damping for a flexible pad and pivot when compared to a rigid pad and pivot using measured operating clearances. Wilkes saw a significant reduction in the predicted bearing damping coefficients with a flexible pad and pivot.

Table 2. Overestimation for direct stiffness and damping for a flexible pad and pivot when compared to a rigid pad and pivot.

Speed [RPM]	Unit Load [kPa]	Direct Stiffness	Direct Damping
4,400	3132	202%	811%
10,200	3132	177%	513%
10,200	783	51%	182%

As with Brockwell et al., Wilkes observed that pivot flexibility has a significant effect on the TPJB's rotordynamic coefficients. However, for the pads Wilkes tested, pad flexibility may have been more important than pivot flexibility. Wilkes still emphasized the need to include both pad and pivot flexibility in the bearing prediction code to accurately model the bearing's performance. Similar to Brockwell et al., Wilkes noted the importance of pad flexibility in larger bearings.

In 2013, Hagemann et al. [27] and Kukla et al. [28] measured and predicted the static and dynamic performance, respectively, of a 500 mm diameter TPJB under high

operating speeds. They predicted the TPJB's static performance using two simulation models that included pad and pivot flexibility and compared the predictions to the measured results. The simpler simulation, COMBROS, used a one-dimensional beam model to approximate pad flexibility. The advanced simulation used COMBROS with a three-dimensional structural mechanics software to approximate the axial pad deflection as the change in gap thickness. The comparison shows the three-dimensional model agreed with their measured results better than the one-dimensional model. Predictions and results also show that for the large TPJB, axial deflections caused by the thermal gradient were larger than axial deflections caused by mechanical loads. They performed an additional static parametric study on a smaller TPJB. They concluded that the bearing's size and design, and the mechanical load should be considered when determining the pad flexibility model used to predict pad deflection.

Although Hagemann et al. suggested that a three-dimensional model be used to predict the static and dynamic performance of large TPJBs, Kukla et al. used COMBROS (one-dimensional) to predict the dynamic performance of the 500 mm diameter TPJB. The measured results were reduced using a [K][C] model. There is good agreement between the predictions and results for the cross-coupled force coefficients, but poor agreement between the predictions and results for the direct force coefficients. The direct stiffness predictions are higher than the measured values, while the direct damping predictions are lower than the measured values.

Several researchers have stressed the importance of including pad and pivot flexibility in computational models to accurately predict the performance of TPJBs. However, there are limited measured results that show the effect of pad flexibility on the dynamic performance of a TPJB. The current work develops test results for a three-pad, 50% pivot offset, rocker-pivot pad, TPJB in the LBP orientation with three different pads having measurably different pad flexibilities. A three-pad TPJB, with a pivot offset of 50% is tested to create a significant change in the pad's flexibility. Three interchangeable pad sets with varying pad thicknesses are tested to determine the effect

of pad flexibility on the dynamic performance of a TPJB. The measured results can be used to validate computational codes that account for pad and pivot contact flexibilities.

Static load characteristics and rotordynamic coefficients presented will be compared to predictions from a computational code, XLTPJB, available from rotordynamic software suite XLTRC^2 at Texas A&M Turbomachinery Laboratory. The code created by Tao [29] and San Andrés and modified by Li and San Andrés includes the effects of pivot flexibility and pad flexibility, respectively. Their model accounts for pivot flexibility, pad flexibility, load configuration (LOP or LBP), and different pad-pivot geometries to predict the static and dynamic performance characteristics of a TPJB.

DESCRIPTION OF THE TEST RIG

Test Apparatus

Figure 7 shows the main section of the oil-bearing test rig at Texas A&M University. This test rig serves to measure the static and dynamic performance of fluid-film bearings. Kaul [30] presents a detailed description of the test rig design and the facility. The rig was originally designed to test oil bushing seals, similar to Glienicke's floating-bearing set-up [31]. It was adapted to test hydrodynamic bearings. The following section describes the test rig's main features.

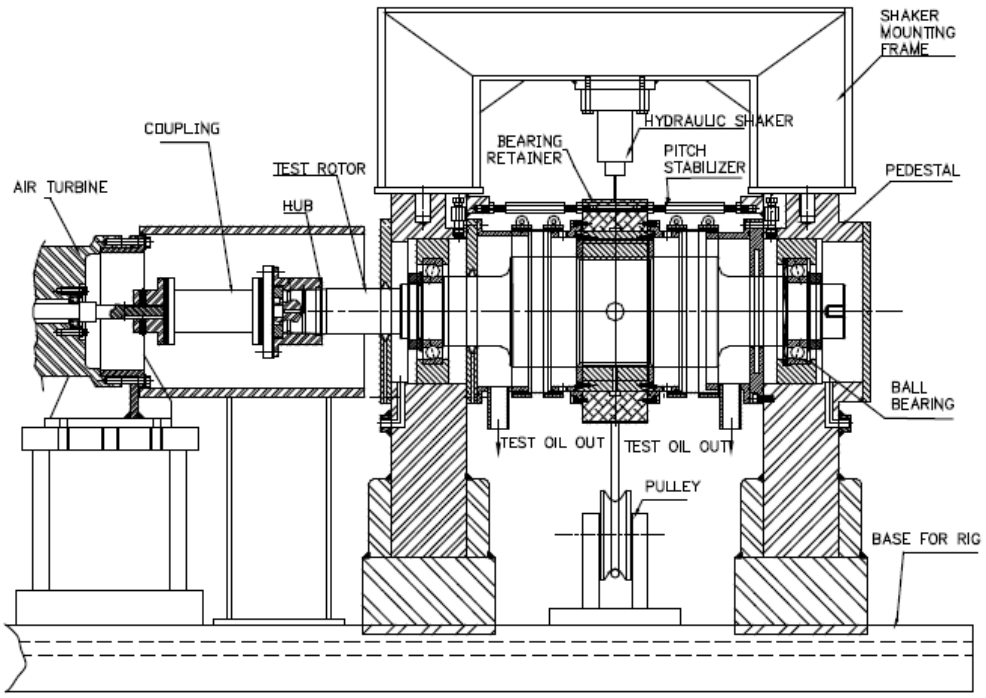

Figure 7. Main section of the oil bearing test rig [32].

The rig consists of a steel base that supports an air turbine, which drives the shaft, and the main test rig section. A flexible coupling connects the steel 4140 shaft to the air turbine. The air turbine can spin the shaft up to 17,000 rpm. The test shaft is machined

to 101.59 mm (3.9995 in) at the bearing location and is supported on the pedestals with two SKF hybrid-ceramic, angular contact ball bearings spaced roughly 457 mm (18 in) apart. An oil mist system lubricates the angular contact ball bearings. Pressurized air buffer seals ensure the oil from the outlet collections chambers does not enter the ball bearing section.

A split stator housing design holds the test bearing and the instruments, consisting of accelerometers, pressure transducers, and proximity probes, which are assembled onto the stator housing. Along with a press fit, an anti-rotation pin hole prevents the bearing from rotating within the stator housing. A pneumatic loader applies a static load while two orthogonal hydraulic shakers apply a dynamic load to the stator-bearing assembly. The hydraulic shakers attach to the stator housing via stingers, as shown in Figure 8.

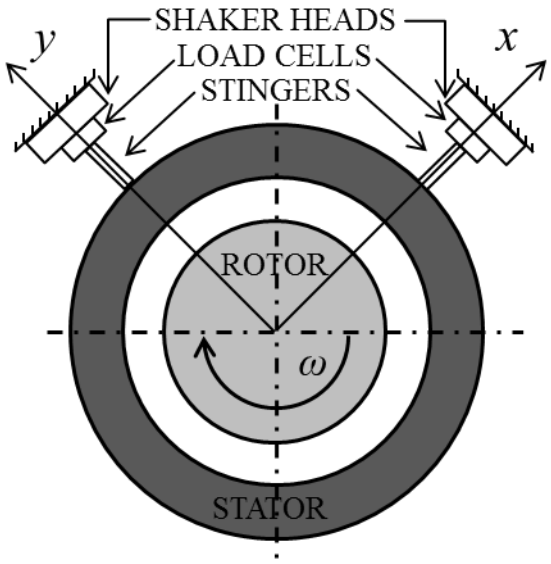

Figure 8. Stator shaker-stinger arrangement as viewed from the non-drive end.

The hydraulic shaker head in the x axis can excite the stator-bearing assembly with dynamic loads up to 4,450 N (1,000 lb_f) in both tension and compression. The hydraulic shaker in the y axis can excite the stator-bearing assembly with dynamic loads up to

4,450 N in tension and 11,125 N (2,500 lb_f) in compression. Both hydraulic shakers can produce excitation frequencies up to 1,000 Hz. Load cells, located between the hydraulic shaker heads and the stingers as seen in Figure 8, measure the dynamic loads applied to the stator-bearing assembly.

A pneumatic loader applies a static tensile load to the stator housing in the -y direction through a yoke, pulley, cable, and spring system, as seen in Figure 9. The static loader can apply a maximum load of 22,240 N (5,000 lb). The cable and spring system makes certain the load is constant and applied in one direction, and a load cell measures the static force applied to the stator housing.

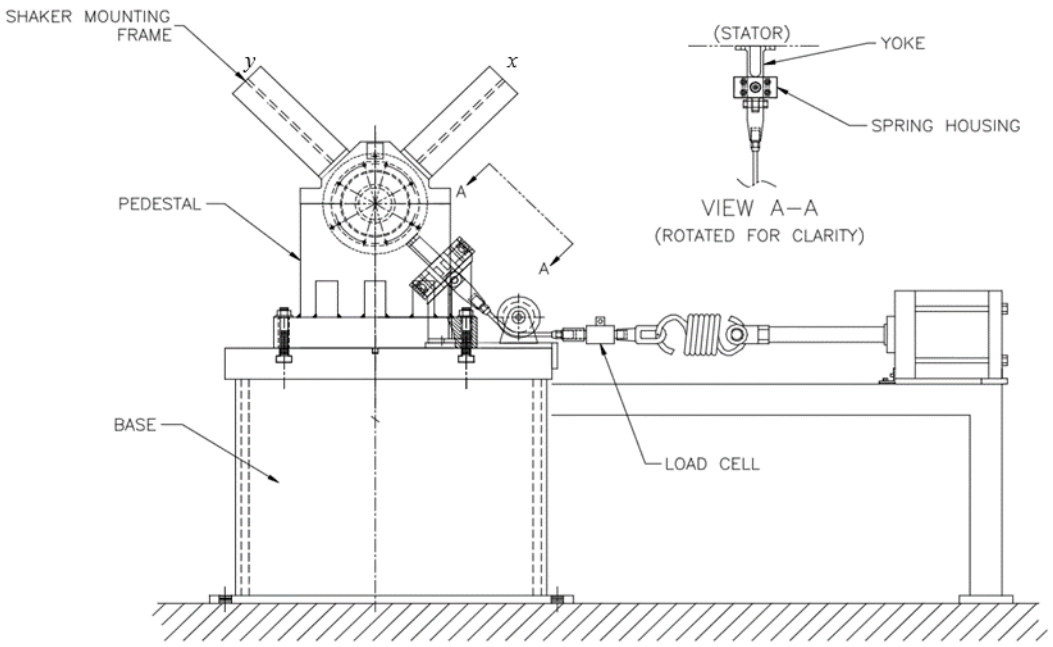

Figure 9. Static loader arrangement for the main test section from the non-drive end [32].

An oil pump system supplies ISO VG 46 turbine oil to the bearing through a port at the bottom of the stator housing. The pump can deliver oil at a maximum pressure of 82.7 bars and a maximum volumetric flow rate of 75 liters per minute. A set of

pneumatic control values and a heat exchanger control the oil temperature delivered to the bearing. Oil flows from the test bearing through end-caps attached to the stator housing and drains back into the oil pump system.

Instrumentation

Figure 10 shows the stator-bearing assembly that includes the instruments, static loader, stator housing, test bearing, and end-caps. The figure also shows the coordinate system viewed from the drive end. Note that the drive end (DE) and non-drive end (NDE) refer to the turbine side (TS) and non-turbine side (NTS), respectively.

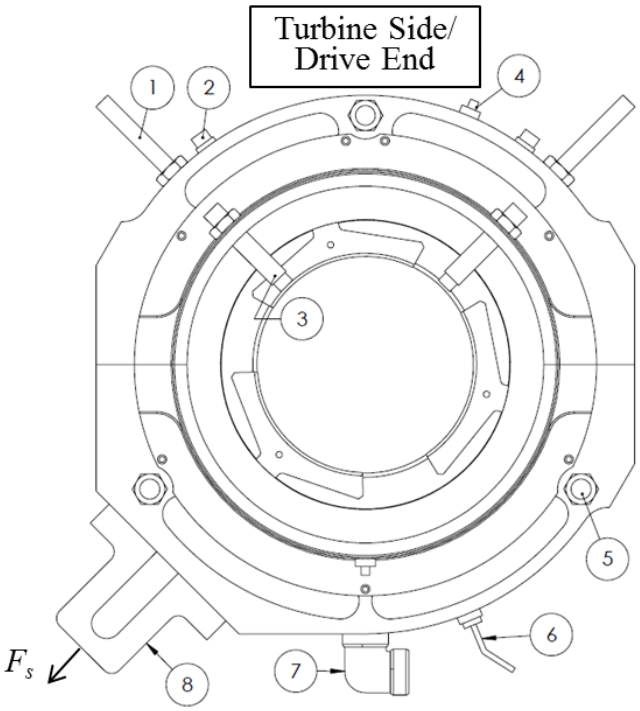

Part	Description	Quantity
1	Stinger	2
2	Accelerometer	2
3	Proximity Probe	4
4	Pressure Transducer	3
5	Pitch Stabelizers	6
6	Inlet Thermocouple	1
7	Inlet Oil Hose	1
8	Static Loader	1

Figure 10. Bearing configuration, instrumentation attachment, and raw coordinate system viewed from the DE for an applied force F_s.

Four proximity probes, placed in the stator end-caps, measure the shaft's relative displacement with respect to the test bearing. Two proximity probes are located on a

plane at the DE, and the remaining two proximity probes are located on a parallel plane on the NDE. The four proximity probes define an average test bearing location and allow for monitoring the stator-bearing assembly's angular alignment. Six pitch stabilizers arranged around the stator housing, three per side, control the angular misalignment between the shaft and the stator-bearing assembly.

Two piezoelectric accelerometers measure the stator-bearing assembly's absolute acceleration in both the x and y directions. Static pressure transducers measure the oil pressures at the inlet and both outlet locations. An oil hose attaches to the stator housing at the bottom and supplies oil to the test bearing. A thermocouple placed near the inlet oil hose measures the inlet oil temperature. Additional thermocouples measure the ball bearing and the oil discharged temperatures from the test bearing.

The coordinate system, shown in Figure 10, is a stator-centric coordinate system. When a static tensile load F_s is applied to the stator housing, it displaces the stator-bearing assembly's center along the y direction. This makes the shaft appear to displace in the +y direction even though the shaft is fixed.

Bearing and Pad Set Description

The test bearing, seen in Figure 11, is a three-pad, rock-pivot, tilting-pad journal bearing (TPJB) manufactured by Kingsbury, Inc. The bearing uses a split-design housing shell, and its assembly uses a flooded supply configuration.

Figure 11. Test bearing from the NDE, manufactured by Kingsbury, Inc.

The test bearing can be fitted with three different pad sets of varying pad thicknesses in order to test for the impact of pad flexibility. The pad sets have a constant 1.5 mm thick Babbitt layer. The total pad thickness, pad and Babbitt layer, for each pad set is 8.5 mm, 10 mm, and 11.5 mm. Figure 12 provides a comparison of the pad sets tested for this thesis. Each pad set has a pivot offset of 50%, a preload of 0.25, and a nominal radial clearance of 0.076 mm (0.003 in).

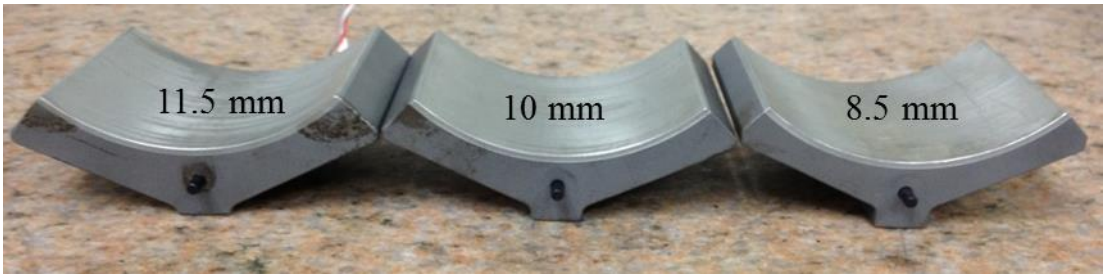

Figure 12. Test bearing pads, from right to left, with a thickness of 11.5 mm (0.456 in), 10 mm (0.396 in), and 8.5 mm (0.335 in).

Table 3 lists the details of the test bearing lubricant type, loading style, and geometry. These parameters are consistent for the three different pad configurations.

Table 3. Test bearing parameters that are constant for each pad set.

Description	Value
Rotor Diameter	101.59 mm (3.9995 in)
Number of pads	3
Load Configuration	LBP
Bearing (Bore) Diameter	101.74 mm (4.0057 in)
Radial Pad Clearance, C_p	0.1016 mm (0.004 in)
Radial Bearing Clearance, C_b	0.0762 mm (0.003 in)
Pad Axial Length	60.96 mm (2.4 in)
Thickness Variation	1.5 mm (0.06 in)
Pad Arc Angle	90°
Pivot Offset	50%
Preload	0.25
Lubricant Type	ISO VG 46
Oil Inlet Temperature	120°F

The loaded pads have an embedded thermocouple placed at a circumferential offset of 75% from the pad's leading edge to measure the maximum temperature in the pad. An additional exposed thermocouple measures the oil's temperature between the back of the pad and the bearing housing. Figure 13 and Figure 14 show the placement of the thermocouples on the pad and their arrangement on the loaded pads.

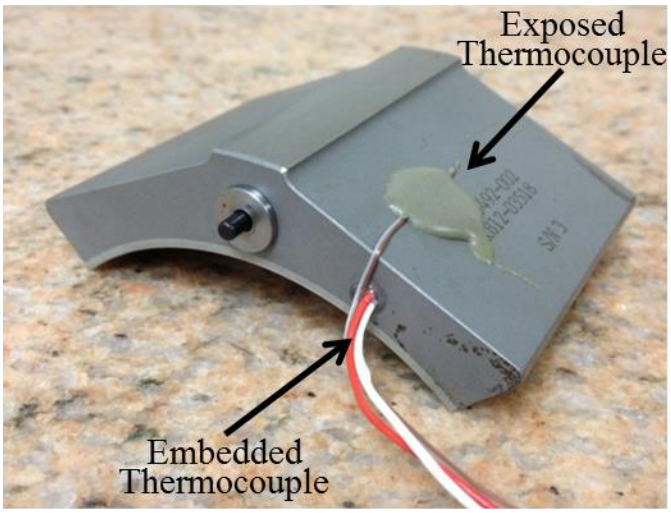

Figure 13. Embedded and exposed thermocouple placement on the pad.

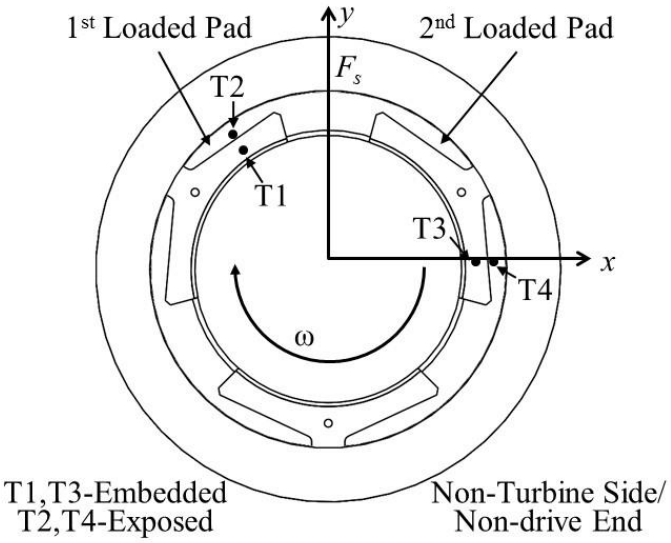

Figure 14. Arrangement of thermocouples on the loaded pads as viewed from the NDE.

EXPERIMENTAL PROCEDURE

Test Procedure Overview

The general testing procedure includes achieving steady-state operating conditions, and performing static and dynamic load tests. Attaining steady-state conditions requires operating the test rig near nominal test conditions, including shaft speed, static load, oil flow rate, and oil inlet temperature. The nominal test conditions include three speeds varying from 6,000 to 12,000 rpm and five unit loads varying from 172 to 1,724 kPa (25 to 250 psi). The flow rate (31 L/min) and inlet temperature (49°C) remained constant for all test conditions. Table 4 presents the nominal test conditions. The actual test conditions are reported in APPENDIX A: MEASURED STATIC LOAD CONDITIONS and APPENDIX B: MEASURED DYNAMIC LOAD CONDITIONS.

Table 4. Matrix of nominal test conditions.

Surface Speed RΩ	Speed [RPM]	Static Load [kPa (psi)], (Flow-rate 31 [L/min] @ 49°C)				
		172 (25)	345 (50)	689 (100)	1034 (150)	1,724 (250)
32 m/s	**6,000**	X	X	X	X	X
48 m/s	**9,000**	X	X	X	X	X
64 m/s	**12,000**	X	X	X	X	X

Static and dynamic load tests are performed once the inlet temperature, shaft speed, and static load have reached steady-state conditions i.e. confidence intervals are small. The test bearing is excited in two orthogonal directions, i.e. x and y directions, by the hydraulic shakers with a pseudo-random [33], dynamic excitation waveform during a dynamic load test. The waveform consists of frequencies that range from approximately 10 to 320 Hz in 10 Hz increments, and are slightly offset to avoid noise at 60 Hz and its multiples.

Static Load Characteristics

Static load characteristics for TPJBs normally include bearing clearance, journal eccentricity, bearing loci, attitude angles, and pad metal temperatures. The following section explains and defines these parameters. The Static Load Characteristics section will discuss the test results and predictions.

The bearing clearance is measured by slowing precessing the stator-bearing assembly about the rigid non-rotating shaft. The hydraulic shakers used for dynamic load testing move the bearing about the shaft while the proximity probes record the relative motion between the test bearing and the shaft. A "cold" clearance refers to this measurement taken at room temperature. The cold-clearance measurement estimates the average test bearing clearance. This clearance measurement provides an approximate clearance boundary for the test bearing to ensure the shaft does not rub the pads as the static load increases during testing. A "hot" clearance refers to this measurement taken immediately after shutting down the test rig. Typically, the hot clearance is smaller due to the influence of operating temperatures and represents the operational bearing clearance. Wilkes suggested that calculating the static load characteristics using the cold bearing clearance could be misleading. Therefore, the test bearing's static load characteristics are reduced using the hot-clearance measurement.

While the stator-bearing assembly is precessing around the shaft, the shaft is forced between the pads. For a 5-pad bearing and a 4-pad bearing, the bearing clearance measurement results in a pentagon and square clearance, respectively. Since the bearing tested in this thesis is a 3-pad TPJB, the clearance measurement yields a triangle clearance. Figure 15 shows an example of the raw clearance measurement (Figure 15 (a)) and the centered cold and hot bearing clearance measurements (Figure 15 (b)). The corner points and pad center points are used to approximate the radial bearing clearance. Figure 15 (b) also shows the circular clearance fit to measured clearance. The circular clearance fit's radius provides a good approximate of the radial bearing clearance.

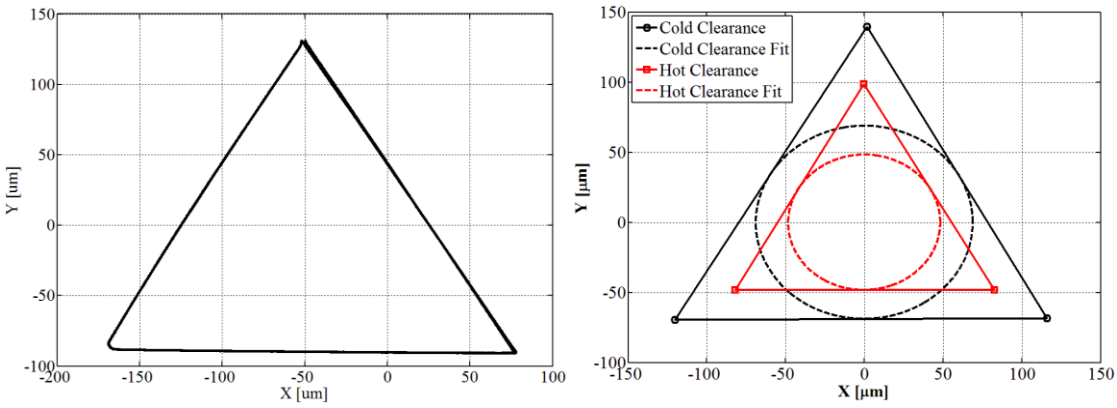

(a) **(b)**

Figure 15. Example of a (a) raw clearance measurement and a (b) measured hot and cold clearance using the corner points, and average fitted bearing clearances.

The static eccentricity ratio ε_o and the attitude angle ϕ describe the shaft's position at steady-state operating conditions. Figure 16 shows a general plot for the bearing loci and a physical representation of eccentricity and attitude angle.

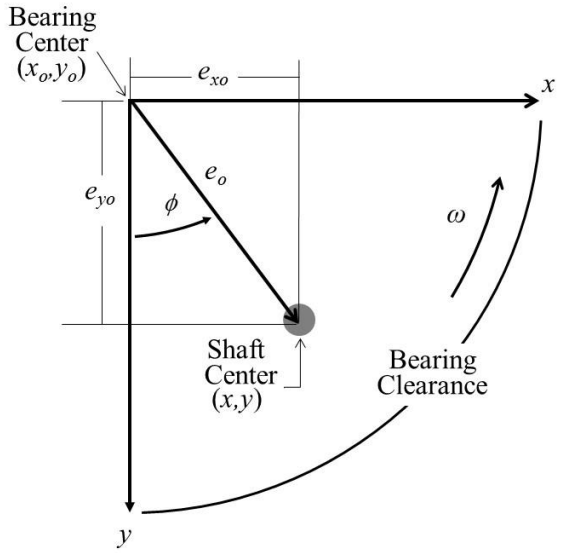

Figure 16. Generic journal eccentricity and attitude angle plot.

Eccentricity is the difference between the shaft center and the bearing center as a ratio with respect to the operational bearing clearance. An eccentricity ratio of zero indicates that the shaft is operating near the bearing's center. An eccentricity ratio of one would suggest contact between the shaft and the bearing but that is not always the case. For LBP orientations, the shaft can displace past the circular clearance fit shown in Figure 15. Eccentricity ratios in the x, y directions and the magnitude are

$$\varepsilon_{xo} = \frac{x - x_o}{C_{hb}} \quad \text{and} \quad \varepsilon_{yo} = \frac{y - y_o}{C_{hb}} \tag{9}$$

$$\varepsilon_o = \sqrt{(\varepsilon_{xo})^2 + (\varepsilon_{yo})^2} \tag{10}$$

where x_o and y_o are the coordinates for the bearing's center as determined by the hot clearance C_{hb}, and x and y are the coordinates for the shaft's position for a given unit load.

Attitude angle represents the shaft relative displacement from the y axis. The attitude angle is

$$\phi = \tan^{-1}\left(\frac{\varepsilon_{xo}}{\varepsilon_{yo}}\right)\frac{180}{\pi}[\text{deg}] \tag{11}$$

Dynamic Load Characteristics

Dynamic-Stiffness Coefficients

Childs and Hale [34] describe a parameter-identification model that extracts the rotordynamic coefficients from the measured dynamic data. By applying Newton's Second Law in the x and y directions, an equation of motion for the stator mass M_s is

$$M_s \begin{Bmatrix} \ddot{x}_s \\ \ddot{y}_s \end{Bmatrix} = \begin{Bmatrix} f_x \\ f_y \end{Bmatrix} - \begin{Bmatrix} f_{bx} \\ f_{by} \end{Bmatrix} \tag{12}$$

where $\ddot{x}_s$ and $\ddot{y}_s$ are measured stator accelerations, f_x and f_y are the excitation forces produced by the hydraulic shakers, and f_{bx} and f_{by} are the bearing reaction forces. The bearing reaction forces can be written in terms of stiffness [K] and damping [C] matrices. The conventional [K][C] model is

$$-\begin{Bmatrix} f_{bx} \\ f_{by} \end{Bmatrix} = \begin{bmatrix} K_{xx} & K_{xy} \\ K_{yx} & K_{yy} \end{bmatrix} \begin{Bmatrix} \Delta x \\ \Delta y \end{Bmatrix} + \begin{bmatrix} C_{xx} & C_{xy} \\ C_{yx} & C_{yy} \end{bmatrix} \begin{Bmatrix} \Delta \dot{x} \\ \Delta \dot{y} \end{Bmatrix}. \tag{13}$$

The conventional [K][C] model frequently yields frequency-dependent stiffness and damping coefficients. Childs et al. [35] suggest that adding a mass matrix and modeling the real part of dynamic-stiffness coefficients as a quadratic function of excitation frequency will yield a [K][C][M] model with frequency-independent rotordynamic coefficients,

$$-\begin{Bmatrix} f_{bx} \\ f_{by} \end{Bmatrix} = \begin{bmatrix} K_{xx} & K_{xy} \\ K_{yx} & K_{yy} \end{bmatrix} \begin{Bmatrix} \Delta x \\ \Delta y \end{Bmatrix} + \begin{bmatrix} C_{xx} & C_{xy} \\ C_{yx} & C_{yy} \end{bmatrix} \begin{Bmatrix} \Delta \dot{x} \\ \Delta \dot{y} \end{Bmatrix} + \begin{bmatrix} M_{xx} & M_{xy} \\ M_{yx} & M_{yy} \end{bmatrix} \begin{Bmatrix} \Delta \ddot{x} \\ \Delta \ddot{y} \end{Bmatrix}. \tag{14}$$

where the added mass matrix [M] contain the fluid-film's virtual-mass coefficients. By substituting the [K][C][M] model into the equation of motion for the stator, the bearing reaction force as a function of the rotordynamic coefficients becomes

$$\begin{Bmatrix} f_x - M_s \ddot{x}_s \\ f_y - M_s \ddot{y}_s \end{Bmatrix} = -\begin{bmatrix} K_{xx} & K_{xy} \\ K_{yx} & K_{yy} \end{bmatrix} \begin{Bmatrix} \Delta x \\ \Delta y \end{Bmatrix} - \begin{bmatrix} C_{xx} & C_{xy} \\ C_{yx} & C_{yy} \end{bmatrix} \begin{Bmatrix} \Delta \dot{x} \\ \Delta \dot{y} \end{Bmatrix} - \begin{bmatrix} M_{xx} & M_{xy} \\ M_{yx} & M_{yy} \end{bmatrix} \begin{Bmatrix} \Delta \ddot{x} \\ \Delta \ddot{y} \end{Bmatrix} \tag{15}$$

where K_{ij}, C_{ij}, and M_{ij} are stiffness, damping, and virtual-mass coefficients. The excitation forces, stator accelerations, and relative motion between the shaft and the stator-bearing assembly, i.e. Δ x and Δ y, are measured functions of time.

Extracting the rotordynamic coefficients occurs in the frequency domain. A Fast Fourier Transform converts the data captured in the time domain into the frequency domain, yielding

$$\begin{Bmatrix} \boldsymbol{F_x} - M_s \boldsymbol{A_x} \\ \boldsymbol{F_y} - M_s \boldsymbol{A_y} \end{Bmatrix} = -\begin{bmatrix} \boldsymbol{H_{xx}} & \boldsymbol{H_{xy}} \\ \boldsymbol{H_{yx}} & \boldsymbol{H_{yy}} \end{bmatrix} \begin{Bmatrix} \boldsymbol{D_x} \\ \boldsymbol{D_y} \end{Bmatrix} \tag{16}$$

where $\mathbf{F_i}$, $\mathbf{A_i}$, and $\mathbf{D_i}$ are the excitation force, stator acceleration, and relative motion between the shaft and the stator-bearing assembly in the x and y directions. The complex dynamic-stiffness function, $\mathbf{H_{ij}}$, relates a force in the "i" direction in response to a displacement, velocity, or acceleration in the "j" direction. The complex dynamic-stiffness written in terms of the rotordynamic coefficients is

$$\boldsymbol{H_{ij}} = \left(K_{ij} - \Omega^2 M_{ij}\right) + \boldsymbol{j}\left(\Omega C_{ij}\right). \tag{17}$$

The real and imaginary components of the dynamic-stiffness are

$$\mathrm{Re}\left(\boldsymbol{H_{ij}}\right) = K_{ij} - \Omega^2 M_{ij} \tag{18}$$

$$\mathrm{Im}\left(\boldsymbol{H_{ij}}\right) = \Omega C_{ij} \tag{19}$$

where Ω represents the excitation frequency. The rotordynamic coefficients are found by curve fitting the Re ($\mathbf{H_{ij}}$) as a quadratic function of Ω and the Im ($\mathbf{H_{ij}}$) as a linear function of Ω. The stiffness and virtual-mass coefficients are the zero-frequency intercept and curvature, respectively, of the quadratic fit while the damping coefficient is the linear curve fit's slope.

The equation for the bearing's dynamic-stiffness provides two equations with four unknowns $\mathbf{H_{xx}}$, $\mathbf{H_{xy}}$, $\mathbf{H_{yx}}$, and $\mathbf{H_{yy}}$. Shaking the stator-bearing assembly in the x and y directions, while measuring the response in each direction, produces four independent equations. The four independent equations are

$$\begin{bmatrix} \boldsymbol{F}_{xx} - M_s \boldsymbol{A}_{xx} & \boldsymbol{F}_{xy} - M_s \boldsymbol{A}_{xy} \\ \boldsymbol{F}_{yx} - M_s \boldsymbol{A}_{yx} & \boldsymbol{F}_{yy} - M_s \boldsymbol{A}_{yy} \end{bmatrix} = -\begin{bmatrix} \boldsymbol{H}_{xx} & \boldsymbol{H}_{xy} \\ \boldsymbol{H}_{yx} & \boldsymbol{H}_{yy} \end{bmatrix} \begin{bmatrix} \boldsymbol{D}_{xx} & \boldsymbol{D}_{xy} \\ \boldsymbol{D}_{yx} & \boldsymbol{D}_{yy} \end{bmatrix} \tag{20}$$

One set of frequency-dependent dynamic-stiffness coefficients ($\mathbf{H_{xx}}$, $\mathbf{H_{xy}}$, $\mathbf{H_{yx}}$, and $\mathbf{H_{yy}}$) is obtained from 32 repeated excitations, from a pseudo-random, dynamic excitation waveform, that are averaged in the frequency domain. As stated earlier, the waveform consists of frequencies that range from 10 to 320 Hz in 10 Hz increments. This process repeats 10 times in the x and y directions for each nominal test conditions. This results in 320 multi-frequency waveforms in each direction, for each nominal test condition. The dynamic repeatability of the dynamic-stiffness coefficients, at each frequency, is twice the standard deviation of the 10 individual impedance values. Frequency values with poor repeatability, i.e. large uncertainty, are eliminated for the purpose of dynamic coefficient extraction.

The dynamic-stiffness functions measures the stiffness, damping and inertia of the test bearing's fluid-film and anything rigidly attached to the stator-bearing assembly, such as the instrumentation, static loader, and pitch stabilizers. Before oil is introduced into the test bearing, a dry dynamic load test, or baseline, accounts for the stiffness and damping of the stator attachments. The fluid-film's dynamic-stiffness is the difference

between the dynamic-stiffness of the baseline and the dynamic-stiffness of a nominal test condition. The fluid-film's dynamic-stiffness is

$$\boldsymbol{H}_{ij} = \boldsymbol{H}_{ij,TEST} - \boldsymbol{H}_{ij,BASELINE} \tag{21}$$

A new baseline is required for each test bearing configuration. Even though the assembly process is the same for each configuration, there might be slight differences in the stator attachments. A new baseline will account for any minor changes across configurations. Figure 17 and Figure 18 show an example of the direct and cross-coupled baseline dynamic-stiffness coefficients.

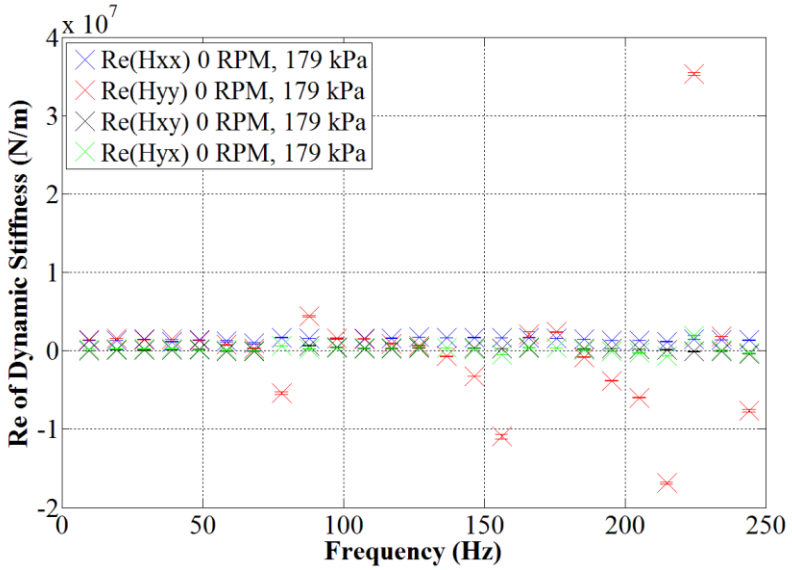

Figure 17. Baseline for the real direct and cross-coupled dynamic-stiffness.

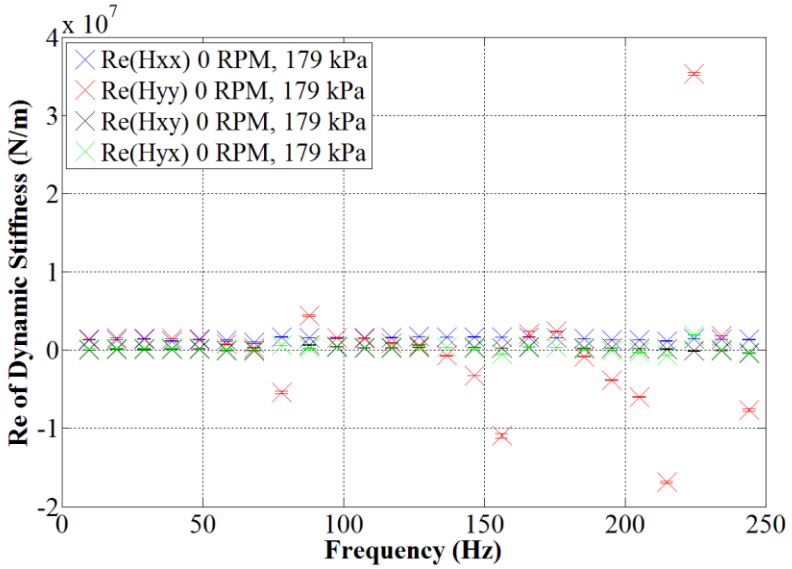

Figure 18. Baseline for the imaginary direct and cross-coupled dynamic-stiffness.

Curve Fitting and Uncertainty Analysis

Recall that for each nominal test condition, there are 10 individual shakes (320 multi-frequency waveforms) in each orthogonal direction. The dynamic-stiffness $\mathbf{h_{ij}}$ is averaged for N number of shakes at each excitation frequency and the uncertainty of each averaged dynamic-stiffness $\mathbf{H_{ij}}$ value can be defined as two times the standard deviation.

$$\boldsymbol{H}_{ij} = \frac{1}{N}\sum_{k=1}^{N}\left(\boldsymbol{h}_{ij}\right)_k \tag{22}$$

$$\Delta\boldsymbol{H}_{ij} = 2\sigma_{\boldsymbol{H}_{ij}} = \boldsymbol{2}\sqrt{\frac{\sum_{k=1}^{N}\left(\left(\boldsymbol{h}_{ij}\right)-\boldsymbol{H}_{ij}\right)}{N-1}} \tag{23}$$

These equations are used to obtain the average dynamic-stiffness and uncertainty for the baseline dynamic-stiffness and the tested dynamic-stiffness. The dynamic-stiffness' uncertainty is considered to be the repeatability of each test condition and is shown as error bars on the dynamic-stiffness plots.

The stiffness and virtual-mass coefficients are the zero-frequency intercept and curvature, respectively, of the quadratic fit to the real part of the dynamic-stiffness $\mathbf{H_{ij}}$. The dynamic-stiffness' real part becomes a linear function of Λ by setting $\Omega^2 = \Lambda$, where K_{ij} is the y-intercept and M_{ij} is the slope, defined by

$$\mathrm{Re}(\boldsymbol{H_{ij}}) = K_{ij} - \Lambda M_{ij} \tag{24}$$

K_{ij} and M_{ij} are reduced from the least squares linear regression, in the slope-intercept form that is applied to Re ($\mathbf{H_{ij}}$) versus Λ data

$$y = mx + b \tag{25}$$

where x represents the independent variable, y represents the dependent variable, m is the slope, and b is the y-intercept. The slope m and y-intercept b of the linear regression are

$$m = \frac{n\sum_{k=1}^{n} x_k y_k - \sum_{k=1}^{n} x_k \sum_{k=1}^{n} y_k}{\sum_{k=1}^{n} x_k^2 - \left(\sum_{k=1}^{n} x_k\right)^2} \tag{26}$$

$$b = \left(\frac{1}{n}\sum_{k=1}^{n} x_k\right) - m\left(\frac{1}{n}\sum_{k=1}^{n} y_k\right) \tag{27}$$

where n is the number of data point pairs and x_k and y_k represent the data point pair's coordinates.

When applying the linear regression to Re ($\mathbf{H_{ij}}$) versus Λ data, the slope is the virtual-mass coefficient M_{ij}, and the y-intercept is the stiffness coefficient K_{ij}. When applying the linear regression to Im ($\mathbf{H_{ij}}$) versus Ω data, the slope is the frequency-independent damping coefficient C_{ij} while the y-intercept has no physical meaning. The least squares linear regression is used to find both the cross-coupled and direct coefficients.

The uncertainties for the rotordynamic coefficients are determined by the correlation coefficient r of the linear regression best fit line with the dynamic-stiffness data. The dynamic-stiffness' uncertainty data (2σ) is different than the uncertainty of the rotordynamic coefficients. The final coefficient uncertainty of the slope and y-intercept

is a function of the sum of squared deviations of observed points from their sample mean S_{xx} and the mean square error $\hat{\sigma}^2$ defined by

$$S_{xx} = \sum_{k=1}^{n} \left(x_k^2 - \bar{x}^2 \right) \tag{28}$$

$$\hat{\sigma}^2 = \frac{\sum_{k=1}^{n} \left(y_k - \hat{y}_k \right)^2}{n-2} \tag{29}$$

where $\bar{x}$ is the sample mean, $\bar{y}_k$ is the dependent variable fit data, and x and y represent the independent and dependent variables, respectively. The uncertainty of the slope m and y-intercept b are

$$\Delta m = t \sqrt{\frac{\hat{\sigma}^2}{S_{xx}}} \tag{30}$$

$$\Delta b = t \sqrt{\hat{\sigma}^2 \left(\frac{1}{n} + \frac{\bar{x}^2}{S_{xx}} \right)} \tag{31}$$

where the statistical variable t is a function of the number of data points n and the confidence interval. The statistical variable t = 1.96 for large data set with a confidence interval of 95%.

Table 5 shows a summary of the rotordynamic coefficients and uncertainties for t_p = 8.5 mm at 6,000 rpm and 1,724 kPa.

Table 5. Experimental rotordynamic coefficients for t_p = 8.5mm at 6,000 rpm and 1,724 kPa.

Coefficient	Units	Value	Uncert.	%Uncert.
$\mathbf{K_{xx}}$	MN/m	404	13	3
$\mathbf{K_{xy}}$		-40	5	12
$\mathbf{K_{yx}}$		-46	7	15
$\mathbf{K_{yy}}$		150	4	2
$\mathbf{C_{xx}}$	kN-s/m	190	11	6
$\mathbf{C_{xy}}$		-46	5	11
$\mathbf{C_{yx}}$		-39	6	16
$\mathbf{C_{yy}}$		100	5	5
$\mathbf{M_{xx}}$	kg	-18	18	97
$\mathbf{M_{xy}}$		-17	7	40
$\mathbf{M_{yx}}$		-17	9	55
$\mathbf{M_{yy}}$		-16	4	30

Large uncertainties occur when the rotordynamic coefficients values are small, as for the cross-coupled terms. These rotordynamic uncertainties are representative of the majority of the test results. The uncertainties for each test condition can be found in APPENDIX C: ROTORDYNAMIC COEFFICIENTS

Input Parameters for Predictive Code

As mentioned earlier, the static and dynamic load characteristics will be compared to predictions. The rotordynamic bearing code used to predict the performance of the bearing was originally developed by Tao and San Andrés at the Texas A&M Turbomachinery Laboratory and later modified by Li and San Andrés. The bearing code uses a laminar-flow Reynolds equation model to predict the static and dynamic performance for a bearing. The original code accounts for pivot flexibility with a user defined load-versus-deflection curve. The modified code accounts for pad flexibility through a user defined ANSYS FEM that specifies pad thickness, pad material, pad arc length, and pivot offset.

The stiffness of each pad set was measured using the test rig. The bearing is assembled in the LOP orientation. The bearing is loaded using the static loader, and the load and the relative displacement between the stator-bearing assembly and the rotor is

recorded. This procedure is intended to measure the stiffness of the pivot but the relative displacement might include the deflection of the pad relative to the pivot i.e. pad flexibility. The pivot stiffness of each pad set is shown in Table 6. As the thickness of the pad increased, the pivot stiffness increased. These pivot stiffness values were input into XL_TPJB©, and FEMs were created for each pad configuration with the help of Yingkun Li.

Table 6. Pivot stiffness for each pad configuration measured on the test apparatus.

Pad Thickness	Pivot Stiffness [MN/m]
t_p = 8.5 mm	505
t_p = 10 mm	664
t_p = 11.5 mm	751

The program also allows the user to input a pad clearance and choose a frequency analysis option and a thermal analysis option.

1. Pad Clearance: The hot clearance is assumed to be more representative of the bearing clearance during tests and will be used in predictions instead of the measured cold clearance
2. Frequency Analysis: This option allows the user to reduce the coefficients using a synchronous or non-synchronous option. The synchronous analysis predicts the rotordynamic coefficients at a specified running speed. The non-synchronous analysis predicts the bearing's performance over a range of excitation frequencies (0-350 Hz).
3. Thermal Analysis: The code uses an adiabatic energy transport equation to predict the temperature distribution in the bearing and gives the user the option to select what type of thermal analysis, adiabatic or isothermal, to use for both the bearing and the rotor. There is an input for the thermal mixing

coefficient that represents the fraction of hot oil carry over from one pad to the adjacent pad.

The output for the bearing program presents the rotordynamic coefficients and the static parameters such as the eccentricity ratio, attitude angle, and maximum temperature rise in the bearing.

STATIC LOAD CHARACTERISITICS

Clearance

Measured cold clearance (CC) and hot clearance (HC) plots for each pad configuration are shown in Figure 19. The fitted clearance curves shown in Figure 19 are for the measured cold clearance and for the measured hot clearance at 12,000 rpm. The radial bearing clearance values are given in Table 7. As mentioned previously, the measured hot clearance is smaller than the measured cold clearance due to the influence of the operating temperatures.

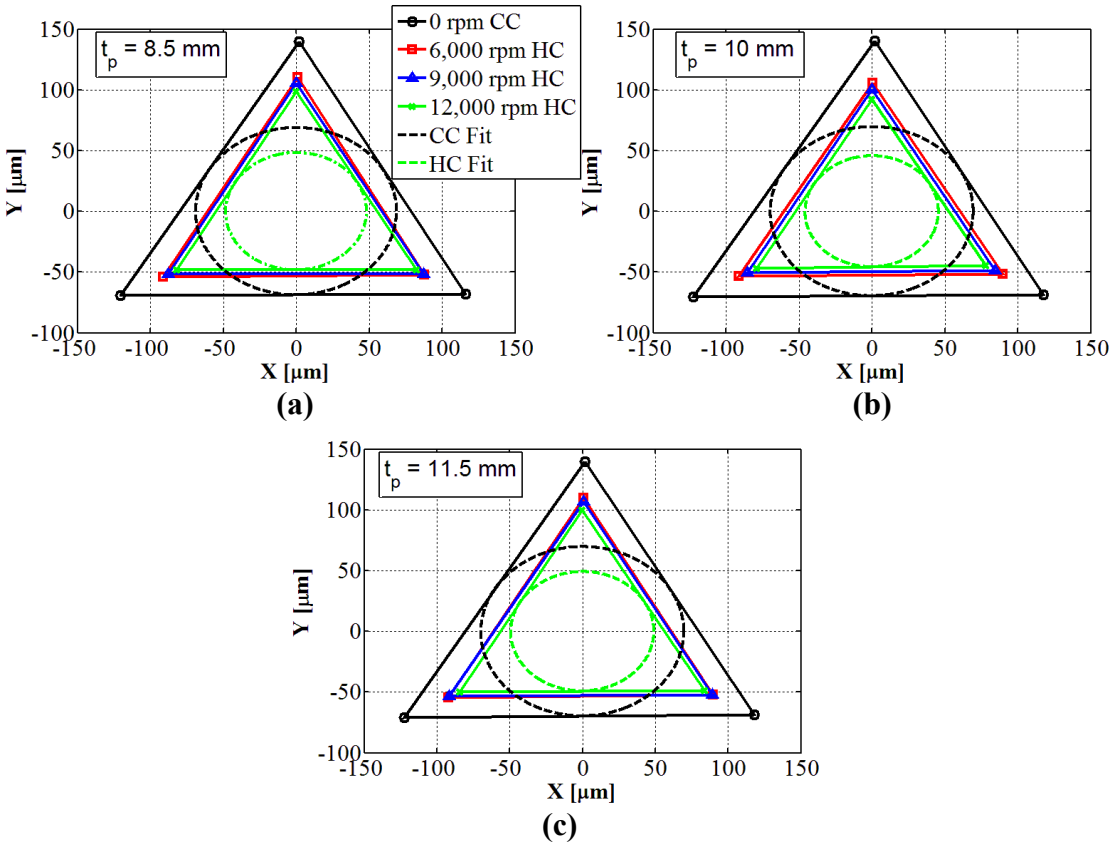

Figure 19. Cold and hot clearances for the nominal speeds for (a) t_p = 8.5 mm, (b) t_p = 10 mm, and (c) t_p = 11.5 mm

Table 7 shows that the nominal operating clearance (cold clearance) is approximately the same for each pad configuration. Increasing the speed results in a decrease in radial bearing clearance due to the increase in operating temperatures in the bearing.

Table 7. Measured test bearing cold and hot clearances for each pad configuration (nominal clearance 76.2 μm).

Speed [RPM]	Radial Bearing Clearance [μm]		
	t_p = 8.5 mm	t_p = 10 mm	t_p = 11.5 mm
0 (CC)	69	70	70
6,000 (HC)	53	53	54
9,000 (HC)	51	50	53
12,000 (HC)	48	46	49

Eccentricity and Attitude Angle

The static eccentricity ratio and attitude angle describe the rotor's position at a given operating position. The following section presents measured and predicted loci for each pad configuration, nominal speed, and nominal static load. Each data point represents a static load condition where the data point near the origin is 172 kPa, and the point furthest from the origin is 1,724 kPa. The solid lines are measured values, and the dashed lines are the predictions. This convention holds for the remainder of this work. Recall that the eccentricity ratios are normalized with the hot bearing clearance. The pad outlines and clearance circle fits in the following graphs represent the hot bearing clearance measurements.

Figure 20 provides the measured loci plots for three rotational speeds and unit loads for the three pad configurations. Increasing the unit load increases the journal displacement along the loaded direction (y-axis), while increasing the rotational speed decreases the journal displacement along the loaded direction. Eccentricity ratios of

over one are measured at the largest unit loads because the rotor can push in between the two loaded pads.

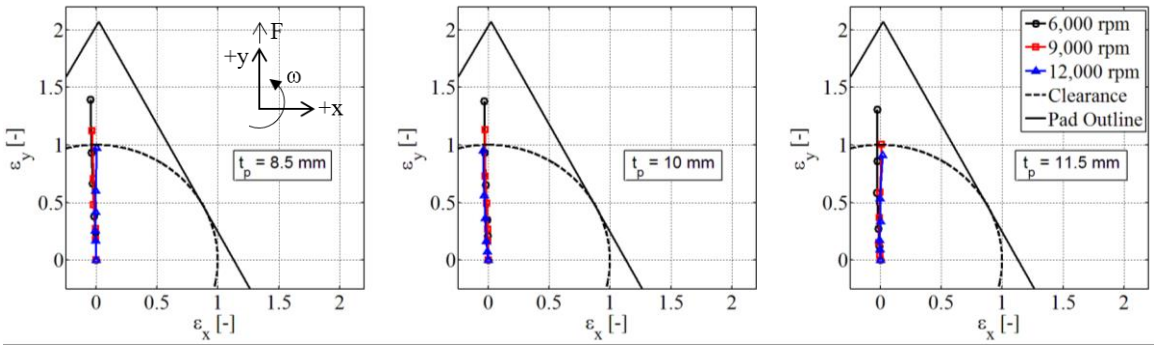

(a) **(b)** **(c)**

Figure 20. Measured loci plots for three pad thicknesses for (a) t_p = 8.5 mm, (b) t_p = 10 mm, and (c) t_p = 11.5 mm.

Figure 21 through Figure 23 show the measured and predicted loci plots using XL_TPJB© for the three pad configurations. Note the x-axis dimension is significantly smaller than the y-axis dimension to determine the agreement between the measured results and predictions. Figure 21 provides the measured and predicted loci plot for t_p = 8.5 mm, Figure 22 shows the measured and predicted loci plots for t_p = 10 mm, and lastly, Figure 23 shows the measured and predicted loci plots for t_p = 11.5 mm.

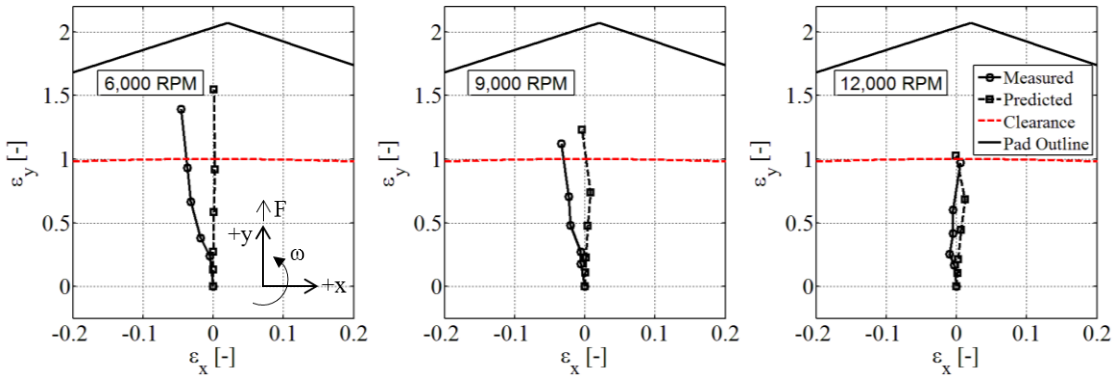

Figure 21. Measured (solid) and predicted (dashed) loci plots for three speeds for (a) 6,000 rpm, (b) 9,000 rpm, and (c) 12,000 rpm for t_p = 8.5 mm.

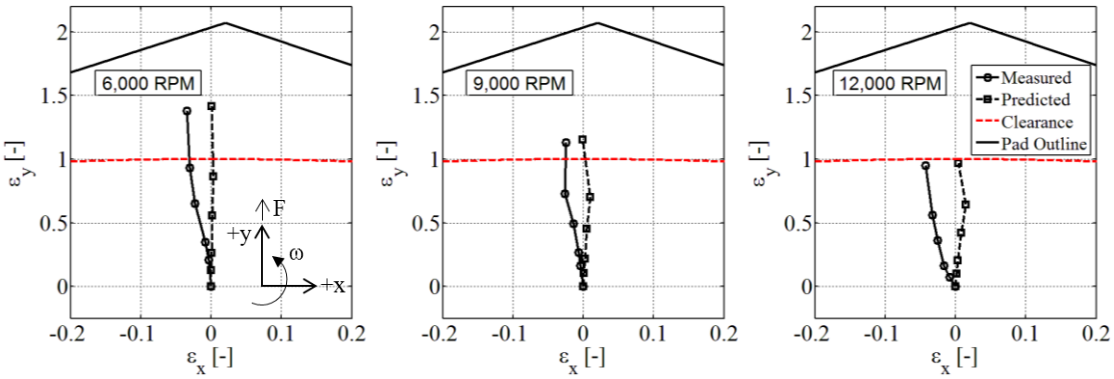

Figure 22. Measured (solid) and predicted (dashed) loci plots for three speeds for (a) 6,000 rpm, (b) 9,000 rpm, and (c) 12,000 rpm for t_p = 10 mm.

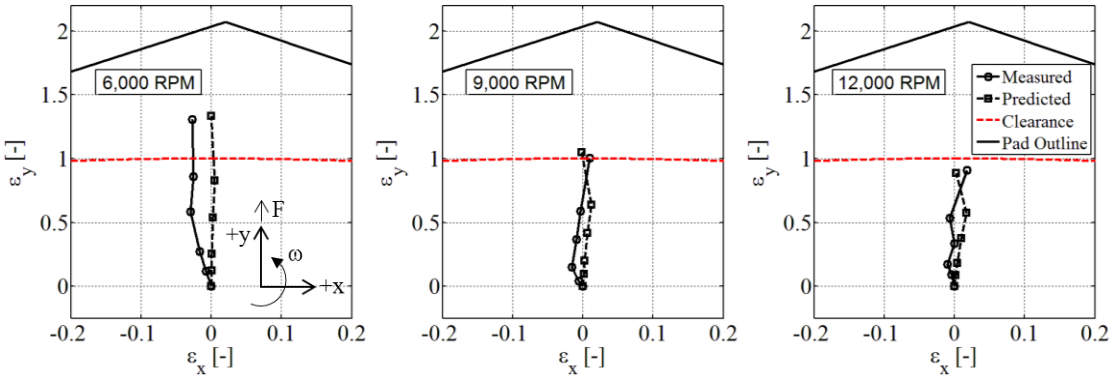

Figure 23. Measured (solid) and predicted (dashed) loci plots for three speeds for (a) 6,000 rpm, (b) 9,000 rpm, and (c) 12,000 rpm for t_p = 11.5 mm.

At lower unit loads, the eccentricity predictions are lower than the measured values for all pad configurations. As the unit load increases, the eccentricity predictions are higher than the measured values. At low speeds, the eccentricity predictions are lower than the measured values. At 12,000 rpm, the eccentricity predictions are higher than the measured values. There is better agreement between the measured values and predictions as the rotational speed increases.

Figure 24 shows the measured and predicted eccentricity ratio in the loaded direction versus unit load for each pad configuration. The dashed line is the bearing clearance limit.

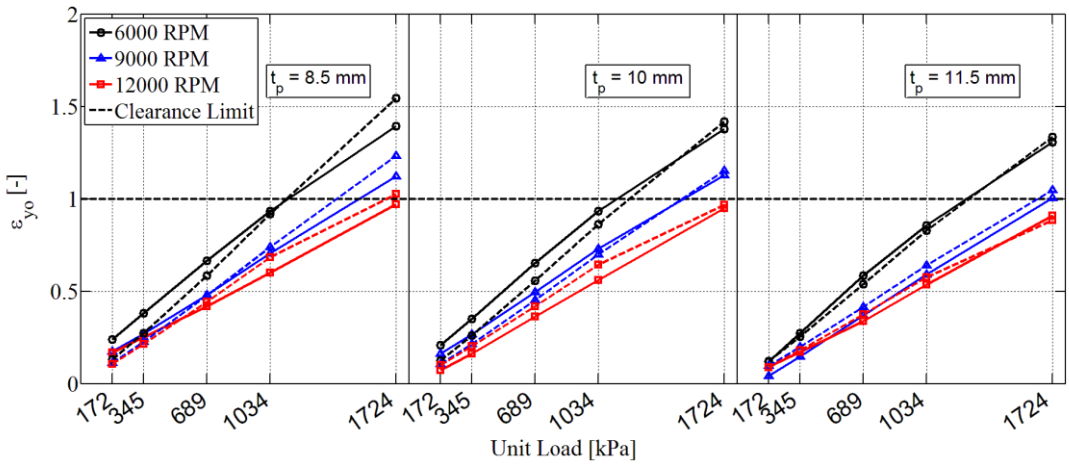

Figure 24. Measured (solid) and predicted (dashed) eccentricity in the loaded directions (y-axis) versus unit load for three pad thicknesses.

Increasing the pad thickness decreases the eccentricity ratio. At low speeds, the predicted values are lower than the measured values across all pad configurations. In general, the predictions are higher than the measured values at higher speeds and higher loads.

Figure 25 shows the measured and predicted attitude angle for three speeds and unit loads for the three pad configurations. For t_p = 8.5 mm and t_p = 10 mm at low rotational speeds, the attitude angles remain fairly consistent as unit load increases. At 12,000 rpm, the attitude angle decreases as unit load increases. For t_p = 11.5 mm, increasing the unit load decreases the attitude angles for all rotational speeds. In general, the attitude angle decreases as rotational speed increases for t_p = 8.5 mm and t_p = 11.5 mm. This trend is opposite for t_p = 10 mm.

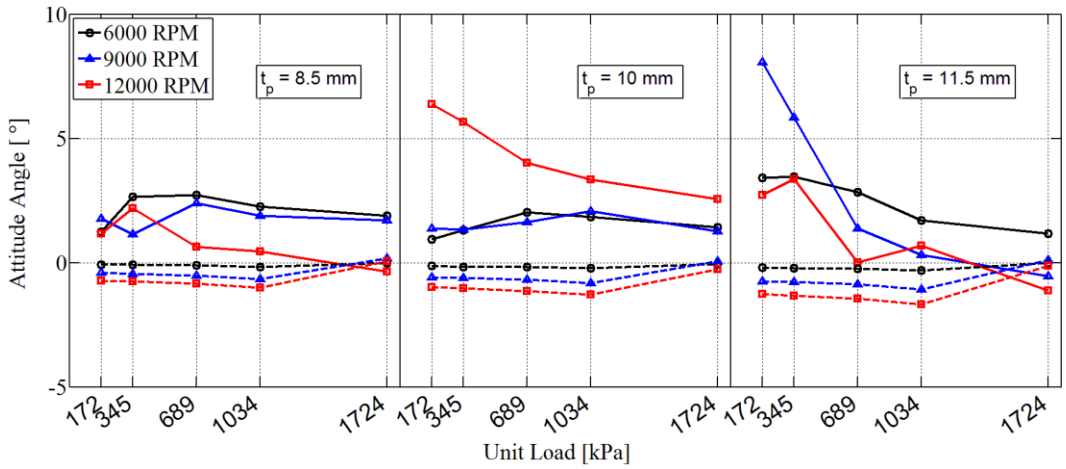

Figure 25. Measured (solid) and predicted (dashed) attitude angle for the three pad configurations.

Pad configurations t_p = 8.5 mm and t_p = 11.5 show negative attitude angles for the highest rotational speed and unit load. XL_TPJB© predicts attitude angles that have a smaller magnitude than the measured results for all rotational speed and unit load conditions and are consistently negative. The predicted attitude angles are fairly consistent across unit loads, and the magnitude of the predicted attitude angles decrease as rotational speed increases.

Pad Metal Temperatures

Figure 14 shows the pad thermocouples' location in and on the loaded pads. There are two thermocouples for each pad, one embedded (T_1 or T_3) in the pad and one exposed (T_2 or T_4) in the oil bath behind the pad.

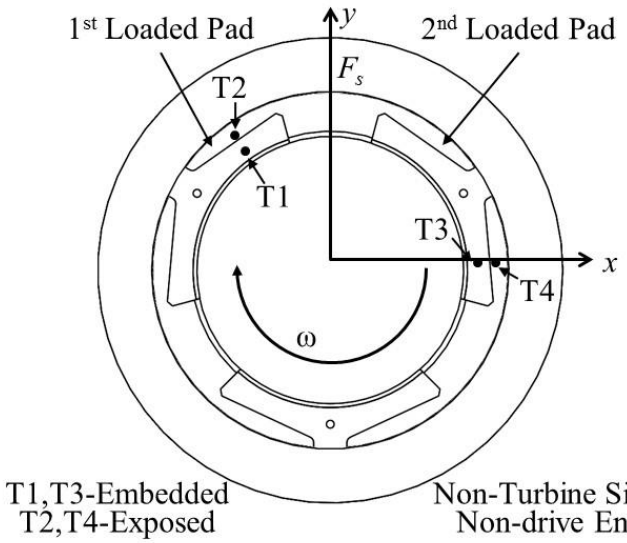

Figure 14. Arrangement of thermocouples on the loaded pads as viewed from the NDE.

Figure 26 and Figure 27 show the measured and predicted pad metal temperatures at the test conditions for the first loaded pad and the second loaded pad, respectively.

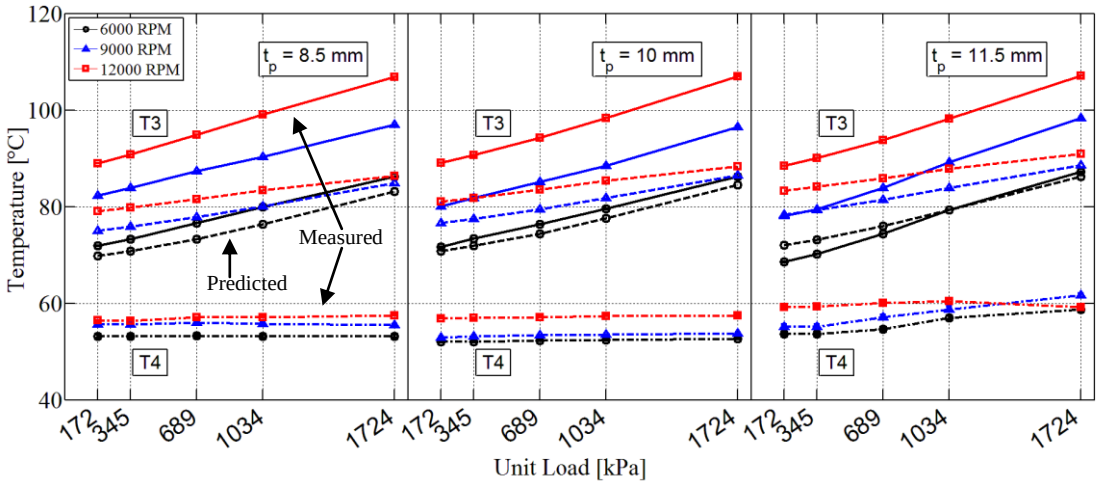

Figure 26. Measured (solid) and predicted (dashed) pad metal temperatures for the embedded thermocouple (T_1) and measured (dash-dot) exposed thermocouple (T_2) for the first loaded pad for the three pad configurations.

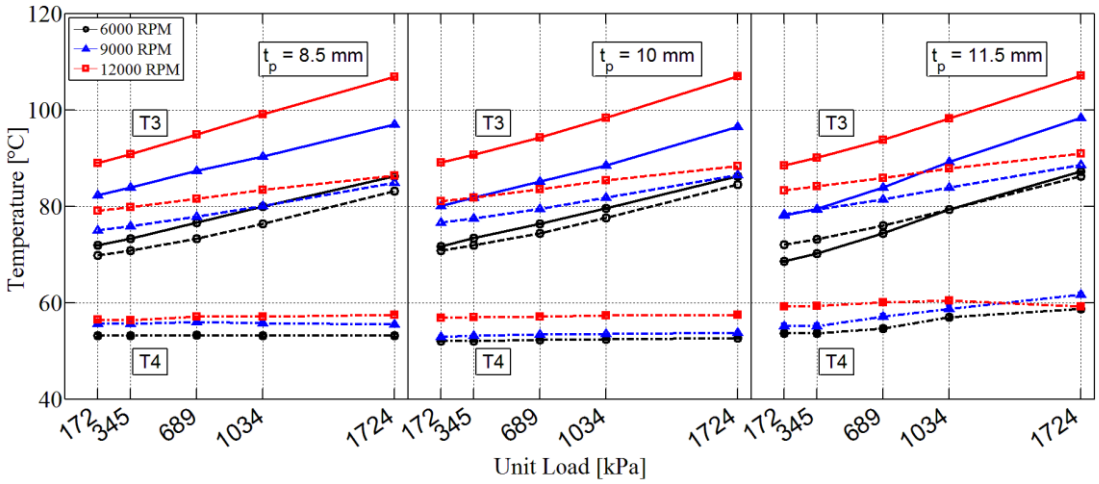

Figure 27. Measured (solid) and predicted (dashed) pad metal temperatures for the embedded thermocouple (T_3) and measured (dash-dot) exposed thermocouple (T_4) for the second loaded pad for the three for the pad configurations.

Both figures show the embedded thermocouples (T_1 or T_3) increase as the unit load increases and increase as rotational speed increases. As the temperature in the bearing increases, the bearing and pads expand. This expansion in the bearing will act to decrease the operating clearance. Therefore, the decrease in operating clearance increases as rotational speed increases. The thermocouples exposed in the oil bath (T_2 or T_4) remain constant as unit load increases but increase slightly as rotational speed increases. The measured temperature values do not vary greatly across pad configurations.

For both loaded pads, the predictions agree well with the measured values at 6,000 rpm. The predicted values are consistently lower than the measured values for 9,000 rpm and 12,000 rpm. As unit load increases, the difference between the measured values and the predicated values increases.

The measured static load characteristics, such as bearing position and pad metal temperatures at the test conditions, can be found in APPENDIX A: MEASURED STATIC LOAD CONDITIONS.

DYNAMIC LOAD CHARACTERISTICS

Dynamic-Stiffness

The following section presents the measured dynamic-stiffness functions for t_p = 8.5 mm at two test conditions. These test conditions include a low rotor speed (6,000 rpm) with a low unit load (172 kPa) and a high rotor speed (12,000 rpm) with a high unit load (1,724 kPa). Erratic data at high frequencies were omitted from the curve fits to obtain the best curve fit to the dynamic-stiffness data. The rotordynamic coefficients were obtained by curve fitting the dynamic-stiffness data up to 200 Hz.

The baseline results, shown in Figure 17 and Figure 18, have already been subtracted from the dynamic-stiffness. Therefore, the dynamic-stiffness presented represents the fluid-film's dynamic response. APPENDIX D: DYNAMIC-STIFFNESS COEFFICIENTS presents the dynamic-stiffness data and uncertainty values used to calculate the rotordynamic coefficients. The rotordynamic coefficients and uncertainty values can be found in APPENDIX C: ROTORDYNAMIC COEFFICIENTS**.**

For brevity, the results for the remaining pad configurations (t_p = 10 mm and t_p = 11.5 mm) can be found in APPENDIX D: DYNAMIC-STIFFNESS COEFFICIENTS**.**

Figure 28 shows the measured dynamic-stiffness functions with uncertainty bars for t_p = 8.5 mm at ω = 6,000 rpm with a 172 kPa unit load. The black vertical line designated by ω in the figure represents the running speed. The direct and cross-coupled, real dynamic-stiffness functions are shown in Figure 28 (a) and Figure 28 (b), respectively. The direct and cross-coupled, imaginary dynamic-stiffness functions are shown in Figure 28 (c) and Figure 28 (d), respectively.

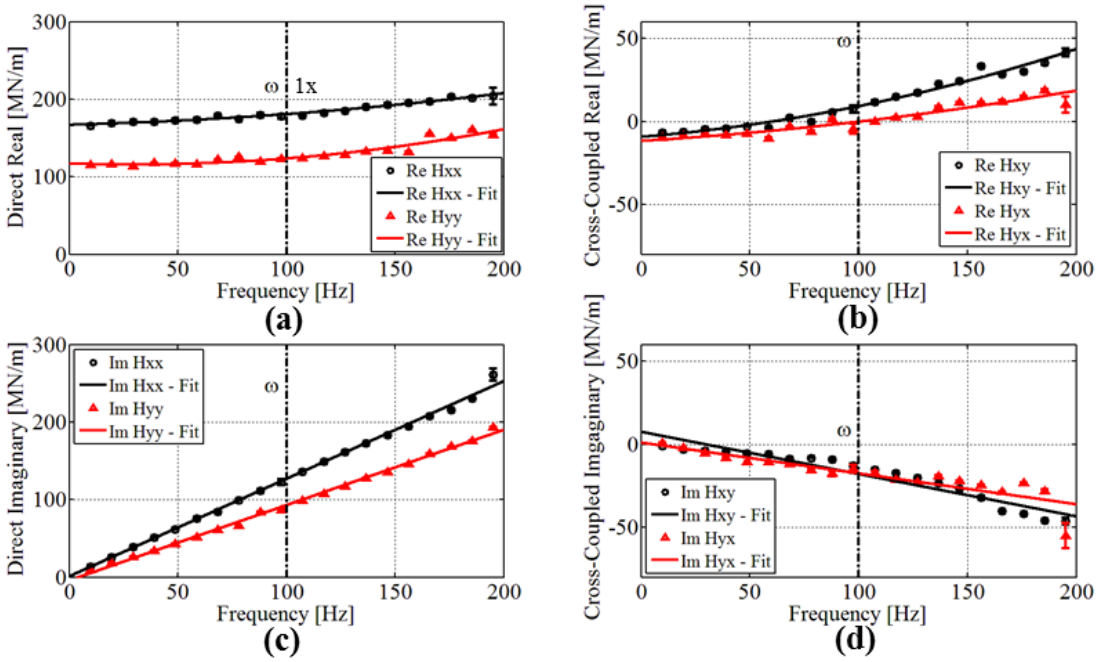

Figure 28. Measured dynamic-stiffness with uncertainty at 6 krpm (100 Hz, 32 m/s) and 172 kPa for t_p = 8.5 mm for (a) direct real, (b) cross-coupled real, (c) direct imaginary, and (d) cross-coupled imaginary.

The measured direct real dynamic-stiffness (Figure 28 (a)) and cross-coupled real dynamic-stiffness (Figure 28 (b)) show a slight increase in value as excitation frequency Ω increases indicating negative virtual-mass coefficients. Measured $\mathrm{Re}(\boldsymbol{H}_{xx})$ is larger than measured $\mathrm{Re}(\boldsymbol{H}_{yy})$. $\mathrm{Re}(\boldsymbol{H}_{xy})$ and $\mathrm{Re}(\boldsymbol{H}_{yx})$ have the same curvature, indicating there is no impact on stability for this test condition. The curve fits show that: (1) $K_{xx} > K_{yy}$, (2) K_{xx} and K_{yy} are positive, (3) $K_{yx} > K_{xy}$, (4) K_{yx} are K_{xy} are negative, (5) all virtual-mass coefficients are negative.

The measured direct imaginary dynamic-stiffness (Figure 28 (c)) and cross-coupled imaginary dynamic-stiffness (Figure 28 (d)) increase and decrease, respectively, linearly as Ω increases. The slope of measured $\mathrm{Im}(\boldsymbol{H}_{xx})$ is larger than the slope of measured $\mathrm{Im}(\boldsymbol{H}_{yy})$. The slope of measured $\mathrm{Im}(\boldsymbol{H}_{xy})$ is larger than the slope of measured

$\mathrm{Im}(\boldsymbol{H}_{yx})$ and both slopes are negative. The curve fits show that: (1) $C_{xx} > C_{yy}$, (2) C_{xx} and C_{yy} are positive, (3) $|C_{xy}| > C_{yx}$, and (4) C_{xy} and C_{yx} are negative.

Figure 29 shows the measured dynamic-stiffness functions with uncertainty bars for t_p = 8.5 mm at a ω = 12,000 rpm with a 1,724 kPa unit load. The black vertical line designated by ω in the figure represents the running speed. The direct and cross-coupled, real dynamic-stiffness functions are shown in Figure 29 (a) and Figure 29 (b), respectively. The direct and cross-coupled, imaginary dynamic-stiffness functions are shown in Figure 29 (c) and Figure 29 (d), respectively.

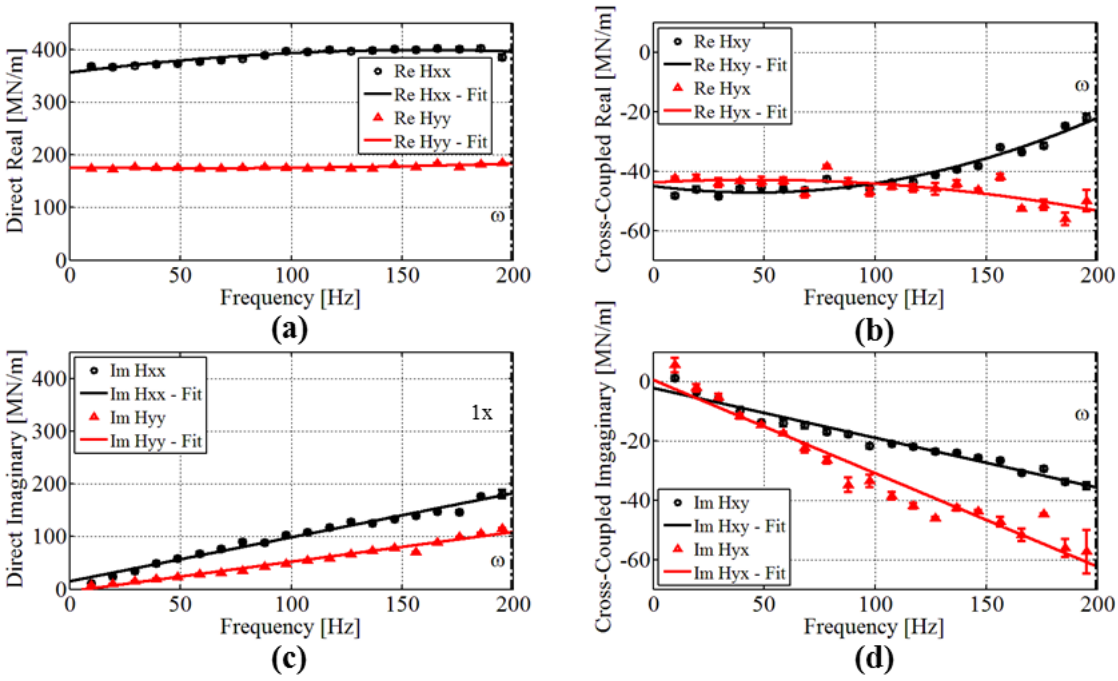

Figure 29. Measured dynamic-stiffness with uncertainty at 12 krpm (200 Hz, 64 m/s) and 1,724 kPa for t_p = 8.5 mm for (a) direct real, (b) cross-coupled real, (c) direct imaginary, and (d) cross-coupled imaginary.

Real $\mathbf{H_{xx}}$ and $\mathbf{H_{yy}}$ (Figure 29 (a)) show a slight increase in value as Ω increases and $\mathrm{Re}(\boldsymbol{H}_{xx}) > \mathrm{Re}(\boldsymbol{H}_{yy})$. When comparing Figure 28 (a) and Figure 29 (a), increasing the

unit load from 172 kPa to 1,724 kPa and the operating speed from 6,000 rpm to 12,000 rpm increases the difference between the measured $\mathrm{Re}(\boldsymbol{H}_{xx})$ and measured $\mathrm{Re}(\boldsymbol{H}_{yy})$. Real $\mathbf{H_{xy}}$ and $\mathbf{H_{yx}}$ (Figure 29 (b)) show a slight decrease in $\mathrm{Re}(\boldsymbol{H}_{yx})$ as the excitation frequency increases, and an increase in $\mathrm{Re}(\boldsymbol{H}_{xy})$, especially after 100 Hz, as Ω increases. $\mathrm{Re}(\boldsymbol{H}_{yx})$ and $\mathrm{Re}(\boldsymbol{H}_{xy})$ have opposite curvatures at larger excitation frequencies, indicating M_{xy} and M_{yx} have opposite signs. A difference in sign of cross-coupled virtual-mass suggests there is a possible impact on stability. The curve fits also show that: (1) $K_{xx} > K_{yy}$, (2) K_{xx} and K_{yy} are positive, (3) $K_{yx} > K_{xy}$, (4) K_{yx} are K_{xy} are negative, (5) M_{xx}, M_{yy}, and M_{xy} are negative, and (6) M_{yx} is positive.

Imaginary $\mathbf{H_{xx}}$ and $\mathbf{H_{yy}}$ (Figure 29 (c)) and imaginary $\mathbf{H_{xy}}$ and $\mathbf{H_{yx}}$ (Figure 29 (d)) increase and decrease, respectively, linearly as Ω increases. The slope of measured $\mathrm{Im}(\boldsymbol{H}_{xx})$ is larger than the slope of measured $\mathrm{Im}(\boldsymbol{H}_{yy})$. The slope of measured $\mathrm{Im}(\boldsymbol{H}_{xy})$ is larger than the slope of measured $\mathrm{Im}(\boldsymbol{H}_{yx})$ and both slopes are negative. The curve fits show that: (1) $C_{xx} > C_{yy}$, (2) C_{xx} and C_{yy} are positive, (3) $|C_{xy}| > C_{yx}$, and (4) C_{xy} and C_{yx} are negative.

Measured and Predicted Rotordynamic Coefficients

For brevity, only the direct rotordynamic coefficients are shown in this section. The cross-coupled rotordynamic coefficients with the predictions can be seen in APPENDIX C: ROTORDYNAMIC COEFFICIENTS. The solid lines are the measured data while the dashed lines are the predictions.

APPENDIX C: ROTORDYNAMIC COEFFICIENTS lists the coefficient of determination (R^2) for each test condition. Rotordynamic coefficients with poor coefficient of determination values (< 0.7) were omitted from the following rotordynamic coefficient graphs and excluded from the pad flexibility analysis. Additionally, if the majority of one rotational speed has poor coefficient of determination values, the entire speed was omitted from the rotordynamic graphs. For

example, the majority of the coefficient of determinations for Re ($\mathbf{H_{yx}}$) are less than 0.7, and therefore, M_{yx} will be excluded from the pad flexibility analysis.

Stiffness Coefficients

Figure 30 and Figure 31 show the measured values and predictions using XL_TPJB© for the direct stiffness coefficients. Figure 30 shows the results for K_{xx} for the three pad configurations.

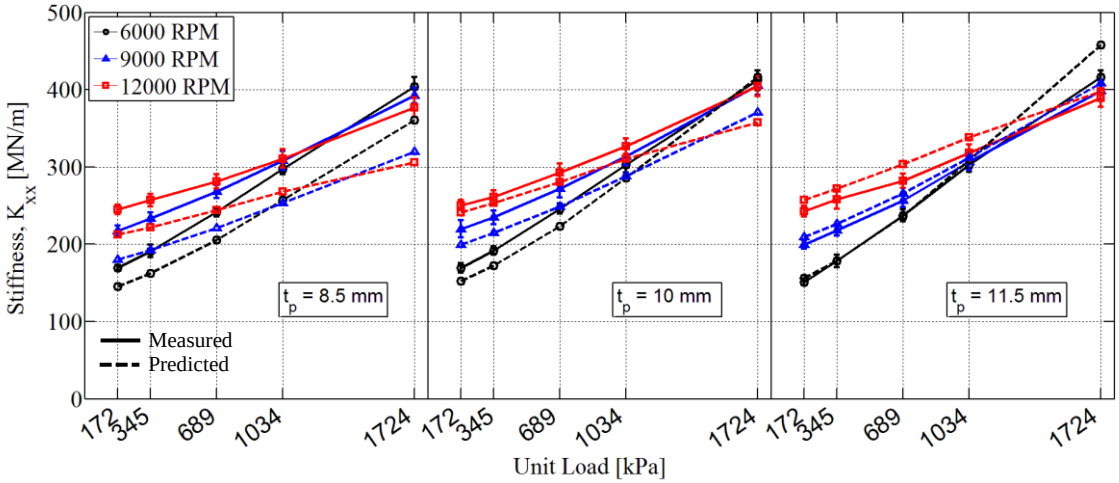

Figure 30. Measured (solid) and predicted (dashed) direct stiffness coefficient, K_{xx}, with uncertainties for three shaft speeds and increasing unit load for the different pad configurations.

Increasing the unit load increases K_{xx} for all pad configurations. At low unit loads, increasing the rotational speed increases K_{xx}. At 1,724 kPa, increasing the rotational speed decreases K_{xx}. For t_p = 8.5 mm and t_p = 10 mm, the measured values are higher than the predicted values. For these pad configurations, XL_TPJB© has a harder time predicting the performance at higher loads. For t_p = 11.5 mm, the predictions are slightly higher than the measured values but show excellent agreement with the measured values at 6,000 rpm.

Figure 31 shows the measured results and predictions for K_{yy} for the three pad configurations versus unit load.

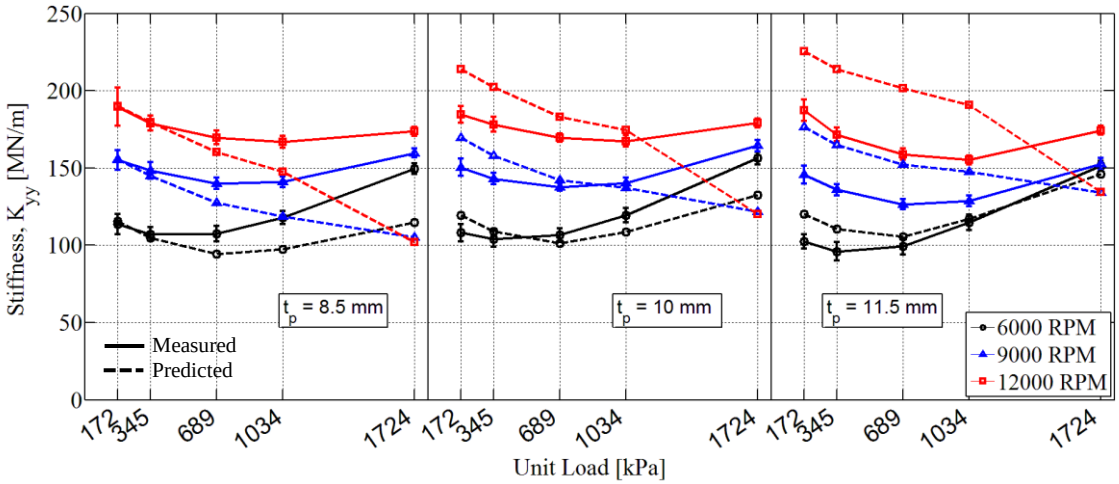

Figure 31. Measured (solid) and predicted (dashed) direct stiffness coefficient, K_{yy}, with uncertainties for three shaft speeds and increasing unit load for the different pad configurations.

Increasing the operating speed increases K_{yy} for all pad configurations. K_{yy} initially decreases as unit load increases but increases at higher unit loads. For t_p = 8.5 mm, the predictions show good agreement with the measured results at low unit loads. The measured values are higher than the predicted values at higher unit loads. For t_p = 10 mm and t_p = 11.5 mm, the predictions are higher than the measured values at low unit loads, and the predictions are lower than the measured values at higher loads.

Table 8 list the correlation between the measured results and the predictions from XL_TPJB© for the direct stiffness coefficient. The correlation is found by dividing the predicted values from XL_TPJB© by the measured results. The correlations range from 0.6 to 1.3 for the direct stiffness coefficients while the average is approximately 1.

Table 8. Correlation between predictions and measured results for the direct stiffness coefficients: Predicted Value/Measured Value.

Speed [RPM]	Unit Load [kPa]	t_p = 8.5 mm K_{xx} [MN/m]	t_p = 8.5 mm K_{yy} [MN/m]	t_p = 10 mm K_{xx} [MN/m]	t_p = 10 mm K_{yy} [MN/m]	t_p = 11.5 mm K_{xx} [MN/m]	t_p = 11.5 mm K_{yy} [MN/m]
6000	172	0.9	1.0	0.9	1.1	1.0	1.2
	345	0.9	1.0	0.9	1.0	1.0	1.2
	689	0.9	0.9	0.9	1.0	1.0	1.1
	1034	0.9	0.8	0.9	0.9	1.0	1.0
	1724	0.9	0.8	1.0	0.8	1.1	1.0
9000	172	0.8	1.0	0.9	1.1	1.1	1.2
	345	0.8	1.0	0.9	1.1	1.0	1.2
	689	0.8	0.9	0.9	1.0	1.0	1.2
	1034	0.8	0.8	0.9	1.0	1.0	1.1
	1724	0.8	0.7	0.9	0.7	1.0	0.9
12000	172	0.9	1.0	1.0	1.2	1.1	1.2
	345	0.9	1.0	1.0	1.1	1.1	1.2
	689	0.9	0.9	1.0	1.1	1.1	1.3
	1034	0.9	0.9	1.0	1.0	1.1	1.2
	1724	0.8	0.6	0.9	0.7	1.0	0.8

Note: The direct stiffness in the non-loaded direction (K_{xx}) is greater than the stiffness in the loaded direction (K_{yy}), and there is stiffness orthotropy even though the bearing is assembled in the LBP orientation. This outcome could be attributed to the three-pad bearing design. Predictions show the minimum film thickness occurs closer to the non-loaded direction instead of the loaded direction which could cause $K_{xx} > K_{yy}$. As mentioned in the introduction, the LBP orientation offers more symmetric ($K_{xx} = K_{yy}$) rotordynamic coefficients, while the LOP orientation provides stiffness orthotropy ($K_{xx} \neq K_{yy}$) causing the bearing to be stiffer in the loaded direction than in the non-loaded direction. At low unit loads, the measured direct stiffness coefficients are more symmetric but, as the unit load increases, K_{xx}'s magnitude (non-loaded direction) almost doubles while K_{yy}'s magnitude (loaded direction) remains fairly consistent.

Damping Coefficients

Figure 32 and Figure 33 show the measured values and predictions using XL_TPJB© for the direct damping coefficients. Figure 32 shows the results for C_{xx} for the three pad configurations.

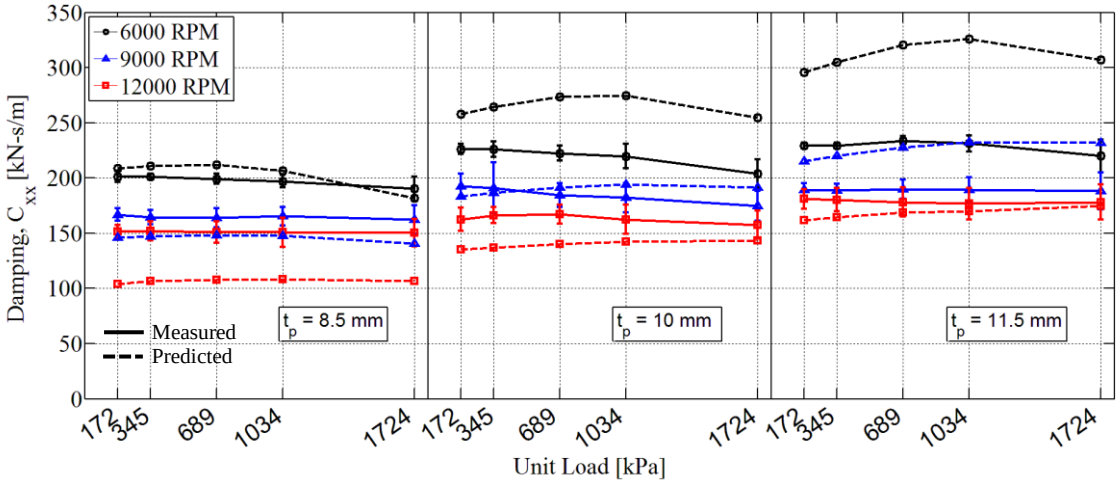

Figure 32. Measured (solid) and predicted (dashed) direct damping coefficient, C_{xx}, with uncertainties for three shaft speeds and increasing unit load for the different pad configurations.

Increasing the operating speed decreases C_{xx}. C_{xx} remains relatively constant as the unit load increases. At 12,000 rpm, the measured values are higher than the predicted values. For t_p = 8.5 mm, the predictions are lower than the measured values at 9,000 rpm and are, in general, higher than the measured values at 6,000 rpm. For t_p = 10 mm and t_p = 11.5 mm, the predictions are generally higher than the measured values.

Figure 33 shows the measured results and predictions for C_{yy} for the three pad configurations versus unit load.

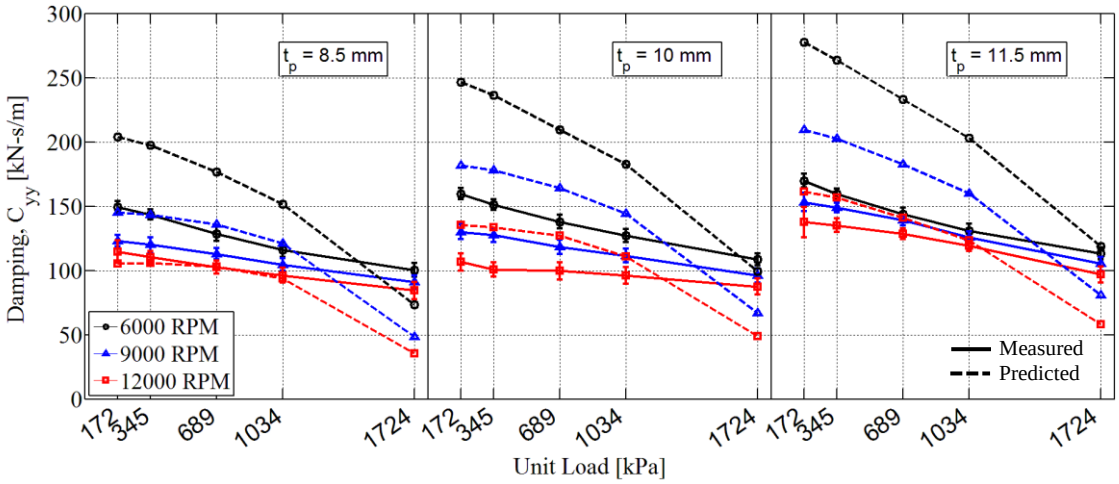

Figure 33. Measured (solid) and predicted (dashed) direct damping coefficient, C_{yy}, with uncertainties for three shaft speeds and increasing unit load for the different pad configurations.

Increasing the unit load decreases C_{yy} for all pad configurations. Increasing the operating speed decreases C_{yy}. The predictions show good agreement with the measured values for t_p = 8.5 mm at low unit loads and an operating speed of 12,000 rpm. At low unit loads, the predictions are higher than the measured results for all pad configurations. At 1,724 kPa, the measured values are higher than the predicted values.

Table 9 list the correlation between the measured results and the predictions from XL_TPJB©. The correlations range from 0.4 to 1.7 for the direct damping coefficients.

Table 9. Correlation between predictions and measured results for the direct damping coefficients: Predicted Value/Measured Value.

Speed [RPM]	Unit Load [kPa]	t_p = 8.5 mm C_{xx} [kN-s/m]	t_p = 8.5 mm C_{yy} [kN-s/m]	t_p = 10 mm C_{xx} [kN-s/m]	t_p = 10 mm C_{yy} [kN-s/m]	t_p = 11.5 mm C_{xx} [kN-s/m]	t_p = 11.5 mm C_{yy} [kN-s/m]
6000	172	1.0	1.4	1.1	1.5	1.3	1.6
	345	1.0	1.4	1.2	1.6	1.3	1.7
	689	1.1	1.4	1.2	1.5	1.4	1.6
	1034	1.0	1.3	1.3	1.4	1.4	1.6
	1724	1.0	0.7	1.2	0.9	1.4	1.1
9000	172	0.9	1.2	1.0	1.4	1.1	1.4
	345	0.9	1.2	1.0	1.4	1.2	1.4
	689	0.9	1.2	1.0	1.4	1.2	1.3
	1034	0.9	1.2	1.1	1.3	1.2	1.3
	1724	0.9	0.5	1.1	0.7	1.2	0.8
12000	172	0.7	0.9	0.8	1.3	0.9	1.2
	345	0.7	1.0	0.8	1.3	0.9	1.2
	689	0.7	1.0	0.8	1.3	0.9	1.1
	1034	0.7	1.0	0.9	1.2	1.0	1.0
	1724	0.7	0.4	0.9	0.6	1.0	0.6

Virtual-Mass Coefficients

Figure 34 and Figure 35 show the measured values and predictions using XL_TPJB© for M_{xx} and M_{yy}, respectively with the exclusions from the poor coefficient of determination values.

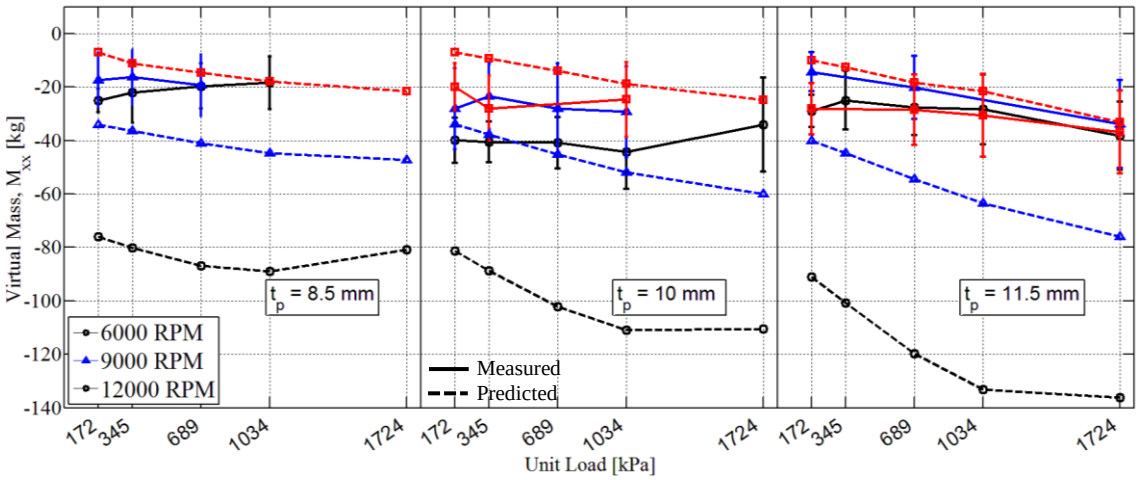

Figure 34. Measured (solid) and predicted (dashed) direct virtual-mass coefficients, M_{xx}, with uncertainties for three shaft speeds and increasing unit load for the different pad configurations.

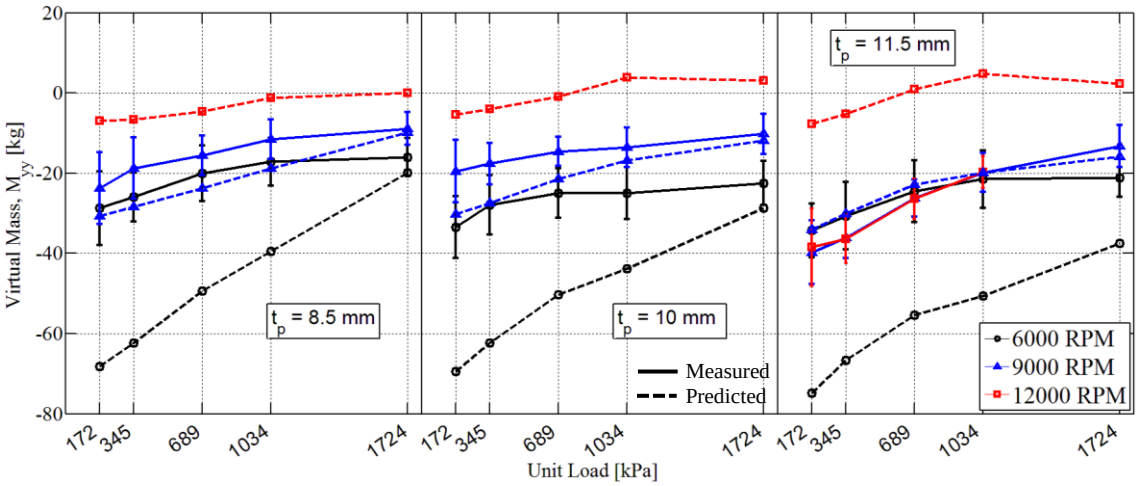

Figure 35. Measured (solid) and predicted (dashed) direct virtual-mass coefficient, M_{yy}, with uncertainties for three shaft speeds and increasing unit load for the different pad configurations.

At low operating speeds, the predicted direct virtual-mass coefficients have a larger magnitude than the measured coefficients and have a smaller magnitude than the measured results at higher operating speeds. The predicted M_{xx} show good agreement

with the measured values for t_p = 8.5 mm at 12,000 rpm. The predicted M_{yy} show good agreement with the measured values for t_p = 11.5 mm at 9,000 rpm.

Note, from the author's experience using XL_TPJB©, the predictions are sensitive to the input parameters used during the prediction analysis. The bearing and lubricant should be modeled as accurately as possible to predict the static and dynamic load characteristics that correlate to the measured results. For example, varying the viscosity at the supply temperature had a large effect on the static load characteristics. XL_TPJB© can be useful when determining how the performance of the bearing will change when varying the input parameters.

Whirl Frequency Ratio

The whirl frequency ratio (WFR) defines the stability characteristic of bearings and seals. The WFR is the ratio between the natural frequency and the onset speed of instability (OSI). If a bearing has zero cross-coupled stiffness, like most TPJBs, the WFR is zero and the bearing has an infinite onset speed of instability. Recall that plain journal bearings have cross-coupled stiffness coefficients. They have a WFR of 0.5 and will go unstable around twice the critical speed. The formulas used to calculate the bearing's WFR tested in this work are from San Andrés [36] and can be found in APPENDIX E:WFR CALCULATION. The WFR is zero for all test conditions and pad configurations, signifying no impact on stability. The bearing, by itself, will not be a cause of a rotor instability.

Pad Flexibility Analysis

Wilkes [26] applied an averaged fluid-film moment at the pad's leading and trailing edge due to the fluid-film pressure. The ratio of applied fluid-film moment to the change in pad radius due to the applied moment is the pad's structural bending stiffness $\bar{k}_p$. This approach could be easily adapted to structural models since the bending moment is applied at the pad's edges as shown in Figure 5.

An FEM of each pad configuration is developed in SolidWorks® to predict the structural bending stiffness of each pad configuration. Each pad model includes a 1.5 mm thick Babbitt layer. Once the pad's pivot is fixed, a uniform pressure distribution of

689 kPa (100 psi) is applied to the pad's rotor-side surface such that the resultant force created by the pressure distribution passes through the pad's pivot. The average applied moment due to the uniform pressure distribution is calculated, and the change in pad radius due to the applied loading is recorded. Figure 36 shows the FEA for t_p = 11.5 mm with a uniform pressure distribution applied to the rotor-side surface of the pad.

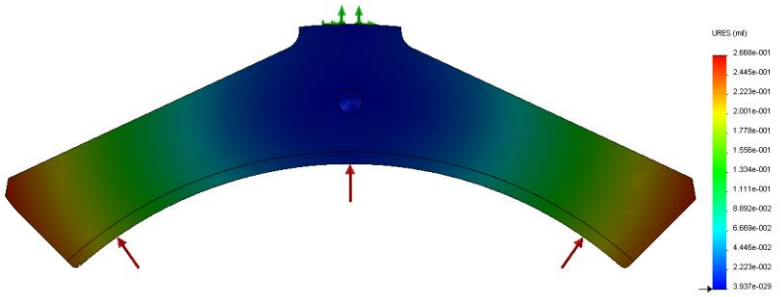

Figure 36. FEA static deflection analysis for t_p = 11.5 mm with a uniform pressure distribution of 689 kPa (100 psi).

Branagan and Barrett compared several analytic bending stiffness formulas, and concluded that the bending stiffness formula by Deutschman et al. in Eq. (8) was the most accurate when predicting the change in pad curvature. Predictions from the FEA are given in Table 10 and are used in the balance of this work. Deutschman et al.'s model agrees reasonably well with the FEA.

Table 10. Bending stiffness (k_p) and pad flexibility ($1/k_p$) for each pad configuration calculated from the FEA analysis.

Pad Thickness	k_p [MN]	$1/k_p$ [1/MN]
t_p = 8.5 mm	2.57	0.39
t_p = 10 mm	3.62	0.28
t_p = 11.5 mm	4.94	0.20

The rotordynamic coefficients are plotted versus pad flexibility values calculated from the FEA analysis to demonstrate the impact of pad flexibility.

Stiffness Coefficients

Figure 37 shows the measured direct stiffness coefficients, K_{yy} (solid black line) and K_{xx} (dashed red line) for the nominal speed and unit load conditions versus pad flexibility.

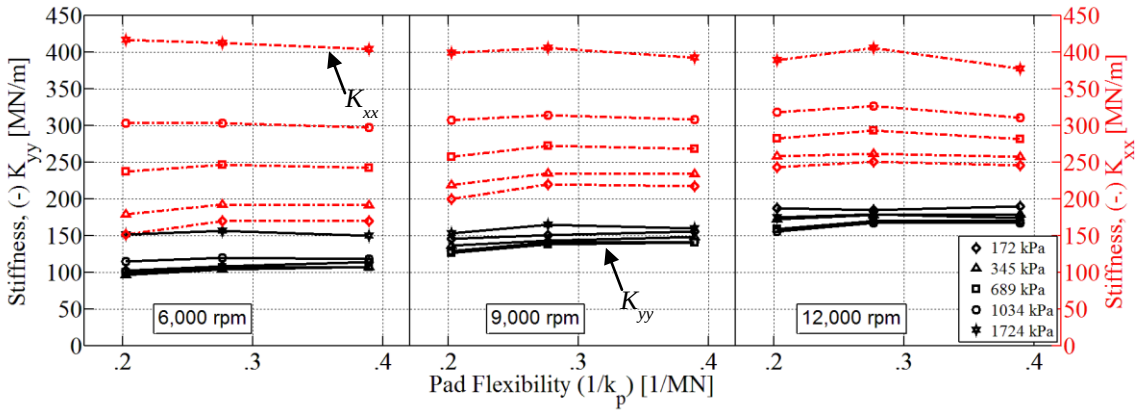

Figure 37. Measured K_{xx} (dashed red) and K_{yy} (solid black) versus pad flexibility for three speeds and unit loads.

At first glance, it appears that K_{xx} and K_{yy} remain relatively constant as pad flexibility increases. The average change in direct stiffness coefficients as pad flexibility increases is an increase of 2% for K_{xx} and increase of 6% for K_{yy}. The direct stiffness coefficients depend on unit load. At lower unit loads, K_{xx} and K_{yy} increase up to 12% as pad flexibility increases. As the unit load increases, they decrease up to 3% as pad flexibility increases. The percent change in direct stiffness coefficients at low unit loads decreases as the speed increases. Table 11 shows an example of the load dependence for the direct stiffness coefficients at 6,000 rpm.

Table 11. Measured percent change in K_{xx} and K_{yy} from the nominally rigid pad to the most flexible pad.

Speed [RPM]	Unit Load [kPa]	K_{xx} [MN/m]	K_{yy} [MN/m]
6,000	172	12%	11%
	345	7%	12%
	689	2%	8%
	1034	-2%	3%
	1,724	-3%	-1%

Figure 38 shows the measured cross-coupled stiffness coefficients, K_{yx} (solid black line) and K_{xx} (dashed red line) for the nominal speed and unit load conditions versus pad flexibility.

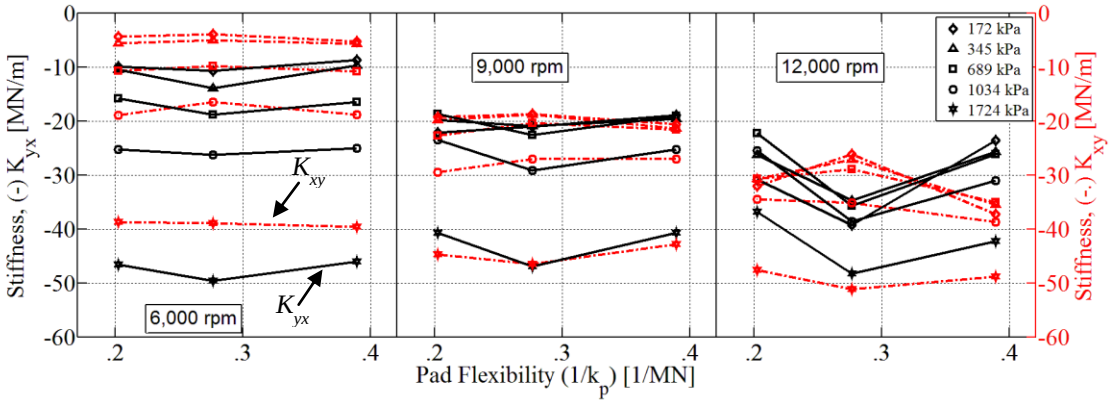

Figure 38. Measured K_{xy} (dashed red) and K_{yx} (solid black) versus pad flexibility for three speeds and unit loads.

Again, it appears that K_{xy} and K_{yx} remain relatively constant as pad flexibility increases, except at 12,000 rpm. The average change in cross-coupled stiffness coefficients as pad flexibility increases is an increase of 5% for K_{xy} and a 0% change for K_{yx}. The cross-coupled coefficients show similar load dependence as the direct stiffness

coefficients, however, they have opposite trends as the unit load increases. At low unit loads, K_{xy} increases up to 18% as pad flexibility increases, and at high unit loads, K_{xy} decreases up to 8% as pad flexibility increases. K_{yx} decreases up to 23% as pad flexibility increases at low unit loads and increases up to 22% as pad flexibility increases at higher unit loads.

The majority of predictions in literature show a decrease in direct stiffness coefficients as pad flexibility increases for high eccentricity ratios or high unit loads and no change at low eccentricity ratios or low unit loads. However, those researchers did not predict results at unit loads as low as the ones tested for this work. Burgier and Pascal predicted similar load dependence for the direct stiffness coefficients. Their predictions show the direct stiffness coefficients increased at low loads and decreased at high loads when pad flexibility was included in the model. The present measured results show that the change in stiffness coefficients as pad flexibility increases depends on the unit load and operating speed.

Damping Coefficients

Figure 39 shows the measured direct damping coefficients, C_{yy} (solid black line) and C_{xx} (dashed red line) for the nominal speed and unit load conditions versus pad flexibility.

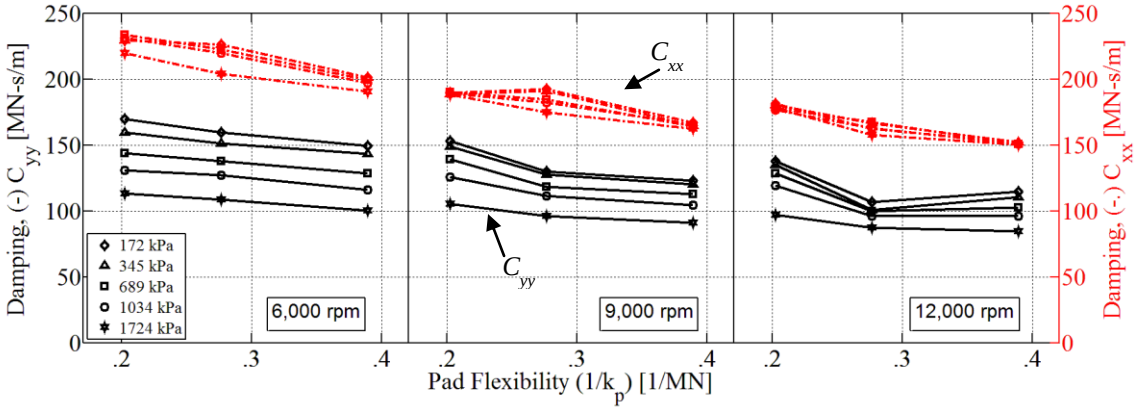

Figure 39. Measured C_{xx} (dashed red) and C_{yy} (solid black) versus pad flexibility for three speeds and unit loads.

The direct damping coefficients decrease as pad flexibility increases. As pad flexibility increases, the average change in the direct damping coefficients is a decrease of 14% for C_{xx} and a decrease of 15% for C_{yy}. The direct damping coefficients show a slight dependence on operating speed. Increasing the operating speed increases the difference in direct damping coefficients from 12% to 16%. They remain relatively constant as unit load increases. Table 12 list the percent change in direct damping coefficients from t_p = 11.5 mm (nominally rigid pad) pad set to t_p = 8.5 mm (flexible pad) pad set.

Table 12. Measured average percent change in C_{xx} and C_{yy} from the nominally rigid pad to the most flexible pad.

Speed [RPM]	C_{xx} [kN-s/m]	C_{yy} [kN-s/m]
6,000	-13%	-11%
9,000	-13%	-18%
12,000	-16%	-17%
Average	-14%	-15%
	-15%	

Figure 40 shows the measured cross-coupled damping coefficients, C_{yx} (solid black line) and C_{xy} (dashed red line) for the nominal speed and unit load conditions versus pad flexibility.

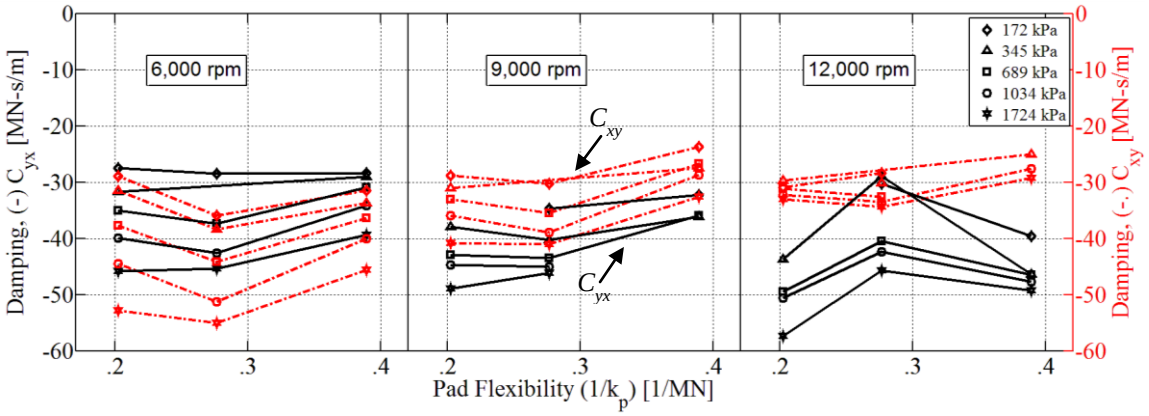

Figure 40. Measured C_{xy} (dashed red) and C_{yx} (solid black) versus pad flexibility for three speeds and unit loads.

The average change in cross-coupled-damping coefficients as pad flexibility increases is a decrease of 12% for C_{xy} and a decrease of 7% for C_{yx}. In general, C_{xy} decreases as pad flexibility increases. C_{yx} shows a dependence on unit load that is similar to the direct stiffness coefficients. C_{yx} increases up to 15% at low unit loads and decreases up to 19% at high unit loads as pad flexibility increases.

The general decrease in damping coefficients as pad flexibility increases agrees well with literature. Including pad flexibility can decrease the direct damping coefficients up to 20% and on average, decrease the cross-coupled coefficients by -10%

Virtual-Mass Coefficients

Figure 41 shows the measured direct virtual-mass coefficients, M_{yy} (solid black line) and M_{xx} (dashed red line) for the nominal speed and unit load conditions versus pad flexibility. Figure 42 shows the measured cross-coupled virtual-mass coefficients, M_{yx} (solid black line) and M_{xy} (dashed red line) for the nominal speed and unit load conditions versus pad flexibility.

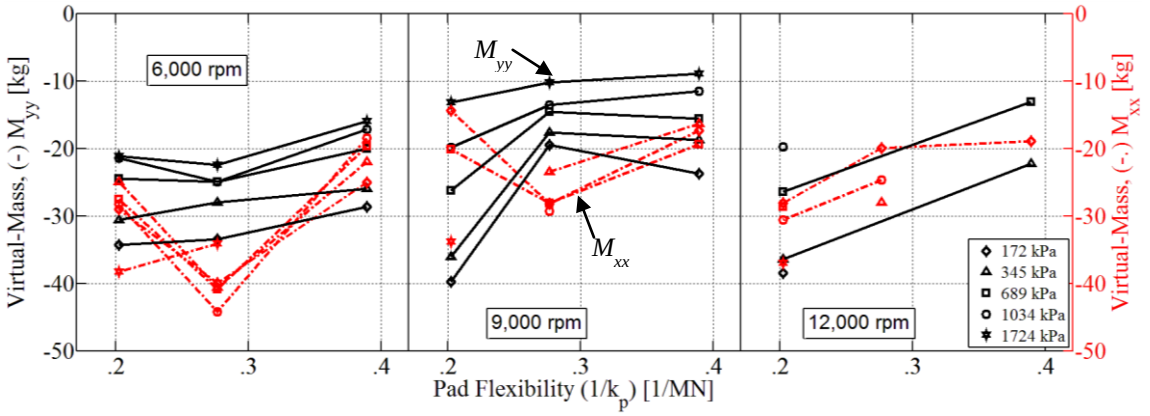

Figure 41. Measured M_{xx} (dashed red) and M_{yy} (solid black) versus pad flexibility for three speeds and unit loads.

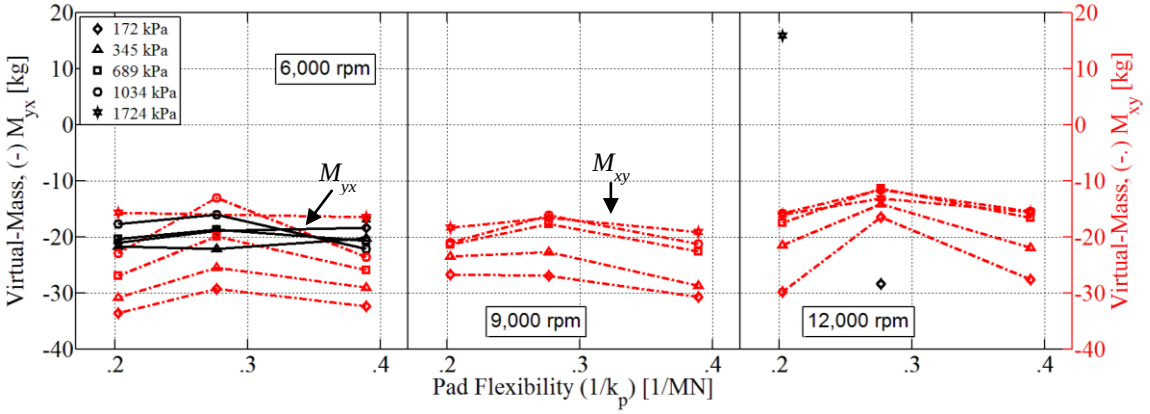

Figure 42. Measured M_{xy} (dashed red) and M_{yx} (solid black) versus pad flexibility for three speeds and unit loads.

The average change in direct virtual-mass coefficients as pad flexibility increases is a decrease of 24% for M_{xx} and a decrease of 33% for M_{yy}. M_{xx} shows a dependence on unit loads, increasing the unit load increases the difference in M_{xx} as pad flexibility increases. The average change in cross-coupled virtual-mass coefficients as pad flexibility increases is an increase of 2% for M_{xy}. Recall that the majority of M_{yx} is excluded from the pad flexibility analysis due to poor coefficient of determination (R^2)

values. In general, at 6,000 rpm, M_{yx} increases by 2% as pad flexibility increases, similar to $M_{xy.}$

Degree of Pad Flexibility

Rotordynamic coefficients were predicted for eight bearings with different properties to determine the influence of pad flexibility on the change in predicted rotordynamic coefficients. XL_TPJB© was used to predict the direct damping coefficients for these different bearings with perceptibly different pad flexibilities for a unit load of 783 kPa (114 psi) and a circumferential surface-speed of 54 m/s. Measured pivot stiffness and bearing parameters were input for each bearing. The pivot stiffness was not specifically defined in the Hagemann et al. so an approximation was used for XL_TPJB©. Table 13 lists the bearing properties for each pad configuration and the respective static load and rotor speed.

Table 13. Bearing properties for each pad configuration

Pad	D [mm]	L [mm]	θ_{pad}	Pivot Offset	Speed [rpm]	F_s [kN]
t_p = 8.5 mm	101.6	60.96	90°	0.5	10,200	4.85
t_p = 10 mm	101.6	60.96	90°	0.5	10,200	4.85
Malcher [6]	119.9	59.9	75°	0.6	8,643	5.62
t_p = 11.5 mm	101.6	60.96	90°	0.5	10,200	4.85
Wilkes [26]	101.6	55.9	58.9°	0.5	10,200	4.45
Hagemann et al.* [27]	500	350	56°	0.6	2,073	137.03
Tschoepe [37]	101.6	60.3	72°	0.57	10,200	4.80
Kulhanek [32]	101.6	60.3	57.87°	0.5	10,200	4.80

*Approximate pivot stiffness

The code outputs the rotordynamic coefficients and the deflection along the surface of the pad. The code was used to predict the rotordynamic coefficients for: (1) rigid pad, flexible pivot, and (2) flexible pad, flexible pivot. Since the direct damping coefficients vary the most when including pad and pivot flexibility, the percent change in direct damping coefficients was defined by

$$\Delta C = \frac{C_{rigid} - C_{flexibile}}{C_{rigid}}. \tag{32}$$

The deflection δ_p at the leading and trailing edge was recorded and the pad arc length L_{arc} was calculated for each pad configuration. Figure 43 shows a schematic of the pad's deflection due to an applied moment at the pad's leading and trailing edge.

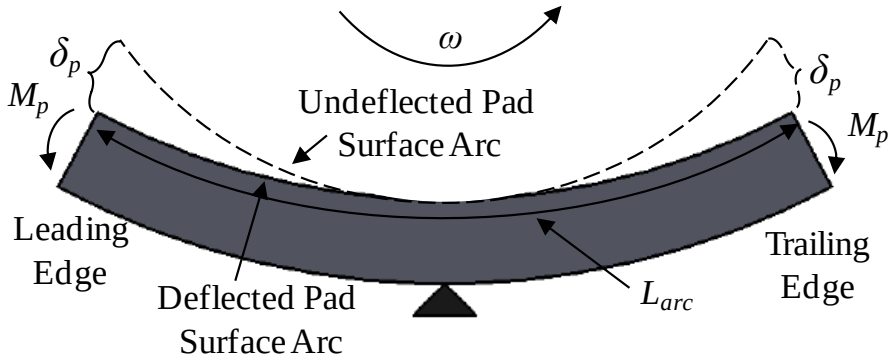

Figure 43. Schematic of pad flexibility and parameters

Using the average deflection from the leading to the trailing edge of the pad $\delta_{p,avg}$ and the pad arc length, the non-dimensional flexibility parameter was defined as

$$\alpha_{flex} = \frac{\delta_{p,avg}}{L_{arc}} \frac{[L]}{[L]}. \tag{33}$$

Table 14 list the results from the study performed on the eight different bearing with measurably different pad flexibilities.

Table 14. Percent change in predicted C_{xx} and C_{yy} for the eight bearings with measurably different pad flexibilities.

	Pad	$\%\Delta C_{xx}$ [-]	$\%\Delta C_{yy}$ [-]	$\delta_{p,avg}$ [μm]	L_{arc} [mm]	α_{flex}[-]
1	**t_p = 8.5 mm**	25%	12%	18	160	11.3 x 10^{-5}
2	**t_p = 10 mm**	20%	11%	13	80	7.94 x 10^{-5}
3	**t_p = 11.5 mm**	12%	9%	7	80	4.48 x 10^{-5}
4	**Malcher [6]**	12%	12%	5	94	3.28 x 10^{-5}
5	**Hagemann et al.* [27]**	8%	8%	16	293	3.19 x 10^{-5}
6	**Wilkes [26]**	9%	9%	3	52	3.12 x 10^{-5}
7	**Tschoepe [37]**	2%	2%	2	73	1.64 x 10^{-5}
8	**Kulhanek [32]**	1%	1%	1	51	1.46 x 10^{-5}

*Approximate pivot stiffness

Figure 44 shows the percent change in predicted direct damping coefficients as pad flexibility increases.

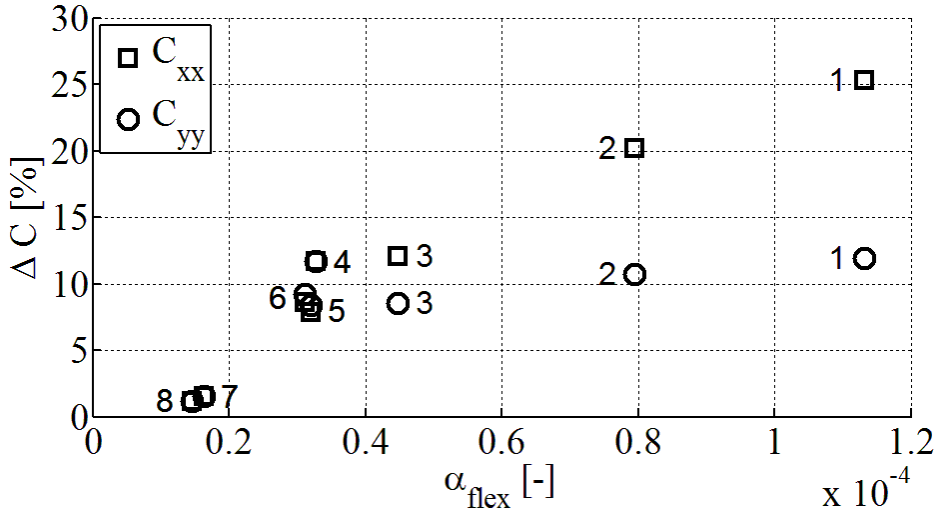

Figure 44. Percent change in predicted C_{xx} and C_{yy} versus the non-dimensional pad flexibility parameter, α_{flex}.

As the non-dimensional pad flexibility parameter α_{flex} increases, the percent change in predicted C_{xx} and C_{yy} also increases. The percent change in C_{xx} is slightly greater than

C_{yy} for low values of α_{flex} or more rigid pads. The difference between C_{xx} and C_{yy} increases as α_{flex} increases or as pad flexibility increases.

Clearly, the pads tested here are extremely flexible. For such pads, the percent change in predicted direct damping coefficients can be up to 25%. For nominally rigid pads, such as those tested by Tschoepe and Kulhanek, the percent change in C_{xx} and C_{yy} is virtually zero, confirming that pad flexibility can be neglected.

SUMMARY, DISCUSSION, AND CONCLUSIONS

The static and dynamic load characteristics were presented for a three-pad, rocker-pivot TPJB in the LBP orientation. Three interchangeable pad configurations were tested with pad thicknesses of 8.5 mm (0.33 in), 10 mm (0.39 in), and 11.5 mm (.45 in) to determine the effect of pad flexibility on the dynamic performance of a TPJB. Tests were performed on a floating-test-bearing rig about a rigid-rotor design with unit loads ranging from 69 to 1,724 kPa (10 to 250 psi) and speeds from 6 to 12 krpm. The measured results were compared to predictions from a computational code, XLTPJB, which includes the effects of pivot and pad flexibility.

Static Load Characteristics

Static performance characteristics for TPJBs normally include cold and hot bearing clearances, journal eccentricity, journal loci, attitude angles, and pad metal temperatures. The bearing clearance is measured by slowing precessing the stator-bearing assembly about the rigid non-rotating shaft. A cold clearance is taken at room temperature while a hot clearance is taken immediately after shut-down to simulate operating clearances. The static eccentricity ratio and attitude angle are used to describe the rotor's position at a given operating position. The pad metal temperatures show the pad's temperature during operation.

The maximum measured eccentricity ratio was over one for each pad configuration. As pad flexibility increased, the static eccentricity ratio decreased. The eccentricity ratio predictions agreed well with the measured results in the loaded direction. The measured attitude angles were as high as approximately 10°. The attitude angles remained fairly constant at low rotational speeds for t_p = 8.5 mm and t_p = 10 mm and decreased as unit load increased for t_p = 11.5 mm. XL_TPJB© predicted attitude angles that had a smaller magnitude than the measured results for all rotational speed and unit load conditions and were negative.

The pad metal temperatures did not vary greatly across pad configurations. The predictions agreed well with the measured values at low speeds and low unit loads. As

the operating speed and unit load increased, the predictions were lower than the measured values.

Dynamic Load Characteristics

Dynamic load tests were performed for all nominal test conditions over a range of excitation frequencies to obtain complex dynamic-stiffness coefficients as a function of excitation frequency. A [K][C][M] model produced frequency-independent rotordynamic coefficients, which are the fluid-film's stiffness, damping, and virtual-mass coefficients.

XL_TPJB© was used to predict the performance of the tilting-pad bearing tested in this work. The predictions using XL_TPJB© agreed well with the measured values for direct stiffness coefficients. For a given pad set, the predictions agreed well with the measured results for one operating-speed case and were either lower or higher than the measured results for the remaining speed cases for C_{xx}. The predicted values were generally higher than the measured values for C_{yy} at low unit loads and were lower than measured values at high unit loads. The measured values had a smaller magnitude than the predictions for the direct virtual-mass coefficients at lower speeds. At higher speeds, the predictions had a lower magnitude than the measured direct virtual-mass coefficients. All cross-coupled-coefficient predictions were nearly zero, and the measured values were typically non-zero and negative.

An FEM was created in SolidWorks® to obtain the structural bending stiffness of each pad configuration. The moment due to the applied loading was calculated as well as the deflection of the pad surface. Results from the FEA show an increase in pad flexibility as the pad's thickness decreased.

To examine the effect of pad flexibility on the rotordynamic coefficients, the measured results were compared across each pad configuration.

The measured results for the stiffness coefficients depended on unit load and rotor speed as pad flexibility increased. The direct stiffness coefficients and K_{xy} increased at low unit loads and decreased at high unit loads as pad flexibility increased. K_{yx} shows similar load dependence but with the opposite trend; K_{yx} decreased at low unit loads and

increased at high unit loads as pad flexibility increased. At low unit loads, the percent difference in direct stiffness coefficients decreased as the operational speed increased.

The majority of past predictions show a decrease in the stiffness coefficients once they include pad flexibility in their models. However, their predictions and test results were not done for unit loads as low as ones tested here. Burgier and Pascal [10] predicted a wider range of loads and show similar load dependence for the direct stiffness coefficients as measurements in this work. The present measured results show that the change in stiffness coefficients as pad flexibility increases depends on the unit load and operating speed.

Measured results for the damping coefficients show a general decrease in value as pad flexibility increased. The direct damping coefficients decreased by approximately 15%, and the cross-coupled damping coefficients decreased by 10% as pad flexibility increased. The general decrease in direct damping coefficients agree well with prior literature.

The measured direct virtual-mass coefficients' magnitude show a general decrease of 29% as pad flexibility increased. The measured results show an increase of 2% for M_{xy} and M_{yx} as pad flexibility increased. Note that changing the excitation frequency used for the curve fits will change the virtual-mass coefficients. Therefore, the change in virtual-mass coefficients as pad flexibility increases could vary if the cut-off excitation frequency is changed.

The WFR was used to determine the TPJB's stability tested in this thesis. Theory shows that rock-pivot TPJB have zero cross-coupled stiffness coefficients, and therefore TPJBs have a WFR of zero and an infinite onset speed of instability. The WFR for all test conditions and pad configurations was negative or zero, and the bearing by itself will have no impact on stability.

A non-dimensional pad flexibility parameter α_{flex} was used to relate the pad flexibility of multiple bearing of different sizes. The parameter related the average deflection across the pad surface to the pad's arc length. XL_TPJB© was used to predict the percent change in direct damping coefficients for a rigid pad, flexible pivot and

flexible pad, flexible pivot for a surface speed of 54 m/s and a unit load of 783 kPa. The results show the pads tested in this thesis are extremely flexible compared to pads used in industry. This non-dimensional parameter could be used to determine if pad flexibility will have an impact on the rotordynamic coefficients.

Measured results show pad flexibility does have an impact on the dynamic performance of TPJB. In general, there is a decrease in the rotordynamic coefficients but caution should be taken when operating at low unit loads due to the increase in stiffness coefficients. Although TPJBs themselves are inherently stable, the bearing force coefficients could have a significant impact on the overall performance of a compressor or turbine. The results show that an appropriate model that includes pad flexibility should be used when predicting the performance of TPJB.

The measured result presented in this work can be used to validate computational codes that account for pad and pivot contact flexibilities. This work also provides measured dynamic load characteristics for a three-pad TPJB, which is limited.

REFERENCES

[1] Hargreaves, D. and Fillon, M., 2007, “Analysis of Tilting Pad Journal Bearing to Avoid Pad Fluttering,” Tribology International, **40**, pp. 607-612.

[2] Lund, J.W., 1964, “Spring and Damping Coefficients for the Tilting-Pad Journal Bearing,” ASLE Trans., **7**, pp. 342-352

[3] Varga, Z., 1977, “900 mm Pivoted-Pad Journal Bearing for Steam Turbosets – Characteristics and Testing,” Brown Boveri Rev, **6**, pp.325-335.

[4] Nilsson, L., 1978, “The Influence of Bearing Flexibility on the Dynamic Performance of Radial Oil-film Bearings,” Proc. 5th Leeds-Lyon Symposium on Tribology, **5**, pp.311-319, Lyon, France, Mechanical Engineering Publications, London (September 1978).

[5] Ettles, C.M., 1980, “The Analysis and Performance of Pivoted Pad Journal Bearings Considering Thermal and Elastic Effects,” ASME Journal of Lubrication Technology, **102**, pp. 182-192.

[6] Malcher, L., 1975, “Die Federungs und Dampfungseigenschaften von Gleitlagern fur Turbomaschinen,” Dipl.-Ing. Thesis, Karlsruhe Technische Hochschule, Karlsruhe, Germany.

[7] Klummp, R., 1975, “Beitrag zur Theoric von Kippsegment-Radiallagern,” Dissertation, Karlsruhe Technische Hochschule, Karlsruhe, Germany.

[8] Hashimoto, H., Wada, S., and Marukawa, T., 1985, “Performance Characteristics of Large Scale Tilting-pad Journal Bearings,” Bull. J.S.M.E., **28**, pp. 1761-1767.

[9] Lund, J.W., and Pedersen, L.B., 1987, "The Influence of Pad Flexibility on the Dynamic Coefficients of a Tilting Pad Journal Bearing," ASME J. Trib., **109**(1), pp. 65-70.

[10] Brugier, D., and Pascal, M., 1989, “Influence of Elastic Deformations of Turbo-Generator Tilting Pad Bearings on the Static Behavior and on the Dynamic Coefficients in Different Designs,” ASME J. Trib., **111**, pp. 364-371.

[11] Earles, L., Palazzolo, A., and Armentrout, R., 1990, “A Finite Element Approach to Pad Flexibility Effects in Tilt Pad Journal Bearings: Part I - Single Pad Analysis,” ASME J. Trib., **112**, pp. 169-177.

[12] Earles, L., Palazzolo, A., and Armentrout, R., 1990, “A Finite Element Approach to Pad Flexibility Effects in Tilt Pad Journal Bearings: Part II - Assembled Bearing and System Analysis,” ASME J. Trib., **112**, pp. 178-182.

[13] Brockwell, K., Kleinbub, D., and Dmochowski, W., 1990, “Measurement and Calculation of the Dynamic Operating Characteristics of the Five Shoe, Tilting Pad Journal Bearing,” Trib. Trans, **33**(4), pp. 481-492.

[14] Kim, J., Palazzolo, A., and Gadangi, R., 1995, "Dynamic Characteristics of TEHD Tilt Pad Journal Bearing Simulation Including Multiple Mode Pad Flexibility Model," ASME J. Vib. Acoust., **117**(1), pp. 123-135.

[15] Ettles, C.M., 1992, "The Analysis of Pivoted Pad Journal Bearing Assemblies Considering Thermoelastic Deformation ad Heat Transfer Effects," Tribology Transactions STLE, **35**(1), pp.156-162.

[16] Fillon, M., Bligoud, J.C., and Frene, J., 1992, "Experimental Study of Tilting-Pad Journal Bearing – Comparison with Theoretical Thermoelastohydrodynamic Results," Journal of Tribology, **114**, pp. 579-587

[17] Desbordes, H., Fillon, M., Chan Hew Wai, C., and Frene, J., 1994, "Dynamic Analysis of Tilting-Pad Journal Bearing—Influence of Pad Deformation," Journal of Tribology, **116**, pp. 621–628.

[18] Desbordes, H., Fillon, M., Frene, J., Chan Hew Wai, C., 1995, "The Effect of Three Dimensional Pad Deformation on Tilting-Pad Journal Bearings under Dynamic Loading," Journal of Tribology, **117**, pp. 379–384.

[19] Fillon, M., Desbordes, H., Frene, J., Chan Hew Wai, C., 1996, "A Global Approach of Thermal Effects Including Pad Deformations in Tilting-Pad Journal Bearings Submitted to Unbalance Load," Journal of Tribology, **118**, pp. 169–174.

[20] El-Butch, A.M., and Ashour, N.M., 1999, "Analysis of heavy duty tilting-pad journal bearing taking into account pad distortion and possible adoption of rubber pad segments," Tribology International, **32**(6), pp. 285-293.

[21] Cerda Varela, A., and Santos, I., 2011, "Stability Analysis of an Industrial Gas Compressor Supported by Tilting-Pad Bearings under Different Lubrication Regimes," Journal of Engineering for Gas Turbines and Power, **134**(2), pp. 022504-022504-11

[22] Cerda Varela, A., and Santos, I., 2012, "Performance improvement of tiliting-pad journal bearing by means of controllable lubrication," Mechanics & Industry, **13**(1), pp. 17-32.

[23] Cerda Varela, A., Fillon, M., and Santos, I., 2012, "On the Simplification for the Thermal Modeling of Tilting-Pad Journal Bearings Under Thermoelastohydrodynamic Regime," Proc. ASME Turbo Expo 2012, Paper GT2012-68329, June 11-15, 2012, Copenhagen, Denmark.

[24] Branagan, L., and Barrett, L., 1988, "Thermal Analysis of Fixed and Tilting Pad Journal Bearings Including Cross-Film Viscosity Variations and Deformations," ROMAC Report No. 276, UVa Report No. UVA/643092/MAE88/376.

[25] Deutschman, A., Michels, W., and Wilson, C., 1975, Machine Design, Macmillan Publishing Co., Inc., New York, pp. 862-863.

[26] Wilkes, J.C., 2012, "Measured and Predicted Rotor-Pad Transfer Functions for a Rocker-Pivot Tilting-Pad Journal Bearing," Ph.D. Dissertation, Mechanical Engineering, Texas A&M University, College Station, TX.

[27] Hagemann, T., Kukla, S., and Schwarze, H., 2013, "Measurement and Prediction of the Static Operating Conditions of a Large Turbine Tilting-Pad Bearing Under High Circumferential Speeds and Heavy Loads," Proc. ASME Turbo Expo 2013, Paper GT2013-95004, June 3-7, 2013, San Antonio, Texas.

[28] Kukla, S., Hagemann, T., and Schwarze, H., 2013, "Measurement and Prediction of the Dynamic Characteristics of a Large Turbine Tilting-Pad Bearing Under High Circumferential Speeds," Proc. ASME Turbo Expo 2013, Paper GT2013-95074, June 3-7, 2013, San Antonio, Texas.

[29] Tao, Y., 2012, "A Novel Computational Model for Tilting Pad Journal Bearings with soft Pivot Stiffnesses," Master's Thesis, Mechanical Engineering, Texas A&M University, College Station, TX.

[30] Kaul, A., 1999, "Design and Development of a Test Setup for the Experimental Determination of the Rotordynamic and Leakage Characteristics of Annular Bushing Oil Seals," M.S. Thesis, Mechanical Engineering, Texas A&M University.

[31] Glienicke, J., 1966, "Experimental Investigation of Stiffness and Damping Coefficients of Turbine Bearings and Their Application to Instability Predictions," Proc. of the International Mech. E., **181** (3B), pp. 116-129.

[32] Kulhanek, C., 2010, "Dynamic and Static Characteristics of a Rocker-Pivot, Tilting-Pad Bearing with 50% and 60% Offsets," M.S. thesis, Texas A&M University, College Station, TX.

[33] Burrows, C.R., Sayed-Esfahani, R., and Stanway, R., 1981, "A Comparison of Multifrequency Techniques for Measuring the Dynamics of Squeeze-Film Bearings," ASME Journal of Lubrication Technology, **103(1)**, pp. 137-143.

[34] Childs, D., and Hale, K., 1994, "A Test Apparatus and Facility to Identify the Rotordynamic Coefficients of High-Speed Hydrostatic Bearings," ASME Journal of Tribology, **116**, pp. 337-344.

[35] Childs, D., and Vannini, G., Delgado, A., 2011, "Tilting-Pad Bearings: Measures Frequency Characteristics of Their Rotordynamic Coefficients," Proc. 40th Turbomachinery Symposium, Turbomachinery Laboratory, Texas A&M University, College Station, TX, pp. 33-45

[36] San Andrés, L., 2010, Modern Lubrication Theory. "Dynamics of a Rigid Rotor-Fluid-film Bearing System", Notes 5, Texas A&M University Digital Libraries, http://repository.tamu.edu/handle/1969.1/93197 [4/16/2014]

[37] Tschoepe, D., 2012, "Measurements Versus Predictions for the Static and Dynamic Characteristics of a Four-Pad Rocker-Pivot, Tilting-Pad Journal Bearing," M.S. thesis, Texas A&M University, College Station, TX.

APPENDIX A:
MEASURED STATIC LOAD TEST CONDITIONS

Table A. 1. Average static load test conditions and uncertainties for t_p= 8.5 mm.

Nominal Speed [rpm]	Running Speed [rpm]	Nominal Unit Load [kPa]	Actual Unit Load [kPa]	Inlet Temperature [°C]	eX [µm]	eY [µm]	Flowrate [L/M]	T1 [°C]	T2 [°C]	T3 [°C]	T4 [°C]
6000	5993 ± 1.68	172	172.67 ± 0.11	49.02 ± 0.01	-0.27 ± 0.01	12.75 ± 0.01	31.25 ± 0.07	69.55 ± 0.02	50.93 ± 0.04	71.87 ± 0.02	53.15 ± 0.36
	5971 ± 1.01	345	348.56 ± 0.22	49.01 ± 0	-0.94 ± 0	20.25 ± 0.01	31.3 ± 0.07	71.14 ± 0.01	50.95 ± 0.07	73.22 ± 0.02	53.2 ± 0.27
	6023 ± 1.08	689	693.1 ± 0.43	48.99 ± 0.01	-1.67 ± 0	35.36 ± 0.01	31.21 ± 0.05	75.41 ± 0.02	51.08 ± 0.07	76.61 ± 0.02	53.27 ± 0.31
	6030 ± 1.4	1034	1033.71 ± 0.64	49.07 ± 0.01	-1.97 ± 0.01	49.66 ± 0.02	31.24 ± 0.08	79.66 ± 0.03	51.21 ± 0.05	79.99 ± 0.03	53.11 ± 0.32
	6043 ± 0.8	1724	1726.08 ± 1.06	48.98 ± 0.01	-2.45 ± 0.01	74.09 ± 0.02	31.12 ± 0.08	87.33 ± 0.02	51.43 ± 0.11	86.27 ± 0.03	53.18 ± 0.3
9000	9035 ± 1.07	172	172.76 ± 0.12	48.94 ± 0.01	-0.28 ± 0.01	9.03 ± 0.01	31.15 ± 0	79.59 ± 0.01	53.07 ± 0.03	82.32 ± 0.01	55.62 ± 0.28
	9042 ± 0.26	345	348.38 ± 0.24	49.03 ± 0.01	-0.28 ± 0.01	13.94 ± 0.01	31.12 ± 0.01	81.22 ± 0.02	53.24 ± 0.04	83.85 ± 0.02	55.62 ± 0.25
	9054 ± 1.45	689	693.98 ± 0.44	48.95 ± 0.01	-1.04 ± 0.01	24.77 ± 0.02	31.13 ± 0.01	85.04 ± 0.02	53.46 ± 0.04	87.33 ± 0.02	55.98 ± 0.24
	8953 ± 2.3	1034	1037.99 ± 0.64	49.05 ± 0	-1.19 ± 0.01	36.23 ± 0.02	31.15 ± 0.01	89.48 ± 0.02	53.62 ± 0.04	90.29 ± 0.01	55.73 ± 0.23
	8967 ± 1.47	1724	1727.83 ± 1.06	48.92 ± 0.01	-1.73 ± 0.01	57.79 ± 0.02	31.11 ± 0.01	98.3 ± 0.01	53.99 ± 0.05	96.96 ± 0.03	55.43 ± 0.21
12000	11991 ± 9.17	172	174.17 ± 0.14	48.84 ± 0.01	-0.16 ± 0.03	8.14 ± 0.03	31.49 ± 0.07	89.58 ± 0.05	56.35 ± 0.04	88.96 ± 0.03	56.43 ± 0.06
	11986 ± 1.3	345	346.14 ± 0.22	48.86 ± 0.01	-0.47 ± 0.01	12.17 ± 0.01	31.56 ± 0.03	91.29 ± 0.02	56.42 ± 0.04	90.81 ± 0.01	56.4 ± 0.05
	12073 ± 2.68	689	692.92 ± 0.43	49.1 ± 0.01	-0.22 ± 0.03	20.14 ± 0.03	31.26 ± 0.02	95.45 ± 0.02	56.99 ± 0.04	94.88 ± 0.03	57.04 ± 0.06
	12049 ± 1.89	1034	1039.07 ± 0.64	49.11 ± 0.01	-0.22 ± 0.03	28.97 ± 0.02	31.2 ± 0.02	99.88 ± 0.02	57.27 ± 0.04	99.03 ± 0.02	57.14 ± 0.06
	12016 ± 2.58	1724	1724.66 ± 1.06	49.24 ± 0.01	0.29 ± 0.01	46.87 ± 0.02	31.2 ± 0.05	108.73 ± 0.02	57.88 ± 0.05	106.85 ± 0.01	57.52 ± 0.07

Table A. 2. Average static load test conditions and uncertainties for t_p= 10 mm.

Nominal Speed [rpm]	Running Speed [rpm]	Nominal Unit Load [kPa]	Actual Unit Load [kPa]	Inlet Temperature [°C]	eX [µm]	eY [µm]	Flowrate [L/M]	T1 [°C]	T2 [°C]	T3 [°C]	T4 [°C]
6000	6051 ± 1.98	172	172.76 ± 0.11	48.84 ± 0	-0.18 ± 0.01	10.93 ± 0.01	31.52 ± 0.07	69.63 ± 0.01	52.1 ± 0.2	71.71 ± 0.02	52.07 ± 0.12
	6055 ± 3.34	345	348.28 ± 0.22	48.99 ± 0.01	-0.42 ± 0.01	18.33 ± 0.01	31.47 ± 0.06	71.61 ± 0.01	52.43 ± 0.22	73.35 ± 0.01	52.1 ± 0.15
	5993 ± 1.6	689	689.66 ± 0.43	49.03 ± 0.01	-1.21 ± 0.01	34.21 ± 0.01	31.44 ± 0.06	75.31 ± 0.01	52.64 ± 0.19	76.31 ± 0.02	52.29 ± 0.11
	5989 ± 1.46	1034	1034.86 ± 0.64	49.12 ± 0.01	-1.57 ± 0.01	49.01 ± 0.01	31.42 ± 0.07	79.1 ± 0.02	53.02 ± 0.32	79.52 ± 0.02	52.38 ± 0.1
	6015 ± 0.95	1724	1731 ± 1.06	49.18 ± 0.01	-1.81 ± 0.01	72.38 ± 0.01	31.53 ± 0.06	87.01 ± 0.01	53.82 ± 0.24	86.22 ± 0.01	52.64 ± 0.14
9000	8961 ± 1.48	172	172.83 ± 0.16	48.97 ± 0.01	-0.19 ± 0.01	8.03 ± 0.01	31.27 ± 0.03	78.85 ± 0.03	54.14 ± 0.16	80.08 ± 0.04	52.92 ± 0.03
	8998 ± 1.48	345	344.98 ± 0.22	49.13 ± 0.01	-0.31 ± 0.01	13.18 ± 0.01	31.38 ± 0.03	80.52 ± 0.02	54.34 ± 0.17	81.74 ± 0.01	53.15 ± 0.02
	9009 ± 3.44	689	695.95 ± 0.45	49.17 ± 0.01	-0.7 ± 0.01	24.53 ± 0.01	31.31 ± 0.03	84.21 ± 0.02	54.3 ± 0.13	85.11 ± 0	53.37 ± 0.02
	8978 ± 1.46	1034	1034.89 ± 0.63	49.17 ± 0.01	-1.3 ± 0.01	36.14 ± 0.02	31.39 ± 0.02	88.15 ± 0.01	54.43 ± 0.09	88.52 ± 0.01	53.48 ± 0.02
	9018 ± 1.22	1724	1728.96 ± 1.06	49.2 ± 0.01	-1.23 ± 0.01	55.98 ± 0.02	31.3 ± 0.01	97.21 ± 0.01	55.08 ± 0.12	96.54 ± 0.02	53.76 ± 0.02
12000	11999 ± 0.51	172	171.21 ± 0.11	49.03 ± 0.01	-0.37 ± 0.01	3.3 ± 0.01	31.27 ± 0.01	85.9 ± 0.01	57.38 ± 0.05	89.08 ± 0.01	56.86 ± 0.07
	12018 ± 2.72	345	347.9 ± 0.22	49.07 ± 0.01	-0.73 ± 0.01	7.42 ± 0.01	31.23 ± 0.01	87.37 ± 0.01	57.55 ± 0.03	90.62 ± 0.01	56.93 ± 0.04
	11971 ± 1.39	689	691.66 ± 0.43	49.08 ± 0.01	-1.16 ± 0.01	16.55 ± 0.01	31.2 ± 0.01	90.68 ± 0.01	57.7 ± 0.05	94.23 ± 0.01	57.13 ± 0.06
	11979 ± 2.99	1034	1035.03 ± 0.64	49.14 ± 0.01	-1.5 ± 0.01	25.57 ± 0.02	31.21 ± 0	94.82 ± 0.01	58.06 ± 0.04	98.28 ± 0.01	57.4 ± 0.05
	11942 ± 4.58	1724	1728.71 ± 1.07	49.06 ± 0	-1.93 ± 0.01	43.32 ± 0.02	31.21 ± 0	103.17 ± 0.04	58.28 ± 0.04	107.03 ± 0.03	57.46 ± 0.09

Table A. 3. Average static load test conditions and uncertainties for t_p= 11.5 mm.

Nominal Speed [rpm]	Running Speed [rpm]	Nominal Unit Load [kPa]	Actual Unit Load [kPa]	Inlet Temperature [°C]	eX [µm]	eY [µm]	Flowrate [L/M]	T1 [°C]	T2 [°C]	T3 [°C]	T4 [°C]
6000	6051 ± 2.3	172	173.83 ± 0.11	49.13 ± 0.01	-0.38 ± 0.01	6.33 ± 0.01	31.67 ± 0.12	70.03 ± 0.03	57.62 ± 0.49	68.53 ± 0.02	53.58 ± 0.2
	5988 ± 5.35	345	347.73 ± 0.22	49.1 ± 0.01	-0.88 ± 0.01	14.63 ± 0.02	31.61 ± 0.13	71.24 ± 0.02	56.41 ± 0.24	70.17 ± 0.02	53.64 ± 0.24
	5957 ± 3.96	689	690.65 ± 0.42	49.04 ± 0.01	-1.56 ± 0.01	31.32 ± 0.02	31.39 ± 0.17	74.66 ± 0.03	57.7 ± 0.42	74.38 ± 0.03	54.59 ± 0.26
	5994 ± 2.54	1034	1035.41 ± 0.63	49.27 ± 0.01	-1.36 ± 0.01	45.94 ± 0.02	31.5 ± 0.15	78.91 ± 0.03	58.33 ± 0.46	79.36 ± 0.02	56.99 ± 0.45
	6037 ± 2.89	1724	1729.51 ± 1.06	48.86 ± 0	-1.43 ± 0.01	70.06 ± 0.04	31.21 ± 0.16	86.12 ± 0.04	60.19 ± 0.58	87.21 ± 0.03	58.71 ± 0.3
9000	9034 ± 1.96	172	174.99 ± 0.11	49.13 ± 0.01	-0.31 ± 0.01	2.18 ± 0.01	31.24 ± 0.05	78.89 ± 0.01	55.84 ± 0.44	78.07 ± 0.02	55.17 ± 0.42
	9010 ± 2.24	345	346.75 ± 0.22	48.85 ± 0.01	-0.8 ± 0.01	7.8 ± 0.02	31.22 ± 0.01	80.33 ± 0.02	55.42 ± 0.23	79.42 ± 0.01	55.13 ± 0.45
	8962 ± 2.72	689	693.75 ± 0.43	49.15 ± 0.01	-0.47 ± 0.01	19.41 ± 0.01	31.23 ± 0.06	84.16 ± 0.01	55.9 ± 0.26	83.83 ± 0.01	57.09 ± 0.46
	9032 ± 0.52	1034	1039.44 ± 0.64	49.18 ± 0.01	-0.17 ± 0.01	31.07 ± 0.01	31.33 ± 0.01	88.75 ± 0.01	56.45 ± 0.23	89.15 ± 0.01	58.74 ± 0.53
	8984 ± 0.74	1724	1728.38 ± 1.06	49.2 ± 0.01	0.5 ± 0.02	52.98 ± 0.03	31.43 ± 0.03	97.42 ± 0.01	56.69 ± 0.26	98.3 ± 0.02	61.63 ± 0.36
12000	12004 ± 1.4	172	173.7 ± 0.14	49 ± 0.01	-0.21 ± 0.03	4.41 ± 0.03	31.4 ± 0.04	90.04 ± 0.03	66.81 ± 0.25	88.48 ± 0.02	59.18 ± 0.28
	11985 ± 2.44	345	345.12 ± 0.23	48.86 ± 0.01	-0.5 ± 0.01	8.42 ± 0.01	31.26 ± 0	91.87 ± 0.01	66.93 ± 0.32	90.07 ± 0.01	59.32 ± 0.27
	12081 ± 2.39	689	692.39 ± 0.43	49.05 ± 0.02	0 ± 0.01	16.58 ± 0.01	31.45 ± 0.01	95.78 ± 0.01	67.63 ± 0.32	93.81 ± 0.01	60.09 ± 0.33
	11953 ± 1.73	1034	1037.76 ± 0.64	48.96 ± 0.01	-0.31 ± 0.02	26.34 ± 0.03	31.28 ± 0.01	99.54 ± 0.02	68.44 ± 0.52	98.25 ± 0.03	60.48 ± 0.3
	12013 ± 4.65	1724	1727.87 ± 1.07	49.03 ± 0.01	0.88 ± 0.01	44.66 ± 0.02	31.38 ± 0	108.7 ± 0.01	69.43 ± 0.44	107.15 ± 0.01	59.18 ± 0.19

APPENDIX B:

MEASURED DYNAMIC LOAD TEST CONDITIONS

Table B. 1. Average dynamic load test conditions and uncertainties for t_p= 8.5 mm.

Nominal Speed (rpm)	Running Speed [rpm]	Nominal Unit Load [psi]	Actual Unit Load [psi]	Inlet Temperature [°F]	DE Outlet Temperature [°F]	NDE Outlet Temperature [°F]	Flowrate [GPM]
6000	6011 ± 6.996	25	24 ± 0.499	120.22 ± 0.027	127.02 ± 0.061	126.27 ± 0.06	8.2 ± 0.055
	5976 ± 8.684	50	50 ± 1.172	120.2 ± 0.022	126.98 ± 0.137	126.23 ± 0.134	8.24 ± 0.058
	6041 ± 11.651	100	100 ± 2.398	120.08 ± 0.055	127.54 ± 0.044	126.54 ± 0.043	8.25 ± 0.014
	6042 ± 17.222	150	149 ± 0.282	120.24 ± 0.028	128.18 ± 0.09	126.88 ± 0.089	8.27 ± 0.04
	6044 ± 23.379	250	250 ± 0.202	120.31 ± 0.031	128.45 ± 0.035	127.2 ± 0.034	8.28 ± 0.013
9000	9038 ± 8.8	25	25 ± 0.543	120.23 ± 0.015	135.04 ± 0.016	133.33 ± 0.016	8.22 ± 0.002
	9013 ± 18.701	50	49 ± 2.605	119.97 ± 0.056	134.77 ± 0.097	133.1 ± 0.095	8.21 ± 0.004
	9069 ± 8.926	100	100 ± 0.409	120.4 ± 0.096	135.53 ± 0.117	133.78 ± 0.115	8.21 ± 0.003
	9063 ± 14.024	150	150 ± 0.071	120.16 ± 0.035	135.4 ± 0.006	133.65 ± 0.006	8.21 ± 0.008
	8952 ± 16.573	250	250 ± 0.067	120.11 ± 0.03	135.42 ± 0.094	133.72 ± 0.092	8.2 ± 0.007
12000	12062 ± 20.108	25	25 ± 1.838	119.8 ± 0.098	142.5 ± 0.148	142.19 ± 0.145	8.23 ± 0.133
	12019 ± 49.124	50	49 ± 1.024	119.9 ± 0.069	142.54 ± 0.07	142.3 ± 0.069	8.19 ± 0.011
	12005 ± 36.605	100	100 ± 0.196	120.39 ± 0.052	142.59 ± 0.177	142.61 ± 0.173	8.29 ± 0.037
	12007 ± 33.865	150	150 ± 1.876	120.31 ± 0.013	142.55 ± 0.072	142.78 ± 0.07	8.35 ± 0.013
	11962 ± 16.694	250	250 ± 0.458	120.63 ± 0.018	142.81 ± 0.128	143.5 ± 0.125	8.3 ± 0.082

Table B. 2. Average dynamic load test conditions and uncertainties for t_p= 10 mm.

Nominal Speed (rpm)	Running Speed [rpm]	Nominal Unit Load [psi]	Actual Unit Load [psi]	Inlet Temperature [°F]	DE Outlet Temperature [°F]	NDE Outlet Temperature [°F]	Flowrate [GPM]
6000	6004 ± 14.807	25	25 ± 7.495	120.02 ± 0.062	127.06 ± 0.108	126.15 ± 0.106	8.26 ± 0.022
	6022 ± 2.566	50	50 ± 1.974	120.19 ± 0.042	127.39 ± 0.021	126.39 ± 0.021	8.28 ± 0.07
	6002 ± 8.666	100	100 ± 0.983	120.25 ± 0.043	127.63 ± 0.005	126.67 ± 0.005	8.26 ± 0.034
	5980 ± 9.389	150	150 ± 2.723	120.4 ± 0.058	127.95 ± 0.114	126.87 ± 0.112	8.27 ± 0.016
	5989 ± 4.964	250	251 ± 0.097	120.48 ± 0.01	128.59 ± 0.056	127.19 ± 0.055	8.26 ± 0.023
9000	9027 ± 6.285	25	24 ± 2.877	119.99 ± 0.065	134.36 ± 0.033	133 ± 0.033	8.26 ± 0.017
	8990 ± 3.283	50	49 ± 0.38	120.45 ± 0.009	134.73 ± 0.067	133.25 ± 0.066	8.25 ± 0.026
	9034 ± 8.108	100	100 ± 0.218	120.55 ± 0.059	135.28 ± 0.025	133.53 ± 0.025	8.24 ± 0.032
	8951 ± 1.532	150	150 ± 2.164	120.54 ± 0.058	135.3 ± 0.053	133.48 ± 0.052	8.26 ± 0.046
	8967 ± 3.241	250	250 ± 1.956	120.48 ± 0.006	135.96 ± 0.006	133.97 ± 0.006	8.22 ± 0.009
12000	11999 ± 3.932	25	24 ± 0.285	120.34 ± 0.025	142.99 ± 0.037	142.5 ± 0.036	8.23 ± 0.001
	12020 ± 9.056	50	50 ± 1.66	120.25 ± 0.033	143.05 ± 0.044	142.53 ± 0.043	8.24 ± 0.005
	11969 ± 10.008	100	100 ± 0.084	120.25 ± 0.049	142.93 ± 0.059	142.35 ± 0.058	8.23 ± 0
	11962 ± 11.873	150	150 ± 0.075	120.56 ± 0.065	143.43 ± 0.05	142.76 ± 0.049	8.23 ± 0.002
	11989 ± 4.439	250	250 ± 0.534	120.18 ± 0.06	143.66 ± 0.028	142.8 ± 0.028	8.23 ± 0.004

Table B. 3. Average dynamic load test conditions and uncertainties for t_p= 11.5 mm.

Nominal Speed (rpm)	Running Speed [rpm]	Nominal Unit Load [psi]	Actual Unit Load [psi]	Inlet Temperature [°F]	DE Outlet Temperature [°F]	NDE Outlet Temperature [°F]	Flowrate [GPM]
6000	5990 ± 12.837	25	24 ± 0.224	120.45 ± 0.01	126.72 ± 0.038	126.22 ± 0.037	8.24 ± 0.053
	6004 ± 18.181	50	50 ± 0.118	120.29 ± 0.024	126.74 ± 0.076	126.02 ± 0.074	8.27 ± 0.098
	6034 ± 5.077	100	99 ± 0.148	120.34 ± 0.049	127.14 ± 0.135	126.27 ± 0.133	8.23 ± 0.075
	6063 ± 5.027	150	150 ± 1.836	120.05 ± 0.1	127.27 ± 0.064	126.24 ± 0.062	8.19 ± 0.125
	6072 ± 19.125	250	250 ± 0.115	119.94 ± 0.022	127.59 ± 0.107	126.52 ± 0.105	8.18 ± 0.052
9000	9051 ± 1.699	25	24 ± 1.107	120.44 ± 0.056	133.26 ± 0.091	132.65 ± 0.089	8.26 ± 0.031
	9026 ± 7.261	50	50 ± 0.381	119.87 ± 0.021	132.71 ± 0.11	132.1 ± 0.108	8.23 ± 0.039
	9071 ± 3.95	100	100 ± 0.413	120.32 ± 0.111	133.62 ± 0.117	132.99 ± 0.114	8.25 ± 0.025
	8991 ± 6.599	150	150 ± 0.638	120.65 ± 0.034	134.08 ± 0.05	133.15 ± 0.049	8.24 ± 0.01
	8988 ± 1.702	250	250 ± 0.345	120.54 ± 0.05	134.79 ± 0.014	133.4 ± 0.014	8.27 ± 0.022
12000	12049 ± 9.338	25	25 ± 2.789	119.94 ± 0.025	141.28 ± 0.041	140.41 ± 0.04	8.26 ± 0.023
	11970 ± 3.711	50	50 ± 3.53	120.12 ± 0.034	141.26 ± 0.02	140.44 ± 0.02	8.25 ± 0.004
	11943 ± 4.329	100	100 ± 1.342	120.24 ± 0.078	141.56 ± 0.113	140.58 ± 0.11	8.23 ± 0.015
	11994 ± 3.818	150	150 ± 0.449	120.25 ± 0.029	142.15 ± 0.046	140.87 ± 0.045	8.27 ± 0.013
	12018 ± 9.491	250	250 ± 0.195	120.11 ± 0.062	142.2 ± 0.132	141.49 ± 0.129	8.22 ± 0

APPENDIX C:

ROTORDYNAMIC COEFFICIENTS

Rotordynamic Coefficient Tables

Table C. 1. Measured stiffness coefficients and uncertainties at specified speed and unit load test conditions for t_p = 8.5 mm.

Speed [RPM]	Unit Load [kPa]	K_{xx} [MN/m]	K_{xy} [MN/m]	K_{yx} [MN/m]	K_{yy} [MN/m]
6,000	172	169.71 ± 3.15	-5.24 ± 4.18	-8.68 ± 4.56	113.43 ± 6.56
	345	191.17 ± 8.13	-5.75 ± 4.36	-9.78 ± 3.4	107.24 ± 4.4
	689	241.74 ± 6.08	-10.89 ± 4.34	-16.5 ± 4.57	107.46 ± 4.92
	1034	297.32 ± 6.99	-18.85 ± 4.8	-25.11 ± 6.3	117.9 ± 4.25
	1,724	403.87 ± 12.74	-39.61 ± 4.72	-46.03 ± 6.68	149.58 ± 3.38
9,000	172	217.12 ± 7.18	-20.66 ± 3.29	-18.94 ± 4.33	155.16 ± 6.39
	345	233.71 ± 7.44	-21.37 ± 6.17	-19.65 ± 8.02	148.33 ± 5.48
	689	268.13 ± 8.19	-21.61 ± 2.74	-19.08 ± 5.42	140.03 ± 3.52
	1034	307.96 ± 12.29	-27.03 ± 3.05	-25.29 ± 6.35	141.14 ± 3.51
	1,724	392.37 ± 10.33	-42.82 ± 3.07	-40.72 ± 4.07	159.64 ± 2.95
12,000	172	245 ± 6.31	-37.32 ± 3.82	-23.65 ± 3.97	189.68 ± 12.45
	345	257.1 ± 8.3	-35.47 ± 2.83	-25.69 ± 2.93	178.95 ± 4.8
	689	281.31 ± 9.28	-35.02 ± 3.46	-26.11 ± 4.4	169.65 ± 4.42
	1034	310.74 ± 11.92	-38.72 ± 3.9	-31.05 ± 6.64	166.85 ± 3.99
	1,724	377.11 ± 12.67	-48.87 ± 3.19	-42.28 ± 4.12	173.66 ± 3.02

Table C. 2. Measured damping coefficients and uncertainties at specified speed and unit load test conditions for t_p = 8.5 mm.

Speed [RPM]	Unit Load [kPa]	C_{xx} [kN-s/m]	C_{xy} [kN-s/m]	C_{yx} [kN-s/m]	C_{yy} [kN-s/m]
6,000	172	201.32 ± 5.02	-31.55 ± 7.21	-28.38 ± 7	149.27 ± 4.82
	345	201.01 ± 2.75	-33.76 ± 6.76	-29.02 ± 6.49	143.4 ± 3.97
	689	199.3 ± 4.77	-36.35 ± 6.41	-31 ± 5.6	128.56 ± 5.46
	1034	197 ± 5.6	-40.1 ± 6.46	-34.15 ± 5.16	116.03 ± 5.64
	1,724	190.3 ± 11.08	-45.62 ± 4.89	-39.44 ± 6.44	100.39 ± 5.24
9,000	172	166.8 ± 5.65	-23.75 ± 5.08	-32.33 ± 6.24	123.1 ± 4.37
	345	164.53 ± 6.33	-27.48 ± 7.99	-36.17 ± 7.81	120.14 ± 5.39
	689	163.9 ± 8.77	-26.75 ± 2.84	-35.93 ± 7.65	112.92 ± 4.36
	1034	165.31 ± 8.53	-28.76 ± 2.45	-37.48 ± 9.6	104.52 ± 4.87
	1,724	162.49 ± 12.89	-32.66 ± 3.28	-39.53 ± 9.48	90.79 ± 5.26
12,000	172	151.55 ± 5.77	-22.49 ± 10.88	-39.59 ± 7.3	114.58 ± 8.64
	345	151.91 ± 8.69	-25.08 ± 1.86	-46.4 ± 6.39	110.53 ± 4.45
	689	150.9 ± 9.75	-27.01 ± 3.04	-46.52 ± 7.42	102.45 ± 5.05
	1034	150.81 ± 13.18	-27.64 ± 3.36	-47.72 ± 6.42	96.23 ± 5.73
	1,724	150.45 ± 12.62	-29.3 ± 2.86	-49.33 ± 5.78	84.3 ± 6.69

Table C. 3. Measured virtual-mass coefficients and uncertainties at specified speed and unit load test conditions for t_p = 8.5 mm.

Speed [RPM]	Unit Load [kPa]	M_{xx} [kg]	M_{xy} [kg]	M_{yx} [kg]	M_{yy} [kg]
6,000	172	-25.04 ± 4.41	-32.38 ± 5.84	-18.34 ± 6.37	-28.7 ± 9.17
	345	-21.97 ± 11.36	-29.08 ± 6.09	-20.3 ± 4.75	-25.98 ± 6.15
	689	-19.64 ± 8.5	-25.91 ± 6.06	-20.68 ± 6.38	-20.05 ± 6.88
	1034	-18.45 ± 9.77	-23.57 ± 6.71	-22.13 ± 8.81	-17.15 ± 5.94
	1,724	-18.38 ± 17.79	-16.51 ± 6.59	-17 ± 9.33	-15.96 ± 4.73
9,000	172	-17.34 ± 10.03	-30.76 ± 4.6	-8.86 ± 6.05	-23.71 ± 8.93
	345	-16.37 ± 10.4	-28.78 ± 8.62	-11.23 ± 11.21	-18.76 ± 7.66
	689	-19.38 ± 11.45	-22.57 ± 3.83	-1.46 ± 7.57	-15.6 ± 4.92
	1034	-16.83 ± 17.18	-21.29 ± 4.26	-1.79 ± 8.87	-11.54 ± 4.91
	1,724	-21.84 ± 14.44	-19.14 ± 4.29	2.49 ± 5.69	-8.89 ± 4.12
12,000	172	-18.91 ± 8.82	-27.62 ± 5.34	5.15 ± 5.55	-23.8 ± 17.39
	345	-14.96 ± 11.6	-21.96 ± 3.95	3.48 ± 4.1	-22.29 ± 6.7
	689	-17.46 ± 12.97	-16.62 ± 4.83	4.87 ± 6.15	-13.06 ± 6.17
	1034	-16.42 ± 16.66	-15.5 ± 5.46	3.53 ± 9.28	-8.42 ± 5.57
	1,724	-19.82 ± 17.7	-15.56 ± 4.45	6.4 ± 5.76	-5.19 ± 4.23

Table C. 4. R^2 value for [K][C][M] model for t_p = 8.5 mm.

Speed [RPM]	Unit Load [kPa]	Re (H_{xx})	Re (H_{xy})	Re (H_{yx})	Re (H_{yy})	Im (H_{xx})	Im (H_{xy})	Im (H_{yx})	Im (H_{yy})
6,000	172	0.969	0.968	0.891	0.906	0.997	0.862	0.79	0.995
	345	0.786	0.957	0.947	0.946	0.999	0.888	0.801	0.997
	689	0.847	0.947	0.911	0.893	0.997	0.908	0.857	0.992
	1034	0.778	0.924	0.861	0.891	0.996	0.922	0.894	0.99
	1724	0.511	0.86	0.765	0.918	0.981	0.96	0.879	0.988
9,000	172	0.746	0.978	0.677	0.874	0.994	0.888	0.769	0.994
	345	0.709	0.916	0.496	0.855	0.992	0.706	0.766	0.991
	689	0.738	0.971	0.035	0.908	0.984	0.952	0.746	0.993
	1034	0.485	0.961	0.038	0.844	0.985	0.967	0.649	0.991
	1724	0.692	0.951	0.158	0.82	0.963	0.96	0.686	0.986
12,000	172	0.819	0.963	0.458	0.647	0.992	0.572	0.811	0.974
	345	0.62	0.968	0.414	0.916	0.982	0.97	0.897	0.992
	689	0.64	0.921	0.381	0.815	0.992	0.572	0.811	0.974
	1034	0.488	0.888	0.124	0.692	0.954	0.908	0.913	0.985
	1724	0.552	0.923	0.548	0.596	0.958	0.948	0.941	0.974

Table C. 5. Measured stiffness coefficients and uncertainties at specified speed and unit load test conditions for t_p = 10 mm.

Speed [RPM]	Unit Load [kPa]	K_{xx} [MN/m]	K_{xy} [MN/m]	K_{yx} [MN/m]	K_{yy} [MN/m]
6,000	172	169.58 ± 6.09	-3.91 ± 4.56	-10.7 ± 6.37	108.16 ± 5.54
	345	191.96 ± 5.52	-5.11 ± 3.88	-13.93 ± 3.48	104.12 ± 5.29
	689	246.06 ± 6.84	-9.79 ± 3.99	-18.8 ± 5.33	106.64 ± 4.43
	1034	302.69 ± 10.04	-16.51 ± 4.16	-26.29 ± 6.86	119.26 ± 4.61
	1,724	412.23 ± 12.59	-38.98 ± 4.75	-49.59 ± 6.25	156.28 ± 3.95
9,000	172	219.81 ± 10.9	-18.68 ± 4.84	-21.01 ± 9.63	150.31 ± 5.57
	345	234.63 ± 8.73	-18.79 ± 4.95	-20.91 ± 5.85	143.05 ± 3.71
	689	272.36 ± 12.07	-20.34 ± 2.99	-22.61 ± 5.18	137.66 ± 2.55
	1034	313.97 ± 12.15	-27.01 ± 3.11	-29.21 ± 5.08	140.16 ± 3.54
	1,724	405.66 ± 12.76	-46.47 ± 3	-46.91 ± 6.68	164.36 ± 3.57
12,000	172	250.67 ± 6.32	-26.12 ± 3.84	-39.24 ± 6.51	184.72 ± 5.38
	345	261.17 ± 8.69	-27.13 ± 3.11	-34.75 ± 10.99	178.17 ± 4.76
	689	292.72 ± 11.92	-28.91 ± 3.11	-35.76 ± 6.13	169.4 ± 2.67
	1034	326.48 ± 10.04	-35.18 ± 3.23	-38.6 ± 4.3	167.29 ± 3.67
	1,724	405.01 ± 13.42	-51.21 ± 3.03	-48.29 ± 4.27	179.02 ± 2.81

Table C. 6. Measured damping coefficients and uncertainties at specified speed and unit load test conditions for t_p = 10 mm.

Speed [RPM]	Unit Load [kPa]	C_{xx} [kN-s/m]	C_{xy} [kN-s/m]	C_{yx} [kN-s/m]	C_{yy} [kN-s/m]
6,000	172	226.16 ± 4.54	-35.94 ± 5.72	-28.48 ± 3.32	159.68 ± 4.52
	345	226.04 ± 7.21	-38.42 ± 5.18	-35.64 ± 10.69	151.14 ± 4.23
	689	222.42 ± 6.83	-44.22 ± 5.59	-37.44 ± 6.72	137.94 ± 5.31
	1034	219.59 ± 11.07	-51.24 ± 4.06	-42.64 ± 7.44	127 ± 5.13
	1,724	204.13 ± 12.79	-55.08 ± 3.94	-45.37 ± 6.14	108.4 ± 4.59
9,000	172	192.3 ± 11.35	-30.29 ± 2.61	-34.76 ± 5.32	129.93 ± 5.78
	345	191.11 ± 22.92	-34.66 ± 14.35	-40.31 ± 7.83	127.54 ± 5.66
	689	184.38 ± 10.8	-35.44 ± 1.84	-43.51 ± 6.03	118.36 ± 5.59
	1034	182.17 ± 13.25	-38.94 ± 1.62	-45.01 ± 8.34	111.48 ± 5.27
	1,724	174.56 ± 13.44	-41.01 ± 2.81	-46.17 ± 8.73	96.15 ± 5.66
12,000	172	162.41 ± 10.52	-28.38 ± 4.12	-30.31 ± 6.15	106.56 ± 6.81
	345	166.29 ± 7.47	-30.15 ± 2.99	-28.97 ± 5.72	100.62 ± 5.57
	689	167.14 ± 8.85	-32.6 ± 3.22	-40.52 ± 8.21	99.67 ± 6.73
	1034	162.54 ± 13.31	-33.49 ± 3.56	-42.34 ± 3.83	96.03 ± 6.31
	1,724	157.67 ± 12.7	-34.42 ± 3.07	-45.7 ± 6.65	87.36 ± 6.25

Table C. 7. Measured virtual-mass coefficients and uncertainties at specified speed and unit load test conditions for t_p = 10 mm.

Speed [RPM]	Unit Load [kPa]	M_{xx} [kg]	M_{xy} [kg]	M_{yx} [kg]	M_{yy} [kg]
6,000	172	-40 ± 8.51	-29.25 ± 6.37	-18.94 ± 8.9	-33.52 ± 7.74
	345	-40.61 ± 7.71	-25.55 ± 5.42	-22.17 ± 4.87	-27.97 ± 7.4
	689	-40.91 ± 9.56	-19.91 ± 5.58	-18.72 ± 7.44	-24.97 ± 6.19
	1034	-44.19 ± 14.02	-13.1 ± 5.81	-16.07 ± 9.59	-24.98 ± 6.44
	1,724	-34.08 ± 17.6	-8.34 ± 6.64	-13.14 ± 8.74	-22.44 ± 5.52
9,000	172	-28.17 ± 15.23	-26.95 ± 6.76	-9.55 ± 13.45	-19.54 ± 7.78
	345	-23.52 ± 12.2	-22.76 ± 6.92	-5.79 ± 8.18	-17.62 ± 5.18
	689	-28.09 ± 16.87	-17.77 ± 4.17	-3.51 ± 7.23	-14.57 ± 3.56
	1034	-29.35 ± 16.97	-16.2 ± 4.35	-0.6 ± 7.1	-13.52 ± 4.95
	1,724	-25.41 ± 17.82	-16.59 ± 4.2	1.54 ± 9.34	-10.22 ± 4.99
12,000	172	-19.96 ± 8.83	-16.51 ± 5.37	-28.43 ± 9.1	-6.2 ± 7.52
	345	-28.01 ± 12.14	-14.21 ± 4.34	-12.42 ± 15.36	-5.82 ± 6.66
	689	-20.47 ± 16.66	-11.34 ± 4.34	-12.19 ± 8.57	-5.4 ± 3.73
	1034	-24.65 ± 14.03	-11.58 ± 4.51	-6.77 ± 6.01	-4.82 ± 5.13
	1,724	-20.84 ± 18.75	-13.2 ± 4.23	2.23 ± 5.97	-4.58 ± 3.93

Table C. 8. R^2 value for [K][C][M] model for t_p = 10 mm.

Speed [RPM]	Unit Load [kPa]	Re (H_{xx})	Re (H_{xy})	Re (H_{yx})	Re (H_{yy})	Im (H_{xx})	Im (H_{xy})	Im (H_{yx})	Im (H_{yy})
6,000	172	0.956	0.954	0.816	0.948	0.998	0.92	0.93	0.996
	345	0.965	0.956	0.953	0.933	0.995	0.938	0.698	0.997
	689	0.947	0.926	0.861	0.941	0.995	0.947	0.85	0.993
	1034	0.907	0.833	0.734	0.936	0.986	0.977	0.833	0.993
	1724	0.786	0.607	0.689	0.942	0.978	0.98	0.898	0.992
9,000	172	0.77	0.94	0.331	0.861	0.983	0.969	0.884	0.991
	345	0.785	0.914	0.33	0.919	0.925	0.477	0.823	0.991
	689	0.731	0.947	0.188	0.943	0.98	0.987	0.893	0.99
	1034	0.746	0.932	0.007	0.88	0.968	0.992	0.811	0.99
	1724	0.666	0.939	0.026	0.805	0.965	0.981	0.791	0.985
12,000	172	0.834	0.903	0.905	0.4	0.977	0.89	0.871	0.982
	345	0.839	0.913	0.391	0.429	0.989	0.947	0.786	0.986
	689	0.597	0.871	0.665	0.674	0.985	0.948	0.854	0.98
	1034	0.752	0.866	0.554	0.464	0.96	0.931	0.962	0.981
	1724	0.548	0.905	0.12	0.571	0.962	0.953	0.902	0.978

Table C. 9. Measured stiffness coefficients and uncertainties at specified speed and unit load test conditions for t_p = 11.5 mm.

Speed [RPM]	Unit Load [kPa]	K_{xx} [MN/m]	K_{xy} [MN/m]	K_{yx} [MN/m]	K_{yy} [MN/m]
6,000	172	151.2 ± 4.24	-4.44 ± 3.33	-9.94 ± 3.64	102.45 ± 4.8
	345	178.38 ± 7.87	-5.67 ± 3.23	-10.47 ± 5.01	95.94 ± 6.04
	689	237.29 ± 7.45	-10.71 ± 3.44	-15.88 ± 5.5	99.34 ± 5.48
	1034	302.67 ± 9.36	-18.94 ± 4.61	-25.29 ± 6.34	114.74 ± 5.11
	1,724	416.01 ± 9.13	-38.77 ± 5.97	-46.58 ± 6.95	151.29 ± 3.33
9,000	172	199.44 ± 5.21	-19.26 ± 3.15	-22.16 ± 6.12	145.66 ± 5.69
	345	218.35 ± 7.36	-19.8 ± 2.92	-19.78 ± 7.79	135.85 ± 3.61
	689	256.89 ± 8.47	-22.78 ± 2.75	-18.77 ± 3.72	126.48 ± 3.29
	1034	306.97 ± 11.05	-29.49 ± 2.36	-23.53 ± 4.74	128.74 ± 3.48
	1,724	398.7 ± 11.69	-44.69 ± 2.72	-40.75 ± 5.26	152.57 ± 3.77
12,000	172	242.68 ± 6.86	-32.06 ± 9.15	-30.79 ± 8.72	187.26 ± 6.91
	345	257.74 ± 11.92	-30.67 ± 3.51	-26.23 ± 9.58	171.68 ± 4.3
	689	282.22 ± 9.44	-30.77 ± 3.41	-22.27 ± 5.37	158.85 ± 3.6
	1034	317.96 ± 11.1	-34.5 ± 3.15	-25.51 ± 5.84	155.24 ± 2.91
	1,724	389.11 ± 11.1	-47.59 ± 3.97	-36.84 ± 7.34	174.31 ± 2.88

Table C. 10. Measured damping coefficients and uncertainties at specified speed and unit load test conditions for t_p = 11.5 mm.

Speed [RPM]	Unit Load [kPa]	C_{xx} [kN-s/m]	C_{xy} [kN-s/m]	C_{yx} [kN-s/m]	C_{yy} [kN-s/m]
6,000	172	229.27 ± 2.92	-28.93 ± 6.02	-27.45 ± 4.7	169.8 ± 5.4
	345	229.19 ± 2.62	-31.52 ± 5.89	-31.72 ± 8.53	159.58 ± 4.3
	689	233.67 ± 4.11	-37.75 ± 6.02	-35.09 ± 8.78	143.56 ± 5.1
	1034	231.24 ± 7.18	-44.48 ± 6.01	-39.95 ± 9.11	130.68 ± 5.73
	1,724	219.85 ± 15.1	-52.86 ± 6.01	-45.85 ± 7.93	113.07 ± 4.55
9,000	172	189.49 ± 5.62	-28.84 ± 2.43	-28.04 ± 7.6	153.07 ± 7.23
	345	188.75 ± 6.02	-31.06 ± 1.88	-37.91 ± 6.58	148.68 ± 3.78
	689	189.89 ± 8.78	-33.02 ± 2.63	-42.93 ± 9.28	139.23 ± 4.22
	1034	189.19 ± 11.22	-35.91 ± 2.71	-44.7 ± 9.97	125.8 ± 4.42
	1,724	188.25 ± 16.72	-40.87 ± 4.14	-49 ± 10.62	105.23 ± 5.37
12,000	172	181.07 ± 8.97	-30.99 ± 4.01	-36.7 ± 9.08	137.63 ± 11.9
	345	180.31 ± 10.54	-29.75 ± 2.08	-43.77 ± 8.03	135.02 ± 5.29
	689	178.24 ± 13.04	-31.2 ± 2.88	-49.52 ± 7.77	128.35 ± 4.08
	1034	176.73 ± 14.41	-32.28 ± 3.07	-50.65 ± 8.27	119.09 ± 3.96
	1,724	178.2 ± 16.01	-33.09 ± 3.32	-57.4 ± 8.43	96.91 ± 6.26

Table C. 11. Measured virtual-mass coefficients and uncertainties at specified speed and unit load test conditions for t_p = 11.5 mm.

Speed [RPM]	Unit Load [kPa]	M_{xx} [kg]	M_{xy} [kg]	M_{yx} [kg]	M_{yy} [kg]
6,000	172	-28.99 ± 5.92	-33.57 ± 4.66	-21.02 ± 5.09	-34.29 ± 6.71
	345	-24.98 ± 11	-30.81 ± 4.51	-21.78 ± 7	-30.63 ± 8.44
	689	-27.53 ± 10.41	-26.91 ± 4.8	-20.35 ± 7.68	-24.53 ± 7.65
	1034	-28.33 ± 13.08	-22.95 ± 6.45	-17.75 ± 8.86	-21.48 ± 7.14
	1,724	-38.29 ± 12.76	-15.74 ± 8.34	-9.96 ± 9.71	-21.19 ± 4.65
9,000	172	-14.38 ± 7.28	-26.76 ± 4.4	-9.7 ± 8.55	-39.75 ± 7.95
	345	-13.81 ± 10.29	-23.48 ± 4.08	-2.76 ± 10.89	-36.1 ± 5.04
	689	-20.13 ± 11.83	-21.38 ± 3.85	3.58 ± 5.19	-26.24 ± 4.59
	1034	-23.25 ± 15.43	-21.07 ± 3.3	7.34 ± 6.62	-19.86 ± 4.86
	1,724	-33.88 ± 16.34	-18.37 ± 3.8	9.59 ± 7.36	-13.2 ± 5.26
12,000	172	-28.11 ± 9.59	-29.8 ± 12.78	-5.42 ± 12.18	-38.47 ± 9.66
	345	-21.12 ± 16.66	-21.55 ± 4.91	3.85 ± 13.39	-36.47 ± 6.01
	689	-28.61 ± 13.2	-17.48 ± 4.77	7.06 ± 7.51	-26.41 ± 5.03
	1034	-30.58 ± 15.51	-15.86 ± 4.4	9.12 ± 8.15	-19.73 ± 4.07
	1,724	-36.97 ± 15.51	-16.04 ± 5.54	15.86 ± 10.26	-5.97 ± 4.02

Table C. 12. R^2 value for [K][C][M] model for t_p = 11.5 mm.

Speed [RPM]	Unit Load [kPa]	Re (H_{xx})	Re (H_{xy})	Re (H_{yx})	Re (H_{yy})	Im (H_{xx})	Im (H_{xy})	Im (H_{yx})	Im (H_{yy})
6,000	172	0.959	0.981	0.944	0.962	0.999	0.874	0.861	0.996
	345	0.865	0.979	0.905	0.928	0.999	0.895	0.755	0.997
	689	0.873	0.969	0.873	0.91	0.999	0.92	0.775	0.995
	1034	0.822	0.926	0.797	0.899	0.995	0.942	0.796	0.992
	1724	0.898	0.777	0.508	0.953	0.975	0.957	0.861	0.993
9,000	172	0.793	0.973	0.558	0.961	0.996	0.967	0.54	0.989
	345	0.639	0.97	0.059	0.981	0.995	0.983	0.821	0.997
	689	0.74	0.968	0.318	0.97	0.988	0.971	0.745	0.996
	1034	0.69	0.976	0.547	0.943	0.98	0.976	0.743	0.995
	1724	0.808	0.958	0.625	0.86	0.954	0.962	0.755	0.989
12,000	172	0.894	0.841	0.162	0.94	0.987	0.928	0.694	0.965
	345	0.612	0.95	0.075	0.973	0.981	0.976	0.79	0.992
	689	0.822	0.929	0.464	0.964	0.969	0.953	0.876	0.995
	1034	0.792	0.927	0.551	0.958	0.96	0.95	0.866	0.995
	1724	0.848	0.891	0.701	0.684	954	0.947	0.906	0.983

Direct Virtual-Mass Coefficients

Figure C. 1 and Figure C. 2 show M_{xx} and M_{yy} , respectively, without any exclusions due to poor coefficient of determination (R^2) values.

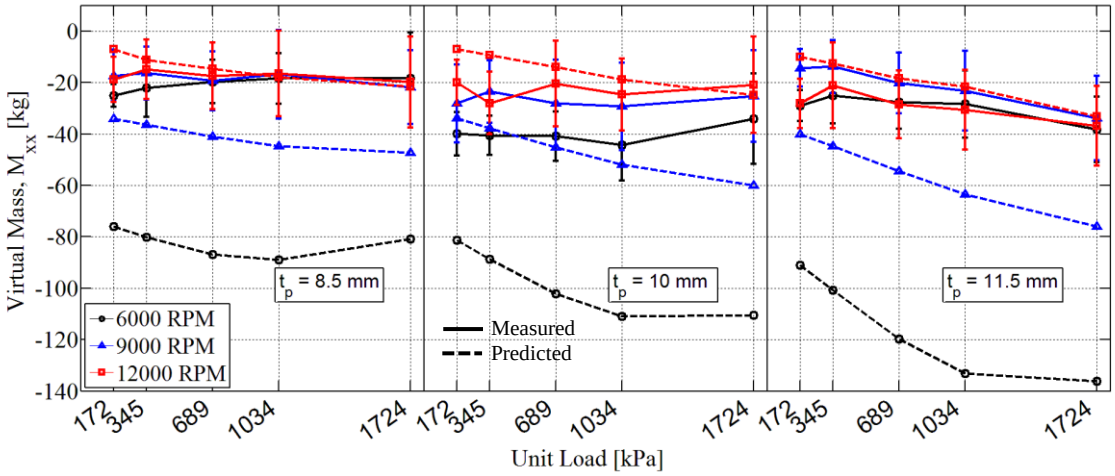

Figure C. 1. Measured (solid) and predicted (dashed) direct virtual-mass coefficients, M_{xx}, with uncertainties for three shaft speeds and increasing unit load for the different pad configurations without exclusions.

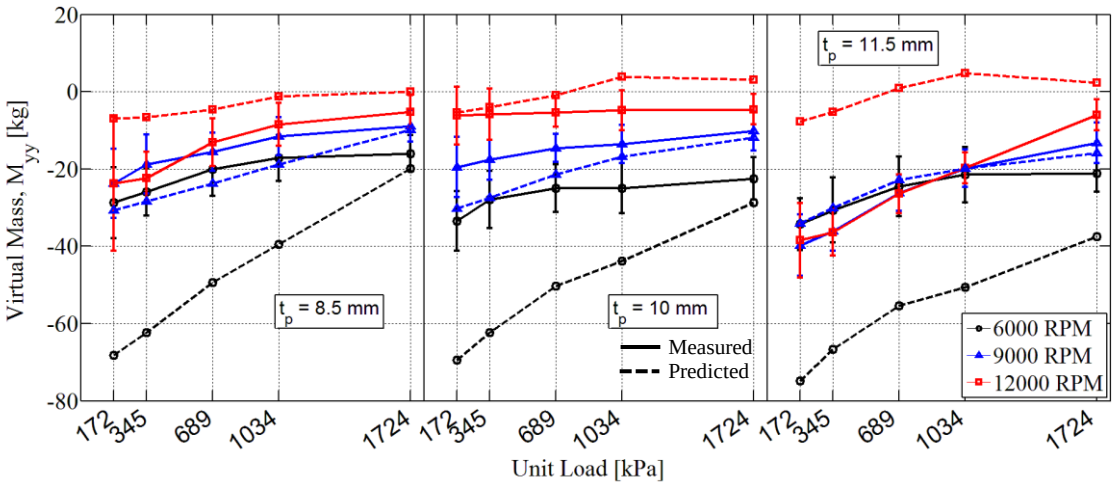

Figure C. 2. Measured (solid) and predicted (dashed) direct virtual-mass coefficient, M_{yy}, with uncertainties for three shaft speeds and increasing unit load for the different pad configurations without exclusions.

Cross-Coupled Rotordynamic Coefficient Plots

Figure C. 3 through Figure C. 8 show the measured cross-coupled stiffness, damping, and virtual-mas coefficients and the predictions using XL_TPJB© without any

coefficient of determination (R^2) exclusions. Figure C. 3 presents the results for K_{xy} and Figure C. 4 presents the results for K_{yx}.

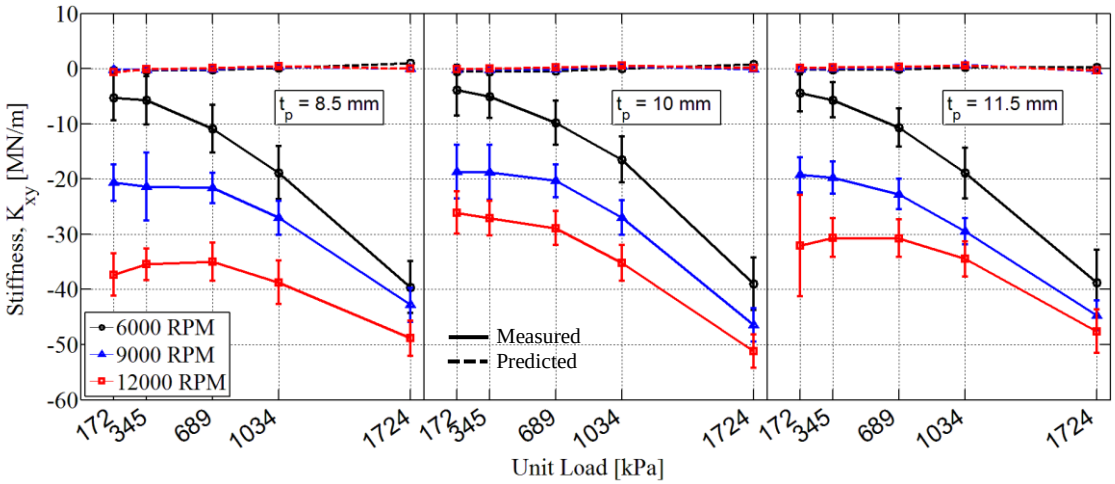

Figure C. 3. Measured (solid) and predicted (dashed) cross-coupled stiffness, K_{xy}, with uncertainties for three speeds and unit load for the different pad configurations.

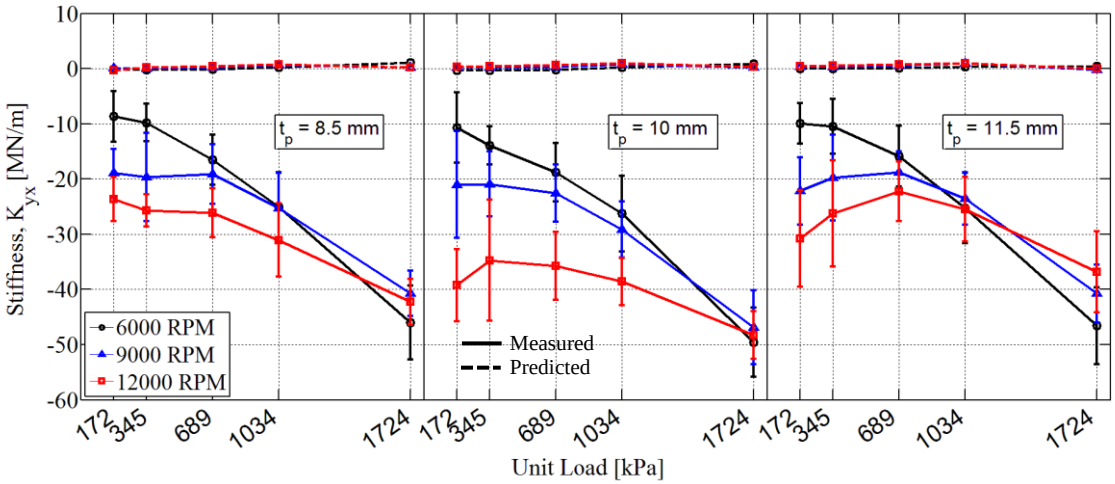

Figure C. 4. Measured (solid) and predicted (dashed) cross-coupled stiffness coefficient, K_{yx}, with uncertainties for three speeds and unit load for the different pad configurations.

Both plots show an increase in magnitude as the unit load increases. Increasing the speed increases the magnitude for the cross-coupled stiffness coefficients. At high loads, increasing the speed decreases the magnitude of K_{yx}. The cross-coupled stiffness coefficient predictions have a significantly smaller magnitude than the measured values. The predictions are nearly zero.

Figure C. 5 and Figure C. 6 present the results for C_{xy} and C_{yx}, respectively.

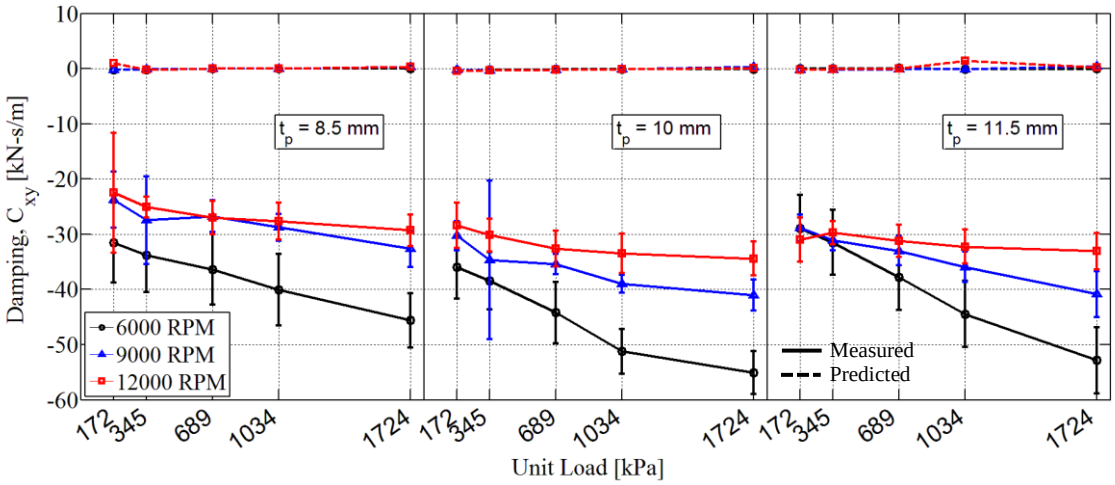

Figure C. 5. Measured (solid) and predicted (dashed) cross-coupled damping coefficient, C_{xy}, with uncertainties for three speeds and unit load for the different pad configurations.

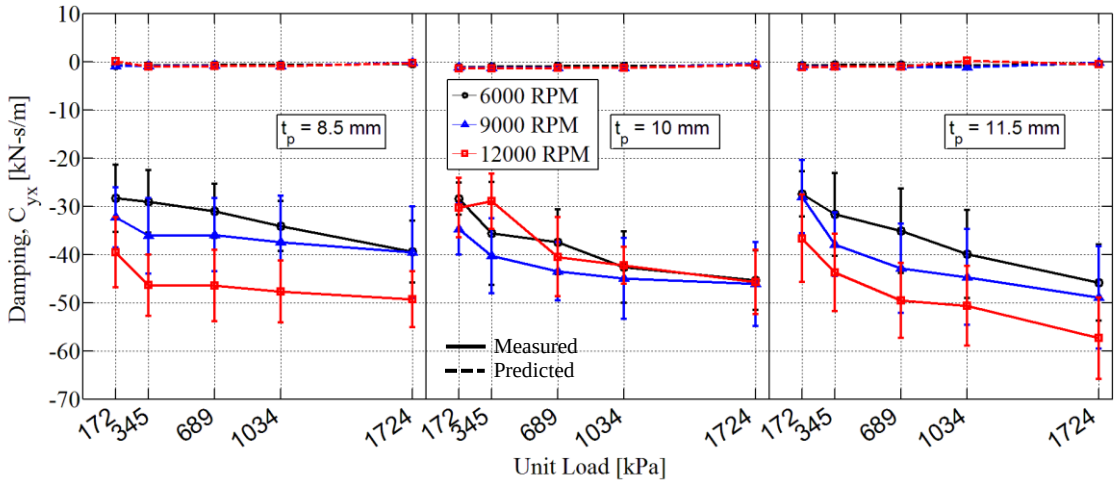

Figure C. 6. Measured (solid) and predicted (dashed) cross-coupled damping coefficient, C_{yx}, with uncertainties for three speeds and unit load for the different pad configurations.

Both plots show an increase in magnitude as the unit load increases. Increasing the speed increases the magnitude of C_{yx}. For C_{xy}, increasing the speed decreases the magnitude. The cross-coupled damping coefficient predictions have a significantly smaller magnitude than the measured values. The predictions are nearly zero.

Figure C. 7 and Figure C. 8 presents the results for M_{xy} and M_{yx}, respectively.

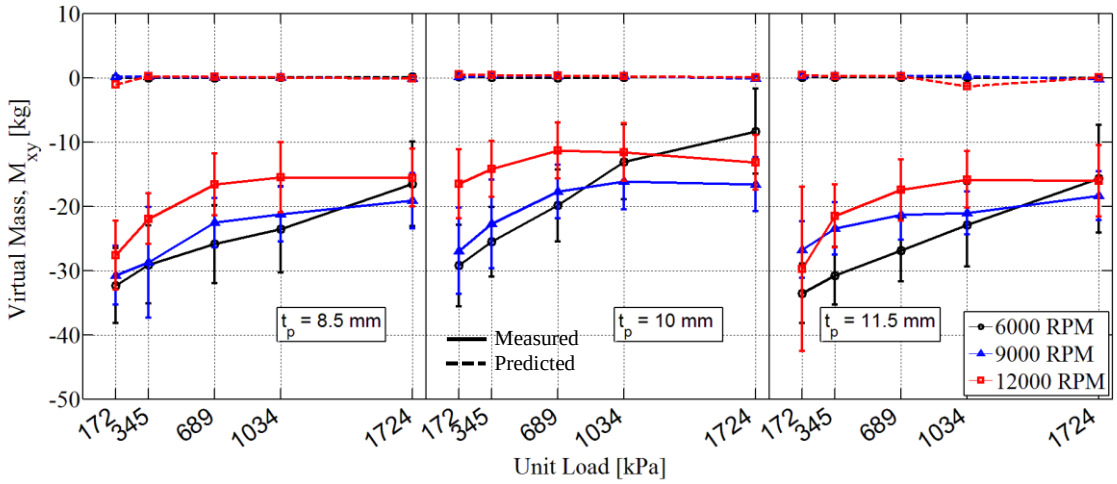

Figure C. 7. Measured (solid) and predicted (dashed) cross-coupled virtual-mass coefficient, M_{xy}, with uncertainties for three speeds and unit load for the different pad configurations.

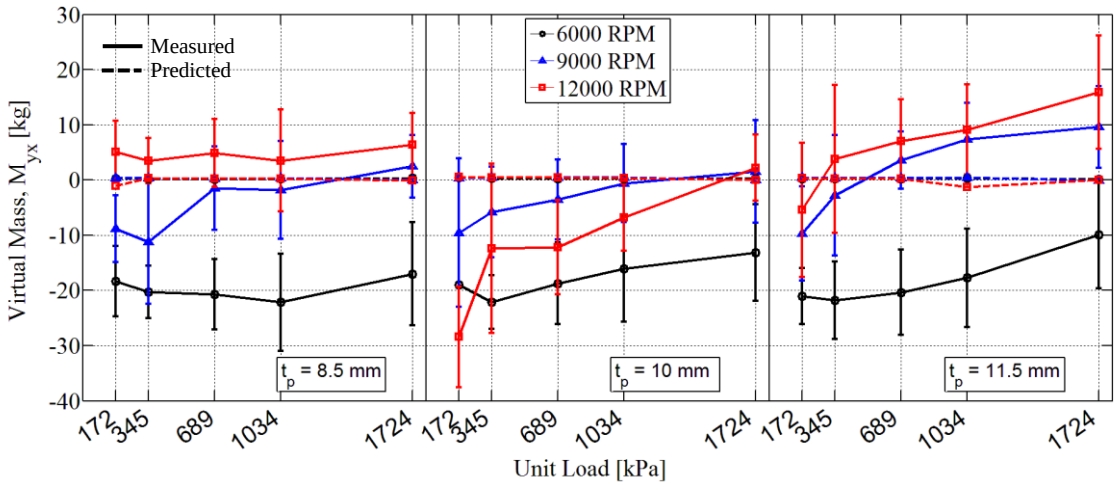

Figure C. 8. Measured (solid) and predicted (dashed) cross-coupled virtual-mass coefficient, M_{yx}, with uncertainties for three speeds and unit load for the different pad configurations.

In general, measured M_{xy} decreases in magnitude as the unit load increases and is always negative. M_{yx} is positive at high speed and high unit loads. For all pad configurations, the cross-coupled virtual-mass predictions are nearly zero.

APPENDIX D:

DYNAMIC-STIFFNESS COEFFICIENTS

Pad Configuration: t_p = 8.5 mm

Table D. 1. Measured dynamic-stiffness real and imaginary parts at 6,000 rpm and 172 kPa for t_p=8.5 mm.

Freq. [Hz.]	Re (H_{xx}) [MN/m]	Re (H_{xy}) [MN/m]	Re (H_{yx}) [MN/m]	Re (H_{yy}) [MN/m]	Im (H_{xx}) [MN/m]	Im (H_{xy}) [MN/m]	Im (H_{yx}) [MN/m]	Im (H_{yy}) [MN/m]
9.77	165.77 ± 0.35	-6.59 ± 0.38	-10.2 ± 0.26	114.79 ± 0.41	13.97 ± 0.52	-0.87 ± 0.13	0.76 ± 0.21	9.1 ± 0.33
19.53	168.96 ± 0.37	-6.21 ± 0.42	-8.97 ± 0.51	115.65 ± 0.27	26.16 ± 0.76	-2.96 ± 0.25	-2.22 ± 0.25	18.25 ± 0.24
29.30	170.91 ± 0.21	-4.63 ± 0.28	-7.49 ± 0.45	113.52 ± 0.36	39.1 ± 0.74	-3.89 ± 0.29	-5.32 ± 0.4	26.04 ± 0.3
39.06	170.84 ± 0.33	-4.46 ± 0.2	-8.3 ± 0.33	117.6 ± 0.47	51.33 ± 0.26	-4.48 ± 0.16	-8.35 ± 0.86	33.82 ± 0.31
48.83	172.53 ± 0.91	-3.05 ± 0.21	-7.73 ± 0.28	117.16 ± 0.48	61.96 ± 0.2	-5.42 ± 0.33	-10.89 ± 0.38	42.47 ± 0.59
58.59	173.38 ± 0.85	-3.91 ± 0.32	-10.45 ± 0.83	115.98 ± 0.44	75.35 ± 1.02	-5.86 ± 0.12	-10.85 ± 0.55	51.35 ± 0.55
68.36	178.53 ± 0.9	2.3 ± 0.48	-3.2 ± 0.31	121.68 ± 0.55	84.31 ± 0.42	-8.64 ± 0.33	-11.95 ± 0.39	60.64 ± 0.57
78.13	174.57 ± 0.88	-0.28 ± 0.35	-6.42 ± 0.99	125.35 ± 0.29	99.56 ± 0.56	-8.29 ± 0.23	-15.68 ± 0.88	65.93 ± 0.54
87.89	179.77 ± 2.71	5.41 ± 0.66	1 ± 0.85	119.03 ± 0.84	111.19 ± 0.87	-9.2 ± 0.44	-17.8 ± 1.71	83.65 ± 0.59
97.66	177.68 ± 2.85	7.35 ± 2.44	-4.5 ± 3.02	123.21 ± 0.95	122.46 ± 3.67	-12.73 ± 1.11	-14.81 ± 2.46	86.54 ± 1.74
107.42	179.29 ± 1.63	11.55 ± 0.86	-0.24 ± 0.97	123.74 ± 0.6	136.44 ± 0.54	-15.17 ± 0.43	-17.48 ± 1.27	98.23 ± 0.54
117.19	182.46 ± 0.72	14.74 ± 0.21	2.18 ± 0.3	126.7 ± 0.66	148.85 ± 0.46	-17.35 ± 0.28	-21.28 ± 0.52	106.8 ± 0.32
126.95	184.84 ± 0.31	17.5 ± 0.46	2.61 ± 0.17	128.46 ± 0.38	161.57 ± 0.8	-20.23 ± 0.11	-23.14 ± 0.46	116.98 ± 0.39
136.72	190.37 ± 0.83	22.64 ± 0.22	8.55 ± 0.62	132.83 ± 0.46	172.37 ± 0.68	-23.63 ± 0.23	-19.38 ± 0.79	127.52 ± 0.33
146.48	193.27 ± 1.22	24.21 ± 0.47	11.13 ± 0.34	132.99 ± 0.37	183.25 ± 0.46	-26.76 ± 0.28	-22.06 ± 0.37	134.81 ± 0.36
156.25	195.72 ± 0.67	33.27 ± 0.31	11.39 ± 0.3	131.78 ± 0.29	194.31 ± 0.7	-32.22 ± 0.34	-24.82 ± 0.43	145.41 ± 0.38
166.02	197.13 ± 0.61	28.47 ± 0.51	11.8 ± 0.89	155.09 ± 0.36	207.89 ± 1.05	-40.18 ± 0.32	-28.89 ± 0.48	159.13 ± 0.44
175.78	202.99 ± 0.97	29.89 ± 0.41	14.93 ± 0.46	149.68 ± 0.56	215.93 ± 0.84	-41.88 ± 0.21	-23.63 ± 0.53	167.99 ± 0.52
185.55	201.97 ± 0.63	35.2 ± 1	18.55 ± 0.81	160.28 ± 0.52	230.88 ± 1.26	-45.93 ± 0.5	-28.47 ± 1.29	175.36 ± 0.72
195.31	203.83 ± 10.68	41.6 ± 2.48	9.95 ± 4.91	153.31 ± 1.89	261.19 ± 7.68	-46.29 ± 1.98	-55.18 ± 7.56	192.94 ± 1.15
205.08	208.18 ± 2.26	39.75 ± 1.55	34.31 ± 1.4	158.93 ± 0.67	251.31 ± 0.81	-52.17 ± 0.64	-18.65 ± 1.04	194.22 ± 0.9
214.84	211.98 ± 0.78	54.93 ± 0.36	44.6 ± 0.95	147.14 ± 0.6	266.92 ± 0.53	-50.65 ± 0.5	-28.76 ± 1.02	231.82 ± 0.8
224.61	219.52 ± 0.95	38.47 ± 0.67	32.98 ± 0.83	185.14 ± 0.86	281.29 ± 1.02	-77.44 ± 0.49	-31.04 ± 0.46	210.07 ± 0.71
234.38	225.78 ± 0.48	42.45 ± 0.49	44.74 ± 0.44	194.04 ± 0.64	290.8 ± 0.42	-61.2 ± 0.49	-24.13 ± 0.58	239.54 ± 0.55
244.14	234.3 ± 0.99	42.06 ± 0.54	50.7 ± 1.17	173.6 ± 0.69	309.26 ± 0.88	-54.41 ± 0.35	-4.89 ± 1.07	251 ± 0.8
253.91	242.27 ± 0.32	60.26 ± 0.84	54.38 ± 0.53	193.75 ± 0.77	319.58 ± 0.76	-51.21 ± 0.35	-6.67 ± 0.29	276.88 ± 0.78
263.67	243.5 ± 0.2	83.89 ± 0.51	74.73 ± 0.8	216.12 ± 2.46	330.39 ± 0.28	-71.23 ± 1.29	17.12 ± 1.06	319.63 ± 1.72
273.44	257.46 ± 1.67	118.93 ± 1.21	123.9 ± 1.39	215.29 ± 1.5	363.71 ± 1.18	-67.62 ± 1.45	50.3 ± 0.99	331.95 ± 3.74
283.20	295.6 ± 1.28	60.26 ± 1.8	107.88 ± 10.32	324.71 ± 2.28	326.52 ± 5.75	-119.2 ± 0.91	-109.45 ± 5.05	309.33 ± 3.44
292.97	437.09 ± 5.91	69.2 ± 1.35	419.98 ± 9.26	224.02 ± 2.69	318.55 ± 6.11	-115.1 ± 1.44	-280.36 ± 13.99	262.71 ± 2.27

Table D. 2. Measured dynamic-stiffness real and imaginary parts at 6,000 rpm and 345 kPa for t_p=8.5 mm.

Freq. [Hz.]	Re (H_{xx}) [MN/m]	Re (H_{xy}) [MN/m]	Re (H_{yx}) [MN/m]	Re (H_{yy}) [MN/m]	Im (H_{xx}) [MN/m]	Im (H_{xy}) [MN/m]	Im (H_{yx}) [MN/m]	Im (H_{yy}) [MN/m]
9.77	186.31 ± 0.72	-6.95 ± 0.2	-8.95 ± 0.28	109.27 ± 0.26	13.36 ± 0.56	-0.58 ± 0.18	0.3 ± 0.81	8.9 ± 0.29
19.53	189.53 ± 0.31	-7.13 ± 0.13	-8.26 ± 0.37	109.64 ± 0.31	26.57 ± 0.59	-3.08 ± 0.29	-2.68 ± 0.65	16.51 ± 0.28
29.30	190.75 ± 0.56	-6.35 ± 0.4	-8.02 ± 0.21	107.98 ± 0.27	39.81 ± 0.33	-3.95 ± 0.23	-6.44 ± 0.38	24.37 ± 0.31
39.06	193.18 ± 0.42	-5.5 ± 0.2	-8.12 ± 0.26	110.49 ± 0.27	52.1 ± 0.47	-5.1 ± 0.21	-9 ± 0.5	31.97 ± 0.17
48.83	193.5 ± 0.75	-4.1 ± 0.29	-10.22 ± 0.59	110.23 ± 0.24	61.31 ± 0.4	-6.04 ± 0.35	-10.42 ± 0.43	39.31 ± 0.3
58.59	194.19 ± 1.11	-3.74 ± 0.39	-9.78 ± 0.74	110.06 ± 0.37	76.28 ± 0.99	-7.47 ± 0.25	-12.19 ± 0.38	48.28 ± 0.34
68.36	199.4 ± 0.43	0.81 ± 0.47	-4.6 ± 0.5	111.55 ± 0.49	87.11 ± 0.74	-7.81 ± 0.42	-11.31 ± 1.07	60.18 ± 0.28
78.13	195.76 ± 0.44	2.27 ± 0.54	-4.96 ± 0.71	119.97 ± 0.73	96.34 ± 1.33	-10.79 ± 0.17	-17.16 ± 0.88	68.67 ± 0.48
87.89	194.21 ± 2.35	-0.43 ± 0.66	2.78 ± 1.87	111.76 ± 0.47	109.1 ± 1.91	-11.36 ± 0.36	-25.46 ± 1.06	75.7 ± 0.44
97.66	197.7 ± 1.97	5.57 ± 1.95	-6.73 ± 2.84	115.8 ± 0.88	123.53 ± 4.56	-14.19 ± 0.89	-14.16 ± 1.73	84.54 ± 1.39
107.42	200.47 ± 1	9.25 ± 0.31	-2.49 ± 0.62	116.74 ± 0.51	137.35 ± 0.9	-16.73 ± 0.53	-19.85 ± 1.21	95.07 ± 0.56
117.19	202.68 ± 0.38	12.78 ± 0.19	-0.22 ± 0.27	119.14 ± 0.47	150.21 ± 0.18	-19.65 ± 0.38	-21.09 ± 0.23	103.25 ± 0.26
126.95	206.33 ± 0.43	16.11 ± 0.13	1.85 ± 0.6	120.88 ± 0.28	163.16 ± 0.76	-22.37 ± 0.27	-24.07 ± 0.99	114.47 ± 0.31
136.72	209.39 ± 0.56	19.05 ± 0.16	6.82 ± 0.82	124.91 ± 0.39	174.61 ± 0.68	-26.24 ± 0.18	-20.91 ± 0.43	123.61 ± 0.42
146.48	214.96 ± 0.47	22.54 ± 0.23	8.7 ± 0.08	127.12 ± 0.28	187.37 ± 0.96	-29.31 ± 0.18	-23.1 ± 0.62	131.58 ± 0.29
156.25	217.5 ± 0.98	29.45 ± 0.19	11.65 ± 0.37	126.54 ± 0.38	196.57 ± 0.91	-34.61 ± 0.39	-27.03 ± 0.78	137.43 ± 0.31
166.02	221.09 ± 0.98	24.48 ± 0.11	10.43 ± 0.62	140.19 ± 0.37	208.39 ± 0.54	-40.69 ± 0.2	-28.87 ± 0.38	149.48 ± 0.37
175.78	223.29 ± 0.54	27.06 ± 0.29	15.49 ± 0.71	139.38 ± 0.34	217.05 ± 1.35	-44.24 ± 0.53	-25.11 ± 0.34	160.73 ± 0.34
185.55	225.5 ± 1.92	29.96 ± 0.47	16.69 ± 0.85	147.36 ± 0.55	232.76 ± 1.86	-48.12 ± 1.05	-27.1 ± 1.5	170.39 ± 0.49
195.31	204.99 ± 10.88	34.13 ± 1.93	21.76 ± 10.61	146.56 ± 2.66	246.74 ± 8.12	-48.58 ± 2.09	-51.18 ± 11.27	183.9 ± 2.15
205.08	232.14 ± 0.43	33.22 ± 0.69	28.55 ± 1.15	153.16 ± 0.73	254.92 ± 2.3	-55.87 ± 1.37	-23.88 ± 0.73	184.97 ± 0.62
214.84	237.68 ± 0.6	36.47 ± 0.36	36.34 ± 0.56	159.52 ± 0.44	267.17 ± 0.78	-57.8 ± 0.69	-26.62 ± 0.54	196.14 ± 0.52
224.61	238.49 ± 0.49	53.3 ± 0.44	44.23 ± 0.89	115.27 ± 0.66	279.61 ± 0.55	-79.61 ± 0.48	-33.79 ± 1.32	261.08 ± 0.68
234.38	248.9 ± 0.87	33.57 ± 0.3	38.1 ± 0.69	176.7 ± 0.43	293.47 ± 0.99	-66.55 ± 0.57	-33.61 ± 0.6	221.83 ± 0.34
244.14	258.78 ± 2.14	36.93 ± 0.37	44.08 ± 1.34	168.81 ± 0.65	304.94 ± 2.3	-65.26 ± 0.66	-23.46 ± 1.25	232.96 ± 0.58
253.91	262.66 ± 1	38.62 ± 0.34	40.92 ± 0.3	190.8 ± 0.65	314.96 ± 0.46	-70.17 ± 0.61	-29.73 ± 0.51	242.45 ± 0.48
263.67	266.28 ± 0.17	44.03 ± 0.4	53.1 ± 0.27	195.53 ± 0.37	327.14 ± 0.32	-62.66 ± 0.55	-17 ± 0.3	238.97 ± 0.34
273.44	270.58 ± 0.34	60.02 ± 0.13	63.19 ± 0.59	182.49 ± 0.53	340.82 ± 0.58	-70.72 ± 0.67	-9.99 ± 0.32	239.49 ± 0.41
283.20	275.25 ± 0.46	62.24 ± 0.64	77.23 ± 0.45	217.34 ± 0.9	363.87 ± 1.74	-69.14 ± 0.64	-16.56 ± 0.95	276.72 ± 0.5
292.97	289.02 ± 0.21	52.47 ± 0.32	82.84 ± 0.29	245.04 ± 0.75	380.13 ± 0.63	-83.32 ± 0.43	13.25 ± 0.1	295.98 ± 0.39

Table D. 3. Measured dynamic-stiffness real and imaginary parts at 6,000 rpm and 689 kPa for t_p=8.5 mm.

Freq. [Hz.]	Re (H_{xx}) [MN/m]	Re (H_{xy}) [MN/m]	Re (H_{yx}) [MN/m]	Re (H_{yy}) [MN/m]	Im (H_{xx}) [MN/m]	Im (H_{xy}) [MN/m]	Im (H_{yx}) [MN/m]	Im (H_{yy}) [MN/m]
9.77	236.53 ± 0.9	-12.56 ± 0.09	-13.66 ± 0.41	111.26 ± 0.3	14.94 ± 0.6	-1.2 ± 0.17	1.69 ± 0.76	7.74 ± 0.27
19.53	238.97 ± 0.82	-12.51 ± 0.1	-13.18 ± 0.21	110.94 ± 0.32	26.65 ± 0.33	-3.2 ± 0.18	-1.88 ± 0.45	13.71 ± 0.25
29.30	240.2 ± 0.53	-13.13 ± 0.11	-11.97 ± 0.73	111.1 ± 0.27	41 ± 0.52	-4 ± 0.23	-6 ± 0.78	19.64 ± 0.39
39.06	241.95 ± 0.6	-10.85 ± 0.35	-12.5 ± 0.33	110.17 ± 0.38	53.36 ± 0.51	-6.37 ± 0.12	-9.37 ± 0.46	28.1 ± 0.23
48.83	245.15 ± 0.38	-9.95 ± 0.26	-13.67 ± 0.34	110.4 ± 0.26	64.89 ± 0.75	-7.91 ± 0.14	-11.13 ± 0.28	35.6 ± 0.26
58.59	246.63 ± 0.29	-9.66 ± 0.19	-14.35 ± 0.34	109.39 ± 0.29	74.39 ± 0.57	-8.13 ± 0.22	-13.83 ± 0.38	43.76 ± 0.34
68.36	244.3 ± 0.3	-7.8 ± 0.18	-16.1 ± 0.82	107.15 ± 0.37	89.59 ± 0.55	-7.71 ± 0.24	-12.08 ± 0.54	55.95 ± 0.22
78.13	247.03 ± 0.96	-2.25 ± 0.43	-10.01 ± 0.75	109.45 ± 0.47	97.24 ± 1.07	-10.87 ± 0.28	-21.18 ± 0.7	58.86 ± 0.4
87.89	249.29 ± 1.94	-1.88 ± 0.3	-10.2 ± 0.95	111.65 ± 0.41	106.92 ± 0.96	-12.77 ± 0.59	-24.63 ± 1.06	68.98 ± 0.35
97.66	249.03 ± 1.39	0.94 ± 0.62	-16.19 ± 2.88	114.67 ± 0.48	118.73 ± 6.82	-16.23 ± 0.99	-18.97 ± 0.69	77 ± 0.7
107.42	250.22 ± 0.85	3.33 ± 0.5	-10.45 ± 0.84	115.15 ± 0.44	137.7 ± 1.2	-18.84 ± 0.38	-22.06 ± 0.43	86.4 ± 0.31
117.19	253.1 ± 0.35	6.41 ± 0.36	-9.85 ± 0.16	117.33 ± 0.35	151.62 ± 0.45	-22.68 ± 0.07	-25.28 ± 0.34	94.42 ± 0.23
126.95	255.68 ± 0.63	9.19 ± 0.35	-7.18 ± 0.69	118.25 ± 0.43	166.64 ± 0.51	-26.23 ± 0.16	-29.36 ± 1.01	103.3 ± 0.35
136.72	258.39 ± 0.69	11.2 ± 0.14	0.09 ± 0.77	122.91 ± 0.27	169.55 ± 0.73	-29.85 ± 0.18	-19.2 ± 0.72	111.25 ± 0.27
146.48	262.77 ± 0.73	13.29 ± 0.31	1.37 ± 0.38	124.23 ± 0.34	182.98 ± 0.39	-33.23 ± 0.13	-23.4 ± 0.57	119.4 ± 0.23
156.25	263.7 ± 0.67	20.25 ± 0.21	7.02 ± 0.52	117.86 ± 0.29	194.93 ± 0.58	-35.81 ± 0.25	-28.07 ± 0.88	114.5 ± 0.26
166.02	267.2 ± 0.59	15.35 ± 0.33	4.86 ± 1.11	135.01 ± 0.31	207.67 ± 1.06	-42.88 ± 0.19	-32.5 ± 0.5	132.35 ± 0.38
175.78	270.62 ± 0.27	16.96 ± 0.26	11.75 ± 0.71	131.3 ± 0.33	212.09 ± 0.87	-45.72 ± 0.25	-25.62 ± 1.04	143.45 ± 0.35
185.55	268.79 ± 1.15	19.63 ± 0.5	12.15 ± 0.5	139.92 ± 0.38	232.95 ± 1.48	-50.73 ± 0.44	-35.49 ± 1.42	155.75 ± 0.5
195.31	257.43 ± 5.62	26.31 ± 1.29	15.47 ± 4.64	137.7 ± 1.11	242.73 ± 8.05	-51.23 ± 1.03	-45.62 ± 4.14	167.03 ± 0.73
205.08	282.04 ± 1.84	23.14 ± 1.04	23.71 ± 1.08	145.26 ± 0.84	252.94 ± 3.75	-60.37 ± 0.84	-28.94 ± 1.2	167.05 ± 0.31
214.84	285.6 ± 0.61	26.81 ± 0.52	26.92 ± 0.45	157 ± 0.47	266.03 ± 0.67	-62.63 ± 0.26	-31.12 ± 0.4	178.88 ± 0.36
224.61	288.99 ± 1.14	40.56 ± 0.43	33.49 ± 0.36	61.75 ± 0.31	276.18 ± 0.87	-63.59 ± 0.5	-29.03 ± 0.3	179.2 ± 0.37
234.38	300.19 ± 1.84	24.44 ± 0.58	26.58 ± 1.16	161.92 ± 0.42	291.56 ± 2.07	-72.83 ± 0.38	-42.97 ± 0.68	203.21 ± 0.67
244.14	301.8 ± 1.3	26.54 ± 0.45	38.39 ± 1.4	161.62 ± 0.44	304.03 ± 1.01	-70.26 ± 0.26	-38.9 ± 0.53	204.65 ± 0.45
253.91	311.75 ± 1.7	30.83 ± 0.77	39.28 ± 0.93	180.23 ± 0.63	312.72 ± 1.82	-84.49 ± 0.86	-38.61 ± 0.7	238.33 ± 0.75
263.67	314.54 ± 0.65	29.62 ± 0.33	41.47 ± 0.24	188.8 ± 0.66	324.04 ± 1.44	-72.96 ± 0.46	-32.95 ± 0.7	214.19 ± 0.28
273.44	322.69 ± 0.45	45.53 ± 0.4	46.8 ± 0.21	140.32 ± 0.54	335.35 ± 0.54	-71.54 ± 0.5	-26.78 ± 0.33	187.89 ± 0.4
283.20	326.32 ± 0.49	34.97 ± 0.23	48.47 ± 0.81	210.33 ± 0.43	355.81 ± 1.1	-80.86 ± 0.22	-45.37 ± 0.72	235.27 ± 0.37
292.97	339.22 ± 0.41	71.84 ± 0.63	59.55 ± 0.3	133.68 ± 0.71	359.74 ± 0.46	-81.22 ± 0.48	-14.99 ± 0.13	315.77 ± 0.34

Table D. 4. Measured dynamic-stiffness real and imaginary parts at 6,000 rpm and 1034 kPa for t_p=8.5 mm.

Freq. [Hz.]	Re (H_{xx}) [MN/m]	Re (H_{xy}) [MN/m]	Re (H_{yx}) [MN/m]	Re (H_{yy}) [MN/m]	Im (H_{xx}) [MN/m]	Im (H_{xy}) [MN/m]	Im (H_{yx}) [MN/m]	Im (H_{yy}) [MN/m]
9.77	288.32 ± 0.85	-21.19 ± 0.18	-21.86 ± 0.79	121.47 ± 0.43	14.86 ± 0.85	-0.42 ± 0.2	3.21 ± 0.39	7.25 ± 0.3
19.53	291.71 ± 0.39	-21.13 ± 0.36	-20.33 ± 0.43	120.64 ± 0.39	29.55 ± 0.53	-3.13 ± 0.19	-2.65 ± 0.39	11.14 ± 0.22
29.30	294.79 ± 0.72	-22.38 ± 0.21	-19.65 ± 0.24	122.77 ± 0.26	43 ± 0.35	-3.85 ± 0.23	-5.5 ± 0.26	16.21 ± 0.3
39.06	298.7 ± 0.92	-19.45 ± 0.3	-20.4 ± 0.2	119.68 ± 0.42	53.34 ± 1.14	-6.71 ± 0.26	-9.46 ± 0.42	24.74 ± 0.31
48.83	299.73 ± 1.33	-18.47 ± 0.41	-20.72 ± 0.58	119.35 ± 0.45	64.44 ± 0.7	-8.54 ± 0.3	-12.35 ± 0.69	31.95 ± 0.25
58.59	301.99 ± 0.61	-17.54 ± 0.49	-21.55 ± 0.39	119.04 ± 0.43	76.75 ± 1.09	-8.88 ± 0.3	-15.19 ± 0.51	40.5 ± 0.29
68.36	299.85 ± 0.51	-15.81 ± 0.21	-25.27 ± 0.33	116.86 ± 0.5	87.62 ± 0.84	-10.33 ± 0.23	-18.99 ± 0.88	45.36 ± 0.38
78.13	302.3 ± 0.49	-10.77 ± 0.33	-17.51 ± 0.94	119.97 ± 0.39	97.39 ± 1.07	-10.71 ± 0.25	-22.65 ± 0.88	51.77 ± 0.24
87.89	307.12 ± 1.83	-9.37 ± 0.56	-18.17 ± 1.26	121.86 ± 0.34	109.55 ± 2.39	-13.91 ± 0.51	-24.54 ± 1.02	61.32 ± 0.33
97.66	310.41 ± 6.6	-7.15 ± 1.5	-23.38 ± 2.5	123.63 ± 0.45	123.65 ± 5.97	-19.51 ± 0.48	-23.47 ± 3.37	70.03 ± 0.74
107.42	305.16 ± 1.89	-5.42 ± 0.31	-20.05 ± 0.34	124.91 ± 0.43	133.51 ± 1.58	-21.94 ± 0.5	-25.1 ± 1.51	77.97 ± 0.51
117.19	308.57 ± 0.64	-2.11 ± 0.26	-19.99 ± 0.43	126 ± 0.35	148.45 ± 0.75	-25.88 ± 0.33	-27.2 ± 0.59	85.72 ± 0.53
126.95	312.15 ± 1.53	0.4 ± 0.18	-16.47 ± 1.36	126.89 ± 0.25	162.72 ± 0.52	-30 ± 0.19	-30.74 ± 0.63	93.93 ± 0.39
136.72	313.89 ± 0.97	2.55 ± 0.22	-9.58 ± 0.56	129.53 ± 0.36	166.27 ± 0.84	-34.55 ± 0.23	-24.67 ± 0.63	104.59 ± 0.33
146.48	317.44 ± 0.61	3.06 ± 0.15	-7.7 ± 0.35	132.67 ± 0.26	178.37 ± 0.47	-36.78 ± 0.14	-24.97 ± 0.47	107.93 ± 0.3
156.25	317.42 ± 0.63	9.45 ± 0.22	-1.55 ± 0.44	129.31 ± 0.25	189.24 ± 0.36	-40.36 ± 0.14	-29.61 ± 0.45	102.56 ± 0.23
166.02	319.69 ± 0.65	4.04 ± 0.16	-2.13 ± 0.77	143.46 ± 0.36	203.01 ± 0.78	-47.06 ± 0.23	-35.15 ± 0.35	120.05 ± 0.34
175.78	321.03 ± 0.8	6.05 ± 0.21	4.27 ± 0.54	137.59 ± 0.31	207.4 ± 1.03	-48.55 ± 0.26	-30.58 ± 0.5	128.44 ± 0.36
185.55	324.04 ± 3.76	9.03 ± 0.49	1.61 ± 2.2	144.78 ± 0.5	229.73 ± 0.35	-54.99 ± 0.52	-39.29 ± 1.76	142.21 ± 0.61
195.31	311.5 ± 7.99	13.98 ± 1.51	17.43 ± 1.67	142.9 ± 0.91	246.6 ± 11.76	-55.02 ± 1.62	-47.27 ± 5.55	149.12 ± 0.72
205.08	331.53 ± 4.53	12.1 ± 2.38	17.1 ± 1.35	152.8 ± 0.43	248.3 ± 2.26	-63.11 ± 2.08	-35.34 ± 1.98	151.64 ± 1.29
214.84	337.9 ± 0.87	15.64 ± 0.37	18.25 ± 0.42	161.79 ± 0.33	261.37 ± 0.51	-65.91 ± 0.68	-38.52 ± 0.48	164.54 ± 0.34
224.61	342.15 ± 0.57	22.71 ± 0.43	20.58 ± 0.57	84.14 ± 0.39	274.11 ± 1.09	-67.49 ± 0.41	-38.52 ± 0.26	147.88 ± 0.27
234.38	350 ± 1.07	12.95 ± 0.36	14.3 ± 0.58	163.92 ± 0.39	285.49 ± 0.95	-75 ± 0.38	-52.37 ± 0.84	185.79 ± 0.4
244.14	354.01 ± 0.52	14.56 ± 0.54	25.36 ± 1.27	163.33 ± 0.8	298.65 ± 2.76	-72.14 ± 0.41	-46.4 ± 0.64	182.18 ± 1.01
253.91	366.56 ± 1.34	19.8 ± 0.54	24.26 ± 0.68	162.97 ± 0.53	307.23 ± 0.61	-81.64 ± 0.36	-45.97 ± 0.25	201.07 ± 0.52
263.67	369.41 ± 0.66	17.4 ± 0.43	28.17 ± 0.41	192.95 ± 0.34	319.64 ± 0.54	-79.13 ± 0.34	-45.05 ± 0.42	193.2 ± 0.4
273.44	375.98 ± 0.68	26.72 ± 0.27	33.15 ± 0.54	157.6 ± 0.39	328.92 ± 0.19	-77.75 ± 0.19	-42.32 ± 0.22	155.02 ± 0.27
283.20	380.42 ± 1.44	19.61 ± 0.38	32.99 ± 0.5	213 ± 0.28	347.15 ± 1.29	-89.05 ± 0.51	-58.26 ± 0.4	215.7 ± 0.57
292.97	392.5 ± 0.9	26.32 ± 0.42	37.63 ± 0.6	168.78 ± 0.46	350.09 ± 0.48	-77.66 ± 0.41	-40.22 ± 0.81	222.83 ± 0.3

Table D. 5. Measured dynamic-stiffness real and imaginary parts at 6,000 rpm and 1,724 kPa for t_p=8.5 mm.

Freq. [Hz.]	Re (H_{xx}) [MN/m]	Re (H_{xy}) [MN/m]	Re (H_{yx}) [MN/m]	Re (H_{yy}) [MN/m]	Im (H_{xx}) [MN/m]	Im (H_{xy}) [MN/m]	Im (H_{yx}) [MN/m]	Im (H_{yy}) [MN/m]
9.77	392.05 ± 1.07	-43.58 ± 0.23	-42.64 ± 1.22	150.18 ± 0.5	21.35 ± 1.04	-0.56 ± 0.2	0.54 ± 0.53	8.33 ± 0.43
19.53	395.43 ± 0.39	-41.73 ± 0.08	-40.55 ± 0.9	149.36 ± 0.35	31.88 ± 0.52	-2.38 ± 0.25	-2.82 ± 0.44	9.25 ± 0.23
29.30	397.35 ± 0.79	-45.05 ± 0.35	-40.93 ± 0.89	154.67 ± 0.55	45.6 ± 0.23	-4.02 ± 0.46	-6.36 ± 0.72	14.65 ± 0.4
39.06	398.73 ± 0.77	-40.24 ± 0.25	-41.6 ± 0.5	150.55 ± 0.27	58.42 ± 0.61	-8.68 ± 0.19	-11.45 ± 0.34	22.56 ± 0.33
48.83	402.43 ± 0.6	-39.54 ± 0.25	-43.63 ± 0.64	150.75 ± 0.51	70.73 ± 0.71	-11.38 ± 0.14	-13.68 ± 0.42	28 ± 0.39
58.59	406.74 ± 0.85	-37.97 ± 0.34	-43.37 ± 1.1	149.5 ± 0.29	82.94 ± 0.98	-11.99 ± 0.49	-19.11 ± 0.3	36.08 ± 0.37
68.36	407.41 ± 0.95	-35.64 ± 0.46	-46.55 ± 1.06	151.29 ± 0.54	92.29 ± 1.08	-14.58 ± 0.38	-23.33 ± 0.19	39.09 ± 0.31
78.13	412.7 ± 0.82	-30.95 ± 0.13	-39.78 ± 1.24	151.62 ± 0.29	102.54 ± 1.35	-15.94 ± 0.21	-23.7 ± 1.53	45.94 ± 0.38
87.89	414.88 ± 2.02	-31.32 ± 0.53	-42.14 ± 2.35	153.99 ± 0.61	104.22 ± 4.51	-18.35 ± 0.66	-29.04 ± 3.01	52.76 ± 0.46
97.66	420.54 ± 13.15	-30.14 ± 1.94	-47.43 ± 3.04	155.91 ± 1.1	114.72 ± 5.17	-24.97 ± 2.02	-23.79 ± 5.09	60.82 ± 1.07
107.42	419.05 ± 2.3	-30.08 ± 0.94	-43.76 ± 0.5	156.89 ± 0.34	131.29 ± 2.95	-27.73 ± 0.52	-28.57 ± 1.53	68.9 ± 0.57
117.19	420.61 ± 0.85	-27.36 ± 0.49	-44.09 ± 0.97	158.22 ± 0.4	143.05 ± 1.38	-33.17 ± 0.49	-29.4 ± 0.98	75.14 ± 0.4
126.95	422.16 ± 1.35	-26.26 ± 0.37	-39.69 ± 0.54	158.42 ± 0.34	157.92 ± 2.44	-37.35 ± 0.36	-33.61 ± 1.58	81.98 ± 0.34
136.72	422.28 ± 1.05	-24.58 ± 0.3	-31.25 ± 0.39	159.79 ± 0.39	160.25 ± 1.92	-40.02 ± 0.25	-27.39 ± 0.46	86.95 ± 0.3
146.48	424.75 ± 1.29	-25.37 ± 0.29	-31.35 ± 0.66	165.42 ± 0.34	169.54 ± 0.99	-42.63 ± 0.34	-30.48 ± 0.93	94.03 ± 0.38
156.25	424.65 ± 1.39	-19.79 ± 0.3	-25.23 ± 1.1	163.41 ± 0.35	181.38 ± 1.04	-46.83 ± 0.24	-32.96 ± 0.93	86.15 ± 0.32
166.02	427.1 ± 0.54	-25.13 ± 0.4	-29.82 ± 1.05	172.92 ± 0.41	194.46 ± 0.53	-52.15 ± 0.17	-37 ± 0.11	104.54 ± 0.28
175.78	429.11 ± 1.91	-24.53 ± 0.24	-23.08 ± 1.31	167.56 ± 0.32	194.87 ± 0.46	-52.61 ± 0.2	-37.19 ± 1.26	110.98 ± 0.33
185.55	433.45 ± 4.07	-19.06 ± 0.89	-28.17 ± 2.31	173.64 ± 0.49	231.58 ± 4.65	-59.98 ± 0.61	-44.72 ± 2.92	124.86 ± 0.62
195.31	404.62 ± 9.67	-15.36 ± 1.55	-11.81 ± 4.72	169.95 ± 1	226.87 ± 13.74	-54.84 ± 2.04	-61.02 ± 6.41	127.92 ± 0.83
205.08	432.84 ± 4.89	-18.51 ± 1.59	-11.86 ± 2.08	178.75 ± 0.8	236.56 ± 3.16	-62.65 ± 0.8	-45.28 ± 1.68	132.29 ± 0.87
214.84	440.16 ± 0.73	-13.88 ± 0.3	-8.76 ± 0.25	187.55 ± 0.5	248.35 ± 0.34	-66.32 ± 0.35	-46.94 ± 0.98	139.79 ± 0.47
224.61	444.82 ± 0.99	-8.36 ± 0.19	-8.16 ± 0.2	119.06 ± 0.34	259.08 ± 0.57	-70.45 ± 0.13	-47.89 ± 0.64	121.49 ± 0.24
234.38	453.87 ± 1.54	-16.53 ± 0.66	-13.6 ± 0.92	188.95 ± 0.62	269.4 ± 0.81	-75.43 ± 0.29	-58.82 ± 0.97	157.32 ± 0.42
244.14	461.79 ± 1.46	-16.48 ± 0.4	-3.51 ± 0.73	192.94 ± 0.54	275.44 ± 1.91	-73.17 ± 0.29	-51.86 ± 0.24	152.96 ± 0.51
253.91	466.14 ± 0.94	-9.06 ± 0.39	-4.02 ± 0.24	186.05 ± 0.36	282.67 ± 0.77	-80.94 ± 0.53	-52.1 ± 0.64	170.07 ± 0.35
263.67	466.12 ± 0.5	-11.24 ± 0.13	2.05 ± 0.33	213.15 ± 0.42	297.5 ± 0.34	-80.81 ± 0.27	-52.72 ± 0.34	166.67 ± 0.35
273.44	472.67 ± 0.26	-6.4 ± 0.13	4.04 ± 0.34	192.66 ± 0.33	306.66 ± 0.26	-82.01 ± 0.26	-53.7 ± 0.39	122.05 ± 0.42
283.20	472.58 ± 0.95	-10.86 ± 0.3	6.19 ± 0.25	237.18 ± 0.45	323.82 ± 0.92	-92.18 ± 0.57	-66.29 ± 0.48	187.47 ± 0.48
292.97	484.63 ± 1.02	-7.08 ± 0.46	10.51 ± 0.56	198.21 ± 0.47	320.17 ± 0.77	-82.22 ± 0.37	-53.3 ± 0.21	185.45 ± 0.32

Table D. 6. Measured dynamic-stiffness real and imaginary parts at 9,000 rpm and 172 kPa for t_p=8.5 mm.

Freq. [Hz.]	Re (H_{xx}) [MN/m]	Re (H_{xy}) [MN/m]	Re (H_{yx}) [MN/m]	Re (H_{yy}) [MN/m]	Im (H_{xx}) [MN/m]	Im (H_{xy}) [MN/m]	Im (H_{yx}) [MN/m]	Im (H_{yy}) [MN/m]
9.77	212.12 ± 1.68	-20.25 ± 0.99	-19.12 ± 0.91	152.46 ± 0.44	11.1 ± 0.85	0.33 ± 0.43	0.79 ± 0.32	7.33 ± 0.3
19.53	209.06 ± 0.24	-18.45 ± 0.63	-16.97 ± 1.1	154.48 ± 0.38	25.98 ± 0.63	-1.67 ± 0.58	-5.02 ± 0.69	17.22 ± 0.53
29.30	214.32 ± 1.67	-17.14 ± 0.86	-16.46 ± 0.81	151.76 ± 0.76	37.64 ± 0.67	-4.74 ± 0.3	-6.84 ± 0.45	25.36 ± 0.35
39.06	215.48 ± 0.96	-19.11 ± 0.32	-18.28 ± 0.62	157.61 ± 0.68	48.58 ± 0.8	-5.9 ± 0.47	-12.23 ± 0.83	31.99 ± 0.8
48.83	214.53 ± 0.46	-18.75 ± 1.12	-16.53 ± 2.06	158.36 ± 1.14	55.26 ± 1.21	-6.03 ± 0.85	-15.95 ± 0.93	39.56 ± 1.03
58.59	217.79 ± 2.08	-18.94 ± 0.7	-22.09 ± 1.15	158.08 ± 1.21	67.25 ± 2.38	-5.64 ± 1	-15.42 ± 1.35	46.97 ± 0.68
68.36	223.12 ± 1.56	-17.92 ± 0.76	-17.24 ± 1.08	160.13 ± 0.57	77.56 ± 1.01	-7.45 ± 1.18	-21.55 ± 0.99	52.04 ± 1.25
78.13	227.77 ± 0.45	-15.34 ± 0.54	-16.74 ± 1.35	167.92 ± 0.47	85.47 ± 2.59	-7.14 ± 0.93	-22.48 ± 1.47	59.95 ± 1.69
87.89	228.05 ± 2.25	-10.91 ± 1.2	-12.79 ± 1.63	164.37 ± 1.28	99.36 ± 1.8	-9.46 ± 0.73	-22.38 ± 2.03	70.13 ± 0.51
97.66	228.44 ± 1.3	-10.25 ± 0.49	-16.77 ± 0.45	167.65 ± 0.69	105.56 ± 0.89	-10.66 ± 1.09	-22.27 ± 2.09	71.86 ± 0.93
107.42	227.98 ± 1.09	-6.83 ± 0.93	-16.14 ± 0.6	167.05 ± 0.75	113.25 ± 0.64	-11.39 ± 0.59	-25.29 ± 1.28	79.88 ± 1.05
117.19	228.77 ± 1.04	-3.65 ± 0.21	-14.54 ± 1.01	166.32 ± 0.58	121.57 ± 0.82	-12.04 ± 0.24	-28.77 ± 0.83	86.41 ± 0.65
126.95	231.82 ± 1.21	0.06 ± 0.46	-15.14 ± 0.8	168.51 ± 0.7	134.91 ± 0.81	-15.77 ± 0.52	-30.6 ± 2.18	95.5 ± 0.76
136.72	232.36 ± 1.89	4.98 ± 0.8	-11.38 ± 1.22	170.99 ± 0.91	142.63 ± 1.05	-17.31 ± 0.53	-24.68 ± 0.72	103.13 ± 0.49
146.48	233.66 ± 1.77	7.12 ± 1.19	-9.76 ± 1.65	170.43 ± 1.35	149.2 ± 2.15	-18.27 ± 1.75	-29.27 ± 2.18	110.27 ± 1.03
156.25	235.27 ± 1.68	15.04 ± 0.56	-11.07 ± 0.84	169.32 ± 0.98	160.42 ± 2.52	-22.47 ± 0.98	-34.07 ± 2.99	113.61 ± 0.61
166.02	236.5 ± 0.92	10.43 ± 0.68	-16.27 ± 2.68	192.55 ± 0.72	173.88 ± 1.75	-32.91 ± 0.64	-31.08 ± 1.72	134.25 ± 0.67
175.78	238.04 ± 2.32	14.39 ± 0.77	-8.5 ± 0.97	181.67 ± 0.83	178.44 ± 1.35	-30.15 ± 0.31	-31.14 ± 1.54	139.16 ± 0.57
185.55	244.11 ± 1.91	19.61 ± 1.04	-9.36 ± 2.35	190.73 ± 1.29	193.55 ± 1.87	-34.68 ± 0.98	-25.5 ± 1.97	145.34 ± 0.53
195.31	230.5 ± 20.62	25.07 ± 1.96	2 ± 13.81	189.12 ± 1.38	202.09 ± 16.37	-33.25 ± 3.35	-38.2 ± 6.18	156.9 ± 2
205.08	236.59 ± 3.77	28.97 ± 1.32	9.87 ± 1.18	189.44 ± 1.22	211.1 ± 1.45	-37.82 ± 0.87	-21.44 ± 2.96	159.75 ± 0.67
214.84	239.78 ± 3.39	41.4 ± 1.51	12.98 ± 1.26	188.28 ± 2.06	226.23 ± 4.26	-41.29 ± 0.66	-30.18 ± 9.31	195.06 ± 0.61
224.61	245.43 ± 4.03	37.28 ± 1.84	-4.55 ± 14	189.95 ± 0.64	239.01 ± 8.04	-60.05 ± 1.75	-22.9 ± 3.41	180.52 ± 3.1
234.38	243.28 ± 3.18	38.03 ± 1.38	19.41 ± 0.78	213.98 ± 1.61	244.26 ± 2.1	-47.83 ± 0.74	-8.69 ± 2.71	199.16 ± 0.72
244.14	256.88 ± 1.89	39.13 ± 0.67	32.81 ± 3.1	198.61 ± 0.84	247.4 ± 2.64	-44.83 ± 0.92	13.87 ± 1.22	202.8 ± 0.82
253.91	272.93 ± 7.82	53.21 ± 0.93	39.55 ± 1.5	207.28 ± 1.14	270.25 ± 3.67	-52.74 ± 1.76	18.4 ± 2.01	225.99 ± 0.73
263.67	264.74 ± 2.74	69.96 ± 0.75	62.55 ± 2.4	214.94 ± 1.07	281.78 ± 2.5	-50.32 ± 0.8	54.36 ± 3.88	232.73 ± 0.68
273.44	304.3 ± 5.33	79.99 ± 2.63	125.74 ± 15.33	228.59 ± 1.98	300.79 ± 10.96	-75.65 ± 1.78	18.97 ± 7.4	236.89 ± 3.69
283.20	275.83 ± 5.35	52.11 ± 2.45	137.91 ± 3.73	356.14 ± 3.74	271.74 ± 2.74	-117.15 ± 3.16	5.32 ± 10.13	239.13 ± 3.17
292.97	279.9 ± 4.91	51.27 ± 1.46	44.03 ± 16.91	252.63 ± 3.92	247.03 ± 5.06	-88.75 ± 2.18	-66.44 ± 16.5	279.9 ± 5.59

Table D. 7. Measured dynamic-stiffness real and imaginary parts at 9,000 rpm and 345 kPa for t_p=8.5 mm.

Freq. [Hz.]	Re (H_{xx}) [MN/m]	Re (H_{xy}) [MN/m]	Re (H_{yx}) [MN/m]	Re (H_{yy}) [MN/m]	Im (H_{xx}) [MN/m]	Im (H_{xy}) [MN/m]	Im (H_{yx}) [MN/m]	Im (H_{yy}) [MN/m]
9.77	226.23 ± 0.87	-18.74 ± 0.66	-18.16 ± 0.92	145.08 ± 0.63	13.5 ± 0.54	-1.96 ± 0.64	0.98 ± 0.78	8.25 ± 0.99
19.53	226.79 ± 1.26	-18.92 ± 0.74	-15.49 ± 1.09	146.2 ± 0.68	25.16 ± 0.8	-4.98 ± 0.59	-3.2 ± 0.36	16 ± 0.42
29.30	228.66 ± 0.62	-18.13 ± 0.45	-15.84 ± 0.48	144.63 ± 0.43	37.14 ± 0.98	-6.04 ± 0.58	-8.33 ± 0.86	24.34 ± 0.31
39.06	231.95 ± 0.84	-18.3 ± 0.73	-15.91 ± 0.34	147.83 ± 0.63	48.01 ± 0.27	-7.05 ± 0.67	-11.51 ± 0.55	30.86 ± 0.66
48.83	234.93 ± 1.41	-17.89 ± 0.83	-17.68 ± 0.94	148.58 ± 0.74	58.04 ± 1.53	-7.97 ± 0.43	-13.75 ± 0.62	35.82 ± 0.86
58.59	232.65 ± 1.6	-17.9 ± 1.18	-13.76 ± 1.16	149.61 ± 1.22	68.99 ± 0.82	-9.58 ± 0.84	-16.63 ± 1.01	42.76 ± 0.61
68.36	245.27 ± 1.35	-16.54 ± 1.06	-13.94 ± 0.7	153.61 ± 0.66	78.47 ± 1.21	-9.22 ± 0.48	-18.71 ± 0.38	53.43 ± 0.39
78.13	237.86 ± 0.79	-27.25 ± 1.17	-18.11 ± 1.27	165.49 ± 0.78	86.68 ± 1.36	-36.9 ± 0.98	-31.43 ± 0.85	42.12 ± 0.72
87.89	243.44 ± 3.35	-15.82 ± 1.45	-17.73 ± 2.03	157.95 ± 0.41	94.02 ± 1.99	-11.07 ± 0.69	-31.85 ± 2.34	68.47 ± 0.44
97.66	246.75 ± 2.19	-10.54 ± 0.32	-21.56 ± 1.55	158.2 ± 0.78	104.06 ± 1.27	-12.87 ± 0.52	-24.74 ± 2.21	71.87 ± 0.78
107.42	245.41 ± 1.21	-9.23 ± 0.66	-17.43 ± 0.51	156.87 ± 0.49	113.16 ± 1.01	-12.94 ± 0.62	-26.72 ± 0.83	79.01 ± 0.88
117.19	246.38 ± 0.99	-5.3 ± 0.56	-17.64 ± 0.72	158.28 ± 0.91	121.95 ± 1.01	-15.06 ± 0.34	-27.78 ± 1.06	86.8 ± 0.89
126.95	246.29 ± 0.66	-1.71 ± 0.63	-16.64 ± 1.18	158.79 ± 0.47	131.59 ± 1	-16.72 ± 0.35	-31.25 ± 0.7	94.66 ± 0.81
136.72	247.82 ± 0.86	2.1 ± 0.6	-13.9 ± 0.62	162.07 ± 0.39	140.71 ± 0.77	-18.88 ± 0.27	-27.99 ± 0.65	103.42 ± 0.66
146.48	249.71 ± 3.12	5.66 ± 1.59	-13.02 ± 1.09	161.99 ± 0.98	149.8 ± 1	-21.68 ± 0.81	-29.05 ± 1.45	109.93 ± 1.36
156.25	250.5 ± 1.4	16.69 ± 0.49	-14.08 ± 2	161.84 ± 0.77	160.2 ± 1.78	-29.21 ± 0.25	-32.82 ± 1.03	119.49 ± 1.05
166.02	251.91 ± 0.36	9.26 ± 0.54	-10.71 ± 1.61	168.14 ± 0.51	169.79 ± 1.62	-29.52 ± 0.24	-31.81 ± 1.13	125.77 ± 0.51
175.78	255.03 ± 0.91	10.66 ± 0.32	-6.16 ± 0.96	173.45 ± 0.33	174.86 ± 0.98	-30.8 ± 0.43	-30.7 ± 0.83	136.38 ± 0.5
185.55	256.78 ± 2.07	15.7 ± 0.6	-9.3 ± 1.52	174.89 ± 1.14	188.94 ± 1.59	-36.38 ± 0.82	-33.78 ± 1.13	142.65 ± 1.01
195.31	246.73 ± 4.74	19.79 ± 0.95	15.46 ± 5.16	175.9 ± 1.11	197.54 ± 4.57	-37.57 ± 0.92	-54.3 ± 6.2	149.22 ± 1.26
205.08	257.85 ± 1.24	20.06 ± 0.35	1.35 ± 1.28	181.95 ± 0.62	203.58 ± 1.36	-39.68 ± 0.55	-22.44 ± 0.71	156.61 ± 0.99
214.84	261.22 ± 0.97	25.91 ± 0.99	4.57 ± 0.57	193.63 ± 0.4	212.92 ± 0.55	-42.6 ± 0.65	-21.75 ± 0.27	166.52 ± 0.62
224.61	262.72 ± 0.42	31.61 ± 1.31	4.39 ± 0.8	133.87 ± 0.68	220.97 ± 1.07	-45.44 ± 1.23	-18.73 ± 0.57	151.09 ± 0.98
234.38	264.9 ± 0.68	34.12 ± 1.14	9.92 ± 0.55	188.74 ± 0.88	228.72 ± 0.64	-55.26 ± 0.42	-12.7 ± 0.96	213.3 ± 1.12
244.14	261.89 ± 2.88	33.46 ± 0.54	11.98 ± 1.76	197.06 ± 0.53	246.25 ± 1.84	-51.8 ± 1.23	-7.91 ± 1.25	194.04 ± 0.84
253.91	264.27 ± 1.19	36.95 ± 1	18.34 ± 1.2	212.11 ± 0.96	250.73 ± 0.67	-59.95 ± 1.1	-3.03 ± 1.6	203.71 ± 1.17
263.67	259.51 ± 0.67	42.49 ± 0.57	25.4 ± 0.93	214.93 ± 0.71	263.93 ± 1.21	-53.05 ± 0.65	9.67 ± 0.14	197.01 ± 0.61
273.44	259.82 ± 0.56	58.63 ± 0.7	40.38 ± 0.25	172.57 ± 0.86	279.29 ± 0.42	-54.16 ± 1.08	24.86 ± 0.47	171.79 ± 0.51
283.20	259.33 ± 1.55	53.43 ± 0.79	72.34 ± 1.2	256.89 ± 1.76	312.11 ± 2.66	-82.3 ± 0.5	12.87 ± 2.01	245.32 ± 0.83
292.97	262.32 ± 0.85	56.2 ± 1.48	112.12 ± 3.64	245.87 ± 2.32	330.53 ± 0.81	-81.81 ± 1.48	73.43 ± 3.5	254.12 ± 0.84

Table D. 8. Measured dynamic-stiffness real and imaginary parts at 9,000 rpm and 689 kPa for t_p=8.5 mm.

Freq. [Hz.]	Re (H_{xx}) [MN/m]	Re (H_{xy}) [MN/m]	Re (H_{yx}) [MN/m]	Re (H_{yy}) [MN/m]	Im (H_{xx}) [MN/m]	Im (H_{xy}) [MN/m]	Im (H_{yx}) [MN/m]	Im (H_{yy}) [MN/m]
9.77	256.17 ± 2.14	-18.93 ± 0.66	-16.94 ± 1.12	141.11 ± 0.35	11.78 ± 1.55	-0.63 ± 0.52	2.02 ± 0.76	7.38 ± 0.61
19.53	259.88 ± 1	-20.03 ± 0.47	-16.36 ± 1.02	141.26 ± 0.44	27.25 ± 1.37	-5.24 ± 0.49	-3.21 ± 0.65	13.31 ± 0.3
29.30	263.37 ± 1.13	-18.98 ± 1.16	-16.13 ± 0.8	141.08 ± 0.52	37.89 ± 1.1	-6.14 ± 0.54	-8.15 ± 0.57	19.73 ± 0.52
39.06	264.48 ± 1.03	-19.31 ± 0.78	-16.9 ± 0.53	142.03 ± 0.5	49.23 ± 0.85	-7.99 ± 0.48	-10.97 ± 0.52	26.49 ± 0.53
48.83	269.53 ± 1.49	-19.49 ± 1.14	-19 ± 1.25	142.78 ± 0.66	59.58 ± 1.12	-9.76 ± 1.29	-14.26 ± 0.34	33.06 ± 0.45
58.59	272.01 ± 0.41	-19.46 ± 0.66	-18.71 ± 0.66	141.41 ± 0.52	70.76 ± 1.32	-11.24 ± 1.01	-18.71 ± 0.31	40.48 ± 0.86
68.36	275.12 ± 2.01	-20.24 ± 1.12	-21.23 ± 0.62	139.36 ± 0.83	84.42 ± 1.38	-9.02 ± 0.83	-15.86 ± 0.64	51.89 ± 0.85
78.13	276.74 ± 1.39	-16.4 ± 0.67	-16.85 ± 0.38	143.44 ± 0.56	87.98 ± 1.26	-11.87 ± 0.25	-27.49 ± 1.28	52.94 ± 0.44
87.89	280.64 ± 3.72	-17.21 ± 0.69	-12.17 ± 1.66	146.03 ± 0.47	93.06 ± 1.38	-13.95 ± 0.58	-30.43 ± 1.03	62.93 ± 0.92
97.66	282.52 ± 1.77	-14.53 ± 0.74	-25.99 ± 0.85	147.03 ± 0.66	106.95 ± 1.74	-14.68 ± 0.45	-29.3 ± 0.59	67.98 ± 0.7
107.42	282.63 ± 1.14	-13.01 ± 0.4	-24.96 ± 0.37	147.7 ± 0.43	116.4 ± 1.35	-15.68 ± 0.59	-29.46 ± 1.18	75.53 ± 0.52
117.19	285.23 ± 0.81	-10.56 ± 0.65	-22.81 ± 0.98	148.78 ± 0.37	121.53 ± 0.54	-17.09 ± 0.57	-33.28 ± 0.53	82.26 ± 0.73
126.95	285.44 ± 0.61	-8.32 ± 0.36	-21.99 ± 0.91	148.42 ± 0.34	130.55 ± 1.11	-18.94 ± 0.35	-36.59 ± 0.85	90.4 ± 0.42
136.72	285.89 ± 1.04	-3.4 ± 0.31	-16.94 ± 1.21	149.82 ± 0.42	138.44 ± 0.91	-20.27 ± 0.61	-31.03 ± 0.68	98.17 ± 0.41
146.48	285.08 ± 1.52	-1.82 ± 0.87	-18.48 ± 0.95	152.7 ± 0.57	146.56 ± 1.25	-21.89 ± 0.91	-30.77 ± 0.6	105.14 ± 0.78
156.25	287.77 ± 0.47	5.22 ± 0.84	-15.93 ± 1.56	148.7 ± 1.24	160.01 ± 2.07	-24.89 ± 1.22	-35.03 ± 0.69	99.4 ± 0.38
166.02	289.19 ± 1.53	2.27 ± 0.92	-19.57 ± 0.85	162.57 ± 0.43	169.82 ± 1.36	-30.16 ± 0.45	-33.76 ± 1.43	115.32 ± 0.48
175.78	289.6 ± 2.89	5.22 ± 0.42	-13.29 ± 2.14	157.51 ± 0.57	173.18 ± 1.18	-30.99 ± 0.7	-32.9 ± 1.14	126.94 ± 0.46
185.55	291.63 ± 2.59	7.89 ± 0.75	-19.07 ± 1.64	161.2 ± 0.78	189.12 ± 1.54	-34.91 ± 0.87	-30.55 ± 1.48	135.4 ± 0.61
195.31	289.01 ± 2.81	12.71 ± 0.98	-12.54 ± 6.96	166.26 ± 1.14	191.57 ± 4.98	-36.71 ± 0.9	-38.53 ± 6.69	144.64 ± 1.22
205.08	295.27 ± 1.05	13.85 ± 1.36	-8.64 ± 0.68	168.1 ± 0.93	199.77 ± 0.94	-39.49 ± 1.24	-21.67 ± 1.41	148.78 ± 0.9
214.84	297.43 ± 1.31	19.06 ± 0.83	-2.27 ± 0.71	178.35 ± 0.69	207.82 ± 0.63	-40.92 ± 0.53	-23.19 ± 0.31	155.35 ± 0.99
224.61	297.1 ± 1.23	30.94 ± 1.15	4.39 ± 0.83	97.72 ± 0.85	216.22 ± 0.87	-46.51 ± 0.86	-21.52 ± 0.6	154.19 ± 0.41
234.38	301.35 ± 1.43	20.67 ± 0.98	-5.9 ± 1.8	181.25 ± 1.11	226.34 ± 2.52	-49.76 ± 1.53	-21.9 ± 0.89	175.39 ± 0.95
244.14	296.29 ± 0.95	24.04 ± 0.98	10.04 ± 0.91	181.49 ± 1.23	234.24 ± 3.49	-48.96 ± 0.55	-20.77 ± 2.56	180.06 ± 0.98
253.91	299.96 ± 1.37	32.07 ± 0.48	7.48 ± 0.88	175.69 ± 0.55	238.75 ± 1.32	-55.52 ± 2.03	-14.95 ± 1.86	192.74 ± 0.55
263.67	295.55 ± 0.45	31.71 ± 1.23	15.97 ± 0.56	202.93 ± 0.77	252.63 ± 0.82	-54.53 ± 0.31	-8.97 ± 0.58	185.39 ± 1.03
273.44	293.94 ± 0.57	44.68 ± 0.72	24.41 ± 0.49	159.57 ± 1.01	262.68 ± 0.37	-55.22 ± 0.49	0.01 ± 0.48	157.49 ± 1.39
283.20	290.03 ± 0.79	35.17 ± 1.15	32.37 ± 0.28	215.1 ± 1.6	281.37 ± 1.14	-61.66 ± 1.07	-5.53 ± 0.82	201.66 ± 0.99
292.97	295.42 ± 0.66	56.84 ± 1.15	39.82 ± 0.36	137.71 ± 1.21	292.44 ± 0.79	-58.9 ± 0.61	13.87 ± 0.91	248.82 ± 0.89

Table D. 9. Measured dynamic-stiffness real and imaginary parts at 9,000 rpm and 1034 kPa for t_p=8.5 mm.

Freq. [Hz.]	Re (H_{xx}) [MN/m]	Re (H_{xy}) [MN/m]	Re (H_{yx}) [MN/m]	Re (H_{yy}) [MN/m]	Im (H_{xx}) [MN/m]	Im (H_{xy}) [MN/m]	Im (H_{yx}) [MN/m]	Im (H_{yy}) [MN/m]
9.77	297.31 ± 0.98	-24.35 ± 0.55	-21.88 ± 1.57	143.4 ± 0.65	13.22 ± 0.69	-1.11 ± 1.05	3.98 ± 1.67	6.79 ± 0.51
19.53	296.75 ± 1.25	-24.69 ± 0.41	-23.48 ± 0.76	143.1 ± 0.24	27.61 ± 0.8	-4.37 ± 0.76	-3.65 ± 0.71	11.85 ± 0.42
29.30	299.9 ± 0.8	-24.61 ± 0.3	-22.57 ± 0.59	143.3 ± 0.47	38.07 ± 0.97	-6.47 ± 0.88	-6.4 ± 0.71	16.75 ± 0.6
39.06	304.97 ± 1.61	-24.39 ± 0.42	-23.31 ± 1	142.99 ± 0.47	49.93 ± 0.69	-8.39 ± 0.76	-11.06 ± 0.66	23.31 ± 0.64
48.83	308.67 ± 2.02	-24.84 ± 0.38	-22.56 ± 0.94	143.3 ± 0.38	61.54 ± 1.12	-11.37 ± 0.63	-17.1 ± 0.48	28.52 ± 0.47
58.59	309.52 ± 0.68	-23.36 ± 0.88	-22.98 ± 0.7	140.78 ± 0.69	69.7 ± 0.49	-10.51 ± 0.86	-17.85 ± 0.34	35.13 ± 0.48
68.36	311.05 ± 1.08	-26.02 ± 0.49	-26.8 ± 0.52	139.75 ± 0.52	79.67 ± 0.77	-13.78 ± 0.31	-20.81 ± 0.86	41.77 ± 0.76
78.13	315.65 ± 2.04	-22.29 ± 0.6	-22.35 ± 0.32	144.28 ± 0.62	90.71 ± 0.97	-13.69 ± 1.03	-28.17 ± 0.97	47.19 ± 0.33
87.89	318.59 ± 1.93	-22.53 ± 0.56	-24.39 ± 1.39	143.54 ± 1.1	95.74 ± 2.08	-14.42 ± 0.93	-35.06 ± 2.88	55.89 ± 0.62
97.66	326.32 ± 0.49	-21.75 ± 0.64	-31.88 ± 0.36	146.03 ± 0.84	109.5 ± 2.7	-17.07 ± 0.45	-29.4 ± 2.39	61.83 ± 0.56
107.42	323.05 ± 0.74	-19.75 ± 0.8	-25.25 ± 0.83	145.46 ± 0.68	110.74 ± 0.95	-17.38 ± 0.59	-33.72 ± 0.84	71.12 ± 0.5
117.19	324.14 ± 0.59	-17.28 ± 0.65	-29.04 ± 1.19	147.46 ± 0.38	123.39 ± 0.77	-19.2 ± 0.42	-35.58 ± 0.6	77.14 ± 0.69
126.95	326.16 ± 0.53	-14.21 ± 0.19	-29.39 ± 1.22	147.07 ± 0.7	133.3 ± 1.01	-20.42 ± 0.36	-39.53 ± 1.32	84.8 ± 0.37
136.72	322.84 ± 1.12	-10.12 ± 0.51	-23.25 ± 1.02	146.56 ± 0.63	137.99 ± 0.98	-22.14 ± 0.41	-34.38 ± 0.92	92.78 ± 0.67
146.48	325.18 ± 1.86	-8.8 ± 0.68	-27.02 ± 1.66	151.13 ± 0.59	146.74 ± 1.01	-23.08 ± 1.07	-35.1 ± 0.85	97.43 ± 0.55
156.25	326.27 ± 2.39	-2.42 ± 0.77	-22.15 ± 0.77	147.9 ± 0.55	159.9 ± 0.3	-27.4 ± 0.82	-36.49 ± 1.99	91.23 ± 0.99
166.02	329.69 ± 1.2	-5.25 ± 0.58	-29.22 ± 1	159.36 ± 0.75	168.02 ± 1.54	-31.92 ± 0.57	-35.68 ± 0.64	108.41 ± 1
175.78	332.48 ± 2.17	-3.27 ± 0.17	-25.01 ± 0.89	154.23 ± 0.71	172.68 ± 1.77	-34.18 ± 0.58	-29.34 ± 1.56	117.95 ± 0.72
185.55	333.29 ± 2.72	1.12 ± 1.05	-23.76 ± 3.69	160.22 ± 1.01	188.01 ± 4.48	-36.76 ± 0.62	-33.79 ± 0.96	126.95 ± 0.9
195.31	309.1 ± 1.28	8.19 ± 0.95	-10.24 ± 9.3	157.68 ± 1.28	205.19 ± 7.16	-36.89 ± 0.73	-34.03 ± 7.75	133.95 ± 0.95
205.08	333.12 ± 1.45	4.33 ± 0.7	-12.2 ± 1.4	165.01 ± 0.77	196.19 ± 1	-42.6 ± 0.46	-26.62 ± 1.73	137.52 ± 0.84
214.84	339.02 ± 0.82	9.25 ± 0.61	-10.23 ± 0.74	173.69 ± 1.12	205.85 ± 0.97	-43.5 ± 0.88	-26.57 ± 1.08	148.43 ± 0.72
224.61	340.09 ± 0.51	18.25 ± 0.59	-6.67 ± 1.1	98.96 ± 0.57	214.62 ± 1.38	-47.09 ± 0.63	-20.14 ± 0.12	133.88 ± 0.49
234.38	342.82 ± 0.95	11.54 ± 0.56	-11.73 ± 0.8	174.19 ± 0.6	221.77 ± 1.77	-51.77 ± 0.78	-27.66 ± 1.18	165.04 ± 1.01
244.14	338.01 ± 1.09	14.4 ± 1.12	2.16 ± 2.78	173.58 ± 0.88	225.55 ± 3.2	-50.85 ± 1.06	-16.34 ± 2.31	166.11 ± 0.67
253.91	341.3 ± 0.59	23.84 ± 1.62	0.55 ± 1.06	170.05 ± 3.37	234.5 ± 1.25	-60.59 ± 0.6	-19.38 ± 0.86	194.59 ± 0.85
263.67	337.14 ± 1.04	23.22 ± 0.75	8.27 ± 0.43	195.04 ± 0.5	246.07 ± 1.27	-55.92 ± 0.79	-16.03 ± 0.45	177.14 ± 1.17
273.44	334.62 ± 0.49	31.4 ± 1.06	15.61 ± 0.42	161.73 ± 0.38	257.47 ± 0.97	-55.66 ± 0.81	-11.07 ± 0.54	135.23 ± 0.87
283.20	332.68 ± 1.51	25.23 ± 0.86	23.01 ± 1.21	209.57 ± 1.15	274.56 ± 0.88	-64.46 ± 0.9	-17.29 ± 1.02	188.49 ± 0.41
292.97	335.14 ± 1.49	32.45 ± 1.36	28.89 ± 0.89	161.54 ± 0.82	283.47 ± 0.4	-59.83 ± 0.73	-6.26 ± 0.5	202.3 ± 1.07

Table D. 10. Measured dynamic-stiffness real and imaginary parts at 9,000 rpm and 1,724 kPa for t_p=8.5 mm.

Freq. [Hz.]	Re (H_{xx}) [MN/m]	Re (H_{xy}) [MN/m]	Re (H_{yx}) [MN/m]	Re (H_{yy}) [MN/m]	Im (H_{xx}) [MN/m]	Im (H_{xy}) [MN/m]	Im (H_{yx}) [MN/m]	Im (H_{yy}) [MN/m]
9.77	378.28 ± 0.89	-43.36 ± 0.6	-40.55 ± 1.25	161.65 ± 0.69	17.59 ± 1.2	-0.89 ± 0.28	0.89 ± 1.05	7.03 ± 0.37
19.53	384.16 ± 1.54	-41.83 ± 0.54	-38.74 ± 0.31	160.49 ± 0.3	26.58 ± 0.46	-3.63 ± 0.24	-0.82 ± 0.53	9.69 ± 0.35
29.30	388.14 ± 1.15	-44.98 ± 0.9	-40.35 ± 0.91	163.64 ± 0.62	41.62 ± 1.25	-5.3 ± 0.65	-8.59 ± 1.43	14.42 ± 0.39
39.06	387.62 ± 1.75	-40.67 ± 0.59	-39.4 ± 0.49	161.41 ± 0.56	53.15 ± 0.82	-9.67 ± 0.29	-10.68 ± 0.72	19.77 ± 0.37
48.83	391.05 ± 2.16	-39.71 ± 0.47	-39.02 ± 1.1	160.25 ± 0.95	64.83 ± 2.09	-11.08 ± 0.77	-17.9 ± 0.47	24.68 ± 0.57
58.59	397.37 ± 2.29	-42.08 ± 0.29	-42.43 ± 1.74	159.23 ± 0.61	74.15 ± 0.81	-11.55 ± 0.74	-19.22 ± 1.17	30.3 ± 0.78
68.36	394.92 ± 0.84	-39.16 ± 0.89	-42.7 ± 1.97	159.95 ± 0.8	82.15 ± 0.85	-14.57 ± 0.94	-23.9 ± 1.69	35.01 ± 0.59
78.13	403.14 ± 1.17	-36.56 ± 0.74	-36.18 ± 0.79	160.73 ± 0.59	91.17 ± 1.26	-12.79 ± 0.52	-27.25 ± 0.55	40.39 ± 0.52
87.89	407.82 ± 1.08	-37.81 ± 0.77	-39.99 ± 0.7	161.45 ± 1.03	97.82 ± 4.42	-15.06 ± 0.7	-36.51 ± 4.8	48.11 ± 1.26
97.66	412.12 ± 2.83	-37.46 ± 0.41	-42.12 ± 2.22	162.45 ± 0.76	104.94 ± 1.7	-17.8 ± 0.39	-31.23 ± 1.4	53.53 ± 0.36
107.42	413.55 ± 1.62	-35.07 ± 0.41	-44.77 ± 0.84	161.72 ± 0.58	110.43 ± 1.79	-17.35 ± 0.67	-34.5 ± 0.24	61.43 ± 0.53
117.19	412.69 ± 1.41	-32.96 ± 0.27	-48.61 ± 1.56	163.65 ± 0.53	119.49 ± 1.87	-21.05 ± 0.34	-37.54 ± 1.46	66.43 ± 0.54
126.95	412.03 ± 1.14	-30.1 ± 0.32	-45.76 ± 1.46	163.65 ± 0.67	127.99 ± 2.76	-23.6 ± 0.69	-39.65 ± 2.34	73.94 ± 0.7
136.72	410.09 ± 2.28	-25.91 ± 0.53	-42.74 ± 1.06	163.69 ± 0.32	135.72 ± 0.65	-26.17 ± 0.29	-38.54 ± 1.15	79.53 ± 0.44
146.48	409.27 ± 2.91	-23.34 ± 0.77	-45.1 ± 1.87	168.86 ± 0.9	138.77 ± 3.64	-27.44 ± 2.18	-30.81 ± 1.55	84.25 ± 0.99
156.25	414.36 ± 2.07	-19.32 ± 0.39	-41.95 ± 1.78	167.28 ± 0.5	152.17 ± 1.81	-32.36 ± 0.53	-37.01 ± 1.43	77.35 ± 0.35
166.02	413.49 ± 0.76	-24.1 ± 0.63	-45.64 ± 1.17	174.48 ± 0.54	163.51 ± 2.42	-36.51 ± 0.54	-38.63 ± 0.82	93.91 ± 0.32
175.78	415.06 ± 1.17	-22.45 ± 0.47	-39.03 ± 1.74	168.22 ± 0.58	162.5 ± 3.35	-37.77 ± 0.36	-29.28 ± 2.43	102.11 ± 0.42
185.55	422.04 ± 3.51	-18.12 ± 1.15	-41.86 ± 1.19	172.56 ± 1.13	184.22 ± 2.27	-42.79 ± 0.67	-35.96 ± 1.6	113.32 ± 0.82
195.31	416.15 ± 7.86	-14.6 ± 0.79	-44.31 ± 4.75	173.51 ± 1.58	213.48 ± 4.15	-44.3 ± 1.07	-42.77 ± 14.79	118.09 ± 0.97
205.08	419.58 ± 0.91	-15.32 ± 1.53	-29.42 ± 0.89	175.75 ± 0.54	189.08 ± 1.72	-45.84 ± 1.18	-31.79 ± 0.79	122.09 ± 0.94
214.84	421.3 ± 1.55	-11.46 ± 0.43	-27.72 ± 0.2	183.9 ± 0.68	198.55 ± 1.18	-46.11 ± 0.29	-29.34 ± 0.67	129.63 ± 0.43
224.61	424.5 ± 1.8	-3.9 ± 1.12	-24.64 ± 1.88	115.36 ± 0.64	206.97 ± 2.14	-51.02 ± 0.97	-27.66 ± 1.26	112.63 ± 0.61
234.38	422.6 ± 0.52	-10.34 ± 0.93	-26.62 ± 0.73	184.56 ± 1.13	213.37 ± 2.52	-53.07 ± 1.22	-32.3 ± 1.05	146.68 ± 0.64
244.14	426.25 ± 2.52	-9.02 ± 1.01	-15.1 ± 2.39	186.18 ± 0.65	216.78 ± 4.33	-53.67 ± 0.65	-25.9 ± 1.68	144.94 ± 0.52
253.91	420.59 ± 0.99	-0.17 ± 0.78	-13.82 ± 1	180.44 ± 0.92	229.19 ± 1.91	-56.46 ± 0.56	-26.01 ± 0.84	157.95 ± 1.1
263.67	418.77 ± 1.02	-1.22 ± 0.79	-3.13 ± 0.7	205.79 ± 0.62	236.2 ± 1.9	-57.94 ± 1.37	-25.18 ± 0.43	153.94 ± 0.81
273.44	416.1 ± 0.62	6.13 ± 0.25	-0.42 ± 0.7	180.93 ± 1.71	246.2 ± 0.98	-60.99 ± 1.14	-27.13 ± 0.58	116.62 ± 0.91
283.20	414.66 ± 1.55	0.86 ± 0.75	4.78 ± 1.12	223.02 ± 0.61	265.24 ± 2.03	-66.26 ± 1.2	-32.39 ± 1.3	172.62 ± 0.65
292.97	416.94 ± 1.08	8.96 ± 1.92	12.01 ± 0.85	180.53 ± 0.57	269.61 ± 1.82	-61.55 ± 1.58	-22.97 ± 1.32	176.77 ± 1.24

Table D. 11. Measured dynamic-stiffness real and imaginary parts at 12,000 rpm and 172 kPa for t_p=8.5 mm.

Freq. [Hz.]	Re (H_{xx}) [MN/m]	Re (H_{xy}) [MN/m]	Re (H_{yx}) [MN/m]	Re (H_{yy}) [MN/m]	Im (H_{xx}) [MN/m]	Im (H_{xy}) [MN/m]	Im (H_{yx}) [MN/m]	Im (H_{yy}) [MN/m]
9.77	239.5 ± 2.07	-34.17 ± 0.8	-23.6 ± 1.5	179.43 ± 0.99	7.93 ± 2.41	-0.26 ± 1	0.3 ± 2.07	9.25 ± 0.84
19.53	242.02 ± 2.76	-35.2 ± 1	-21.31 ± 1.23	183.52 ± 0.51	26.65 ± 1.45	-4.15 ± 1.01	-9.7 ± 1.64	18.78 ± 1.1
29.30	246.63 ± 0.79	-34.59 ± 1.48	-26.72 ± 3.04	182.48 ± 1.05	32.76 ± 2.86	-6.26 ± 1.2	-10.12 ± 2.55	24.31 ± 0.61
39.06	245.47 ± 4.13	-37.15 ± 1.32	-27.79 ± 1.64	191.3 ± 1.87	45.43 ± 1.24	-6.16 ± 1.17	-17.3 ± 1.58	33.7 ± 0.95
48.83	245.82 ± 1	-33.18 ± 1.36	-23.58 ± 1.3	185.48 ± 1	49.73 ± 1.92	-6.26 ± 0.86	-14.7 ± 1.79	35.86 ± 0.96
58.59	237.88 ± 3.58	-38.54 ± 3.46	-21.59 ± 7.81	215.59 ± 4.21	57 ± 2.23	27.59 ± 0.64	-8.29 ± 4.48	19.66 ± 3.36
68.36	254.35 ± 1.23	-32.21 ± 1.67	-21.23 ± 1.5	192.75 ± 1.64	69.67 ± 2.68	-7.84 ± 1.71	-19.37 ± 0.9	48.78 ± 0.79
78.13	249.03 ± 2.2	-30.49 ± 1.33	-28.1 ± 2.06	201.94 ± 1.68	82.11 ± 1.97	-10.33 ± 0.72	-22.56 ± 2.13	59.22 ± 1.24
87.89	252.63 ± 3.35	-27.21 ± 1.83	-21.14 ± 1.57	195.12 ± 2.27	85.51 ± 3.71	-15.11 ± 0.9	-21.51 ± 3.12	71.09 ± 0.64
97.66	258.28 ± 1.4	-29.3 ± 0.5	-28.46 ± 1.25	203.75 ± 1.04	96.74 ± 1.54	-14.2 ± 0.75	-30.99 ± 1.01	67.62 ± 1.29
107.42	256.66 ± 0.68	-27.12 ± 0.96	-26.18 ± 1.02	199.79 ± 0.67	105.99 ± 1.23	-14.65 ± 1.44	-33.26 ± 1.31	78.48 ± 1.5
117.19	261.05 ± 1.51	-20 ± 1.94	-31.52 ± 1.68	217.58 ± 1.26	115.84 ± 1.54	-21.53 ± 1.16	-38.32 ± 1.54	80.93 ± 1.45
126.95	260.94 ± 0.44	-22.7 ± 0.77	-26.77 ± 0.74	202.8 ± 0.64	122.55 ± 0.84	-16.12 ± 0.62	-37.2 ± 1.48	90.27 ± 0.9
136.72	261.54 ± 1.27	-18.19 ± 0.53	-24.2 ± 1.2	204.08 ± 0.67	128.19 ± 1.35	-18.36 ± 0.66	-37.85 ± 1.29	94.73 ± 0.82
146.48	260.71 ± 2.65	-14.75 ± 0.82	-25.39 ± 2.4	202.91 ± 0.87	137.41 ± 2.81	-17.9 ± 0.74	-41.56 ± 2.64	101.65 ± 0.55
156.25	263.06 ± 3.27	-4.63 ± 0.35	-28.46 ± 3.14	204.22 ± 0.67	145.94 ± 1.01	-24.19 ± 0.43	-40.39 ± 1.67	118.72 ± 0.94
166.02	264.8 ± 0.96	-10.43 ± 0.93	-28.75 ± 1.98	226.5 ± 1.27	151.89 ± 2.59	-27.88 ± 1.34	-34.98 ± 1.74	116.56 ± 1.75
175.78	261.92 ± 1.15	-3.7 ± 0.22	-31.49 ± 1.41	216.57 ± 0.96	166.57 ± 1.76	-24.87 ± 1.03	-38.55 ± 2.09	128.88 ± 0.61
185.55	265.77 ± 1.87	-0.82 ± 1.79	-28.72 ± 3.76	224.64 ± 3.02	170.81 ± 3.41	-31.61 ± 1.37	-35.59 ± 2.69	127.71 ± 2.42
195.31	276.22 ± 3.23	6.48 ± 2.91	-33.72 ± 2.49	220.34 ± 1.84	185.45 ± 7.33	-28.16 ± 1.76	-41.87 ± 5.02	150.44 ± 2.11
205.08	262.76 ± 1.59	3.8 ± 1.4	-14.94 ± 3.56	218.14 ± 2.06	188.66 ± 2.67	-32.94 ± 2.76	-31.27 ± 1.77	149.57 ± 3.6
214.84	264.8 ± 0.94	25.26 ± 1.9	-12.23 ± 1.15	221.28 ± 2.58	206.94 ± 2.02	-32.81 ± 1.89	-35.05 ± 2.68	206.7 ± 2.94
224.61	268.47 ± 2.45	8.85 ± 1.26	8.41 ± 3.5	252.43 ± 1.47	220.15 ± 1.81	-56.83 ± 1.77	-21.46 ± 1.95	154.28 ± 2.37
234.38	272.95 ± 0.4	23.6 ± 1.71	-1.09 ± 1.64	270.16 ± 5.26	228.4 ± 1.1	-33.48 ± 0.86	-20.02 ± 1.81	199.07 ± 4.94
244.14	267.23 ± 2.41	29.44 ± 1.53	2.81 ± 2.15	234.84 ± 2.73	231.39 ± 2.42	-20.86 ± 1.79	-2.06 ± 1.51	216.02 ± 3.6
253.91	281.42 ± 3.98	51.23 ± 2.07	9.26 ± 4.48	239.64 ± 0.91	282.22 ± 4.34	-19.52 ± 2.63	41.19 ± 4.53	257.83 ± 3.82
263.67	319.52 ± 6.26	77.59 ± 5.83	98.31 ± 11.23	308.95 ± 4.05	285.89 ± 5.39	-66.25 ± 3.65	128.3 ± 10.81	243.36 ± 16.35
273.44	398.75 ± 10.27	125.17 ± 5.49	131.37 ± 10.51	260.38 ± 38.68	305.22 ± 15.73	-77.92 ± 4.96	75 ± 9.91	343.44 ± 3.93
283.20	323.92 ± 7.22	82.5 ± 4.07	102.5 ± 24.12	471.41 ± 15.67	262.49 ± 15.55	-105.09 ± 3.14	-93.78 ± 21.27	210.06 ± 13.59
292.97	368.47 ± 4.17	60.02 ± 3.19	64.85 ± 8.03	340.67 ± 18.15	241.98 ± 7.82	-119.56 ± 6.17	-21.42 ± 14.65	204.19 ± 13.88

Table D. 12. Measured dynamic-stiffness real and imaginary parts at 12,000 rpm and 345 kPa for t_p=8.5 mm.

Freq. [Hz.]	Re (H_{xx}) [MN/m]	Re (H_{xy}) [MN/m]	Re (H_{yx}) [MN/m]	Re (H_{yy}) [MN/m]	Im (H_{xx}) [MN/m]	Im (H_{xy}) [MN/m]	Im (H_{yx}) [MN/m]	Im (H_{yy}) [MN/m]
9.77	247.54 ± 0.7	-32.98 ± 0.57	-23.73 ± 0.75	173.35 ± 0.33	12.3 ± 0.93	-0.37 ± 0.58	0.79 ± 1.16	8.84 ± 1.07
19.53	250.77 ± 1.94	-33.17 ± 1.03	-25.55 ± 0.55	176.59 ± 1.01	23.18 ± 0.41	-4.53 ± 0.24	-5.17 ± 1.11	16.95 ± 0.36
29.30	249.49 ± 0.95	-32.67 ± 0.72	-22.06 ± 1.73	173.71 ± 0.78	36.32 ± 0.67	-6.99 ± 0.77	-11.62 ± 1	24.7 ± 0.51
39.06	254.45 ± 1.49	-32.89 ± 0.58	-27.06 ± 0.58	180.86 ± 0.62	44.21 ± 0.88	-7.02 ± 0.46	-13.99 ± 0.94	29.09 ± 0.42
48.83	257.94 ± 0.94	-33.85 ± 1.19	-27.43 ± 1.12	181.7 ± 0.92	55.71 ± 1.93	-9.6 ± 1.08	-17.47 ± 0.79	35.3 ± 0.83
58.59	262.07 ± 0.3	-35.95 ± 0.51	-29.29 ± 1.21	182.45 ± 1.16	65.3 ± 0.72	-11 ± 1.15	-20.52 ± 1.34	41.52 ± 1.09
68.36	261.74 ± 1.06	-29.94 ± 1.07	-23.77 ± 0.67	185.42 ± 1.01	73.56 ± 1.47	-12.27 ± 1.18	-22.22 ± 1.52	52.19 ± 0.66
78.13	260.86 ± 1.6	-29.33 ± 1.05	-25.56 ± 0.7	191.16 ± 0.99	80.97 ± 0.94	-12.8 ± 0.32	-29.92 ± 0.75	57.44 ± 0.43
87.89	264.27 ± 1.57	-30.14 ± 0.33	-28.02 ± 3.64	189.63 ± 0.96	97.11 ± 2.77	-16.74 ± 1.25	-34.44 ± 2.77	66.58 ± 1.26
97.66	271.39 ± 1.99	-29.02 ± 0.79	-30.35 ± 1.96	191.32 ± 0.93	97.85 ± 1.97	-17.11 ± 1.09	-29.55 ± 1.82	64.39 ± 1.1
107.42	272.04 ± 1.02	-28.3 ± 0.55	-29.24 ± 0.65	190 ± 1	107.79 ± 2.07	-16.9 ± 0.68	-34.9 ± 1.37	72.62 ± 0.51
117.19	270.06 ± 1.99	-25.12 ± 1.14	-29.16 ± 1.05	192.59 ± 0.45	114.61 ± 1.67	-17.21 ± 0.53	-38.75 ± 0.66	77.11 ± 0.37
126.95	271.88 ± 1.82	-23.55 ± 0.67	-28 ± 1.71	191.8 ± 0.47	125.85 ± 0.99	-19.57 ± 0.39	-43.93 ± 2.41	86.6 ± 0.52
136.72	270.42 ± 1.26	-20.29 ± 0.45	-26.81 ± 0.67	196.01 ± 0.67	128.71 ± 1.59	-20.32 ± 0.82	-36.41 ± 1.06	94.26 ± 0.73
146.48	274.5 ± 0.7	-16.84 ± 0.27	-26.92 ± 1	195 ± 0.69	137.07 ± 1.02	-20.97 ± 0.21	-40.71 ± 1.09	99.19 ± 0.87
156.25	272.69 ± 0.49	-10.67 ± 0.74	-25.74 ± 1.78	196.77 ± 0.47	143.14 ± 1.78	-24.06 ± 0.37	-44.63 ± 1	102.42 ± 0.56
166.02	270.96 ± 0.88	-11.67 ± 0.8	-30.45 ± 0.79	205.53 ± 0.53	157.3 ± 1.02	-27.09 ± 0.82	-49.38 ± 1.51	113.45 ± 0.69
175.78	277.12 ± 0.56	-10.2 ± 0.7	-30.53 ± 1.63	203.33 ± 0.76	159.06 ± 1.12	-27.37 ± 0.54	-42.62 ± 0.86	124 ± 0.48
185.55	275.63 ± 1.61	-4.1 ± 0.76	-30.3 ± 3.1	208.75 ± 0.6	171.21 ± 2.55	-29.41 ± 0.55	-43.27 ± 1.46	128.39 ± 0.94
195.31	267.87 ± 10.05	-1.41 ± 1.77	-31.5 ± 8.54	213.81 ± 2.24	179.35 ± 9.33	-29.59 ± 3.22	-58.86 ± 5.74	142.08 ± 2.9
205.08	275.03 ± 1.54	1.75 ± 0.79	-18.09 ± 0.47	212.44 ± 1.76	188.08 ± 2.22	-32.25 ± 1.26	-30.83 ± 1.78	139.19 ± 0.87
214.84	274.69 ± 0.91	7.89 ± 1.53	-20.46 ± 2.75	221.49 ± 1.39	198.38 ± 1.47	-33.64 ± 0.96	-32.23 ± 1.08	153.33 ± 1.6
224.61	274.91 ± 0.44	18.35 ± 0.68	-16.86 ± 1.43	173.24 ± 1.15	211.83 ± 1.08	-47.62 ± 1.07	-39.99 ± 3.26	169.15 ± 1.48
234.38	284.13 ± 4.25	9.54 ± 1.44	-11.38 ± 2.88	230.25 ± 2.37	212.14 ± 2.96	-39.52 ± 2.03	-31.37 ± 2.14	175.05 ± 1.43
244.14	289.35 ± 2.64	15.53 ± 0.46	-20.22 ± 5.46	222.37 ± 0.97	226.1 ± 4.01	-35.94 ± 1.05	-25.95 ± 3.1	186.77 ± 1.53
253.91	276.23 ± 2.58	25.79 ± 0.86	-16.78 ± 2.14	239.97 ± 1.83	243.4 ± 3.06	-41.92 ± 1.53	-10.91 ± 1.63	194.58 ± 1.26
263.67	284.97 ± 1.54	34.08 ± 0.49	-13.26 ± 1.87	246.65 ± 1.71	263.41 ± 2.17	-41.62 ± 1.6	0.65 ± 3.15	193.69 ± 0.97
273.44	289.35 ± 2.48	51.69 ± 1.43	1.88 ± 0.55	228.58 ± 2.79	282.04 ± 1.46	-49.62 ± 1.29	13.78 ± 2.83	186.48 ± 1.15
283.20	336.72 ± 13.7	67.63 ± 3.74	-106.91 ± 7.85	280.97 ± 5.4	262.03 ± 8.51	-73.52 ± 2.45	25.04 ± 47.58	269.47 ± 4.18
292.97	243.33 ± 15.78	57.57 ± 1.82	200.53 ± 12.42	329.32 ± 3.78	357.09 ± 10.17	-70.96 ± 3.12	205.82 ± 23.15	221.4 ± 4.82

Table D. 13. Measured dynamic-stiffness real and imaginary parts at 12,000 rpm and 689 kPa for t_p=8.5 mm.

Freq. [Hz.]	Re (H_{xx}) [MN/m]	Re (H_{xy}) [MN/m]	Re (H_{yx}) [MN/m]	Re (H_{yy}) [MN/m]	Im (H_{xx}) [MN/m]	Im (H_{xy}) [MN/m]	Im (H_{yx}) [MN/m]	Im (H_{yy}) [MN/m]
9.77	271.74 ± 0.61	-31.73 ± 0.3	-25.57 ± 1.68	168.19 ± 0.93	10.08 ± 1.16	-1.68 ± 1.03	1.58 ± 1.15	6.9 ± 1.11
19.53	273.87 ± 1.17	-33.28 ± 0.51	-25.69 ± 0.71	168.67 ± 0.4	23.32 ± 0.81	-4.01 ± 1.35	-2.14 ± 0.97	13.16 ± 0.68
29.30	274.59 ± 1.93	-33.24 ± 0.43	-25.27 ± 0.85	166.85 ± 0.55	32.5 ± 0.82	-6.55 ± 0.48	-8.15 ± 0.79	20.78 ± 0.58
39.06	277.75 ± 0.68	-32.85 ± 0.7	-26.42 ± 0.74	171.33 ± 0.87	44.27 ± 1.2	-10.91 ± 0.92	-13.07 ± 0.55	25.7 ± 0.54
48.83	279.68 ± 1.95	-33.3 ± 1.78	-25.04 ± 0.75	171.79 ± 0.92	57.26 ± 1.89	-12.4 ± 0.33	-18.66 ± 1.85	30.81 ± 1.23
58.59	284.47 ± 1.21	-32.61 ± 0.78	-28.61 ± 1.21	172.22 ± 0.97	65.62 ± 1.97	-10.9 ± 0.4	-20.95 ± 0.73	36.59 ± 0.61
68.36	289.34 ± 1.91	-29.88 ± 0.37	-24.48 ± 1.02	172.5 ± 1.17	78.34 ± 0.65	-13.44 ± 1.27	-20.22 ± 0.78	48.37 ± 0.49
78.13	289.22 ± 1.17	-31.1 ± 1.89	-24.49 ± 0.92	173.28 ± 0.5	82.78 ± 0.28	-16.52 ± 0.93	-29.22 ± 1.04	48.11 ± 0.54
87.89	286.13 ± 1.76	-29.17 ± 0.2	-24.67 ± 2.59	176.31 ± 0.7	94.12 ± 3.33	-18.51 ± 0.76	-34.92 ± 3.22	56.75 ± 0.66
97.66	294.64 ± 2.28	-32.83 ± 0.89	-32.77 ± 0.98	177.84 ± 0.6	98.93 ± 1.39	-19.61 ± 0.68	-32.29 ± 1.12	60.73 ± 0.74
107.42	295.98 ± 1.67	-30.2 ± 0.57	-30.05 ± 0.76	176.28 ± 0.53	107.77 ± 1.53	-19.6 ± 0.83	-37.18 ± 1.03	68.82 ± 0.84
117.19	299.36 ± 0.7	-29.39 ± 0.42	-34.39 ± 1.08	178.39 ± 0.48	115.93 ± 0.51	-21.62 ± 0.78	-41.39 ± 1.05	73.46 ± 0.77
126.95	300.51 ± 1.64	-27.66 ± 0.43	-33.6 ± 0.58	177.13 ± 0.28	127.54 ± 1.62	-22.6 ± 0.56	-47.04 ± 1.24	82.26 ± 0.77
136.72	297.36 ± 1.12	-23.95 ± 0.73	-26.29 ± 0.9	177.79 ± 0.79	127.48 ± 0.93	-21.46 ± 0.27	-39.14 ± 1.06	87.85 ± 0.45
146.48	300.79 ± 0.9	-21.9 ± 0.7	-28.77 ± 0.54	180.23 ± 0.64	135.51 ± 0.65	-23.11 ± 0.46	-42.51 ± 0.18	94.73 ± 0.49
156.25	300.1 ± 0.43	-16.2 ± 0.1	-28.34 ± 0.82	174.18 ± 0.84	140.91 ± 1.42	-23.34 ± 0.25	-47.01 ± 0.54	87.84 ± 0.43
166.02	302.04 ± 1.74	-19.62 ± 0.37	-34.87 ± 1.89	189.84 ± 0.71	151.95 ± 0.89	-27.54 ± 0.24	-49.59 ± 1.25	103.09 ± 0.68
175.78	300.74 ± 2.36	-15.44 ± 0.84	-30.69 ± 2.09	182.21 ± 1	157.74 ± 1.59	-28.71 ± 0.81	-43.93 ± 1.47	116.23 ± 0.88
185.55	303.28 ± 2.83	-10.8 ± 1.33	-35.81 ± 1.72	185.88 ± 1.7	167.15 ± 2.3	-28.42 ± 0.62	-46.9 ± 2.61	123.89 ± 1.05
195.31	293.28 ± 10.14	-5.75 ± 2.33	-29.04 ± 13.69	193.25 ± 2.6	180.55 ± 11.73	-32.63 ± 2.12	-45.06 ± 5.97	133.22 ± 2.71
205.08	303.39 ± 2.72	-7.48 ± 1.35	-29.28 ± 2.61	193.28 ± 1.77	183.06 ± 1.81	-33.17 ± 1.82	-37.11 ± 2.12	134.75 ± 2.44
214.84	304.08 ± 1.46	-0.15 ± 1.09	-29.53 ± 1.09	203.97 ± 0.9	193.59 ± 0.75	-36.33 ± 0.89	-33.87 ± 0.97	143.67 ± 1.04
224.61	306.7 ± 1.5	11.05 ± 1.75	-20.33 ± 0.97	121.54 ± 1.17	200.91 ± 2.47	-37.92 ± 0.63	-35.92 ± 0.78	145.94 ± 2
234.38	313.57 ± 3.56	0.19 ± 1.21	-32.1 ± 2.01	211.7 ± 1.76	205.54 ± 1.87	-39.73 ± 1.57	-36.23 ± 3.16	167.02 ± 0.62
244.14	296.13 ± 4.94	9.08 ± 2.91	-26.37 ± 1.44	210.82 ± 1.64	217.72 ± 3.82	-36.21 ± 1.26	-28.89 ± 1.79	172.45 ± 1.86
253.91	307.47 ± 2.15	18.73 ± 0.9	-26.48 ± 1.97	207.48 ± 1.23	223.76 ± 2.1	-41.18 ± 2.55	-21.33 ± 1.17	183.34 ± 0.79
263.67	305.44 ± 2.51	21.77 ± 0.88	-17.99 ± 0.95	232.48 ± 1.3	237.77 ± 1.45	-44.92 ± 0.61	-15.27 ± 1.12	175.04 ± 1.21
273.44	306.23 ± 1.06	36.41 ± 1.51	-10.43 ± 0.46	189.96 ± 1.56	248.77 ± 1.23	-49.99 ± 1.08	-6.76 ± 0.67	148.75 ± 1.25
283.20	305.53 ± 2.21	28.7 ± 1.04	-3.19 ± 1.44	251.53 ± 0.84	264.5 ± 1.65	-58.71 ± 1.08	-9.04 ± 0.92	189.18 ± 1.39
292.97	311.42 ± 0.83	48 ± 0.63	3.1 ± 0.66	170.92 ± 1.16	271.53 ± 0.7	-57.64 ± 1.84	16.59 ± 0.59	238.7 ± 1.26

Table D. 14. Measured dynamic-stiffness real and imaginary parts at 12,000 rpm and 1034 kPa for t_p=8.5 mm.

Freq. [Hz.]	Re (H_{xx}) [MN/m]	Re (H_{xy}) [MN/m]	Re (H_{yx}) [MN/m]	Re (H_{yy}) [MN/m]	Im (H_{xx}) [MN/m]	Im (H_{xy}) [MN/m]	Im (H_{yx}) [MN/m]	Im (H_{yy}) [MN/m]
9.77	297.91 ± 1.3	-34.82 ± 0.77	-31.67 ± 1.08	166.64 ± 0.61	12.66 ± 1.75	-1.59 ± 0.41	2.04 ± 0.42	8.11 ± 0.59
19.53	302.35 ± 0.55	-36.63 ± 0.86	-30.74 ± 0.5	166.78 ± 0.83	23.05 ± 0.97	-3.94 ± 0.4	-1.67 ± 0.53	12.09 ± 0.79
29.30	303.38 ± 0.68	-34.91 ± 0.42	-28.6 ± 0.49	166.71 ± 0.65	36.09 ± 0.64	-6.63 ± 0.99	-7.63 ± 0.48	16.37 ± 0.49
39.06	308.03 ± 1.14	-35.23 ± 0.76	-30.4 ± 0.45	168.8 ± 0.52	46.56 ± 0.39	-8.51 ± 0.22	-11.61 ± 0.91	22.42 ± 0.4
48.83	307.95 ± 0.72	-35.87 ± 1.31	-31.34 ± 0.54	168.88 ± 0.65	55.09 ± 0.77	-11.55 ± 1.12	-16.06 ± 0.84	26.61 ± 0.64
58.59	312.81 ± 1.02	-36.69 ± 0.91	-30.24 ± 1.12	168.22 ± 0.52	69.36 ± 1.78	-13.51 ± 0.5	-20.46 ± 0.93	33.09 ± 0.6
68.36	312.61 ± 2.16	-37.56 ± 0.69	-34.98 ± 0.84	163.61 ± 1.02	79.79 ± 0.71	-15.65 ± 0.43	-21.23 ± 0.73	40.48 ± 1.1
78.13	318.75 ± 0.89	-35.27 ± 0.81	-28.97 ± 0.88	170.93 ± 0.51	88.64 ± 1	-16.62 ± 0.71	-26.97 ± 1.46	42.48 ± 0.57
87.89	318.94 ± 3.04	-35.81 ± 0.6	-32.26 ± 1.97	171.64 ± 1.32	95.22 ± 1.13	-19.16 ± 1.08	-32.55 ± 2.13	50.68 ± 0.51
97.66	325.05 ± 0.62	-34.72 ± 0.26	-34.39 ± 0.62	171.77 ± 0.4	107.28 ± 1.9	-21.46 ± 0.47	-36.88 ± 2.02	55.55 ± 0.93
107.42	326.8 ± 0.64	-35.08 ± 0.51	-34.05 ± 0.67	171.45 ± 0.61	109.23 ± 1.16	-20.88 ± 0.31	-35.93 ± 0.84	63.64 ± 0.62
117.19	331.91 ± 0.59	-33.02 ± 0.82	-34.41 ± 0.66	170.7 ± 0.43	117.7 ± 0.89	-21.45 ± 0.49	-42.12 ± 1.14	69.1 ± 0.48
126.95	331.06 ± 0.71	-33.42 ± 0.44	-35.44 ± 1.22	171.11 ± 0.7	126.14 ± 1.63	-23.07 ± 0.64	-46.3 ± 1.74	77.04 ± 0.7
136.72	326.98 ± 1.49	-29.23 ± 0.21	-29.9 ± 1.02	169.96 ± 0.53	127.71 ± 0.7	-23.93 ± 0.26	-40.69 ± 0.49	85 ± 0.47
146.48	330.41 ± 0.64	-26.88 ± 0.19	-32.41 ± 1.03	174 ± 0.54	134.47 ± 1.15	-22.97 ± 0.38	-44.2 ± 0.95	89.04 ± 0.44
156.25	330.16 ± 0.43	-21.73 ± 0.18	-30.36 ± 0.76	169.22 ± 0.32	141.51 ± 1.39	-23.56 ± 0.41	-47.9 ± 0.9	81.47 ± 0.69
166.02	330.96 ± 1.16	-23.38 ± 0.37	-41.66 ± 0.63	182.25 ± 0.66	153.14 ± 0.67	-28.18 ± 0.5	-50.64 ± 0.79	98.6 ± 0.54
175.78	331.37 ± 1.59	-21.24 ± 0.39	-37.29 ± 2.84	175.43 ± 0.79	150 ± 1.53	-26.77 ± 0.67	-43.5 ± 1.62	109.22 ± 0.55
185.55	329.72 ± 2.99	-15.33 ± 1.11	-46.15 ± 4.73	181.74 ± 1.08	175.47 ± 2.38	-31.94 ± 0.82	-51.06 ± 4.51	118.66 ± 1.55
195.31	315.11 ± 6.56	-10.15 ± 1.62	-23.88 ± 11.45	178.22 ± 1.72	167.78 ± 13.48	-31.26 ± 2.63	-49.4 ± 2.63	127.57 ± 2.04
205.08	332.22 ± 2.29	-9.38 ± 0.97	-34.87 ± 1.86	186.56 ± 1.7	180.73 ± 0.87	-36.89 ± 2.63	-37.76 ± 2.42	130.28 ± 2.02
214.84	335.39 ± 1.67	-4.76 ± 0.54	-37.18 ± 1.22	197.28 ± 1.67	188.56 ± 1.18	-35.49 ± 2.14	-36.89 ± 0.72	138.76 ± 0.92
224.61	339.29 ± 1.62	4.3 ± 0.36	-30.86 ± 0.82	117.6 ± 1.36	200.67 ± 1.45	-40.35 ± 0.86	-33.21 ± 2.37	124.15 ± 0.75
234.38	348.72 ± 3.37	-1.18 ± 0.71	-43.81 ± 2.88	202.27 ± 0.88	208.49 ± 1.87	-40.97 ± 0.66	-38.35 ± 2.03	159.45 ± 2.12
244.14	336.12 ± 1.85	6.33 ± 1.73	-34.75 ± 1.28	200.13 ± 0.88	214.96 ± 2.72	-41 ± 1.62	-34.43 ± 3.6	163.69 ± 1.45
253.91	344.49 ± 1.54	11.75 ± 1.45	-34.45 ± 2.27	207.95 ± 1.99	222.5 ± 0.5	-50.85 ± 1.07	-21.75 ± 2.95	185.31 ± 1.78
263.67	342.96 ± 1.34	14.88 ± 1.28	-24.19 ± 1.99	222.41 ± 1.1	232.57 ± 1.21	-51.53 ± 1.52	-17.72 ± 1.08	169.61 ± 1.64
273.44	344.53 ± 1	22.8 ± 0.58	-17.89 ± 0.88	191.12 ± 0.97	239.75 ± 0.55	-53.83 ± 0.83	-13.4 ± 0.55	124.42 ± 1.45
283.20	343.52 ± 0.73	15.65 ± 1.05	-17.66 ± 0.9	242.98 ± 1.27	253.52 ± 1.09	-59.64 ± 0.62	-16.46 ± 1.42	177.23 ± 0.79
292.97	345.5 ± 1.07	23.32 ± 0.61	-9.22 ± 0.46	192.62 ± 1.34	256.78 ± 0.88	-55.45 ± 0.7	-2.83 ± 0.7	192.15 ± 1.1

Table D. 15. Measured dynamic-stiffness real and imaginary parts at 12,000 rpm and 1,724 kPa for t_p=8.5 mm.

Freq. [Hz.]	Re (H_{xx}) [MN/m]	Re (H_{xy}) [MN/m]	Re (H_{yx}) [MN/m]	Re (H_{yy}) [MN/m]	Im (H_{xx}) [MN/m]	Im (H_{xy}) [MN/m]	Im (H_{yx}) [MN/m]	Im (H_{yy}) [MN/m]
9.77	368.05 ± 2.28	-48.23 ± 0.74	-42.4 ± 0.41	173.89 ± 0.57	10.57 ± 1.04	1.32 ± 0.69	5.58 ± 2.5	7.14 ± 0.54
19.53	367.34 ± 1.48	-46.17 ± 0.93	-42.27 ± 1.04	172.78 ± 0.56	24.12 ± 1.21	-3.36 ± 0.38	-2.08 ± 1.31	9.63 ± 0.69
29.30	369.82 ± 1.08	-48.45 ± 0.26	-43.94 ± 1.5	176.32 ± 0.61	35.28 ± 2.13	-5.98 ± 0.74	-5.25 ± 1.14	14.63 ± 0.45
39.06	371.92 ± 1.45	-45.91 ± 0.59	-43.39 ± 0.67	175.71 ± 0.33	49.4 ± 0.64	-10.04 ± 1.43	-11.61 ± 0.81	18.86 ± 0.85
48.83	373.44 ± 0.99	-45.45 ± 0.55	-43.45 ± 1.52	175.22 ± 0.65	58.52 ± 1.18	-13.61 ± 0.54	-14.67 ± 0.51	22.68 ± 0.88
58.59	377.55 ± 1.4	-46.15 ± 0.5	-43.28 ± 1.11	173.93 ± 1.05	68.2 ± 1.51	-13.93 ± 1.09	-17.45 ± 0.46	28.34 ± 0.78
68.36	380.19 ± 1.94	-46.33 ± 0.39	-47.39 ± 1.49	173.47 ± 0.4	76.74 ± 1.26	-14.7 ± 1.14	-22.41 ± 1.56	31.09 ± 1.11
78.13	382.97 ± 1.02	-42.63 ± 0.84	-38.41 ± 0.57	175.63 ± 0.58	90.34 ± 1.87	-16.87 ± 0.75	-26.43 ± 1.15	35.26 ± 0.62
87.89	388.49 ± 1.99	-44.64 ± 1.04	-43.73 ± 1.45	177.08 ± 0.49	87.94 ± 2.15	-17.67 ± 0.78	-34.83 ± 2.49	43.14 ± 0.57
97.66	396.84 ± 1.74	-45.54 ± 0.84	-46.99 ± 1.47	175.52 ± 1.16	102.72 ± 1.77	-21.7 ± 0.76	-33.52 ± 2.01	47.31 ± 0.48
107.42	395.25 ± 1.3	-43.83 ± 0.42	-45.13 ± 0.89	174.11 ± 0.48	108.52 ± 0.59	-20.82 ± 0.42	-38.52 ± 1.19	54.88 ± 0.77
117.19	399.66 ± 1.37	-43.79 ± 1.02	-45.73 ± 1.32	174.91 ± 0.59	116.9 ± 0.91	-21.75 ± 0.58	-41.81 ± 0.92	58.07 ± 0.71
126.95	397.46 ± 0.79	-41.31 ± 0.39	-45.9 ± 1.97	174.14 ± 0.43	128.37 ± 1.74	-23.47 ± 0.61	-45.99 ± 0.46	66.3 ± 0.69
136.72	398.18 ± 1.36	-39.35 ± 0.32	-44.25 ± 1.25	174.35 ± 0.33	124.82 ± 0.43	-23.93 ± 0.2	-42.7 ± 0.88	72.56 ± 0.35
146.48	400.85 ± 0.52	-38.06 ± 0.58	-46.28 ± 0.43	179.79 ± 0.67	133.47 ± 1.22	-25.5 ± 0.41	-43.85 ± 0.58	78.19 ± 1
156.25	399.4 ± 1.01	-31.91 ± 0.57	-41.97 ± 1.04	176.33 ± 0.55	139.35 ± 0.85	-26.52 ± 0.49	-47.25 ± 1.55	69.86 ± 0.53
166.02	401.62 ± 0.72	-33.6 ± 0.2	-52.68 ± 0.54	183.26 ± 0.64	147.18 ± 1.2	-30.66 ± 0.4	-51.74 ± 2.13	88.26 ± 0.93
175.78	401.13 ± 1.88	-31.36 ± 0.78	-51.39 ± 1.82	177.06 ± 0.44	146.68 ± 2.53	-29.29 ± 0.6	-44.66 ± 0.31	98.63 ± 0.42
185.55	401.83 ± 4.13	-24.61 ± 0.52	-56.16 ± 2.17	181.9 ± 1.31	176.42 ± 1.44	-33.68 ± 0.8	-56.06 ± 3.09	106.14 ± 1.18
195.31	384.46 ± 5.27	-21.9 ± 1.22	-50.03 ± 3.64	183.81 ± 0.67	180.63 ± 7.83	-35.24 ± 1.18	-57.4 ± 7.25	114.74 ± 1.77
205.08	398.36 ± 1.2	-20.85 ± 1.34	-46.9 ± 1.71	188.61 ± 1.69	178.96 ± 1.98	-36.16 ± 1.27	-43.26 ± 2.72	117.29 ± 0.76
214.84	409.62 ± 1.04	-17.2 ± 0.77	-46.99 ± 1.09	198.65 ± 1.62	186.67 ± 1.84	-39.49 ± 0.72	-41.84 ± 1.31	124.77 ± 0.99
224.61	410.79 ± 1.08	-8.77 ± 0.71	-45.57 ± 2.02	127.97 ± 1.18	191.9 ± 1.08	-42.23 ± 0.15	-37.78 ± 1.46	107.3 ± 1.07
234.38	410.43 ± 1.81	-13.62 ± 1.19	-57.28 ± 2.93	202.04 ± 0.96	202.24 ± 2.09	-47.79 ± 0.63	-45.2 ± 2.29	143.75 ± 0.44
244.14	412.63 ± 2.86	-9.44 ± 0.54	-45.89 ± 0.94	202.65 ± 1.11	205.38 ± 3.34	-48.79 ± 0.83	-34.92 ± 1.11	142.32 ± 0.55
253.91	417 ± 1.28	-7.47 ± 0.84	-45 ± 1.03	197.94 ± 1.1	210.88 ± 1.89	-55.79 ± 0.81	-31.86 ± 1.02	152.24 ± 0.65
263.67	411.51 ± 1.41	-5.34 ± 0.65	-33.07 ± 1.4	223.9 ± 1.02	218.65 ± 0.61	-56.54 ± 0.45	-24.12 ± 0.87	149.36 ± 0.98
273.44	413.37 ± 0.47	0.01 ± 1.37	-29.64 ± 0.66	200.48 ± 0.61	225.37 ± 0.55	-60.62 ± 0.82	-26.11 ± 0.72	110.11 ± 0.85
283.20	411.7 ± 1.06	-6.73 ± 0.72	-30.02 ± 1	245.44 ± 0.56	241.8 ± 0.57	-68.68 ± 1.12	-29.1 ± 1.66	165.1 ± 0.66
292.97	412.6 ± 0.89	0.26 ± 1.11	-18.98 ± 1.36	199.45 ± 1.72	241.1 ± 1.13	-61.43 ± 0.54	-19.29 ± 0.93	169.52 ± 0.63

Pad Configuration: t_p = 10 mm

Figure D. 1 shows the measured dynamic-stiffness functions for t_p = 10 mm at a rotor speed of 6,000 rpm with a 172 kPa unit load. The black vertical line designated by ω represents the running speed. The direct and cross-coupled, real dynamic-stiffness functions are shown in Figure D. 1 (a) and Figure D. 1 (b), respectively. The direct and cross-coupled, imaginary dynamic-stiffness functions are shown in Figure D. 1 (c) and Figure D. 1 (d), respectively.

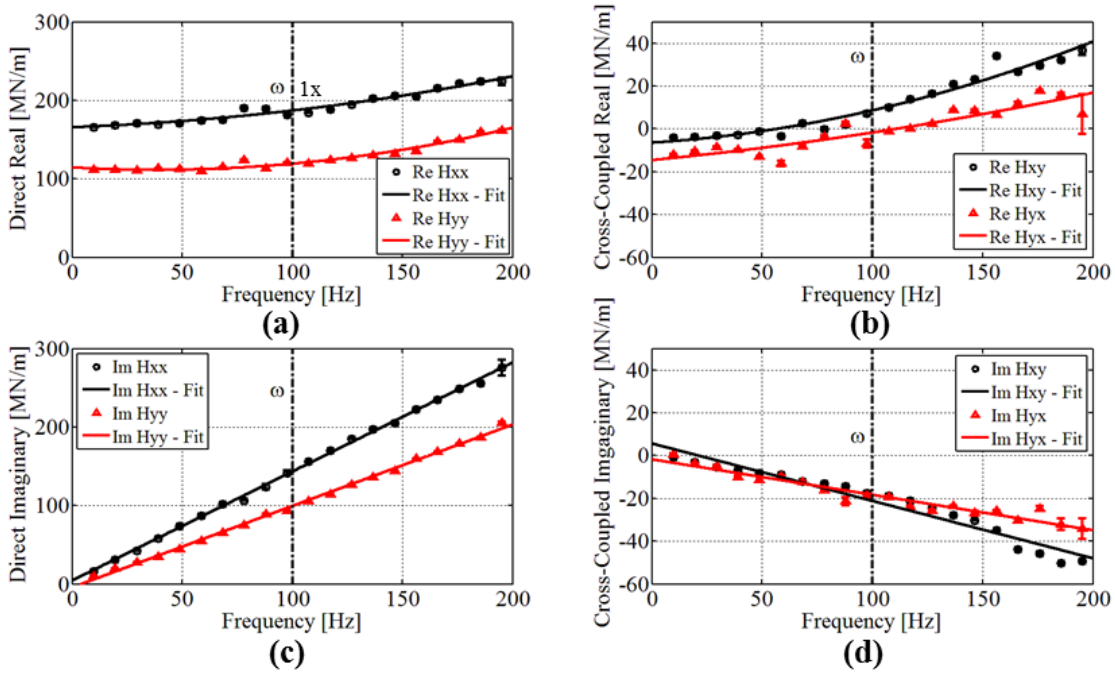

Figure D. 1. Measured dynamic-stiffness at 6 krpm (100 Hz, 32 m/s) and 172 kPa for t_p = 10 mm for (a) direct real, (b) cross-coupled real, (c) direct imaginary, and (d) cross-coupled imaginary.

The measured direct real dynamic-stiffness (Figure D. 1 (a)) and cross-coupled real dynamic-stiffness (Figure D. 1 (b)) show a slight increase in value as excitation frequency Ω increases indicating negative virtual-mass coefficients. Measured $\mathrm{Re}(\boldsymbol{H}_{xx})$ is larger than measured $\mathrm{Re}(\boldsymbol{H}_{yy})$. $\mathrm{Re}(\boldsymbol{H}_{xy})$ and $\mathrm{Re}(\boldsymbol{H}_{yx})$ have the same sign, indicating there is no impact on stability for this test condition. The curve fits

show that: (1) $K_{xx} > K_{yy}$, (2) K_{xx} and K_{yy} are positive, (3) $K_{yx} > K_{xy}$, (4) K_{yx} are K_{xy} are negative, (5) all virtual-mass coefficients are negative.

The measured direct imaginary dynamic-stiffness (Figure D. 1 (c)) and cross-coupled imaginary dynamic-stiffness (Figure D. 1 (d)) increase and decrease, respectively, linearly as Ω increases. The slope of measured $\mathrm{Im}(\boldsymbol{H}_{xx})$ is larger than the slope of measured $\mathrm{Im}(\boldsymbol{H}_{yy})$. The slope of measured $\mathrm{Im}(\boldsymbol{H}_{xy})$ is larger than the slope of measured $\mathrm{Im}(\boldsymbol{H}_{yx})$ and both slopes are negative. The curve fits show that: (1) $C_{xx} > C_{yy}$, (2) C_{xx} and C_{yy} are positive, (3) $|C_{xy}| > C_{yx}$, and (4) C_{xy} and C_{yx} are negative.

Figure D. 2 shows the measured dynamic-stiffness functions for t_p = 10 mm at a rotor speed of 12,000 rpm with a 1,724 kPa unit load. The black vertical line designated by ω represents the running speed. The direct and cross-coupled, real dynamic-stiffness functions are shown in Figure D. 2 (a) and Figure D. 2 (b), respectively. The direct and cross-coupled, imaginary dynamic-stiffness functions are shown in Figure D. 2 (c) and Figure D. 2 (d), respectively.

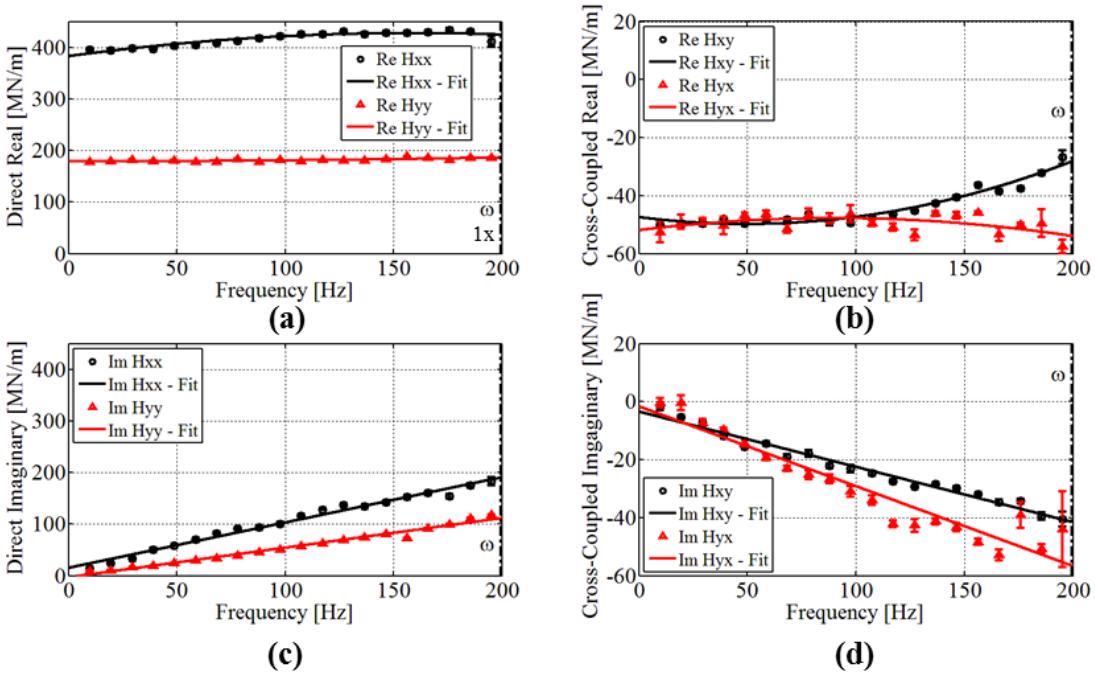

Figure D. 2. Measured dynamic-stiffness at 12 krpm (200 Hz, 64 m/s) and 1,724 kPa for t_p = 10 mm for (a) direct real, (b) cross-coupled real, (c) direct imaginary, and (d) cross-coupled imaginary.

Real $\mathbf{H_{xx}}$ and $\mathbf{H_{yy}}$ (Figure D. 2 (a)) show a slight increase in value as Ω increases and $\mathrm{Re}(\boldsymbol{H}_{xx}) > \mathrm{Re}(\boldsymbol{H}_{yy})$. Real $\mathbf{H_{xy}}$ and $\mathbf{H_{yx}}$ (Figure D. 2 (b)) show a slight decrease in $\mathrm{Re}(\boldsymbol{H}_{yx})$ as the excitation frequency increases, and an increase in $\mathrm{Re}(\boldsymbol{H}_{xy})$ as Ω increases. $\mathrm{Re}(\boldsymbol{H}_{yx})$ and $\mathrm{Re}(\boldsymbol{H}_{xy})$ have opposite signs at larger excitation frequencies, indicating M_{xy} and M_{yx} have opposite signs. The curve fits also show that: (1) $K_{xx} > K_{yy}$, (2) K_{xx} and K_{yy} are positive, (3) $K_{yx} > K_{xy}$, (4) K_{yx} are K_{xy} are negative, (5) M_{xx}, M_{yy}, and M_{xy} are negative, and (6) M_{yx} is positive.

Imaginary $\mathbf{H_{xx}}$ and $\mathbf{H_{yy}}$ (Figure D. 2 (c)) and imaginary $\mathbf{H_{xy}}$ and $\mathbf{H_{yx}}$ (Figure D. 2 (d)) increase and decrease, respectively, linearly as Ω increases. The slope of measured $\mathrm{Im}(\boldsymbol{H}_{xx})$ is larger than the slope of measured $\mathrm{Im}(\boldsymbol{H}_{yy})$. The slope of measured $\mathrm{Im}(\boldsymbol{H}_{xy})$ is larger than the slope of measured $\mathrm{Im}(\boldsymbol{H}_{yx})$ and both slopes are negative.

The curve fits show that: (1) $C_{xx} > C_{yy}$, (2) C_{xx} and C_{yy} are positive, (3) $|C_{xy}| > C_{yx}$, and (4) C_{xy} and C_{yx} are negative.

Table D. 16. Measured dynamic-stiffness real and imaginary parts at 6,000 rpm and 172 kPa for t_p=10 mm.

Freq. [Hz.]	Re (H_{xx}) [MN/m]	Re (H_{xy}) [MN/m]	Re (H_{yx}) [MN/m]	Re (H_{yy}) [MN/m]	Im (H_{xx}) [MN/m]	Im (H_{xy}) [MN/m]	Im (H_{yx}) [MN/m]	Im (H_{yy}) [MN/m]
9.77	166.06 ± 0.23	-3.95 ± 0.31	-12.1 ± 0.3	111.13 ± 0.25	16.35 ± 0.97	-0.79 ± 0.4	0.6 ± 0.46	9.91 ± 0.22
19.53	168.73 ± 0.65	-3.76 ± 0.24	-10.34 ± 0.22	111.9 ± 0.37	30.86 ± 0.45	-3.07 ± 0.23	-3.68 ± 0.15	19.35 ± 0.17
29.30	171.2 ± 0.84	-3.05 ± 0.1	-8.51 ± 0.21	110.38 ± 0.25	42.73 ± 0.42	-5.28 ± 0.3	-5.14 ± 0.51	27.53 ± 0.35
39.06	169.32 ± 0.23	-2.66 ± 0.24	-9.89 ± 0.31	113.26 ± 0.42	58.56 ± 0.16	-6.83 ± 0.11	-10.14 ± 0.52	34.86 ± 0.28
48.83	171.01 ± 0.46	-0.99 ± 0.31	-13.07 ± 0.34	112.23 ± 0.42	73.6 ± 0.74	-8.24 ± 0.33	-11.4 ± 0.59	43.92 ± 0.52
58.59	174.12 ± 1.16	-3.33 ± 0.24	-16.14 ± 1.22	109.62 ± 0.38	87.12 ± 1.79	-9.01 ± 0.24	-9.89 ± 0.58	54.94 ± 0.29
68.36	175.1 ± 1.02	2.77 ± 0.29	-8.09 ± 0.62	114.73 ± 0.59	102.24 ± 0.77	-12.13 ± 0.33	-12.33 ± 0.72	65.09 ± 0.34
78.13	190.29 ± 1.32	-0.06 ± 0.37	-3.71 ± 0.5	123.9 ± 0.32	106.59 ± 0.39	-13.11 ± 0.35	-16.15 ± 0.37	74.61 ± 0.6
87.89	189.62 ± 1.67	2.07 ± 0.39	2.3 ± 1.04	113.25 ± 0.52	123.43 ± 3.4	-14.2 ± 0.7	-21.37 ± 1.84	88.83 ± 0.59
97.66	181.77 ± 1.39	7.2 ± 1.05	-6.89 ± 1.96	120.03 ± 1.15	141.39 ± 3	-17.62 ± 0.89	-18.72 ± 0.8	93.3 ± 1.2
107.42	184.3 ± 0.56	10.1 ± 0.45	-1.29 ± 0.51	119.28 ± 0.33	155.72 ± 0.7	-18.64 ± 0.39	-19.54 ± 0.76	105.37 ± 0.37
117.19	188.29 ± 0.56	13.76 ± 0.26	0.01 ± 0.69	123.69 ± 0.4	170.06 ± 0.32	-21.16 ± 0.36	-23.84 ± 0.39	114.24 ± 0.38
126.95	194.93 ± 0.74	16.58 ± 0.17	2.35 ± 0.31	126.23 ± 0.3	185.32 ± 0.44	-24.57 ± 0.24	-25.7 ± 0.47	126.7 ± 0.31
136.72	202.81 ± 0.53	20.91 ± 0.22	8.82 ± 0.21	129.88 ± 0.37	197.17 ± 0.92	-27.81 ± 0.18	-23.47 ± 0.23	136.08 ± 0.21
146.48	205.56 ± 0.58	23.07 ± 0.3	8.55 ± 0.5	131.94 ± 0.34	205.52 ± 1.01	-30.2 ± 0.25	-26.89 ± 1.15	143.56 ± 0.35
156.25	204.94 ± 0.57	34.01 ± 0.22	6.39 ± 0.32	135.29 ± 0.32	222.37 ± 0.88	-34.93 ± 0.2	-26 ± 0.42	159.23 ± 0.59
166.02	215.35 ± 1.31	26.82 ± 0.49	11.76 ± 0.9	147.6 ± 0.37	234.97 ± 0.9	-43.75 ± 0.38	-30.33 ± 0.99	167.98 ± 0.47
175.78	222.12 ± 0.79	29.56 ± 0.31	17.84 ± 0.14	150.07 ± 0.47	248.44 ± 0.26	-45.78 ± 0.59	-24.77 ± 1.15	178.66 ± 0.42
185.55	224.11 ± 0.75	32.1 ± 0.39	15.89 ± 1.03	159.61 ± 0.72	255.82 ± 1.74	-50.26 ± 0.19	-32.23 ± 2.73	187.13 ± 0.61
195.31	224.15 ± 4.63	36.6 ± 2.18	6.78 ± 9.26	161.26 ± 1.48	275.63 ± 9.75	-49.34 ± 0.71	-34.18 ± 4.68	205.19 ± 1.78
205.08	238.29 ± 2.77	42.44 ± 0.95	41.5 ± 2.42	161.84 ± 1.41	295.25 ± 1.59	-54.45 ± 0.49	-7.08 ± 0.97	204.7 ± 1.2
214.84	247.83 ± 1.07	53.9 ± 0.82	50.77 ± 0.22	150.27 ± 0.48	317.32 ± 0.47	-53.38 ± 0.42	-7.79 ± 0.57	227.89 ± 0.68
224.61	254.7 ± 2.43	41.95 ± 0.71	47.61 ± 1.52	205.37 ± 1.19	345.02 ± 1.02	-91.78 ± 0.73	5.81 ± 1.91	223.81 ± 1.41
234.38	279.24 ± 0.57	44.93 ± 0.24	87.53 ± 0.54	206.1 ± 0.52	351.77 ± 0.7	-72.05 ± 0.31	24.97 ± 1.02	238.38 ± 0.73
244.14	292.92 ± 1.17	53.24 ± 0.47	98.75 ± 2.97	201.34 ± 0.7	412.31 ± 1.15	-71.05 ± 0.17	123.46 ± 2.81	245.94 ± 0.64
253.91	348.2 ± 2.69	56.85 ± 0.87	189.77 ± 5.57	202.25 ± 1.27	333.84 ± 4.06	-80.79 ± 0.97	-39.79 ± 6.16	240.6 ± 1.47
263.67	495.62 ± 2.03	78.31 ± 2	488.68 ± 7.75	207.91 ± 3.17	308.02 ± 9.14	-117.39 ± 0.81	-1.07 ± 14.48	216.08 ± 2.5
273.44	360.85 ± 1.87	72.29 ± 0.67	193 ± 2.75	188.98 ± 1.3	298.37 ± 1.85	-91.36 ± 1.48	-86.97 ± 1.72	304.62 ± 1.23
283.20	334.21 ± 1.65	63.44 ± 0.45	204.22 ± 3.64	302.43 ± 1.82	317.78 ± 0.92	-128.52 ± 1.27	-63.75 ± 3.71	308.1 ± 2.62
292.97	324.81 ± 1.43	54.28 ± 0.78	88.12 ± 1.89	238.59 ± 0.71	313.29 ± 1.03	-87.25 ± 0.41	-112.27 ± 1.99	321.27 ± 0.49

Table D. 17. Measured dynamic-stiffness real and imaginary parts at 6,000 rpm and 345 kPa for t_p=10 mm.

Freq. [Hz.]	Re (H_{xx}) [MN/m]	Re (H_{xy}) [MN/m]	Re (H_{yx}) [MN/m]	Re (H_{yy}) [MN/m]	Im (H_{xx}) [MN/m]	Im (H_{xy}) [MN/m]	Im (H_{yx}) [MN/m]	Im (H_{yy}) [MN/m]
9.77	188.63 ± 0.31	-5.88 ± 0.2	-10.76 ± 0.19	107.48 ± 0.31	15.75 ± 0.36	-1.44 ± 0.22	0.62 ± 0.07	8.86 ± 0.25
19.53	189.17 ± 0.43	-5.59 ± 0.32	-11.27 ± 0.38	107.53 ± 0.46	30.38 ± 0.43	-3.64 ± 0.05	-3.89 ± 0.09	17.76 ± 0.16
29.30	192.24 ± 0.41	-5.15 ± 0.15	-10.03 ± 0.36	106.88 ± 0.34	44.6 ± 0.2	-5.43 ± 0.26	-6.83 ± 0.27	25.41 ± 0.15
39.06	194.35 ± 0.32	-3.82 ± 0.14	-11.16 ± 0.2	108.67 ± 0.27	59.08 ± 0.14	-7.91 ± 0.27	-8.88 ± 0.4	32.97 ± 0.19
48.83	195.55 ± 0.72	-3.32 ± 0.32	-11.84 ± 0.17	108.05 ± 0.3	74.07 ± 0.58	-10.17 ± 0.26	-12.53 ± 0.54	42.34 ± 0.14
58.59	198.35 ± 0.81	-3.36 ± 0.27	-13.75 ± 0.27	105.97 ± 0.31	86.87 ± 0.24	-11.49 ± 0.23	-15.13 ± 0.48	51.1 ± 0.36
68.36	201.52 ± 0.7	0.36 ± 0.25	-8.81 ± 0.41	108.29 ± 0.23	98.64 ± 0.73	-11.45 ± 0.11	-17.77 ± 0.57	64.15 ± 0.39
78.13	196.96 ± 0.25	2.94 ± 0.41	-7.08 ± 0.68	110.91 ± 0.4	114.57 ± 0.61	-15.05 ± 0.32	-25.39 ± 0.45	71.96 ± 0.55
87.89	214.49 ± 1.86	-2.27 ± 0.72	-9.27 ± 0.65	106.29 ± 0.51	145.45 ± 2.09	-17.36 ± 0.73	-19.07 ± 1.98	81.99 ± 0.36
97.66	209.03 ± 2.08	5.1 ± 1.19	-10.4 ± 3.15	113.61 ± 1.13	135.26 ± 4.58	-18.65 ± 1.65	-20.55 ± 1.3	90.45 ± 0.67
107.42	208.17 ± 0.52	7.22 ± 0.45	-7.1 ± 0.53	114.99 ± 0.47	151.58 ± 1.39	-20.86 ± 0.6	-23.98 ± 0.8	101.15 ± 0.61
117.19	211.91 ± 0.75	9.97 ± 0.26	-5.12 ± 0.36	117.65 ± 0.34	167.59 ± 0.23	-23.47 ± 0.19	-29.59 ± 0.69	109.88 ± 0.39
126.95	214.67 ± 0.89	13.17 ± 0.29	-1.82 ± 0.52	121.24 ± 0.45	183.55 ± 0.77	-27.2 ± 0.33	-34.96 ± 0.42	122.81 ± 0.24
136.72	226.77 ± 0.71	16.05 ± 0.12	4.17 ± 1.08	124.98 ± 0.42	194.51 ± 0.39	-30.68 ± 0.12	-20.08 ± 0.38	130.8 ± 0.32
146.48	229.21 ± 0.14	18.96 ± 0.17	5.01 ± 0.51	127.4 ± 0.36	206.36 ± 0.32	-32.78 ± 0.23	-25.42 ± 0.25	139.1 ± 0.26
156.25	232.73 ± 0.35	27.04 ± 0.24	8.69 ± 0.34	121.7 ± 0.2	219.16 ± 0.45	-36.04 ± 0.37	-33.81 ± 0.44	140.37 ± 0.27
166.02	236.38 ± 0.84	21.01 ± 0.14	8.22 ± 0.83	139.77 ± 0.27	231.19 ± 0.4	-44.94 ± 0.29	-35.9 ± 0.84	159.15 ± 0.23
175.78	245.41 ± 1.06	24.19 ± 0.43	14.11 ± 0.91	141.86 ± 0.38	245.39 ± 0.98	-47.77 ± 0.39	-21.45 ± 0.79	168.91 ± 0.36
185.55	245.49 ± 1.55	26.21 ± 0.68	18.39 ± 0.23	147.29 ± 0.33	258.11 ± 1.2	-51.94 ± 0.72	-35.91 ± 0.36	178.05 ± 0.51
195.31	247.1 ± 5.19	31.05 ± 1.29	20.63 ± 3.1	143.97 ± 0.56	277.88 ± 1.03	-53.63 ± 1	-69.96 ± 1.3	192.91 ± 1.17
205.08	261.25 ± 1.6	29.04 ± 2.04	33.24 ± 1.37	156.43 ± 1.35	282.47 ± 0.91	-60.16 ± 0.88	-15.86 ± 0.74	192.25 ± 0.96
214.84	261.03 ± 1.01	35.16 ± 0.7	40.33 ± 0.59	161.63 ± 0.4	298.22 ± 1	-61.29 ± 0.68	-14.5 ± 0.41	201.62 ± 0.33
224.61	256.22 ± 0.45	68.49 ± 0.94	59.37 ± 1.07	117.04 ± 1.34	323.85 ± 0.88	-97.72 ± 0.84	-71.9 ± 0.91	326.03 ± 0.58
234.38	280.96 ± 0.47	31.17 ± 0.56	46.24 ± 1.13	183.82 ± 0.59	326.57 ± 0.69	-73.28 ± 0.62	-8.3 ± 0.58	227.15 ± 0.56
244.14	303.42 ± 0.75	32.76 ± 0.37	42 ± 0.99	172.66 ± 0.6	346.5 ± 1.58	-72.75 ± 0.53	-2.77 ± 1.02	239.1 ± 0.49
253.91	302.71 ± 0.52	38.88 ± 0.52	69.61 ± 1.26	203.77 ± 0.73	362.66 ± 0.63	-77.39 ± 0.24	18.37 ± 0.75	247.2 ± 0.46
263.67	310.18 ± 0.61	46.95 ± 0.45	64.53 ± 1.56	199.39 ± 0.62	373.12 ± 1.08	-66.47 ± 0.6	-15.14 ± 2.62	253.81 ± 0.68
273.44	361.61 ± 0.65	57.65 ± 1.06	189.17 ± 1.4	260.58 ± 0.91	383.62 ± 0.58	-121.18 ± 0.23	5.04 ± 1.94	295.04 ± 1.35
283.20	340.85 ± 0.96	61.08 ± 0.57	39.69 ± 1.14	217.6 ± 0.38	410.23 ± 0.87	-80.06 ± 0.33	25.78 ± 0.97	267.68 ± 0.45
292.97	307.77 ± 0.61	29.73 ± 0.49	-93.42 ± 2.86	218.34 ± 0.62	304.34 ± 2.91	-78.1 ± 0.28	-141.52 ± 0.96	308.84 ± 0.87

Table D. 18. Measured dynamic-stiffness real and imaginary parts at 6,000 rpm and 689 kPa for t_p=10 mm.

Freq. [Hz.]	Re (H_{xx}) [MN/m]	Re (H_{xy}) [MN/m]	Re (H_{yx}) [MN/m]	Re (H_{yy}) [MN/m]	Im (H_{xx}) [MN/m]	Im (H_{xy}) [MN/m]	Im (H_{yx}) [MN/m]	Im (H_{yy}) [MN/m]
9.77	188.63 ± 0.31	-5.88 ± 0.2	-10.76 ± 0.19	107.48 ± 0.31	15.75 ± 0.36	-1.44 ± 0.22	0.62 ± 0.07	8.86 ± 0.25
19.53	189.17 ± 0.43	-5.59 ± 0.32	-11.27 ± 0.38	107.53 ± 0.46	30.38 ± 0.43	-3.64 ± 0.05	-3.89 ± 0.09	17.76 ± 0.16
29.30	192.24 ± 0.41	-5.15 ± 0.15	-10.03 ± 0.36	106.88 ± 0.34	44.6 ± 0.2	-5.43 ± 0.26	-6.83 ± 0.27	25.41 ± 0.15
39.06	194.35 ± 0.32	-3.82 ± 0.14	-11.16 ± 0.2	108.67 ± 0.27	59.08 ± 0.14	-7.91 ± 0.27	-8.88 ± 0.4	32.97 ± 0.19
48.83	195.55 ± 0.72	-3.32 ± 0.32	-11.84 ± 0.17	108.05 ± 0.3	74.07 ± 0.58	-10.17 ± 0.26	-12.53 ± 0.54	42.34 ± 0.14
58.59	198.35 ± 0.81	-3.36 ± 0.27	-13.75 ± 0.27	105.97 ± 0.31	86.87 ± 0.24	-11.49 ± 0.23	-15.13 ± 0.48	51.1 ± 0.36
68.36	201.52 ± 0.7	0.36 ± 0.25	-8.81 ± 0.41	108.29 ± 0.23	98.64 ± 0.73	-11.45 ± 0.11	-17.77 ± 0.57	64.15 ± 0.39
78.13	196.96 ± 0.25	2.94 ± 0.41	-7.08 ± 0.68	110.91 ± 0.4	114.57 ± 0.61	-15.05 ± 0.32	-25.39 ± 0.45	71.96 ± 0.55
87.89	214.49 ± 1.86	-2.27 ± 0.72	-9.27 ± 0.65	106.29 ± 0.51	145.45 ± 2.09	-17.36 ± 0.73	-19.07 ± 1.98	81.99 ± 0.36
97.66	209.03 ± 2.08	5.1 ± 1.19	-10.4 ± 3.15	113.61 ± 1.13	135.26 ± 4.58	-18.65 ± 1.65	-20.55 ± 1.3	90.45 ± 0.67
107.42	208.17 ± 0.52	7.22 ± 0.45	-7.1 ± 0.53	114.99 ± 0.47	151.58 ± 1.39	-20.86 ± 0.6	-23.98 ± 0.8	101.15 ± 0.61
117.19	211.91 ± 0.75	9.97 ± 0.26	-5.12 ± 0.36	117.65 ± 0.34	167.59 ± 0.23	-23.47 ± 0.19	-29.59 ± 0.69	109.88 ± 0.39
126.95	214.67 ± 0.89	13.17 ± 0.29	-1.82 ± 0.52	121.24 ± 0.45	183.55 ± 0.77	-27.2 ± 0.33	-34.96 ± 0.42	122.81 ± 0.24
136.72	226.77 ± 0.71	16.05 ± 0.12	4.17 ± 1.08	124.98 ± 0.42	194.51 ± 0.39	-30.68 ± 0.12	-20.08 ± 0.38	130.8 ± 0.32
146.48	229.21 ± 0.14	18.96 ± 0.17	5.01 ± 0.51	127.4 ± 0.36	206.36 ± 0.32	-32.78 ± 0.23	-25.42 ± 0.25	139.1 ± 0.26
156.25	232.73 ± 0.35	27.04 ± 0.24	8.69 ± 0.34	121.7 ± 0.2	219.16 ± 0.45	-36.04 ± 0.37	-33.81 ± 0.44	140.37 ± 0.27
166.02	236.38 ± 0.84	21.01 ± 0.14	8.22 ± 0.83	139.77 ± 0.27	231.19 ± 0.4	-44.94 ± 0.29	-35.9 ± 0.84	159.15 ± 0.23
175.78	245.41 ± 1.06	24.19 ± 0.43	14.11 ± 0.91	141.86 ± 0.38	245.39 ± 0.98	-47.77 ± 0.39	-21.45 ± 0.79	168.91 ± 0.36
185.55	245.49 ± 1.55	26.21 ± 0.68	18.39 ± 0.23	147.29 ± 0.33	258.11 ± 1.2	-51.94 ± 0.72	-35.91 ± 0.36	178.05 ± 0.51
195.31	247.1 ± 5.19	31.05 ± 1.29	20.63 ± 3.1	143.97 ± 0.56	277.88 ± 1.03	-53.63 ± 1	-69.96 ± 1.3	192.91 ± 1.17
205.08	261.25 ± 1.6	29.04 ± 2.04	33.24 ± 1.37	156.43 ± 1.35	282.47 ± 0.91	-60.16 ± 0.88	-15.86 ± 0.74	192.25 ± 0.96
214.84	261.03 ± 1.01	35.16 ± 0.7	40.33 ± 0.59	161.63 ± 0.4	298.22 ± 1	-61.29 ± 0.68	-14.5 ± 0.41	201.62 ± 0.33
224.61	256.22 ± 0.45	68.49 ± 0.94	59.37 ± 1.07	117.04 ± 1.34	323.85 ± 0.88	-97.72 ± 0.84	-71.9 ± 0.91	326.03 ± 0.58
234.38	280.96 ± 0.47	31.17 ± 0.56	46.24 ± 1.13	183.82 ± 0.59	326.57 ± 0.69	-73.28 ± 0.62	-8.3 ± 0.58	227.15 ± 0.56
244.14	303.42 ± 0.75	32.76 ± 0.37	42 ± 0.99	172.66 ± 0.6	346.5 ± 1.58	-72.75 ± 0.53	-2.77 ± 1.02	239.1 ± 0.49
253.91	302.71 ± 0.52	38.88 ± 0.52	69.61 ± 1.26	203.77 ± 0.73	362.66 ± 0.63	-77.39 ± 0.24	18.37 ± 0.75	247.2 ± 0.46
263.67	310.18 ± 0.61	46.95 ± 0.45	64.53 ± 1.56	199.39 ± 0.62	373.12 ± 1.08	-66.47 ± 0.6	-15.14 ± 2.62	253.81 ± 0.68
273.44	361.61 ± 0.65	57.65 ± 1.06	189.17 ± 1.4	260.58 ± 0.91	383.62 ± 0.58	-121.18 ± 0.23	5.04 ± 1.94	295.04 ± 1.35
283.20	340.85 ± 0.96	61.08 ± 0.57	39.69 ± 1.14	217.6 ± 0.38	410.23 ± 0.87	-80.06 ± 0.33	25.78 ± 0.97	267.68 ± 0.45
292.97	307.77 ± 0.61	29.73 ± 0.49	-93.42 ± 2.86	218.34 ± 0.62	304.34 ± 2.91	-78.1 ± 0.28	-141.52 ± 0.96	308.84 ± 0.87

Table D. 19. Measured dynamic-stiffness real and imaginary parts at 6,000 rpm and 1034 kPa for t_p=10 mm.

Freq. [Hz.]	Re (H_{xx}) [MN/m]	Re (H_{xy}) [MN/m]	Re (H_{yx}) [MN/m]	Re (H_{yy}) [MN/m]	Im (H_{xx}) [MN/m]	Im (H_{xy}) [MN/m]	Im (H_{yx}) [MN/m]	Im (H_{yy}) [MN/m]
9.77	290.96 ± 0.33	-19.05 ± 0.25	-22.35 ± 0.39	123.74 ± 0.17	17.58 ± 0.61	-1.76 ± 0.31	0.9 ± 0.35	8.07 ± 0.29
19.53	294.8 ± 0.57	-18.87 ± 0.27	-21.45 ± 0.2	123.07 ± 0.24	34.17 ± 0.29	-4.65 ± 0.34	-3.56 ± 0.2	12.59 ± 0.25
29.30	298.88 ± 0.52	-18.96 ± 0.3	-20.88 ± 0.12	124.94 ± 0.31	50.57 ± 0.41	-6.54 ± 0.37	-9.59 ± 0.57	19.19 ± 0.29
39.06	303.55 ± 0.54	-17.02 ± 0.16	-20.68 ± 0.24	121.38 ± 0.19	64.44 ± 0.19	-9.39 ± 0.19	-12.88 ± 0.46	27.48 ± 0.35
48.83	307.15 ± 0.47	-16.43 ± 0.29	-22.1 ± 0.44	121.57 ± 0.38	77.83 ± 0.77	-12.71 ± 0.3	-16.96 ± 0.71	35.53 ± 0.23
58.59	309.94 ± 0.5	-15.55 ± 0.46	-22.76 ± 0.37	120.46 ± 0.35	90.66 ± 0.96	-15.07 ± 0.42	-21.89 ± 0.48	44.64 ± 0.17
68.36	307.22 ± 0.83	-16.25 ± 0.44	-29.31 ± 0.57	117.12 ± 0.33	104.31 ± 0.68	-17.06 ± 0.21	-23.44 ± 0.57	52.07 ± 0.21
78.13	314.55 ± 2	-10.02 ± 0.24	-19.85 ± 0.6	125.61 ± 0.43	116.54 ± 0.54	-18.72 ± 0.48	-31.17 ± 0.83	60.33 ± 0.21
87.89	319.79 ± 1.52	-11.19 ± 0.62	-22.69 ± 1.87	121.45 ± 0.53	127.53 ± 0.94	-23.45 ± 0.38	-32.2 ± 1.51	68.39 ± 0.38
97.66	325.5 ± 5.78	-9.4 ± 1.79	-27.58 ± 6.47	128.08 ± 1.08	148.74 ± 15.92	-28.76 ± 1.34	-33.3 ± 4.52	79.49 ± 0.7
107.42	333.29 ± 0.77	-8.81 ± 0.76	-23.74 ± 1.17	129.14 ± 0.42	152.48 ± 2.72	-32.56 ± 0.33	-29.24 ± 0.52	87.31 ± 0.48
117.19	331.47 ± 1.29	-6.36 ± 0.12	-25.23 ± 0.9	131.91 ± 0.35	167.24 ± 0.56	-36.33 ± 0.32	-35.56 ± 0.55	95.01 ± 0.41
126.95	336.69 ± 1.14	-5.04 ± 0.52	-22.24 ± 0.57	133.99 ± 0.38	182.92 ± 1.02	-41.02 ± 0.23	-42.32 ± 0.96	104.37 ± 0.18
136.72	339.88 ± 0.48	-3.21 ± 0.28	-13.97 ± 0.56	136.11 ± 0.37	190.28 ± 0.56	-44.91 ± 0.12	-30.31 ± 0.4	112.69 ± 0.34
146.48	345.61 ± 0.27	-3.51 ± 0.2	-14.37 ± 0.57	141.41 ± 0.34	199.13 ± 0.17	-47.08 ± 0.31	-33.68 ± 0.6	118.03 ± 0.31
156.25	348.09 ± 0.86	1.15 ± 0.21	-9.02 ± 0.27	144.99 ± 0.29	211.32 ± 1.06	-51 ± 0.14	-39.23 ± 0.64	111.72 ± 0.26
166.02	353.37 ± 1.26	-5.46 ± 0.31	-11.61 ± 0.59	150.97 ± 0.25	223.64 ± 1.51	-57.64 ± 0.14	-42.89 ± 1.07	132.24 ± 0.41
175.78	362.3 ± 0.65	-4.48 ± 0.23	-2.07 ± 0.4	148.92 ± 0.32	226.7 ± 0.59	-59.36 ± 0.41	-36.52 ± 0.89	139.72 ± 0.52
185.55	354.4 ± 2.75	-2.33 ± 0.46	-6.31 ± 0.53	156.41 ± 0.43	245.66 ± 1.58	-63.35 ± 0.61	-43.85 ± 1.05	151.65 ± 0.38
195.31	353.94 ± 6.98	2.23 ± 1.36	6.04 ± 1.57	153.82 ± 1.15	265.02 ± 10.28	-65.16 ± 1.93	-54.78 ± 2.82	161.19 ± 0.68
205.08	373.81 ± 1.09	-1.51 ± 0.63	6.27 ± 0.74	165.29 ± 0.68	263.63 ± 1	-69.31 ± 1	-39.56 ± 1.21	161.4 ± 0.34
214.84	376.55 ± 0.82	2.91 ± 0.61	6.53 ± 0.88	171.78 ± 0.3	279.76 ± 0.81	-73.63 ± 0.32	-40.81 ± 0.47	171.91 ± 0.25
224.61	385.4 ± 0.57	9.59 ± 0.62	13.59 ± 0.64	107.89 ± 0.32	292.43 ± 0.45	-76.1 ± 0.34	-38.4 ± 0.17	156.93 ± 0.25
234.38	396.74 ± 1.05	-1.79 ± 0.6	6.82 ± 0.75	179.09 ± 0.35	301.13 ± 0.74	-81.01 ± 0.42	-43.7 ± 0.58	190 ± 0.38
244.14	405.31 ± 1.32	-0.69 ± 0.41	16.44 ± 1.33	174.84 ± 0.52	314.89 ± 1.63	-78.64 ± 0.43	-43.06 ± 1.14	185.48 ± 0.25
253.91	411.03 ± 0.6	8.39 ± 0.87	27.1 ± 1.05	176.95 ± 1.73	319.47 ± 0.97	-94.8 ± 0.44	-32.2 ± 1.12	232.56 ± 0.28
263.67	413.98 ± 1.11	1.96 ± 0.97	23.97 ± 0.97	202.74 ± 0.47	334.4 ± 0.87	-81.92 ± 0.43	-32.78 ± 0.61	200.07 ± 0.24
273.44	425.07 ± 0.25	10.95 ± 0.38	32.95 ± 0.47	185.37 ± 0.47	345.58 ± 0.27	-81.76 ± 0.82	-20.07 ± 0.29	193.78 ± 0.28
283.20	429.99 ± 0.98	4.02 ± 0.34	42.21 ± 0.3	218.23 ± 0.35	369.9 ± 0.76	-92.33 ± 0.36	-30.44 ± 1.15	219.62 ± 0.4
292.97	450.24 ± 0.88	11.62 ± 0.28	62.62 ± 0.57	188.52 ± 0.43	379.94 ± 0.37	-81.63 ± 0.45	12.2 ± 0.39	215.24 ± 0.46

Table D. 20. Measured dynamic-stiffness real and imaginary parts at 6,000 rpm and 1,724 kPa for t_p=10 mm.

Freq. [Hz.]	Re (H_{xx}) [MN/m]	Re (H_{xy}) [MN/m]	Re (H_{yx}) [MN/m]	Re (H_{yy}) [MN/m]	Im (H_{xx}) [MN/m]	Im (H_{xy}) [MN/m]	Im (H_{yx}) [MN/m]	Im (H_{yy}) [MN/m]
9.77	399.42 ± 0.3	-43.49 ± 0.33	-44.51 ± 0.56	158.15 ± 0.4	19.98 ± 0.73	-1.66 ± 0.15	0.25 ± 0.43	7.91 ± 0.3
19.53	401.24 ± 0.71	-42.15 ± 0.31	-44.61 ± 0.57	157.52 ± 0.29	33.6 ± 0.16	-4.76 ± 0.47	-4.39 ± 0.77	11.81 ± 0.2
29.30	406.92 ± 0.81	-43.89 ± 0.29	-45.21 ± 0.42	161.74 ± 0.41	45.32 ± 0.48	-6.54 ± 0.2	-8.72 ± 0.59	16.97 ± 0.17
39.06	411.27 ± 0.69	-39.77 ± 0.28	-44.52 ± 0.16	157.69 ± 0.25	58.63 ± 0.39	-10.31 ± 0.22	-13.8 ± 0.32	23.6 ± 0.34
48.83	415.51 ± 1.1	-38.91 ± 0.78	-46.06 ± 0.65	158.21 ± 0.36	72.83 ± 1.05	-14.45 ± 0.29	-17.36 ± 0.63	31.33 ± 0.24
58.59	418.29 ± 0.75	-37.91 ± 0.39	-47.72 ± 0.63	156.23 ± 0.42	87.87 ± 0.61	-16.5 ± 0.16	-23.85 ± 0.29	39.17 ± 0.33
68.36	417.42 ± 0.7	-36.84 ± 0.25	-50.4 ± 0.67	157.34 ± 0.34	99.62 ± 0.97	-19.4 ± 0.27	-27.54 ± 0.47	44.57 ± 0.33
78.13	425.62 ± 1.95	-31.6 ± 0.29	-43.57 ± 1.47	162.53 ± 0.35	113 ± 1.1	-21.04 ± 0.36	-30.86 ± 0.89	52.12 ± 0.36
87.89	427.6 ± 2.78	-33.96 ± 0.81	-50.39 ± 1.37	158.63 ± 0.3	116.76 ± 3.98	-25.3 ± 0.48	-29.51 ± 2.17	58.01 ± 0.8
97.66	420.23 ± 11.72	-32.45 ± 1.59	-49.41 ± 3.83	165.54 ± 1.75	136.66 ± 8.61	-31.91 ± 3.97	-29.88 ± 4.56	68.25 ± 1
107.42	438.14 ± 1.41	-32.41 ± 0.5	-49.4 ± 1.31	164.42 ± 0.77	147.57 ± 1.89	-37.58 ± 1.06	-35.43 ± 1.05	76.24 ± 0.57
117.19	438.91 ± 1.13	-31.63 ± 0.49	-49.47 ± 0.71	168.08 ± 0.4	160.4 ± 0.81	-42.03 ± 0.4	-38.39 ± 0.42	81.78 ± 0.2
126.95	446.19 ± 0.5	-30.64 ± 0.28	-48.23 ± 0.75	169.14 ± 0.34	176.79 ± 0.96	-47.7 ± 0.44	-39.45 ± 0.3	89.4 ± 0.18
136.72	443.66 ± 0.65	-30.94 ± 0.2	-41.16 ± 0.4	172.03 ± 0.23	170.86 ± 0.95	-49.25 ± 0.33	-34.69 ± 0.85	94.96 ± 0.38
146.48	447.65 ± 0.51	-31.26 ± 0.13	-39.05 ± 0.24	177.28 ± 0.24	181.22 ± 0.32	-51.36 ± 0.3	-36.92 ± 0.71	101.61 ± 0.19
156.25	448.89 ± 1.1	-28.05 ± 0.21	-34.33 ± 0.86	183.49 ± 0.34	194.72 ± 0.93	-56.06 ± 0.21	-41.68 ± 0.35	93.86 ± 0.15
166.02	454.04 ± 1.33	-34.74 ± 0.19	-35.44 ± 0.41	183.49 ± 0.28	208.71 ± 1.27	-61.48 ± 0.34	-47.4 ± 0.55	112.93 ± 0.16
175.78	457.65 ± 1.41	-33.68 ± 0.39	-30.55 ± 0.4	182.1 ± 0.38	207.89 ± 0.95	-61.3 ± 0.32	-42.39 ± 1	119.02 ± 0.27
185.55	452.23 ± 2.12	-29.88 ± 0.53	-32.4 ± 0.9	188.23 ± 0.42	228.89 ± 2.47	-66 ± 0.14	-47.22 ± 0.68	130.88 ± 0.37
195.31	442.04 ± 12.29	-25.26 ± 1.07	-23.38 ± 2.19	186.16 ± 0.8	243.41 ± 4.3	-65.44 ± 1.61	-56.48 ± 5.12	135.02 ± 0.64
205.08	469.17 ± 2.19	-29.82 ± 0.52	-22.05 ± 0.98	194.97 ± 0.44	243.77 ± 1.64	-71.03 ± 0.4	-48.55 ± 0.75	139.42 ± 0.5
214.84	473.5 ± 1.09	-26.46 ± 0.14	-19.93 ± 0.63	201.84 ± 0.53	257.43 ± 0.49	-73.84 ± 0.55	-49.47 ± 0.93	144.92 ± 0.22
224.61	480.32 ± 0.7	-22.11 ± 0.3	-18.05 ± 0.27	141.47 ± 0.25	268.04 ± 0.58	-77.28 ± 0.15	-49.28 ± 0.59	126.8 ± 0.31
234.38	497.97 ± 1.39	-33.13 ± 0.42	-22.58 ± 0.83	206.83 ± 0.47	273.72 ± 0.95	-80.78 ± 0.41	-53.08 ± 0.7	160.92 ± 0.35
244.14	495.8 ± 2.1	-30.36 ± 0.51	-12.57 ± 0.5	205.41 ± 0.41	286.81 ± 1.07	-79.15 ± 0.32	-53.34 ± 0.69	158.56 ± 0.41
253.91	502.65 ± 0.93	-26.05 ± 0.46	-8.69 ± 0.31	203.06 ± 0.31	287.26 ± 0.41	-85.28 ± 0.33	-44.1 ± 0.51	175.2 ± 0.24
263.67	498.03 ± 0.82	-26.64 ± 0.58	0.67 ± 0.78	225.69 ± 0.5	302.97 ± 0.67	-84.09 ± 0.52	-44.9 ± 0.38	172.94 ± 0.6
273.44	510.23 ± 0.28	-23.04 ± 0.57	1.87 ± 0.44	220 ± 0.42	311.71 ± 0.19	-85.01 ± 0.26	-42.43 ± 0.3	158.06 ± 0.27
283.20	510.23 ± 1.1	-25.97 ± 0.25	8.15 ± 0.64	238.83 ± 0.36	328.32 ± 0.92	-94.73 ± 0.71	-53.46 ± 0.13	194.45 ± 0.29
292.97	525.46 ± 0.6	-23.55 ± 0.26	19.92 ± 0.24	217.07 ± 0.37	329.54 ± 0.77	-85.31 ± 0.38	-31.47 ± 0.44	181.43 ± 0.23

Table D. 21. Measured dynamic-stiffness real and imaginary parts at 9,000 rpm and 172 kPa for t_p=10 mm.

Freq. [Hz.]	Re (H_{xx}) [MN/m]	Re (H_{xy}) [MN/m]	Re (H_{yx}) [MN/m]	Re (H_{yy}) [MN/m]	Im (H_{xx}) [MN/m]	Im (H_{xy}) [MN/m]	Im (H_{yx}) [MN/m]	Im (H_{yy}) [MN/m]
9.77	210.5 ± 0.74	-16.13 ± 0.51	-23.32 ± 0.67	148.54 ± 0.59	14.41 ± 0.7	-0.72 ± 0.2	-2.26 ± 0.26	8.84 ± 0.32
19.53	213.06 ± 0.55	-16.04 ± 0.58	-22.67 ± 0.52	149.84 ± 0.53	27.43 ± 0.86	-4.36 ± 0.45	-4.57 ± 0.59	17.99 ± 0.6
29.30	212.26 ± 1.09	-14.82 ± 0.32	-18.95 ± 0.36	148.87 ± 0.58	40.46 ± 0.98	-6.28 ± 0.46	-6.52 ± 0.65	25.61 ± 0.37
39.06	216.97 ± 0.58	-14.9 ± 0.36	-21.07 ± 0.13	153.46 ± 0.3	52.27 ± 1.46	-7.77 ± 0.22	-9.82 ± 0.69	31.05 ± 0.37
48.83	218.36 ± 0.62	-13.91 ± 1.56	-24.21 ± 0.94	153.92 ± 0.98	65.67 ± 0.95	-8.27 ± 0.47	-12.62 ± 0.58	38.84 ± 0.3
58.59	216.83 ± 0.6	-15.62 ± 0.68	-28.72 ± 0.8	151.14 ± 0.87	76.49 ± 1.52	-7.97 ± 0.54	-13.86 ± 0.78	47.76 ± 0.44
68.36	244.93 ± 0.61	-21 ± 1.14	-16.11 ± 1.32	152.14 ± 0.56	104.93 ± 5.63	-15.24 ± 1.03	-12.96 ± 2.09	54.07 ± 0.35
78.13	234.64 ± 1.03	-11.48 ± 1.22	-19.3 ± 1.05	164.79 ± 0.71	92.33 ± 1.02	-13.37 ± 0.35	-20.2 ± 0.91	63.86 ± 0.64
87.89	238.86 ± 3.26	-15.15 ± 0.78	-16.21 ± 1.34	156.57 ± 0.33	105.85 ± 0.94	-14.55 ± 0.38	-25.5 ± 1.08	71.92 ± 1.33
97.66	233.1 ± 1.76	-8.18 ± 1.03	-18.7 ± 2.91	159.94 ± 0.65	124.39 ± 1.79	-17.85 ± 0.67	-23.21 ± 1.89	72.95 ± 0.5
107.42	235.24 ± 1.89	-7.7 ± 0.83	-14.71 ± 0.63	159.11 ± 0.44	129.13 ± 0.67	-20.55 ± 0.63	-25.03 ± 0.92	82.81 ± 0.6
117.19	237.56 ± 1.22	-6.8 ± 0.43	-15.12 ± 0.53	160.5 ± 0.46	138.09 ± 0.36	-21.35 ± 0.39	-29.22 ± 0.72	88.54 ± 0.3
126.95	239.36 ± 1.45	-2.9 ± 0.2	-12.58 ± 1.64	160.93 ± 0.49	146.04 ± 1.5	-21.97 ± 0.61	-35.43 ± 1.32	99.58 ± 0.59
136.72	242.52 ± 2.09	1.93 ± 0.54	-8.58 ± 1.18	162.66 ± 0.44	160.76 ± 0.81	-24.21 ± 0.48	-25.3 ± 0.91	107.32 ± 0.36
146.48	241.87 ± 1.87	4.51 ± 0.84	-9.11 ± 1.72	160.72 ± 0.97	166.7 ± 2.25	-24.09 ± 1.18	-27.5 ± 1.46	114.66 ± 0.38
156.25	244.48 ± 0.71	14.54 ± 0.92	-7.44 ± 3.17	162.64 ± 0.91	182.37 ± 2.55	-31.11 ± 1.11	-35.97 ± 1.46	135.75 ± 0.86
166.02	251.32 ± 0.93	7.7 ± 0.73	-7.29 ± 1.92	176.34 ± 0.59	193.08 ± 1.84	-34.57 ± 0.65	-35.22 ± 1.71	134.57 ± 0.47
175.78	256.39 ± 0.7	10.48 ± 0.81	-0.38 ± 1.43	172.23 ± 0.6	200.52 ± 1.47	-33.98 ± 0.68	-37.52 ± 1.13	146.59 ± 0.4
185.55	261.24 ± 2.22	17.57 ± 0.89	-3.54 ± 0.83	182.77 ± 0.9	230.06 ± 6.48	-39.77 ± 0.69	-29.07 ± 4.21	151.94 ± 0.56
195.31	251.1 ± 7.31	25.5 ± 1.1	-29.05 ± 5.51	180.09 ± 1.06	254.98 ± 1.4	-37.04 ± 1.35	-46.82 ± 4.45	170.61 ± 1.83
205.08	266.31 ± 1.53	26.4 ± 0.42	29.67 ± 2.01	181.47 ± 0.8	241.66 ± 1.64	-43.27 ± 0.69	-10.03 ± 2.14	167.57 ± 0.92
214.84	276.97 ± 0.59	43.05 ± 0.49	44.99 ± 1.06	165.46 ± 0.77	263.07 ± 0.66	-40.7 ± 0.41	-18.27 ± 1.41	197.23 ± 0.7
224.61	304.01 ± 3.41	27.13 ± 1.46	22.03 ± 1.82	222.72 ± 1.22	268.87 ± 2.13	-77.56 ± 1.61	-17.21 ± 1.5	178.44 ± 1.7
234.38	350.01 ± 3.92	16.03 ± 1.92	157.25 ± 13.89	176.85 ± 1.86	181.17 ± 11.75	-59.68 ± 1.29	-191.46 ± 13.41	200.76 ± 3.13
244.14	316.34 ± 5.32	29.49 ± 0.65	76.6 ± 2.8	181.14 ± 1.22	253.2 ± 2.6	-49.92 ± 1.45	-8.53 ± 2.65	213.41 ± 0.63
253.91	292.59 ± 3.02	49.66 ± 1.27	34.36 ± 6.49	188.48 ± 0.77	246.64 ± 3.82	-51.72 ± 0.86	-99.02 ± 3.34	242.76 ± 1.26
263.67	371.78 ± 3.98	64.59 ± 1.05	108.18 ± 5.41	194.85 ± 1.69	233.64 ± 3.79	-82.09 ± 1.37	20.77 ± 2.23	258.81 ± 1.54
273.44	317.66 ± 3.08	70.76 ± 1.23	121.09 ± 6.79	211.96 ± 1.47	230.66 ± 0.47	-83.27 ± 0.84	-69.09 ± 1.14	286.73 ± 1.65
283.20	304.47 ± 2.08	39.92 ± 2.2	196.7 ± 13.4	304.41 ± 5.6	220.4 ± 6.43	-114 ± 1.8	-44.11 ± 14.3	256.48 ± 3.49
292.97	309.53 ± 3.01	42.18 ± 2.39	107.43 ± 13.08	240.59 ± 1.89	247.98 ± 5.92	-87.48 ± 1.63	-50.39 ± 3.96	275.62 ± 2.97

Table D. 22. Measured dynamic-stiffness real and imaginary parts at 9,000 rpm and 345 kPa for t_p=10 mm.

Freq. [Hz.]	Re (H_{xx}) [MN/m]	Re (H_{xy}) [MN/m]	Re (H_{yx}) [MN/m]	Re (H_{yy}) [MN/m]	Im (H_{xx}) [MN/m]	Im (H_{xy}) [MN/m]	Im (H_{yx}) [MN/m]	Im (H_{yy}) [MN/m]
9.77	223.77 ± 0.5	-15.9 ± 0.36	-21.75 ± 0.31	142.4 ± 0.26	13.84 ± 1.32	-1.71 ± 0.45	0.38 ± 0.39	8.67 ± 0.57
19.53	227.09 ± 0.52	-16.09 ± 0.24	-21.82 ± 0.49	143.71 ± 0.38	27.55 ± 0.78	-4.76 ± 0.62	-4.45 ± 0.62	16.67 ± 0.44
29.30	229.29 ± 1.03	-15.59 ± 0.38	-19.87 ± 0.52	142.12 ± 0.19	40.01 ± 0.46	-6.62 ± 0.38	-7.46 ± 0.38	24.22 ± 0.44
39.06	232.55 ± 0.96	-15.69 ± 0.43	-20.42 ± 0.44	145.43 ± 0.45	54.17 ± 1.64	-8.29 ± 0.36	-12.26 ± 0.93	29.43 ± 0.44
48.83	234.4 ± 0.84	-16.23 ± 0.82	-20.95 ± 0.76	146.4 ± 0.5	66.92 ± 1.01	-10.24 ± 0.99	-14.39 ± 0.98	36.94 ± 0.28
58.59	236.89 ± 0.56	-15.88 ± 0.68	-23.63 ± 0.7	145.06 ± 0.57	75.29 ± 1.15	-11.98 ± 1.24	-16.53 ± 1.38	41.94 ± 0.55
68.36	239.42 ± 1.59	-13.71 ± 0.72	-19.48 ± 0.68	147.03 ± 0.6	86.81 ± 1.12	-13.66 ± 0.76	-21.02 ± 0.38	54.94 ± 0.38
78.13	248.23 ± 3.56	-21.61 ± 1.54	-26.17 ± 2.2	153.88 ± 0.75	167.62 ± 2.8	-65.08 ± 1.07	-31.94 ± 1.91	65.65 ± 0.88
87.89	251.08 ± 4.34	-18.61 ± 0.9	-12.92 ± 0.86	144.06 ± 0.45	105.72 ± 4.26	-16.11 ± 0.88	-30.34 ± 5.09	68.46 ± 1.17
97.66	249.55 ± 1.48	-10.34 ± 0.1	-18.37 ± 0.53	150.79 ± 0.35	115.54 ± 2.07	-17.63 ± 0.49	-23.54 ± 0.64	73.53 ± 0.46
107.42	250.75 ± 0.72	-9.68 ± 0.27	-17.32 ± 0.49	149.83 ± 0.46	126.4 ± 0.88	-20.23 ± 0.56	-27.13 ± 0.9	81.42 ± 0.26
117.19	251.78 ± 1.62	-6.71 ± 0.25	-17.38 ± 0.64	151.23 ± 0.57	137.99 ± 0.82	-22.31 ± 0.34	-31.85 ± 0.46	88.06 ± 0.4
126.95	250.94 ± 0.81	-4.12 ± 0.27	-14.98 ± 1.65	151.21 ± 0.37	148.79 ± 1.24	-23.85 ± 0.29	-36.63 ± 0.52	99.51 ± 0.2
136.72	257.61 ± 1.47	-0.98 ± 0.54	-12.04 ± 0.69	154.38 ± 0.25	157.52 ± 0.77	-26.65 ± 0.24	-29.39 ± 1.2	105.87 ± 0.17
146.48	257.94 ± 2.39	2.44 ± 0.68	-12.01 ± 1.5	154.66 ± 0.75	164.85 ± 2.11	-25.95 ± 0.8	-31.47 ± 2.12	113.22 ± 0.45
156.25	258.57 ± 2.07	11.02 ± 0.27	-24.86 ± 1.63	163.68 ± 0.7	184.81 ± 1.14	-36.62 ± 0.54	-45.38 ± 1.68	138.5 ± 1.09
166.02	260.94 ± 1.32	4.1 ± 0.24	-11.2 ± 0.97	163.04 ± 0.59	191.35 ± 2.33	-34.56 ± 0.55	-36.89 ± 1.05	133 ± 0.42
175.78	264.46 ± 1.54	7.23 ± 0.61	-8.38 ± 2.06	163.58 ± 1.06	196.26 ± 1.13	-37.28 ± 0.31	-35.88 ± 1.15	142.2 ± 0.44
185.55	263.01 ± 1.22	10.73 ± 0.58	-15.33 ± 3.7	169.67 ± 0.49	220.29 ± 3.29	-39.78 ± 0.47	-35.79 ± 0.92	148.26 ± 0.57
195.31	258.48 ± 5.08	15.75 ± 0.51	-16.8 ± 1.91	169.25 ± 0.93	241.02 ± 1.82	-40.8 ± 0.7	-60.85 ± 5.04	162.48 ± 0.72
205.08	275.61 ± 0.61	17.02 ± 0.69	5.9 ± 1.36	173.29 ± 1.07	232.13 ± 1.09	-46.63 ± 0.49	-19.61 ± 1.15	163.37 ± 0.6
214.84	274.41 ± 0.83	23.24 ± 0.8	6.59 ± 0.51	178.64 ± 0.51	247.02 ± 1.21	-45.79 ± 0.62	-17.49 ± 0.37	172.6 ± 0.36
224.61	279.72 ± 0.9	38.55 ± 0.72	15.56 ± 1.26	134.6 ± 0.93	261.76 ± 1.51	-63.71 ± 0.61	-20.01 ± 1.04	212.44 ± 0.8
234.38	293.46 ± 1.15	23.57 ± 0.99	30.34 ± 1.41	195.6 ± 0.75	268.24 ± 2.06	-56.29 ± 0.63	-0.1 ± 2	196.24 ± 0.91
244.14	299.61 ± 1.05	29.67 ± 1.2	25.56 ± 1.86	194.51 ± 0.64	301.01 ± 3.36	-59.99 ± 0.81	40.8 ± 1.66	198.97 ± 0.99
253.91	325.68 ± 2.48	39.55 ± 1.04	113.5 ± 2.01	215.09 ± 1.03	324.95 ± 2.53	-68.07 ± 1.83	62.26 ± 3.46	190.63 ± 0.96
263.67	331.85 ± 1.65	45.17 ± 0.94	107.85 ± 2.55	204.59 ± 0.75	326.34 ± 5.82	-64.08 ± 1.23	51.64 ± 1.89	199.98 ± 0.77
273.44	366.63 ± 1.36	56.47 ± 1.33	206.42 ± 1.92	184.33 ± 1.33	297.32 ± 1.15	-89.18 ± 0.63	-0.05 ± 2.21	244.67 ± 0.64
283.20	361.69 ± 4.57	41.66 ± 1.41	126.3 ± 4	208.08 ± 1.46	308.74 ± 5.33	-79.09 ± 1.39	-53.37 ± 7.85	229.44 ± 0.69
292.97	343.21 ± 8.51	27.88 ± 1.55	66.38 ± 8.59	204.41 ± 2.06	273.35 ± 4.51	-82.52 ± 2.59	-106.59 ± 4.56	261.29 ± 2.41

Table D. 23. Measured dynamic-stiffness real and imaginary parts at 9,000 rpm and 689 kPa for t_p=10 mm.

Freq. [Hz.]	Re (H_{xx}) [MN/m]	Re (H_{xy}) [MN/m]	Re (H_{yx}) [MN/m]	Re (H_{yy}) [MN/m]	Im (H_{xx}) [MN/m]	Im (H_{xy}) [MN/m]	Im (H_{yx}) [MN/m]	Im (H_{yy}) [MN/m]
9.77	261.45 ± 0.92	-18.19 ± 0.69	-21.49 ± 0.64	138.19 ± 0.39	15.5 ± 0.51	-2.1 ± 0.39	-0.01 ± 1.24	8.67 ± 0.15
19.53	264.58 ± 1.02	-18.98 ± 0.44	-20.03 ± 0.42	139.16 ± 0.38	30.37 ± 0.83	-4.92 ± 0.5	-5 ± 0.45	15.43 ± 0.36
29.30	265.21 ± 1.04	-18.16 ± 0.31	-19.78 ± 0.9	138.95 ± 0.46	42.31 ± 0.76	-7.5 ± 0.37	-8.41 ± 0.86	21.46 ± 0.47
39.06	269.27 ± 1.02	-19.05 ± 0.31	-21.36 ± 1.09	139.89 ± 0.48	56.22 ± 0.74	-9.85 ± 0.4	-13.72 ± 0.67	27.45 ± 0.2
48.83	271.14 ± 1.47	-18.29 ± 0.8	-22.06 ± 1.63	139.99 ± 0.56	69.37 ± 2.11	-13.39 ± 0.52	-16.03 ± 0.69	34.55 ± 0.61
58.59	274.4 ± 1.73	-19.09 ± 0.85	-22.58 ± 0.81	138.93 ± 0.39	80.18 ± 1.12	-13.65 ± 0.28	-20.3 ± 1.34	40.75 ± 0.18
68.36	280.74 ± 1.01	-15.98 ± 0.12	-19.29 ± 1.03	139.64 ± 0.59	96.16 ± 0.94	-13.67 ± 0.79	-17.27 ± 0.55	57.51 ± 0.6
78.13	279.09 ± 0.86	-14.56 ± 0.46	-18.49 ± 1.09	141.94 ± 0.29	100.27 ± 1.81	-16.99 ± 0.59	-28.39 ± 1.28	55.93 ± 0.33
87.89	280.96 ± 3.03	-17.82 ± 0.7	-23.09 ± 2.81	139.83 ± 1.33	108.97 ± 1.91	-20 ± 0.96	-33.39 ± 4.3	64.46 ± 0.75
97.66	297.82 ± 1.15	-16.49 ± 0.9	-23.77 ± 1.73	143.42 ± 0.42	119.36 ± 1.38	-21.93 ± 0.51	-29.79 ± 0.64	69.12 ± 0.69
107.42	296.06 ± 0.94	-15.02 ± 0.65	-24.31 ± 1.08	143.36 ± 0.31	129.65 ± 1.08	-24.2 ± 0.5	-34.26 ± 1.1	78.66 ± 0.28
117.19	295.14 ± 1.05	-12.14 ± 0.4	-24.35 ± 0.96	145.46 ± 0.36	136.81 ± 1.88	-24.32 ± 0.65	-35.85 ± 0.46	83.93 ± 0.29
126.95	296.84 ± 1.3	-9.82 ± 0.49	-26.45 ± 0.49	145.32 ± 0.39	151.12 ± 1.36	-26.3 ± 0.25	-42.57 ± 1.58	94.38 ± 0.21
136.72	298.7 ± 0.55	-6.95 ± 0.64	-18.1 ± 1.63	148.98 ± 0.31	156.98 ± 1.74	-29.31 ± 0.46	-35.58 ± 1.17	101.58 ± 0.58
146.48	300.09 ± 3.65	-3.98 ± 1.66	-20.94 ± 1.85	148.63 ± 0.4	166.42 ± 2.02	-30.23 ± 1.04	-37.91 ± 1.74	108.53 ± 1.06
156.25	301.6 ± 3.87	1.25 ± 0.89	-20.62 ± 1.11	148.69 ± 0.61	174.98 ± 1.56	-33.13 ± 0.52	-42.07 ± 2.16	103.11 ± 0.63
166.02	306.87 ± 1.31	-2.61 ± 0.58	-21.91 ± 1.75	155.53 ± 0.37	185.52 ± 1.89	-38.57 ± 0.41	-43.12 ± 1.14	122.31 ± 0.65
175.78	308.49 ± 1.12	-0.36 ± 0.64	-16.28 ± 0.66	153.06 ± 0.76	192.13 ± 0.85	-39.76 ± 0.64	-38.26 ± 1.34	134.83 ± 0.36
185.55	309.09 ± 2.18	2.2 ± 0.92	-21.81 ± 0.69	161.98 ± 0.74	208.97 ± 1.27	-44.08 ± 0.52	-45.7 ± 2	143.85 ± 0.52
195.31	293.25 ± 5	9.36 ± 1.23	-7.63 ± 6.85	159.7 ± 1.08	222.8 ± 4.29	-44.28 ± 0.89	-51.64 ± 2.88	152.6 ± 1.01
205.08	317.29 ± 2.03	8.17 ± 0.99	-9.17 ± 1.21	163.3 ± 0.41	220.96 ± 2.37	-48.48 ± 0.43	-29.52 ± 1.35	155.17 ± 0.63
214.84	318.64 ± 0.94	11.51 ± 0.54	-6.95 ± 0.71	174.15 ± 0.41	232.09 ± 0.81	-51.56 ± 0.75	-27.88 ± 0.85	163.53 ± 0.7
224.61	319.27 ± 1	25.33 ± 0.63	0.14 ± 0.63	89.15 ± 0.85	242.4 ± 1.3	-53.39 ± 0.63	-26.2 ± 0.83	160.74 ± 0.4
234.38	325.79 ± 0.7	12.74 ± 0.32	-8.27 ± 1.47	184.74 ± 0.93	251.49 ± 1.95	-59.86 ± 0.51	-19.22 ± 0.9	184.78 ± 0.52
244.14	326.29 ± 2.44	15.02 ± 0.66	1.9 ± 1.08	179.88 ± 0.94	267.85 ± 2.61	-59.31 ± 0.33	-10.04 ± 1.44	186.75 ± 0.82
253.91	331.18 ± 0.24	17.54 ± 1.25	9.79 ± 1.09	196.92 ± 0.7	273.12 ± 2.43	-70.1 ± 0.28	-6.8 ± 1.26	208.95 ± 0.57
263.67	323.31 ± 0.88	22.03 ± 0.33	14.07 ± 1.17	199.05 ± 1.07	288.58 ± 0.96	-63.24 ± 0.99	9.87 ± 0.36	196.88 ± 0.24
273.44	326.87 ± 0.67	37.76 ± 0.72	30.82 ± 0.65	164.63 ± 1.22	305.39 ± 0.39	-61.01 ± 1.04	38.1 ± 0.65	196.88 ± 1.43
283.20	331.94 ± 2.46	29.44 ± 0.72	83.48 ± 1.26	205.03 ± 1.31	349.6 ± 2.71	-75.03 ± 1.1	32.89 ± 1	204.55 ± 0.95
292.97	414.46 ± 3.34	65.34 ± 2	255.15 ± 5.81	163.41 ± 3.5	376.59 ± 7.28	-86.23 ± 1.82	203.12 ± 12.64	246.73 ± 3.41

Table D. 24. Measured dynamic-stiffness real and imaginary parts at 9,000 rpm and 1034 kPa for t_p=10 mm.

Freq. [Hz.]	Re (H_{xx}) [MN/m]	Re (H_{xy}) [MN/m]	Re (H_{yx}) [MN/m]	Re (H_{yy}) [MN/m]	Im (H_{xx}) [MN/m]	Im (H_{xy}) [MN/m]	Im (H_{yx}) [MN/m]	Im (H_{yy}) [MN/m]
9.77	300.66 ± 1.11	-25.54 ± 0.19	-28.42 ± 1.04	141.94 ± 0.36	17.61 ± 0.56	-2.51 ± 0.22	1 ± 0.59	7.37 ± 0.28
19.53	302.99 ± 1.02	-25.18 ± 0.46	-26.17 ± 0.82	142.38 ± 0.52	29.29 ± 0.29	-4.38 ± 0.53	-4.55 ± 0.46	12.81 ± 0.5
29.30	307.01 ± 0.34	-24.97 ± 0.17	-26.21 ± 0.39	143.69 ± 0.21	44.71 ± 0.64	-7.44 ± 0.27	-9.25 ± 0.62	19.06 ± 0.35
39.06	312.4 ± 0.12	-24.79 ± 0.5	-27 ± 0.67	142.31 ± 0.44	55.41 ± 1.05	-11.05 ± 0.49	-14.31 ± 0.4	24.81 ± 0.34
48.83	315.36 ± 1.52	-25.21 ± 0.21	-27.37 ± 0.88	142.68 ± 0.52	65.88 ± 1.26	-13.63 ± 0.53	-16.36 ± 1.52	30.64 ± 0.36
58.59	319.66 ± 1.41	-26.61 ± 0.4	-27.6 ± 0.77	141.59 ± 0.55	81.76 ± 0.79	-15.34 ± 0.63	-20.62 ± 0.48	38.43 ± 0.75
68.36	316.59 ± 0.86	-27.59 ± 0.16	-33.04 ± 0.73	135.81 ± 0.69	92.63 ± 0.77	-15.96 ± 0.57	-24.41 ± 0.91	46.66 ± 0.54
78.13	323.09 ± 2.06	-22.06 ± 0.84	-23.03 ± 1.36	145.65 ± 0.66	100.37 ± 1.3	-18.2 ± 0.37	-29.54 ± 0.39	51.95 ± 0.48
87.89	329.9 ± 3.39	-25.17 ± 1.12	-30.92 ± 2.82	141.01 ± 0.72	111.72 ± 0.83	-20.54 ± 0.96	-36.04 ± 1.98	60.25 ± 0.65
97.66	332.51 ± 1.48	-20.94 ± 0.33	-33.36 ± 1	145.13 ± 0.71	123.04 ± 0.78	-22.88 ± 0.17	-34.49 ± 2.28	66.46 ± 0.55
107.42	336.14 ± 1.54	-20.88 ± 0.33	-33.11 ± 0.5	145.96 ± 0.58	139.78 ± 1.05	-25.96 ± 0.32	-31.39 ± 0.99	72.72 ± 0.47
117.19	340.29 ± 0.39	-19.69 ± 0.34	-32.35 ± 0.74	146.7 ± 0.34	139.25 ± 0.81	-27.02 ± 0.23	-42.06 ± 0.93	80.6 ± 0.48
126.95	341.9 ± 1.02	-17.25 ± 0.11	-32.83 ± 1.19	146.99 ± 0.63	149.03 ± 0.73	-28.84 ± 0.58	-47.77 ± 1.32	89.37 ± 0.29
136.72	342.55 ± 1.04	-13.29 ± 0.62	-29.44 ± 1.02	148.02 ± 0.23	155.64 ± 1.13	-33.24 ± 0.49	-37.59 ± 0.24	99.65 ± 0.4
146.48	342.85 ± 3.44	-10.99 ± 1.6	-31.4 ± 1.13	150.62 ± 1.02	163.13 ± 1.94	-34.01 ± 1.5	-39.02 ± 2.45	101.72 ± 1.16
156.25	344.45 ± 2.85	-6.42 ± 0.58	-26.65 ± 0.33	154.87 ± 0.63	175.99 ± 1.72	-37.45 ± 0.69	-43.17 ± 1.28	97.06 ± 0.37
166.02	347.76 ± 1.21	-11.31 ± 0.8	-31.14 ± 1.65	158.13 ± 0.68	182.78 ± 0.77	-42.08 ± 0.32	-45.43 ± 2.93	115.95 ± 0.46
175.78	354.17 ± 1.22	-10.26 ± 0.42	-25.63 ± 1.25	155.11 ± 0.66	186.99 ± 1.71	-44.31 ± 0.37	-37.97 ± 1.61	125.54 ± 0.29
185.55	347.85 ± 2.24	-4.8 ± 0.39	-30.51 ± 2.76	160.1 ± 0.5	203.01 ± 1.27	-47.64 ± 0.37	-40.57 ± 2.76	135.25 ± 0.68
195.31	338.46 ± 6.09	-2.21 ± 0.94	-21.49 ± 1.23	160.69 ± 0.77	211.15 ± 5.05	-48.58 ± 0.62	-52.55 ± 4.61	145.26 ± 0.73
205.08	358.31 ± 0.56	-3.14 ± 0.45	-19.46 ± 0.89	166.14 ± 0.52	214.09 ± 1.07	-52.84 ± 0.47	-31.09 ± 1.13	146.86 ± 0.78
214.84	359.98 ± 0.65	1.08 ± 0.52	-15.92 ± 0.36	174.24 ± 0.61	223.95 ± 0.93	-56.75 ± 0.47	-30.39 ± 0.89	156.43 ± 0.54
224.61	360.98 ± 0.65	8.74 ± 0.38	-8.62 ± 0.74	103.13 ± 0.68	235.29 ± 1.01	-56.82 ± 0.7	-28.56 ± 0.78	138.46 ± 0.49
234.38	370.63 ± 0.86	-1.93 ± 0.59	-17.31 ± 1.85	180.71 ± 1.05	239.24 ± 1.32	-61.32 ± 0.35	-28.85 ± 0.55	174.89 ± 0.52
244.14	366.8 ± 1.83	1.1 ± 0.87	-5.68 ± 1.49	179.68 ± 0.62	252.77 ± 3.24	-62.9 ± 0.71	-27.54 ± 1.64	175.82 ± 0.8
253.91	367.73 ± 1.09	8.81 ± 0.5	-2.78 ± 0.89	175.17 ± 0.79	259.96 ± 1.2	-66.67 ± 0.17	-13.7 ± 1.59	191.02 ± 0.67
263.67	361.33 ± 1.27	7.49 ± 0.94	4.32 ± 1.48	198.91 ± 0.63	272.38 ± 0.58	-64.12 ± 0.65	-8.32 ± 0.25	184.84 ± 0.73
273.44	363.71 ± 0.3	17.83 ± 1.02	15.24 ± 0.35	174.62 ± 1.09	286.14 ± 0.81	-66.05 ± 1.14	0.93 ± 0.56	177.29 ± 0.85
283.20	363.4 ± 1.3	11.82 ± 1	31.58 ± 1.03	208.15 ± 0.86	314.85 ± 2.13	-76.72 ± 0.91	-3.62 ± 1.01	199.04 ± 1.06
292.97	370.59 ± 1.54	19.34 ± 1.08	45.9 ± 1.37	172.83 ± 1.65	331.91 ± 1.88	-68.17 ± 2	36.17 ± 1.91	202.8 ± 0.8

Table D. 25. Measured dynamic-stiffness real and imaginary parts at 9,000 rpm and 1,724 kPa for t_p=10 mm.

Freq. [Hz.]	Re (H_{xx}) [MN/m]	Re (H_{xy}) [MN/m]	Re (H_{yx}) [MN/m]	Re (H_{yy}) [MN/m]	Im (H_{xx}) [MN/m]	Im (H_{xy}) [MN/m]	Im (H_{yx}) [MN/m]	Im (H_{yy}) [MN/m]
9.77	390.95 ± 1.45	-46.19 ± 0.67	-45.91 ± 0.5	165.42 ± 0.42	17.1 ± 0.54	-0.9 ± 0.29	0.94 ± 0.85	7.54 ± 0.35
19.53	393.71 ± 0.76	-45.21 ± 0.57	-45.69 ± 0.52	165.32 ± 0.59	30.26 ± 0.67	-4.19 ± 0.59	-4.91 ± 0.43	10.28 ± 0.65
29.30	396.74 ± 0.99	-46.91 ± 0.55	-43.85 ± 0.96	168.93 ± 0.35	42.31 ± 1.64	-6.3 ± 0.87	-10.33 ± 0.68	15.07 ± 0.27
39.06	402.6 ± 0.84	-45.44 ± 0.24	-43.53 ± 1.6	166.32 ± 0.52	54.06 ± 1.01	-10.41 ± 0.6	-12.53 ± 1.19	19.97 ± 0.23
48.83	406.75 ± 1.19	-44.73 ± 0.52	-46.17 ± 1.1	165.82 ± 0.36	65.95 ± 1.85	-13.69 ± 0.73	-18.91 ± 0.55	27.25 ± 0.24
58.59	408.85 ± 0.95	-45.87 ± 0.55	-44.76 ± 0.94	163.6 ± 0.36	78.73 ± 1.17	-14.5 ± 0.53	-21.66 ± 0.77	32.48 ± 0.48
68.36	410.45 ± 1.87	-45.04 ± 0.41	-48.87 ± 0.85	163.17 ± 0.79	87.55 ± 1.43	-16.52 ± 0.28	-26.52 ± 1.62	36.46 ± 0.6
78.13	418.39 ± 1.6	-40.54 ± 0.8	-43.78 ± 1.36	169.4 ± 0.28	101.61 ± 0.76	-17.79 ± 0.5	-30.15 ± 0.72	44.07 ± 0.87
87.89	421.29 ± 0.55	-43.57 ± 0.36	-43.32 ± 2.63	163.73 ± 0.75	105.29 ± 3.13	-19.88 ± 0.75	-33.27 ± 1.6	48.97 ± 0.66
97.66	424.85 ± 0.9	-41.41 ± 0.55	-49.56 ± 1.13	167.21 ± 0.37	113.95 ± 2.33	-22.76 ± 0.47	-37.07 ± 2.3	57.13 ± 0.42
107.42	430.22 ± 1.61	-40.37 ± 0.63	-52.94 ± 1.03	166.63 ± 0.5	124.79 ± 1.68	-24.51 ± 0.56	-39.83 ± 1.04	64.34 ± 0.41
117.19	427.41 ± 0.41	-36.99 ± 0.37	-51.84 ± 0.86	169.14 ± 0.7	132.81 ± 0.94	-27.95 ± 0.83	-43.29 ± 1.15	70.2 ± 0.5
126.95	428.35 ± 0.83	-33.96 ± 0.24	-56.04 ± 1.08	168.94 ± 0.48	154.58 ± 3.13	-31.63 ± 0.7	-46.98 ± 1.42	78.43 ± 0.56
136.72	429.24 ± 1.7	-31.76 ± 0.41	-49.34 ± 1	170 ± 0.41	144.35 ± 2.83	-33.67 ± 0.47	-41.23 ± 1.38	83.61 ± 0.38
146.48	430.21 ± 4.54	-29.36 ± 1.32	-52.19 ± 3.12	174.27 ± 0.9	152.47 ± 6.54	-36.02 ± 1.73	-40.32 ± 2.51	88.75 ± 0.72
156.25	432.4 ± 2.13	-25.57 ± 0.67	-48.53 ± 0.78	179.04 ± 0.46	164.66 ± 2.17	-40.09 ± 0.49	-44.64 ± 2.31	81.74 ± 0.41
166.02	435.95 ± 1.32	-30.73 ± 0.25	-52.92 ± 2.02	177.83 ± 0.43	176.65 ± 2.49	-45.26 ± 0.35	-44.44 ± 1.71	100.59 ± 0.32
175.78	437.64 ± 2.42	-29.26 ± 0.44	-47.25 ± 1.57	174.81 ± 0.68	177.21 ± 1.96	-46.82 ± 0.23	-41.02 ± 1.62	108.8 ± 0.41
185.55	438.22 ± 0.96	-24.64 ± 0.54	-51.91 ± 1.43	180.04 ± 0.51	203.34 ± 3.79	-53.72 ± 1.09	-45.54 ± 1.21	120.53 ± 0.89
195.31	423.55 ± 3.84	-22.57 ± 1.07	-36.33 ± 5.03	178 ± 1.02	201.46 ± 6.69	-51.48 ± 1	-44.71 ± 5.11	124.54 ± 0.66
205.08	444.27 ± 1.29	-25.57 ± 0.56	-41.58 ± 1.44	185.4 ± 0.39	202.24 ± 1.32	-56.67 ± 0.34	-35.4 ± 1.59	128.99 ± 0.4
214.84	443.81 ± 0.69	-20.9 ± 0.51	-36.97 ± 1.2	190.82 ± 0.8	213.5 ± 1.17	-58.78 ± 0.37	-36.23 ± 0.66	136.03 ± 0.37
224.61	450.33 ± 0.51	-15.02 ± 0.38	-33.58 ± 1.4	129.31 ± 0.34	221.84 ± 1.32	-62.1 ± 0.56	-31.58 ± 0.52	117.15 ± 0.3
234.38	451.14 ± 2.31	-24.92 ± 0.8	-41.17 ± 2.18	198.23 ± 0.66	224.11 ± 3.53	-63.28 ± 0.67	-28.07 ± 0.96	151.42 ± 0.74
244.14	447.94 ± 1.76	-21.41 ± 0.46	-26.51 ± 1.84	192.64 ± 0.53	234.7 ± 2.32	-64.06 ± 0.58	-30.79 ± 2.45	151.01 ± 0.47
253.91	452.22 ± 0.52	-16.39 ± 0.45	-19.69 ± 1.9	190.82 ± 1.04	239.41 ± 2.51	-69.24 ± 0.52	-20.3 ± 1.61	164.76 ± 0.54
263.67	444.68 ± 0.49	-14.97 ± 0.52	-8.98 ± 1.27	208.87 ± 0.52	254.61 ± 1.03	-68.26 ± 0.8	-25.64 ± 1.1	167.08 ± 0.69
273.44	443.12 ± 0.57	-9.67 ± 0.89	-4.87 ± 0.55	202.65 ± 0.76	263.41 ± 0.66	-67.97 ± 0.29	-18.28 ± 0.52	150.49 ± 0.58
283.20	441.79 ± 0.87	-14.52 ± 0.52	0.83 ± 0.98	224.86 ± 0.67	287.72 ± 2.23	-78.32 ± 0.64	-28.12 ± 0.85	182.21 ± 0.23
292.97	446.54 ± 1.72	-10.63 ± 1.21	12.78 ± 1.01	195.78 ± 0.69	291.49 ± 0.65	-69.47 ± 0.62	-8.7 ± 1.34	174.43 ± 0.85

Table D. 26. Measured dynamic-stiffness real and imaginary parts at 12,000 rpm and 172 kPa for t_p=10 mm.

Freq. [Hz.]	Re (H_{xx}) [MN/m]	Re (H_{xy}) [MN/m]	Re (H_{yx}) [MN/m]	Re (H_{yy}) [MN/m]	Im (H_{xx}) [MN/m]	Im (H_{xy}) [MN/m]	Im (H_{yx}) [MN/m]	Im (H_{yy}) [MN/m]
9.77	246.24 ± 2.49	-27.88 ± 2.18	-41.94 ± 2.14	182.15 ± 2.07	18.38 ± 1.62	-2.93 ± 2.09	-0.3 ± 1.03	7.5 ± 1.01
19.53	244.67 ± 2.88	-25.2 ± 1.15	-37.13 ± 0.72	184.97 ± 0.94	22.34 ± 1.58	-2.73 ± 1.76	2.64 ± 1.63	13.23 ± 0.32
29.30	250.99 ± 2.22	-24.54 ± 1.31	-34.65 ± 0.64	182.13 ± 0.85	31.52 ± 1.87	-3.7 ± 0.84	-5.16 ± 1.36	21.17 ± 0.29
39.06	249.47 ± 1.63	-24.69 ± 1.23	-36.11 ± 1.17	184.38 ± 0.86	46.16 ± 1.23	-7.47 ± 1.58	-7.07 ± 1.15	26.96 ± 0.96
48.83	250.49 ± 3.85	-22.2 ± 1.55	-42.55 ± 1.36	184.99 ± 1.22	59.88 ± 1.9	-11.95 ± 2.66	-7.24 ± 2.41	31.72 ± 1.29
58.59	249.07 ± 2.58	-20.85 ± 2.14	-43.66 ± 2.77	181.42 ± 1.69	79.22 ± 4.52	-13.18 ± 1.3	-2.34 ± 1.68	40.23 ± 0.83
68.36	254.16 ± 1.2	-19.22 ± 2.09	-30.2 ± 1.57	183.69 ± 1.63	74.99 ± 2.16	-13.59 ± 1.69	-12.37 ± 1.34	45.35 ± 1.53
78.13	256.86 ± 3.14	-22.21 ± 1.24	-34.65 ± 2.53	195.8 ± 1.49	83.35 ± 3.23	-13.26 ± 1.57	-16.24 ± 2.15	55.07 ± 1.81
87.89	260.21 ± 1.87	-22.5 ± 1.15	-27.58 ± 1.43	186.95 ± 1.71	89.81 ± 3.06	-18.48 ± 2.26	-21.14 ± 1.53	56.1 ± 1.31
97.66	261.5 ± 1.81	-20.6 ± 1.61	-27.43 ± 1.82	190.39 ± 1.67	108.18 ± 1.91	-20.72 ± 2.69	-14.9 ± 1.59	59.36 ± 0.74
107.42	264.49 ± 1.12	-22.7 ± 1.27	-26.01 ± 1.46	188.68 ± 0.95	113.53 ± 2.55	-20.33 ± 1.3	-17.69 ± 1.55	66.26 ± 0.94
117.19	265.81 ± 1.29	-21.25 ± 0.85	-23.27 ± 1.06	188.63 ± 1.28	125.43 ± 1.68	-23.52 ± 0.84	-21.53 ± 2.29	71 ± 1.36
126.95	267.23 ± 2.07	-17.39 ± 1.1	-17.12 ± 2.35	189.51 ± 0.55	135.72 ± 1.95	-24.61 ± 1.96	-22.72 ± 0.58	78.53 ± 0.91
136.72	268.74 ± 1.22	-17 ± 0.59	-15.9 ± 1.52	189.12 ± 0.66	142.13 ± 4.21	-25.85 ± 0.65	-25.9 ± 1.56	86.09 ± 0.34
146.48	273.6 ± 2.28	-12.11 ± 0.71	-17.25 ± 2.1	186.61 ± 0.91	143.73 ± 1.48	-22.62 ± 0.81	-21.88 ± 1.82	92.57 ± 0.93
156.25	271.96 ± 1.67	-4.73 ± 0.99	-2.08 ± 2.29	187.08 ± 0.89	156.11 ± 1.67	-33.37 ± 0.94	-22.5 ± 1.36	118.87 ± 1.5
166.02	271.89 ± 3.86	-10.09 ± 0.58	-13.59 ± 2.2	198.63 ± 1.3	170.73 ± 3.87	-32.67 ± 1.64	-37.02 ± 2.33	108.4 ± 1.44
175.78	273.66 ± 3.77	-7.3 ± 1.98	-3.61 ± 1.42	192.99 ± 2.25	174.15 ± 1.97	-29.91 ± 2.37	-29.57 ± 2.67	122.54 ± 0.75
185.55	278.65 ± 0.35	-3.42 ± 2.41	-8.25 ± 4.14	194.99 ± 1.15	168.69 ± 3.95	-29.2 ± 1.22	-40.79 ± 4.27	125.37 ± 1.62
195.31	269.47 ± 10.17	2.01 ± 3.16	5.24 ± 12.22	188.41 ± 4.78	199.87 ± 15.34	-26.31 ± 3.83	-47.81 ± 17.86	138.75 ± 3.16
205.08	263.91 ± 2.61	3.74 ± 3.63	37.55 ± 4.64	187.62 ± 4.03	208.94 ± 3.18	-30.98 ± 4.49	-22.44 ± 2.36	142.69 ± 2.57
214.84	270.46 ± 2.22	23.41 ± 2.6	49.41 ± 2.27	159.64 ± 2.35	241.13 ± 3.5	-26.89 ± 3.85	-41.25 ± 3.76	175.21 ± 2.42
224.61	369.36 ± 5.99	-10.67 ± 1.63	-72.38 ± 23.17	244.99 ± 4.95	272.5 ± 7.69	-61.38 ± 2.17	29.15 ± 8.98	162.89 ± 5.53
234.38	429.08 ± 11.95	8.1 ± 2.71	227.17 ± 15.46	190.19 ± 2.38	310.36 ± 12.3	-37.38 ± 4.35	-132.68 ± 8.75	217.85 ± 1.85
244.14	307.19 ± 18.85	18.42 ± 2.69	-77.16 ± 14.09	178.69 ± 2.85	156.13 ± 11.64	-20.89 ± 2.92	-196.12 ± 29.7	224.21 ± 2.43
253.91	333.64 ± 6.55	50.18 ± 1.61	-23.87 ± 6.94	194.77 ± 3.6	209.73 ± 6.87	-3.2 ± 2.43	-95.97 ± 7.44	263.56 ± 3.72
263.67	287.55 ± 16.54	99.53 ± 3.05	11.6 ± 5.57	146.19 ± 3.36	187.44 ± 6.01	-30.59 ± 3.64	-181.98 ± 15.81	319.23 ± 2.68
273.44	292.98 ± 9.59	113.41 ± 6.33	11.51 ± 3.47	229.46 ± 5.89	213.76 ± 7.92	-44.21 ± 5.75	-170.83 ± 14.9	441.12 ± 7.23
283.20	279.48 ± 16.38	86.64 ± 5.97	-1.48 ± 47.67	408.76 ± 6.54	205.19 ± 20.29	-135.58 ± 8.26	-203.25 ± 22.08	281 ± 15.99
292.97	252.68 ± 2.85	48.76 ± 2.82	-8.11 ± 10.02	296.3 ± 4.29	208.68 ± 4.97	-94.09 ± 5.19	-176.17 ± 9.61	245.97 ± 4

Table D. 27. Measured dynamic-stiffness real and imaginary parts at 12,000 rpm and 345 kPa for t_p=10 mm.

Freq. [Hz.]	Re (H_{xx}) [MN/m]	Re (H_{xy}) [MN/m]	Re (H_{yx}) [MN/m]	Re (H_{yy}) [MN/m]	Im (H_{xx}) [MN/m]	Im (H_{xy}) [MN/m]	Im (H_{yx}) [MN/m]	Im (H_{yy}) [MN/m]
9.77	258.01 ± 1.53	-24.6 ± 0.59	-35.87 ± 0.64	176.45 ± 0.34	14.59 ± 1.4	-1.86 ± 0.54	-1.46 ± 2.12	8 ± 0.88
19.53	256.37 ± 0.31	-27.36 ± 1.1	-36.95 ± 1.69	178.34 ± 0.69	24.87 ± 2.09	-4.51 ± 1.01	-3.34 ± 1.49	15.01 ± 0.45
29.30	257.44 ± 1.66	-25.67 ± 0.41	-37.31 ± 1.47	178.41 ± 1.19	32.25 ± 1.62	-5.85 ± 1.01	-5.25 ± 1.12	21.13 ± 0.52
39.06	259.3 ± 1.11	-27.28 ± 0.84	-35.16 ± 0.93	180.8 ± 0.96	47.31 ± 1.07	-8.44 ± 1.41	-11.82 ± 1.3	24.67 ± 0.35
48.83	264.82 ± 1.02	-24.58 ± 1.16	-40.25 ± 1.48	181.25 ± 1.73	53.95 ± 1.6	-10.35 ± 1.16	-12.9 ± 1.93	30.56 ± 1.7
58.59	261.06 ± 1.67	-24.29 ± 1.05	-39.97 ± 1.55	177.92 ± 1.05	68.76 ± 0.59	-12.05 ± 0.81	-12.24 ± 0.73	35.01 ± 0.7
68.36	268.92 ± 1.96	-23.25 ± 2.01	-29.82 ± 1.39	178.84 ± 1.14	77.64 ± 1.02	-13.8 ± 0.38	-16.15 ± 0.59	43.91 ± 1.41
78.13	274.39 ± 1.29	-22.56 ± 0.84	-28.93 ± 1.05	180.19 ± 1.23	90.49 ± 1.22	-16.37 ± 1.6	-24.26 ± 0.55	48.51 ± 0.66
87.89	279.43 ± 2.39	-26.04 ± 0.85	-30.08 ± 4.12	176.82 ± 1.88	101.03 ± 2.16	-21.48 ± 3.33	-23.47 ± 2.1	56.33 ± 1.81
97.66	273.8 ± 2.38	-23.15 ± 1.54	-33.76 ± 0.9	183.34 ± 1.21	107.33 ± 2.32	-21.31 ± 0.95	-13.8 ± 1.77	58.47 ± 0.58
107.42	275.51 ± 0.76	-21.18 ± 0.63	-29.21 ± 1.27	181.21 ± 0.59	118.33 ± 1.5	-23.77 ± 1.39	-19.79 ± 1.14	64.09 ± 0.89
117.19	279.51 ± 0.58	-20.22 ± 0.91	-24.95 ± 0.9	182.45 ± 0.81	126.88 ± 0.84	-23.44 ± 1.03	-22.15 ± 0.92	69.04 ± 0.56
126.95	280.32 ± 1.93	-19.13 ± 1.04	-22.59 ± 1.32	181.97 ± 1.25	134.22 ± 1.12	-25.24 ± 0.5	-24.79 ± 1.9	76.94 ± 1.13
136.72	283.12 ± 1.2	-18.23 ± 0.48	-15.02 ± 0.62	182.72 ± 0.46	138.1 ± 0.73	-27.32 ± 0.56	-23.41 ± 0.85	84.01 ± 0.74
146.48	288.33 ± 1.2	-16.14 ± 0.52	-17.65 ± 0.64	181.18 ± 0.62	147.62 ± 1.41	-24.92 ± 1.02	-26.21 ± 0.5	89.95 ± 0.76
156.25	284.56 ± 1.15	-8.68 ± 0.62	-18.44 ± 0.63	173.13 ± 0.3	156.83 ± 0.72	-26.34 ± 0.43	-27.69 ± 0.69	88.82 ± 0.42
166.02	289.67 ± 1.95	-15.76 ± 0.8	-16.05 ± 1.72	190.61 ± 0.74	169.81 ± 1.98	-31.67 ± 1.51	-27.18 ± 1.71	105 ± 0.35
175.78	291.46 ± 1.43	-11.66 ± 0.69	-7.31 ± 2.12	184.1 ± 0.5	178.19 ± 3.32	-29.44 ± 1.74	-32.09 ± 1.05	115.23 ± 0.81
185.55	284.49 ± 5.32	-6.24 ± 1.23	-22.61 ± 2.91	187.26 ± 1.22	185.53 ± 5.56	-31.45 ± 1.37	-38.67 ± 3.83	123.67 ± 0.62
195.31	315.55 ± 27.23	-2.9 ± 2.91	-38.83 ± 9.5	189.31 ± 2.83	207.78 ± 12.56	-38.78 ± 4.88	-24.64 ± 11.48	134.02 ± 1.97
205.08	290.66 ± 1.12	-0.14 ± 1.6	-0.17 ± 3.51	187.26 ± 3.92	207.49 ± 3.2	-34.14 ± 3.28	-22.56 ± 1.9	140.04 ± 1.49
214.84	300.55 ± 1.66	5.37 ± 0.85	12.24 ± 1.39	187.13 ± 1.67	223.32 ± 0.78	-35 ± 1.48	-24.09 ± 0.76	148.98 ± 1.24
224.61	296.95 ± 2.16	27.02 ± 1.91	36.92 ± 1.81	179 ± 2.81	240.99 ± 1.3	-74.39 ± 2	-21.27 ± 4.98	269.03 ± 4.07
234.38	307.53 ± 2.6	11.27 ± 1.38	23.57 ± 2.26	203.98 ± 1.1	251.21 ± 0.9	-34.89 ± 0.72	-13.14 ± 0.8	173.73 ± 0.79
244.14	332.68 ± 2.46	15.66 ± 2.6	37.7 ± 3.04	194.53 ± 4.5	279.49 ± 5.28	-36.16 ± 2.21	15.05 ± 1.69	181.45 ± 0.46
253.91	340.52 ± 3.38	31.36 ± 1.82	79.72 ± 10.52	212.46 ± 2.39	280.01 ± 4.57	-38.03 ± 3.63	-5.93 ± 5.89	197.16 ± 4.21
263.67	390.37 ± 3.41	41.2 ± 2.02	134.4 ± 6.67	218.61 ± 2.64	306.99 ± 3.98	-45.21 ± 2.37	50.39 ± 6.88	188.63 ± 2.03
273.44	366.75 ± 2	38.42 ± 2.42	71.87 ± 9.21	251.96 ± 1.7	259.15 ± 6.94	-78.2 ± 1.84	-116.45 ± 5.23	234.93 ± 2.79
283.20	410.25 ± 14.01	47.71 ± 3.81	42.49 ± 24.44	200.33 ± 1.83	217.15 ± 14.81	-65.61 ± 2.45	-103.48 ± 4.29	214.36 ± 3.64
292.97	336.15 ± 2.67	28.84 ± 1.7	-22.07 ± 4.97	225.98 ± 0.76	224.67 ± 2.99	-62.11 ± 1.41	-100.96 ± 2.41	233.55 ± 1.36

Table D. 28. Measured dynamic-stiffness real and imaginary parts at 12,000 rpm and 689 kPa for t_p=10 mm.

Freq. [Hz.]	Re (H_{xx}) [MN/m]	Re (H_{xy}) [MN/m]	Re (H_{yx}) [MN/m]	Re (H_{yy}) [MN/m]	Im (H_{xx}) [MN/m]	Im (H_{xy}) [MN/m]	Im (H_{yx}) [MN/m]	Im (H_{yy}) [MN/m]
9.77	286.09 ± 1.98	-27.15 ± 1.25	-34.61 ± 2.84	167.61 ± 0.81	8.31 ± 1.25	-1.82 ± 1	-0.35 ± 1.05	8.22 ± 0.57
19.53	286.35 ± 1.34	-27.27 ± 1.44	-36.49 ± 0.54	168.51 ± 0.78	22.91 ± 1.09	-3.04 ± 0.67	-2.78 ± 0.48	14.44 ± 0.35
29.30	286.54 ± 1.61	-26.68 ± 1.24	-33.92 ± 0.6	168.4 ± 0.81	36.95 ± 1.43	-6.99 ± 0.89	-6.63 ± 1.09	19.06 ± 0.82
39.06	288.87 ± 1.02	-28.15 ± 0.77	-34.91 ± 0.86	170.34 ± 1.32	48.6 ± 0.72	-9.08 ± 0.82	-11.74 ± 0.99	23.59 ± 0.86
48.83	291.16 ± 2.22	-25.86 ± 1.52	-33.18 ± 0.32	168.75 ± 1.15	62.07 ± 2.16	-12.73 ± 0.82	-12.82 ± 2.65	28.77 ± 1.44
58.59	295.62 ± 1.57	-27.72 ± 0.34	-34.87 ± 1.33	170.13 ± 1.09	68.18 ± 2.18	-16.45 ± 1.12	-16.09 ± 0.61	34.74 ± 0.53
68.36	298.62 ± 1.83	-25.88 ± 1.08	-28.93 ± 1.2	171.5 ± 1.05	87.04 ± 1.44	-10.73 ± 0.82	-12.64 ± 1.65	49.9 ± 0.76
78.13	297.17 ± 1.57	-25.9 ± 1.14	-27.31 ± 1.29	174.48 ± 0.71	87.8 ± 0.83	-16.81 ± 1	-20.61 ± 0.42	44.95 ± 0.89
87.89	296.35 ± 4.24	-25.19 ± 0.95	-35.72 ± 1.69	170.56 ± 0.87	102.59 ± 1.66	-23.08 ± 1.47	-26.81 ± 3.01	54.63 ± 0.74
97.66	307.32 ± 3.72	-27.63 ± 0.43	-34.64 ± 3.02	174.38 ± 0.74	107.26 ± 3.27	-24.24 ± 0.41	-22.96 ± 1.11	58.19 ± 1.08
107.42	308.92 ± 1.19	-25.7 ± 1.18	-32.91 ± 1.44	170.25 ± 0.56	113.8 ± 1.8	-23.54 ± 0.27	-23.3 ± 1.27	63.91 ± 0.67
117.19	309.13 ± 1.49	-24.03 ± 0.53	-29.36 ± 0.38	172.61 ± 0.58	125.18 ± 0.87	-26.77 ± 0.61	-28.89 ± 0.67	70.02 ± 0.85
126.95	312.59 ± 1.21	-23.56 ± 0.88	-30.25 ± 1.61	171.85 ± 0.45	137.23 ± 0.4	-27.01 ± 0.6	-32.13 ± 1.17	77.61 ± 0.67
136.72	315.69 ± 2.65	-23.38 ± 0.26	-25.3 ± 1.54	174.83 ± 0.54	141.62 ± 1.58	-29.16 ± 0.58	-27.43 ± 2.35	84.62 ± 0.69
146.48	317.18 ± 0.91	-20.2 ± 0.51	-25.11 ± 1.41	172.97 ± 0.72	150.07 ± 1.22	-28.84 ± 0.62	-34.17 ± 1.33	90.22 ± 0.38
156.25	318.02 ± 1.58	-16.75 ± 0.43	-26.84 ± 1.11	174.34 ± 0.46	159.52 ± 0.87	-30.38 ± 0.37	-35.31 ± 1.16	83.44 ± 0.27
166.02	319.57 ± 1.2	-19.4 ± 0.71	-27.66 ± 1.62	175.67 ± 0.73	168.38 ± 2.14	-33.13 ± 0.29	-39.61 ± 2.21	101.36 ± 0.5
175.78	322.23 ± 4.5	-16.7 ± 0.42	-20.94 ± 2.64	172.66 ± 0.54	171.74 ± 1.88	-32.63 ± 0.69	-40 ± 2.81	114.86 ± 0.62
185.55	321.08 ± 5.89	-12.2 ± 1.72	-25.66 ± 4.26	180.12 ± 1.85	193.07 ± 3.06	-35.42 ± 1.12	-43.31 ± 3.05	123.57 ± 0.56
195.31	297 ± 11.47	-6.3 ± 3.25	-4.95 ± 15.3	176.48 ± 2.34	205.09 ± 16.21	-38.62 ± 2.34	-73.97 ± 16.21	133.24 ± 3.39
205.08	322.19 ± 1.82	-7.2 ± 1.51	-7.35 ± 3.41	179.85 ± 1.61	202.56 ± 3.3	-35.15 ± 0.89	-34.15 ± 3.05	137.33 ± 2.46
214.84	323.7 ± 1.19	-1.77 ± 0.69	-17.13 ± 0.7	189.7 ± 1.35	215.36 ± 1.4	-37.59 ± 0.58	-28.97 ± 1.22	147.5 ± 1.28
224.61	326.71 ± 0.62	12.4 ± 1.72	-8.72 ± 1	112.03 ± 0.88	227.1 ± 2.26	-38.89 ± 1.59	-26.22 ± 2.6	143.12 ± 0.53
234.38	334 ± 1.12	1.95 ± 0.74	-11.31 ± 1.33	196.91 ± 0.74	234.67 ± 3.2	-42.56 ± 1.84	-21.46 ± 3.8	167.24 ± 1.36
244.14	333.62 ± 1.8	6.39 ± 1.72	-5.08 ± 5.48	192.77 ± 2.68	251.08 ± 1.7	-44.44 ± 2.25	-17 ± 3.6	179.14 ± 3.12
253.91	342.98 ± 1.81	18.32 ± 3.13	8.53 ± 2.41	210.4 ± 2.8	255.58 ± 0.4	-55.05 ± 2.39	-10.92 ± 2.65	197.24 ± 3.18
263.67	339.37 ± 2.39	20.36 ± 2.09	8.96 ± 1.5	221.79 ± 2	275.41 ± 1.54	-50.62 ± 1.08	5.83 ± 1.13	181.91 ± 1.94
273.44	351.21 ± 0.89	40.47 ± 1.53	29.5 ± 1.25	194.04 ± 1.7	288.81 ± 1.29	-50.53 ± 0.66	37.19 ± 0.61	188.39 ± 1.62
283.20	343.87 ± 4.68	31.91 ± 3.1	80.44 ± 2.82	229.72 ± 1.1	342.37 ± 1.98	-65 ± 3.33	29.88 ± 3.99	188.71 ± 1.58
292.97	478.51 ± 16.56	62.68 ± 1.76	295.52 ± 11.49	181.83 ± 1.63	332.87 ± 6.34	-78.28 ± 2.72	80.1 ± 8.43	203.06 ± 2.34

Table D. 29. Measured dynamic-stiffness real and imaginary parts at 12,000 rpm and 1034 kPa for t_p=10 mm.

Freq. [Hz.]	Re (H_{xx}) [MN/m]	Re (H_{xy}) [MN/m]	Re (H_{yx}) [MN/m]	Re (H_{yy}) [MN/m]	Im (H_{xx}) [MN/m]	Im (H_{xy}) [MN/m]	Im (H_{yx}) [MN/m]	Im (H_{yy}) [MN/m]
9.77	316.98 ± 1.5	-34.83 ± 0.62	-37.2 ± 0.36	166.46 ± 0.48	14.42 ± 0.77	-2.26 ± 0.68	0.94 ± 1.31	8.32 ± 0.89
19.53	319.1 ± 0.51	-33.66 ± 0.58	-37.12 ± 1.02	167.13 ± 0.56	26.16 ± 0.66	-5.65 ± 0.41	-3.9 ± 1.35	13.32 ± 0.89
29.30	319.39 ± 2.04	-32.09 ± 0.99	-36.92 ± 1.22	168.93 ± 0.79	38.46 ± 1.55	-6.67 ± 0.78	-7.13 ± 1.31	17.82 ± 0.57
39.06	323.5 ± 1.55	-31.37 ± 0.52	-39.18 ± 0.68	169.1 ± 1.01	46.21 ± 1.6	-9.92 ± 0.86	-8.58 ± 1.45	21.72 ± 0.62
48.83	325.97 ± 2.34	-32.95 ± 0.88	-37.23 ± 0.67	168.63 ± 0.42	59.79 ± 1.38	-13.23 ± 0.47	-11.63 ± 0.7	27.25 ± 0.49
58.59	332.03 ± 0.96	-34.46 ± 0.67	-39.13 ± 1.03	168.95 ± 0.54	66.89 ± 0.98	-15.58 ± 0.74	-18.12 ± 1.64	32.81 ± 0.66
68.36	326.12 ± 1.51	-35.37 ± 0.4	-43.55 ± 1.62	160.78 ± 0.7	85.09 ± 1.02	-17.5 ± 0.43	-18.43 ± 0.92	40.09 ± 0.66
78.13	333.27 ± 1.77	-29.27 ± 0.68	-33.09 ± 1.16	172.91 ± 1.09	94.41 ± 1.7	-19.77 ± 0.63	-26.34 ± 2.18	43.94 ± 0.91
87.89	340.21 ± 1.75	-33.66 ± 0.84	-36.33 ± 3.72	166.82 ± 0.97	103.84 ± 3.83	-22.98 ± 0.64	-27.19 ± 2.91	49.86 ± 0.82
97.66	343.95 ± 0.76	-31.89 ± 0.85	-39.04 ± 0.85	170.32 ± 0.41	113.57 ± 2.46	-24.59 ± 0.56	-27.6 ± 3.1	55.89 ± 0.79
107.42	348.99 ± 0.75	-32.55 ± 0.43	-36.96 ± 1.67	170.77 ± 0.66	117.09 ± 2.13	-25.04 ± 0.68	-30.36 ± 0.68	62.76 ± 0.58
117.19	349.81 ± 1.58	-30.89 ± 0.49	-38.22 ± 1.63	170.93 ± 0.86	126.77 ± 0.66	-27.84 ± 0.45	-35.15 ± 1	68.44 ± 0.45
126.95	349.65 ± 3.04	-29.99 ± 0.68	-34.33 ± 1.38	169.16 ± 0.36	136.94 ± 1.23	-28.23 ± 0.17	-39.02 ± 2.68	75.84 ± 0.66
136.72	347.39 ± 1.04	-27.51 ± 0.25	-27.17 ± 1.41	168.14 ± 0.59	139.84 ± 1.93	-29.06 ± 0.58	-34.9 ± 1.26	84.55 ± 0.19
146.48	352.56 ± 0.82	-26.88 ± 0.33	-29.67 ± 0.79	170.43 ± 0.33	146.91 ± 0.75	-28.35 ± 0.37	-36.97 ± 1.11	86.79 ± 0.32
156.25	354.14 ± 1.43	-22.46 ± 0.27	-30.13 ± 0.5	174.37 ± 0.54	156.07 ± 1.08	-31.55 ± 0.94	-40.21 ± 1.43	80.71 ± 0.46
166.02	352.75 ± 1.05	-25.51 ± 0.65	-31.64 ± 2.28	174.14 ± 0.44	165.15 ± 2.68	-33.88 ± 0.44	-43.17 ± 2.26	96.78 ± 0.44
175.78	354.91 ± 1.11	-21.6 ± 0.68	-30.73 ± 1.11	170.64 ± 0.62	171.08 ± 2.09	-35.16 ± 0.33	-40.55 ± 2.94	110.64 ± 0.58
185.55	351.89 ± 4.36	-17.97 ± 1.65	-33.95 ± 3.18	172.95 ± 0.86	185.21 ± 4.32	-36.86 ± 1.14	-47.36 ± 2.98	119.47 ± 0.57
195.31	353.32 ± 11.63	-13.51 ± 3.4	-27.37 ± 10.7	176.32 ± 1.99	174.04 ± 13.97	-35.48 ± 2.52	-52.67 ± 8.28	129.06 ± 1.79
205.08	360.45 ± 1.73	-11.92 ± 1.98	-28.94 ± 1.73	176.85 ± 1.37	199.24 ± 1.34	-40.88 ± 2.05	-38.51 ± 2.83	132.75 ± 1.09
214.84	359.88 ± 0.46	-5.23 ± 1.2	-25.92 ± 1.04	187.24 ± 0.56	211.23 ± 3.73	-41.37 ± 1.71	-36.96 ± 1.29	143.71 ± 0.85
224.61	365.28 ± 1.11	0.89 ± 1.05	-19.58 ± 1.54	118.67 ± 0.71	222.56 ± 1.99	-44.03 ± 0.51	-30.9 ± 1.03	127.88 ± 1.28
234.38	378.3 ± 2.77	-5.04 ± 1.25	-20.76 ± 4.27	192.7 ± 0.82	231.83 ± 1.73	-46.88 ± 1.26	-29.29 ± 2.59	163.6 ± 1.6
244.14	375.91 ± 3.92	2.86 ± 1.86	-20.22 ± 3.6	186.24 ± 1.88	238.33 ± 2.47	-50.65 ± 0.89	-25.02 ± 1.35	183.15 ± 2.04
253.91	375.05 ± 2.32	11.51 ± 1.86	-14.81 ± 1.9	188.4 ± 1.02	249.22 ± 1.72	-53.45 ± 1.41	-18.96 ± 2.06	184.83 ± 1.65
263.67	373.27 ± 1.11	10.61 ± 1.81	-7.26 ± 1.73	215.58 ± 1.52	256.59 ± 2.24	-54.89 ± 0.57	-10.61 ± 3.1	180.35 ± 0.56
273.44	377.15 ± 1	19.39 ± 1.5	0.78 ± 1.16	196.03 ± 0.91	269.33 ± 0.68	-56.43 ± 0.95	0.91 ± 0.56	171.07 ± 1.83
283.20	368.78 ± 0.87	14.42 ± 0.93	11.89 ± 2.42	227.62 ± 0.48	286.88 ± 2.59	-64.6 ± 0.99	-1.66 ± 1.02	189.45 ± 0.84
292.97	386.16 ± 0.73	22.68 ± 1.58	37.89 ± 1.71	194.31 ± 0.55	311.43 ± 1.78	-62.18 ± 1.36	38 ± 0.84	196.28 ± 0.88

Table D. 30. Measured dynamic-stiffness real and imaginary parts at 12,000 rpm and 1,724 kPa for t_p=10 mm.

Freq. [Hz.]	Re (H_{xx}) [MN/m]	Re (H_{xy}) [MN/m]	Re (H_{yx}) [MN/m]	Re (H_{yy}) [MN/m]	Im (H_{xx}) [MN/m]	Im (H_{xy}) [MN/m]	Im (H_{yx}) [MN/m]	Im (H_{yy}) [MN/m]
9.77	395.7 ± 1.45	-50.02 ± 0.34	-52.56 ± 3.54	178.39 ± 0.77	13.51 ± 2.07	-1.91 ± 1.03	-0.48 ± 1.65	9.12 ± 1.03
19.53	394.04 ± 1.7	-49.61 ± 0.48	-49.1 ± 2.49	178.57 ± 0.89	24.43 ± 1.84	-5.31 ± 0.57	-0.46 ± 2.58	10.12 ± 0.86
29.30	398.71 ± 1.36	-49.51 ± 0.88	-48.88 ± 1.13	181.41 ± 1.04	33.56 ± 1.9	-7.43 ± 0.59	-7.31 ± 1.36	15.83 ± 0.65
39.06	397.47 ± 2.38	-47.87 ± 0.6	-50.29 ± 3.1	179.54 ± 0.94	50.93 ± 2.71	-11.72 ± 0.59	-9.77 ± 0.78	18.99 ± 0.59
48.83	403.16 ± 1.02	-49.68 ± 0.28	-46.75 ± 0.91	180.78 ± 0.72	58.1 ± 0.25	-15.56 ± 0.29	-14.45 ± 1.2	24.26 ± 0.34
58.59	404.66 ± 1.4	-48.48 ± 0.44	-46.47 ± 1.26	178.06 ± 0.54	69.9 ± 1.64	-14.49 ± 0.64	-19.28 ± 0.85	28.94 ± 0.63
68.36	408.25 ± 1.66	-48.32 ± 0.44	-51.39 ± 1.5	178.4 ± 0.66	82.28 ± 1.75	-19.02 ± 0.8	-23.01 ± 0.99	33.89 ± 0.26
78.13	413.08 ± 2.63	-46.45 ± 0.43	-46.51 ± 1.99	183.38 ± 0.7	91.22 ± 1.2	-17.92 ± 1.15	-25.18 ± 1.55	39.02 ± 0.46
87.89	418.5 ± 3.2	-49.08 ± 1.34	-47.96 ± 1.73	177.86 ± 0.96	94.02 ± 4.14	-22.09 ± 0.71	-26.66 ± 1.51	44.79 ± 0.79
97.66	421.34 ± 2.26	-49.28 ± 0.33	-46.25 ± 2.85	181.18 ± 0.8	100.08 ± 2.3	-23.12 ± 1.27	-30.96 ± 1.88	50.6 ± 0.34
107.42	425.09 ± 0.44	-47.43 ± 0.26	-49.58 ± 1.08	179.61 ± 0.54	116.01 ± 1.35	-24.71 ± 0.65	-34.06 ± 1.66	56.8 ± 0.43
117.19	425.27 ± 0.62	-46.28 ± 0.61	-50.96 ± 1.27	181.57 ± 0.48	128.33 ± 0.65	-27.55 ± 0.45	-42.19 ± 1.22	61.86 ± 0.33
126.95	431.01 ± 0.41	-45.22 ± 0.39	-53.56 ± 1.9	180.58 ± 0.8	137.15 ± 1.66	-29.29 ± 0.25	-42.72 ± 2.15	68.99 ± 0.36
136.72	426.38 ± 1.63	-42.65 ± 0.41	-46.16 ± 0.82	180.6 ± 0.32	133.98 ± 0.62	-28.41 ± 0.35	-41.27 ± 1.09	74.48 ± 0.41
146.48	427.97 ± 1.81	-40.61 ± 0.46	-46.89 ± 1.15	183.53 ± 0.58	142.51 ± 1.57	-29.69 ± 0.38	-43.35 ± 1.34	80.33 ± 0.36
156.25	428.86 ± 0.86	-36.22 ± 0.28	-45.93 ± 0.56	187.89 ± 0.76	152.28 ± 1.26	-32.01 ± 0.37	-48.39 ± 1.1	72.91 ± 0.24
166.02	429.6 ± 1.03	-38.47 ± 0.35	-53.32 ± 2.27	185.8 ± 0.39	160.14 ± 1.74	-34.76 ± 0.92	-52.86 ± 1.82	91.37 ± 0.57
175.78	433.97 ± 3.39	-37.41 ± 0.45	-50.12 ± 0.76	181.61 ± 0.56	153.96 ± 3.83	-34.27 ± 0.68	-39.05 ± 4.39	99.35 ± 1.01
185.55	430.88 ± 1.16	-32.08 ± 0.66	-49.54 ± 4.75	185.37 ± 1.3	175.55 ± 3.79	-39.47 ± 1.24	-50.81 ± 1.71	111.23 ± 0.59
195.31	411.38 ± 10.04	-26.78 ± 2.25	-57.57 ± 2.27	185.61 ± 2	182.89 ± 7.38	-40.58 ± 2.62	-44 ± 13.03	117.23 ± 1.47
205.08	427.26 ± 3.86	-25.47 ± 1.6	-41.48 ± 4.83	188.71 ± 0.81	191.41 ± 4.9	-44.4 ± 1.62	-37.14 ± 2.86	120.76 ± 1.53
214.84	438.26 ± 1.56	-22.38 ± 0.81	-43.91 ± 0.58	197.96 ± 0.95	201.79 ± 0.74	-49.02 ± 1.04	-39.7 ± 1.95	129.47 ± 0.67
224.61	442.19 ± 2.88	-13.06 ± 0.4	-45.52 ± 2.25	135.26 ± 0.62	210.47 ± 0.78	-50.54 ± 0.62	-40.04 ± 2.1	115.23 ± 0.36
234.38	451.11 ± 3.25	-19.84 ± 0.88	-43.07 ± 5.63	202.62 ± 1.03	210.25 ± 3.74	-54.17 ± 0.98	-36.32 ± 4.56	148.67 ± 0.81
244.14	441.87 ± 4.47	-14.01 ± 0.61	-42.03 ± 5.18	202.15 ± 2.35	224.65 ± 3.01	-56.19 ± 1.13	-37.94 ± 4.43	151.92 ± 0.97
253.91	445.85 ± 1.27	-10.33 ± 0.53	-35.88 ± 2.33	203.77 ± 0.94	225.85 ± 0.53	-61.8 ± 0.35	-28.86 ± 1.59	166.43 ± 1.19
263.67	443.13 ± 1.27	-11.84 ± 0.47	-21.36 ± 2.3	222.45 ± 1.49	237.21 ± 1.78	-63.18 ± 1.1	-27 ± 0.72	166.19 ± 0.43
273.44	443.5 ± 0.19	-6.75 ± 0.6	-18.65 ± 0.86	218.23 ± 0.58	246.53 ± 0.54	-65.64 ± 0.67	-19.19 ± 0.47	148.09 ± 0.42
283.20	438.05 ± 2.18	-8.94 ± 0.89	-12.85 ± 2.46	240.55 ± 0.94	263.49 ± 1.14	-73.81 ± 0.65	-25.49 ± 0.87	181.27 ± 1.05
292.97	446.79 ± 1	-6.38 ± 0.7	-1.86 ± 0.76	209.38 ± 0.5	271.11 ± 0.71	-68.18 ± 1.41	-4.17 ± 1.11	172.91 ± 0.44

Pad Configuration: t_p = 11.5 mm

Figure D. 3 shows the measured dynamic-stiffness functions for t_p = 11.5 mm at a rotor speed of 6,000 rpm with a 172 kPa unit load. The black vertical line designated by ω represents the running speed. The direct and cross-coupled, real dynamic-stiffness functions are shown in Figure D. 3 (a) and Figure D. 3 (b), respectively. The direct and cross-coupled, imaginary dynamic-stiffness functions are shown in Figure D. 3 (c) and Figure D. 3 (d), respectively.

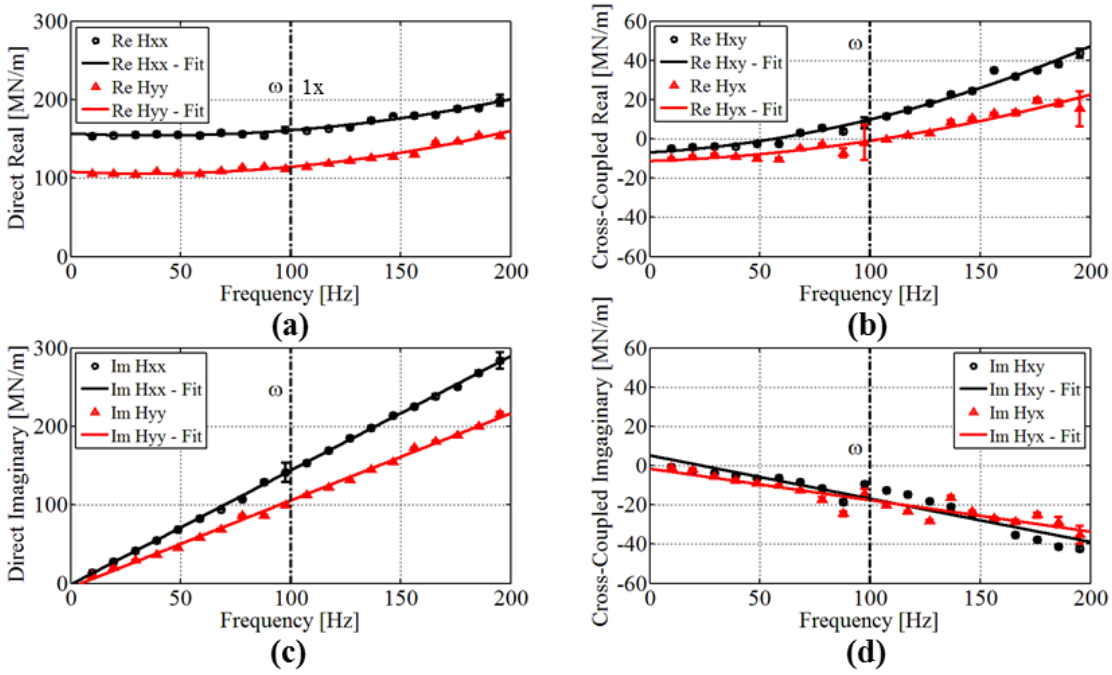

Figure D. 3. Measured dynamic-stiffness at 6 krpm (100 Hz, 32 m/s) and 172 kPa for t_p = 11.5 mm for (a) direct real, (b) cross-coupled real, (c) direct imaginary, and (d) cross-coupled imaginary.

The measured direct real dynamic-stiffness (Figure D. 3 (a)) and cross-coupled real dynamic-stiffness (Figure D. 3 (b)) show a slight increase in value as excitation frequency Ω increases indicating negative virtual-mass coefficients. Measured

$\mathrm{Re}(\boldsymbol{H}_{xx})$ is larger than measured $\mathrm{Re}(\boldsymbol{H}_{yy})$. The curve fits show that: (1) $K_{xx} > K_{yy}$, (2) K_{xx} and K_{yy} are positive, (3) $K_{yx} > K_{xy}$, (4) K_{yx} are K_{xy} are negative, (5) all virtual-mass coefficients are negative.

The measured direct imaginary dynamic-stiffness (Figure D. 3 (c)) and cross-coupled imaginary dynamic-stiffness (Figure D. 3 (d)) increase and decrease, respectively, linearly as Ω increases. The slope of measured $\mathrm{Im}(\boldsymbol{H}_{xx})$ is larger than the slope of measured $\mathrm{Im}(\boldsymbol{H}_{yy})$. The slope of measured $\mathrm{Im}(\boldsymbol{H}_{xy})$ is larger than the slope of measured $\mathrm{Im}(\boldsymbol{H}_{yx})$ and both slopes are negative. The curve fits show that: (1) $C_{xx} > C_{yy}$, (2) C_{xx} and C_{yy} are positive, (3) $|C_{xy}| > C_{yx}$, and (4) C_{xy} and C_{yx} are negative.

Figure D. 4 shows the measured dynamic-stiffness functions for t_p = 11.5 mm at a rotor speed of 12,000 rpm with a 1,724 kPa unit load. The black vertical line designated by ω represents the running speed. The direct and cross-coupled, real dynamic-stiffness functions are shown in Figure D. 4 (a) and Figure D. 4 (b), respectively. The direct and cross-coupled, imaginary dynamic-stiffness functions are shown in Figure D. 4 (c) and Figure D. 4 (d), respectively.

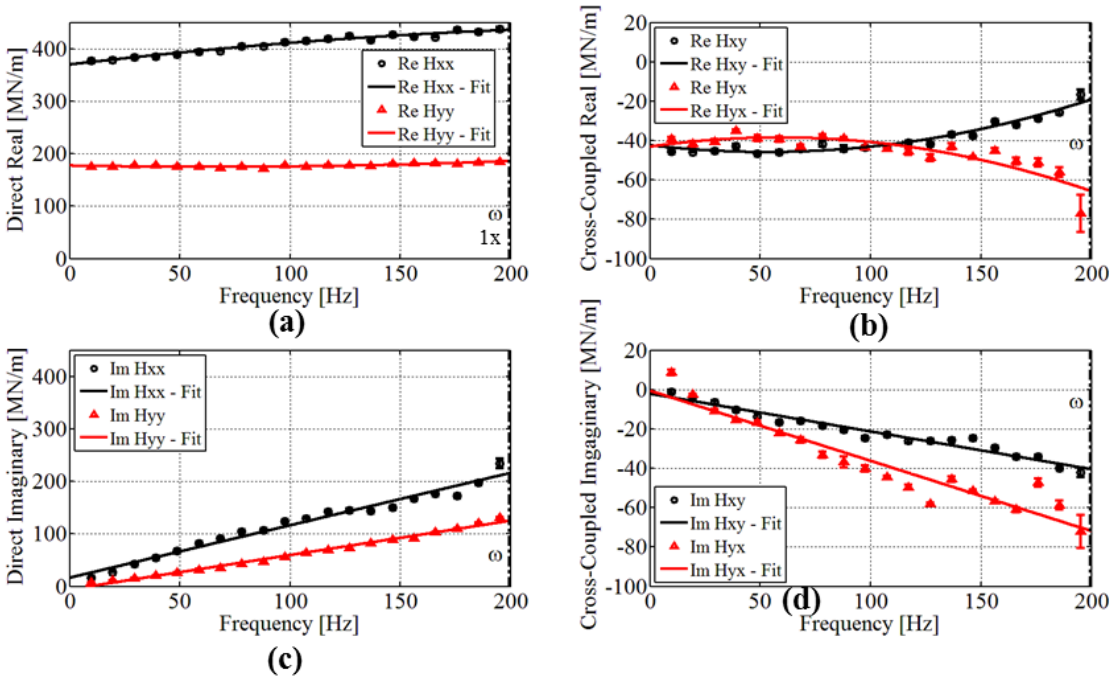

Figure D. 4. Measured dynamic-stiffness at 12 krpm (200 Hz, 64 m/s) and 1,724 kPa for t_p = 11.5 mm for (a) direct real, (b) cross-coupled real, (c) direct imaginary, and (d) cross-coupled imaginary.

Real $\mathbf{H_{xx}}$ and $\mathbf{H_{yy}}$ (Figure D. 4 (a)) show a slight increase in value as Ω increases and $\mathrm{Re}(\boldsymbol{H}_{xx}) > \mathrm{Re}(\boldsymbol{H}_{yy})$. Real $\mathbf{H_{xy}}$ and $\mathbf{H_{yx}}$ (Figure D. 4 (b)) show a slight decrease in $\mathrm{Re}(\boldsymbol{H}_{yx})$ as the excitation frequency increases, and an increase in $\mathrm{Re}(\boldsymbol{H}_{xy})$ as Ω increases. $\mathrm{Re}(\boldsymbol{H}_{yx})$ and $\mathrm{Re}(\boldsymbol{H}_{xy})$ have opposite signs at larger excitation frequencies, indicating M_{xy} and M_{yx} have opposite signs. The curve fits also show that: (1) $K_{xx} > K_{yy}$, (2) K_{xx} and K_{yy} are positive, (3) $K_{yx} > K_{xy}$, (4) K_{yx} are K_{xy} are negative, (5) M_{xx}, M_{yy}, and M_{xy} are negative, and (6) M_{yx} is positive.

Imaginary $\mathbf{H_{xx}}$ and $\mathbf{H_{yy}}$ (Figure D. 4 (c)) and imaginary $\mathbf{H_{xy}}$ and $\mathbf{H_{yx}}$ (Figure D. 4 (d)) increase and decrease, respectively, linearly as Ω increases. The slope of measured $\mathrm{Im}(\boldsymbol{H}_{xx})$ is larger than the slope of measured $\mathrm{Im}(\boldsymbol{H}_{yy})$. The slope of measured $\mathrm{Im}(\boldsymbol{H}_{xy})$ is larger than the slope of measured $\mathrm{Im}(\boldsymbol{H}_{yx})$ and both slopes are negative.

The curve fits show that: (1) $C_{xx} > C_{yy}$, (2) C_{xx} and C_{yy} are positive, (3) $|C_{xy}| > C_{yx}$, and (4) C_{xy} and C_{yx} are negative.

Table D. 31. Measured dynamic-stiffness real and imaginary parts at 6,000 rpm and 172 kPa for t_p=11.5 mm.

Freq. [Hz.]	Re (H_{xx}) [MN/m]	Re (H_{xy}) [MN/m]	Re (H_{yx}) [MN/m]	Re (H_{yy}) [MN/m]	Im (H_{xx}) [MN/m]	Im (H_{xy}) [MN/m]	Im (H_{yx}) [MN/m]	Im (H_{yy}) [MN/m]
9.77	153.29 ± 0.24	-4.73 ± 0.29	-10.03 ± 0.32	105.49 ± 0.31	13.48 ± 0.27	-0.7 ± 0.24	-0.9 ± 0.3	10.15 ± 0.22
19.53	154.7 ± 0.47	-4.21 ± 0.25	-9.09 ± 0.32	105.81 ± 0.27	27.64 ± 0.59	-2.43 ± 0.22	-1.99 ± 0.28	19.37 ± 0.22
29.30	155.13 ± 0.37	-3.98 ± 0.17	-8.09 ± 0.39	104.7 ± 0.46	41.68 ± 0.15	-3.83 ± 0.2	-5.68 ± 0.45	28.94 ± 0.34
39.06	156.15 ± 0.85	-3.8 ± 0.14	-9.12 ± 0.36	107.62 ± 0.25	54.64 ± 0.79	-5.16 ± 0.42	-7.78 ± 0.71	36.4 ± 0.28
48.83	154.98 ± 0.91	-2.45 ± 0.24	-10.08 ± 0.84	105.48 ± 0.28	68.45 ± 0.39	-6.79 ± 0.56	-8.93 ± 0.4	45.45 ± 0.39
58.59	154.1 ± 0.94	-2.59 ± 0.22	-10.46 ± 0.69	105.02 ± 0.17	82.56 ± 0.83	-6.38 ± 0.23	-10.16 ± 0.37	58.2 ± 0.42
68.36	158.05 ± 1.01	3.05 ± 0.62	-4.92 ± 0.43	109.07 ± 0.4	94.39 ± 0.54	-8.45 ± 0.34	-12.68 ± 0.35	68.54 ± 0.61
78.13	156.1 ± 1.17	5.73 ± 0.45	-2.9 ± 0.49	113.11 ± 0.58	106.77 ± 0.74	-11.53 ± 0.28	-17.38 ± 1.14	86.02 ± 0.61
87.89	154.34 ± 2.21	3.74 ± 1.21	-7.2 ± 2.32	113.92 ± 0.37	129.05 ± 1.6	-18.38 ± 0.9	-24.66 ± 1.39	86.55 ± 0.91
97.66	161.75 ± 3.42	8.02 ± 2.66	-1.93 ± 8.86	111.81 ± 0.72	141.52 ± 12.31	-9.41 ± 0.48	-14.21 ± 2.46	99.63 ± 2.02
107.42	160.8 ± 0.34	11.41 ± 0.99	-0.44 ± 0.31	113.92 ± 0.47	153.14 ± 1	-12.56 ± 0.44	-20.15 ± 0.23	112.6 ± 0.53
117.19	163.32 ± 0.43	14.83 ± 0.77	1.79 ± 0.16	118.85 ± 0.56	168.9 ± 0.71	-14.73 ± 0.47	-23.31 ± 0.3	122.13 ± 0.25
126.95	165.05 ± 1.08	18.34 ± 0.14	2.92 ± 0.72	121.97 ± 0.17	185.23 ± 0.37	-18.23 ± 0.36	-28.18 ± 0.43	131.29 ± 0.36
136.72	173.58 ± 0.86	22.71 ± 0.48	8.53 ± 0.78	125.53 ± 0.41	198.18 ± 1.02	-20.92 ± 0.27	-16.45 ± 1.13	144.97 ± 0.45
146.48	178.95 ± 0.34	24.44 ± 0.23	10.59 ± 0.35	126.91 ± 0.3	213.66 ± 0.56	-25.2 ± 0.28	-23.52 ± 0.45	154.17 ± 0.48
156.25	179.43 ± 1.02	34.93 ± 0.37	12.96 ± 0.4	130.11 ± 0.33	225.58 ± 0.92	-27.41 ± 0.21	-27.05 ± 0.7	172.55 ± 0.23
166.02	180.97 ± 1.01	31.68 ± 0.5	13.12 ± 1.22	145.88 ± 0.36	237.92 ± 2.74	-35.33 ± 0.45	-28.64 ± 0.98	180.85 ± 0.39
175.78	188.64 ± 1.62	35.02 ± 0.57	19.45 ± 1.16	146.35 ± 0.46	250.51 ± 0.71	-37.78 ± 0.35	-25.35 ± 1.3	188.38 ± 0.64
185.55	189.18 ± 1.17	38.27 ± 0.81	18.03 ± 1.48	154.23 ± 0.65	267.97 ± 2.55	-41.22 ± 0.56	-28.92 ± 2.53	200.05 ± 0.71
195.31	198.83 ± 6.91	43.56 ± 2.27	15.23 ± 8.89	153.74 ± 1.69	284.02 ± 10.36	-42.43 ± 1.05	-35.37 ± 4.45	216.03 ± 1.9
205.08	196.78 ± 3.22	45.71 ± 1.26	27.39 ± 2.27	159.13 ± 1.42	292.36 ± 2.14	-47.15 ± 1	-19.06 ± 3.44	220.5 ± 1.26
214.84	203.9 ± 0.67	54.39 ± 0.75	36.57 ± 0.79	149.26 ± 0.48	305.82 ± 1.33	-44.29 ± 0.37	-20.17 ± 1.03	249.82 ± 1.16
224.61	206.58 ± 0.72	56.54 ± 1.42	43.72 ± 0.85	233.9 ± 0.59	321.4 ± 1.07	-65.35 ± 0.49	-35.11 ± 1.15	244.09 ± 0.45
234.38	218 ± 1.47	52.1 ± 0.8	47.8 ± 1.73	183.78 ± 0.75	327.78 ± 1.14	-56.11 ± 0.49	-36.11 ± 3.14	280.62 ± 0.64
244.14	226.3 ± 1.29	47.06 ± 0.8	52.27 ± 0.44	177.28 ± 0.68	350.73 ± 0.93	-55.9 ± 0.57	-15.21 ± 1.09	284.32 ± 0.71
253.91	238.96 ± 1.59	65.62 ± 1.35	36.03 ± 1.32	199.54 ± 1.25	359.74 ± 1.9	-47.1 ± 0.36	-5.92 ± 2.64	312.17 ± 0.61
263.67	237.44 ± 1.68	86.31 ± 1.46	69.24 ± 1.04	191.79 ± 0.68	380.55 ± 1.74	-46.15 ± 0.63	14.18 ± 2.17	356.13 ± 0.97
273.44	245.03 ± 0.93	106.78 ± 1.16	81.27 ± 1.16	218.87 ± 0.51	397.15 ± 0.82	-50.82 ± 1.19	2.97 ± 0.82	354.71 ± 0.33
283.20	1191.43 ± 474.5	-50.2 ± 50.69	-325.11 ± 180.69	-129.16 ± 241.02	137.73 ± 94.3	-394.33 ± 157.14	-1524.4 ± 735.69	591.59 ± 93.28
292.97	348.68 ± 8.79	97.51 ± 1.59	257.64 ± 4.13	265.38 ± 2.66	426.78 ± 6.07	-91.15 ± 2.75	-80.07 ± 9.31	337.62 ± 1.64

Table D. 32. Measured dynamic-stiffness real and imaginary parts at 6,000 rpm and 345 kPa for t_p=11.5 mm.

Freq. [Hz.]	Re (H_{xx}) [MN/m]	Re (H_{xy}) [MN/m]	Re (H_{yx}) [MN/m]	Re (H_{yy}) [MN/m]	Im (H_{xx}) [MN/m]	Im (H_{xy}) [MN/m]	Im (H_{yx}) [MN/m]	Im (H_{yy}) [MN/m]
9.77	176.02 ± 0.23	-5.55 ± 0.17	-8.7 ± 0.19	100.47 ± 0.26	14.59 ± 0.3	-1.19 ± 0.31	1.9 ± 0.26	8.92 ± 0.25
19.53	178.28 ± 0.35	-5.81 ± 0.3	-9.86 ± 0.32	100.21 ± 0.25	29.01 ± 0.43	-2.96 ± 0.27	-1.7 ± 0.25	18.03 ± 0.15
29.30	179.13 ± 0.31	-5.05 ± 0.21	-9.15 ± 0.28	99.13 ± 0.19	42.61 ± 0.37	-4.2 ± 0.2	-4.54 ± 0.2	26.39 ± 0.3
39.06	181.86 ± 0.27	-4.25 ± 0.23	-8.43 ± 0.34	100 ± 0.25	55.97 ± 0.43	-5.8 ± 0.14	-6.5 ± 0.32	34.79 ± 0.28
48.83	181.42 ± 0.49	-4.41 ± 0.53	-10 ± 0.28	100.43 ± 0.33	69.25 ± 0.22	-8.37 ± 0.17	-9.76 ± 0.31	43.1 ± 0.28
58.59	183.5 ± 0.62	-3.01 ± 0.3	-10.1 ± 0.37	100.31 ± 0.33	83.7 ± 0.45	-8.25 ± 0.58	-11.63 ± 0.16	52.94 ± 0.35
68.36	182.68 ± 0.43	1.11 ± 0.4	-6.08 ± 0.22	102.31 ± 0.2	97.09 ± 0.62	-8.05 ± 0.5	-14.72 ± 0.26	65.83 ± 0.21
78.13	182.13 ± 0.64	3.05 ± 0.32	-2.68 ± 0.26	100.66 ± 0.59	109.44 ± 0.69	-11.31 ± 0.21	-19.4 ± 0.63	74.49 ± 0.15
87.89	183.31 ± 1.94	2.28 ± 0.5	0.15 ± 1.02	99.24 ± 0.28	123.9 ± 1.18	-13.31 ± 0.69	-19.76 ± 1.3	84.12 ± 0.48
97.66	188.29 ± 1.82	3.36 ± 1.45	-3.9 ± 1.14	105.5 ± 0.55	137.69 ± 1.49	-11.95 ± 0.98	-20.17 ± 0.97	96.45 ± 0.9
107.42	187.26 ± 0.69	8.25 ± 0.68	-1.36 ± 0.45	106.45 ± 0.4	154.29 ± 1.25	-15.13 ± 0.49	-23.27 ± 0.42	106.83 ± 0.74
117.19	189.21 ± 0.36	12.78 ± 0.3	-0.87 ± 0.16	110.75 ± 0.26	170.68 ± 0.89	-17.75 ± 0.34	-30.58 ± 0.44	116.44 ± 0.29
126.95	190.09 ± 0.78	16.25 ± 0.42	-0.82 ± 0.98	114.92 ± 0.46	187.53 ± 0.78	-21.91 ± 0.25	-33.6 ± 0.73	126.76 ± 0.24
136.72	198.68 ± 0.16	19.44 ± 0.29	4.48 ± 0.71	118.04 ± 0.22	200.15 ± 1.06	-24.48 ± 0.37	-17.8 ± 0.43	138.57 ± 0.22
146.48	207.42 ± 0.72	21.31 ± 0.34	11.08 ± 0.77	119.99 ± 0.25	212.8 ± 0.89	-28.57 ± 0.31	-23.5 ± 0.5	146.52 ± 0.28
156.25	205.11 ± 0.25	30.58 ± 0.21	15.47 ± 0.52	114.08 ± 0.2	225.2 ± 0.83	-28.25 ± 0.3	-30.76 ± 0.49	153.37 ± 0.19
166.02	209.19 ± 0.69	27.09 ± 0.11	10.91 ± 0.8	133.84 ± 0.33	239.69 ± 0.53	-38.12 ± 0.39	-30.33 ± 0.41	169.9 ± 0.21
175.78	220.23 ± 1.02	29.95 ± 0.48	12.53 ± 1.13	138.72 ± 0.41	251.59 ± 0.85	-42.51 ± 0.28	-17.03 ± 0.82	177.6 ± 0.36
185.55	214.03 ± 1.15	33.11 ± 0.5	12.85 ± 0.34	142.76 ± 0.61	267.78 ± 1.73	-44.5 ± 0.71	-38.31 ± 0.63	188.57 ± 0.33
195.31	199.63 ± 5.34	39.16 ± 1.81	30.45 ± 2.54	141.95 ± 1.15	278.43 ± 3.27	-44.25 ± 1.44	-54.25 ± 2.98	202.39 ± 0.91
205.08	228.17 ± 4.11	37.85 ± 1.79	25.45 ± 3.71	153.03 ± 1.13	290.96 ± 4.28	-53.08 ± 1.52	-14.21 ± 1.15	205.75 ± 1.14
214.84	233.31 ± 1.92	40.54 ± 0.91	47.4 ± 0.9	152.35 ± 0.76	302.97 ± 1.44	-54.31 ± 1.08	-15.56 ± 0.33	214.8 ± 0.37
224.61	225.61 ± 1.15	88.45 ± 0.75	78.18 ± 0.69	134.43 ± 0.92	320.93 ± 0.9	-79.38 ± 1.55	-62.28 ± 1.08	359.63 ± 0.82
234.38	253.81 ± 1.21	37.89 ± 0.55	34.17 ± 1.44	176.95 ± 0.64	329.75 ± 0.89	-65.34 ± 0.7	-29.12 ± 1.02	247.16 ± 0.49
244.14	253.7 ± 1.09	43.99 ± 0.59	45.51 ± 0.78	163.9 ± 0.34	358.81 ± 0.97	-63.47 ± 0.61	-26.18 ± 1.04	254.76 ± 0.65
253.91	262.02 ± 1.22	46.01 ± 0.38	47.31 ± 0.4	195.46 ± 0.63	362.48 ± 0.52	-66.96 ± 0.26	-18.44 ± 0.79	268.16 ± 0.58
263.67	259.05 ± 1.96	51.76 ± 0.79	69.5 ± 0.98	182.06 ± 0.24	380.34 ± 2.12	-57.2 ± 0.85	-10.67 ± 1.5	272.01 ± 0.6
273.44	272.92 ± 1.16	78.13 ± 1	68.2 ± 0.69	254.96 ± 0.89	398.31 ± 1	-107.87 ± 0.83	-13.76 ± 1.13	360.97 ± 0.72
283.20	302.88 ± 2.68	68.99 ± 0.6	63.31 ± 2.91	212.82 ± 0.93	427.64 ± 1.61	-60.41 ± 0.9	-87.03 ± 2.5	309 ± 0.73
292.97	296.05 ± 1.65	62.3 ± 0.37	121.95 ± 1.73	239.88 ± 0.86	471.55 ± 0.96	-67.08 ± 0.36	100.74 ± 1.59	300.8 ± 0.66

Table D. 33. Measured dynamic-stiffness real and imaginary parts at 6,000 rpm and 689 kPa for t_p=11.5 mm.

Freq. [Hz.]	Re (H_{xx}) [MN/m]	Re (H_{xy}) [MN/m]	Re (H_{yx}) [MN/m]	Re (H_{yy}) [MN/m]	Im (H_{xx}) [MN/m]	Im (H_{xy}) [MN/m]	Im (H_{yx}) [MN/m]	Im (H_{yy}) [MN/m]
9.77	233.53 ± 0.31	-11.7 ± 0.3	-12.65 ± 0.29	105.33 ± 0.21	14.75 ± 0.14	-1.38 ± 0.11	3.34 ± 0.15	7.6 ± 0.23
19.53	236.86 ± 0.24	-11.8 ± 0.38	-15.02 ± 0.13	104.47 ± 0.31	29.49 ± 0.18	-2.88 ± 0.15	-0.81 ± 0.13	13.56 ± 0.26
29.30	238.03 ± 0.41	-10.79 ± 0.05	-12.54 ± 0.29	104.4 ± 0.23	43.19 ± 0.28	-4.34 ± 0.2	-4.83 ± 0.3	21.02 ± 0.22
39.06	240.42 ± 0.23	-10.23 ± 0.32	-11.86 ± 0.26	102.06 ± 0.24	58.32 ± 0.34	-7.27 ± 0.34	-8.54 ± 0.31	29.96 ± 0.09
48.83	241.82 ± 0.37	-10.29 ± 0.24	-13.62 ± 0.32	101.92 ± 0.29	71.16 ± 0.42	-9.88 ± 0.31	-11.78 ± 0.33	37.93 ± 0.2
58.59	242.16 ± 0.65	-8.73 ± 0.45	-13.23 ± 0.33	102.48 ± 0.45	84.6 ± 0.49	-10.19 ± 0.31	-15.43 ± 0.33	47.57 ± 0.18
68.36	243.73 ± 0.23	-5.8 ± 0.44	-11.61 ± 0.56	101.51 ± 0.33	102.91 ± 0.79	-7.47 ± 0.39	-13.96 ± 0.16	62.4 ± 0.31
78.13	242.99 ± 0.64	-2.34 ± 0.54	-8.43 ± 0.57	100.65 ± 0.26	112.22 ± 0.57	-12.97 ± 0.47	-22.42 ± 0.53	66.69 ± 0.51
87.89	244.81 ± 0.92	-3.84 ± 0.6	-7.71 ± 1.69	100.74 ± 0.16	120.82 ± 1.23	-15.49 ± 0.78	-18.48 ± 1.37	73.35 ± 0.41
97.66	243.99 ± 2.44	1.29 ± 1.56	-15.62 ± 0.73	108.38 ± 0.45	143.52 ± 1.08	-17.44 ± 0.74	-25.16 ± 1.17	87.19 ± 0.78
107.42	248.83 ± 1.16	2.61 ± 0.65	-9.09 ± 0.53	107.33 ± 0.28	160.05 ± 0.51	-19.6 ± 0.48	-27.87 ± 0.74	95.44 ± 0.29
117.19	249.36 ± 0.41	6.77 ± 0.44	-9.4 ± 0.73	110.88 ± 0.34	176.14 ± 0.22	-23.66 ± 0.69	-34.05 ± 0.38	105.61 ± 0.31
126.95	251.21 ± 0.68	9.77 ± 0.18	-10.32 ± 0.43	112.77 ± 0.32	192.73 ± 0.69	-27.17 ± 0.08	-38.62 ± 0.57	112.78 ± 0.26
136.72	260.84 ± 0.16	11.18 ± 0.2	-2.34 ± 0.51	117.88 ± 0.16	199.82 ± 0.53	-31.44 ± 0.28	-20.86 ± 0.56	124.44 ± 0.12
146.48	268.07 ± 0.27	11.92 ± 0.23	3.29 ± 0.28	119.07 ± 0.18	214.95 ± 0.45	-34.42 ± 0.13	-27.05 ± 0.45	132.05 ± 0.09
156.25	264.99 ± 0.45	20.89 ± 0.16	7.61 ± 0.25	117.14 ± 0.19	228.76 ± 0.61	-35.89 ± 0.24	-33.07 ± 0.42	136.64 ± 0.13
166.02	269.48 ± 0.61	17.28 ± 0.37	6.65 ± 0.27	128.21 ± 0.22	244.3 ± 0.69	-43.43 ± 0.38	-35.09 ± 0.45	151.32 ± 0.37
175.78	281.65 ± 0.5	19.05 ± 0.32	8.66 ± 0.77	131.69 ± 0.42	251.38 ± 1.21	-48.24 ± 0.49	-19.64 ± 1.06	158.86 ± 0.27
185.55	276.9 ± 1.55	22.24 ± 1.08	7.46 ± 0.17	140.15 ± 0.63	274.83 ± 0.67	-53.25 ± 0.48	-42.21 ± 0.95	173.67 ± 0.41
195.31	263.55 ± 2.23	29.06 ± 1.43	22.06 ± 2.02	134.66 ± 0.69	287.42 ± 3.05	-50.83 ± 0.52	-54.5 ± 1.69	183.11 ± 0.79
205.08	291.6 ± 1.79	28.52 ± 1.19	18.37 ± 0.7	151.1 ± 1.13	298.54 ± 1.25	-67.09 ± 1.5	-23.62 ± 0.86	184.94 ± 0.95
214.84	297.44 ± 1.04	27.98 ± 0.5	31.7 ± 0.42	151.85 ± 0.52	311.06 ± 0.68	-65.86 ± 0.25	-27.59 ± 0.82	196.06 ± 0.59
224.61	307.52 ± 0.48	39.39 ± 0.5	32.07 ± 0.39	143.52 ± 0.61	326.43 ± 0.74	-61.92 ± 0.28	-28.6 ± 0.76	173.96 ± 0.44
234.38	325.26 ± 0.68	24.96 ± 0.58	23.72 ± 0.8	166.19 ± 0.29	340.14 ± 0.93	-75.16 ± 0.85	-32.36 ± 0.94	221.55 ± 0.29
244.14	319.98 ± 0.62	27.55 ± 0.51	35.33 ± 0.64	161.93 ± 0.64	357.28 ± 1.16	-71.93 ± 0.46	-38.04 ± 0.75	223.08 ± 0.36
253.91	334.26 ± 0.79	35.28 ± 0.42	41.83 ± 0.45	184.81 ± 0.46	362.42 ± 0.39	-84.6 ± 0.52	-29.79 ± 0.38	261.2 ± 0.55
263.67	333.5 ± 0.91	29.45 ± 0.47	46.51 ± 0.43	185.62 ± 0.9	372.31 ± 0.67	-74.43 ± 0.55	-22.45 ± 1.06	242.02 ± 0.57
273.44	347.23 ± 0.58	44.62 ± 0.33	41.41 ± 0.59	151.07 ± 0.3	393.14 ± 0.23	-70.11 ± 0.25	-16.76 ± 0.55	210.85 ± 0.46
283.20	349.04 ± 0.64	39.17 ± 0.7	53.45 ± 0.8	226.54 ± 0.43	421.5 ± 0.58	-83.01 ± 0.52	-32.94 ± 1.28	265.91 ± 0.32
292.97	377.44 ± 0.69	64.37 ± 0.36	66.42 ± 0.73	143.91 ± 0.55	427.64 ± 0.23	-66.08 ± 0.98	30.86 ± 1.12	295.58 ± 0.53

Table D. 34. Measured dynamic-stiffness real and imaginary parts at 6,000 rpm and 1034 kPa for t_p=11.5 mm.

Freq. [Hz.]	Re (H_{xx}) [MN/m]	Re (H_{xy}) [MN/m]	Re (H_{yx}) [MN/m]	Re (H_{yy}) [MN/m]	Im (H_{xx}) [MN/m]	Im (H_{xy}) [MN/m]	Im (H_{yx}) [MN/m]	Im (H_{yy}) [MN/m]
9.77	292.79 ± 0.89	-22.28 ± 0.14	-21.06 ± 0.27	120.86 ± 0.54	18.03 ± 0.47	-0.1 ± 0.26	4.05 ± 0.45	7.25 ± 0.23
19.53	297.61 ± 0.83	-21.63 ± 0.25	-23.09 ± 0.17	120 ± 0.33	34.12 ± 0.72	-2.2 ± 0.4	-0.87 ± 0.37	11.4 ± 0.24
29.30	301.25 ± 0.5	-21.3 ± 0.5	-20.26 ± 0.64	120.88 ± 0.18	46.2 ± 0.7	-3.32 ± 0.2	-4.46 ± 0.68	17.8 ± 0.23
39.06	304.25 ± 0.41	-18.73 ± 0.3	-19.25 ± 0.22	117.1 ± 0.29	60.48 ± 0.46	-6.69 ± 0.26	-10.94 ± 0.5	26.05 ± 0.19
48.83	307 ± 0.83	-18.51 ± 0.37	-21.68 ± 0.27	116.97 ± 0.17	74.35 ± 0.29	-10 ± 0.64	-14.26 ± 0.29	33.77 ± 0.27
58.59	309.79 ± 1	-17.05 ± 0.31	-21.68 ± 0.37	116.22 ± 0.51	89.29 ± 0.82	-11.31 ± 0.52	-18.33 ± 0.27	43.4 ± 0.47
68.36	308.13 ± 1.13	-15.32 ± 0.29	-26.52 ± 0.18	113.82 ± 0.45	101.92 ± 0.33	-12.78 ± 0.51	-21.19 ± 0.28	50.24 ± 0.31
78.13	310.15 ± 0.85	-9.6 ± 0.52	-18.31 ± 0.71	116.11 ± 0.39	113.68 ± 1.75	-14.8 ± 0.51	-27.24 ± 0.72	59.96 ± 0.54
87.89	315.14 ± 2.15	-11.84 ± 0.56	-19.81 ± 0.81	114.81 ± 0.53	120.71 ± 1.78	-17.32 ± 0.24	-25.45 ± 2.27	64.8 ± 0.52
97.66	313.22 ± 1.46	-7.52 ± 1.01	-26.22 ± 2.02	121.53 ± 1.09	139.15 ± 3.53	-21.19 ± 1.34	-29.1 ± 1.29	80.34 ± 0.54
107.42	315.78 ± 1.81	-5.46 ± 1.26	-23.63 ± 0.92	122.76 ± 0.21	161.45 ± 1.14	-25.93 ± 0.28	-30.06 ± 0.68	87.77 ± 0.35
117.19	318.54 ± 0.94	-1.79 ± 0.51	-21.52 ± 0.46	125.29 ± 0.52	175.22 ± 0.53	-29.52 ± 0.36	-36.59 ± 0.4	96.34 ± 0.42
126.95	321.78 ± 1.04	0.01 ± 0.27	-22.7 ± 0.52	127.24 ± 0.32	192.31 ± 0.27	-33.84 ± 0.26	-39.58 ± 1.19	102.66 ± 0.23
136.72	327.05 ± 0.38	1.4 ± 0.24	-12.95 ± 0.76	128.78 ± 0.26	194.86 ± 0.21	-38.44 ± 0.17	-23.95 ± 0.49	116.58 ± 0.36
146.48	334.84 ± 0.44	-0.28 ± 0.27	-8.19 ± 0.24	132.95 ± 0.14	208.81 ± 0.36	-41.51 ± 0.19	-31.28 ± 0.28	120.33 ± 0.25
156.25	332.43 ± 0.61	7.72 ± 0.28	-4.5 ± 0.3	133 ± 0.14	224.41 ± 0.26	-44.52 ± 0.13	-35.47 ± 0.39	124.88 ± 0.16
166.02	334 ± 0.64	3.07 ± 0.4	-4.77 ± 0.85	141.2 ± 0.22	238.47 ± 0.41	-50.68 ± 0.22	-39.75 ± 0.51	138.44 ± 0.19
175.78	347.33 ± 0.85	3.96 ± 0.42	-1.53 ± 0.89	143.95 ± 0.32	241.78 ± 0.78	-54.92 ± 0.53	-26.09 ± 0.92	143.53 ± 0.23
185.55	343.42 ± 1.54	9.18 ± 0.71	-2.3 ± 0.62	148.02 ± 0.47	270.64 ± 0.86	-58.57 ± 0.57	-45.21 ± 0.81	157.25 ± 0.21
195.31	325.07 ± 2.67	15.25 ± 1.14	5.88 ± 2.57	145.27 ± 0.75	293.48 ± 4.83	-59.15 ± 1.6	-62.57 ± 1.85	168.07 ± 0.58
205.08	357.48 ± 1.98	8.49 ± 2.59	9.96 ± 0.57	156.66 ± 1.78	287.59 ± 1.19	-66.55 ± 4.17	-33.7 ± 1.21	168.26 ± 1.84
214.84	362.36 ± 0.83	12.58 ± 0.54	18.95 ± 0.62	159.78 ± 0.49	302.03 ± 1.35	-70 ± 0.79	-37.38 ± 0.82	179.36 ± 0.56
224.61	373.31 ± 0.55	18.1 ± 0.33	19.71 ± 0.23	171.59 ± 0.42	317.45 ± 0.61	-69.88 ± 0.34	-38.34 ± 0.96	148.93 ± 0.51
234.38	389.23 ± 1.19	8.46 ± 0.54	8.9 ± 0.67	172.36 ± 0.39	333.63 ± 1.07	-80.45 ± 0.79	-48.03 ± 1.26	201.53 ± 0.2
244.14	386.99 ± 0.85	9.26 ± 0.17	21.86 ± 0.69	170.27 ± 0.65	347.99 ± 0.87	-75.95 ± 0.36	-46.97 ± 0.54	196.33 ± 0.45
253.91	398.72 ± 0.55	15.83 ± 0.44	22.99 ± 0.46	178.83 ± 0.35	352.38 ± 0.48	-83.7 ± 0.45	-41.19 ± 0.47	219.7 ± 0.34
263.67	398.73 ± 0.72	14.04 ± 0.43	30.41 ± 0.74	196.71 ± 0.47	362.99 ± 0.36	-84.15 ± 0.52	-38.62 ± 1.81	222.96 ± 0.53
273.44	413.11 ± 0.42	23.81 ± 0.38	28.11 ± 0.62	172.34 ± 0.16	377.71 ± 0.29	-80.33 ± 0.65	-38.5 ± 0.55	181.95 ± 0.39
283.20	416.55 ± 0.87	18.86 ± 0.65	31.68 ± 0.61	230.21 ± 0.44	399.9 ± 0.69	-89.49 ± 0.77	-53.05 ± 1.31	239.69 ± 0.32
292.97	435.23 ± 0.61	22.79 ± 0.19	41.4 ± 0.72	182.88 ± 0.48	406.64 ± 0.51	-78.77 ± 0.25	-22.46 ± 0.74	233.97 ± 0.32

Table D. 35. Measured dynamic-stiffness real and imaginary parts at 6,000 rpm and 1,724 kPa for t_p=11.5 mm.

Freq. [Hz.]	Re (H_{xx}) [MN/m]	Re (H_{xy}) [MN/m]	Re (H_{yx}) [MN/m]	Re (H_{yy}) [MN/m]	Im (H_{xx}) [MN/m]	Im (H_{xy}) [MN/m]	Im (H_{yx}) [MN/m]	Im (H_{yy}) [MN/m]
9.77	403.5 ± 1.07	-44.52 ± 0.17	-44.14 ± 0.7	154.51 ± 0.28	22.44 ± 0.54	0.36 ± 0.36	3.32 ± 1.02	8.64 ± 0.39
19.53	407.75 ± 0.63	-43.28 ± 0.23	-45.51 ± 0.62	153.14 ± 0.22	36.78 ± 0.54	-2.64 ± 0.38	-2.39 ± 0.54	10.47 ± 0.2
29.30	413.42 ± 0.69	-44.34 ± 0.26	-43.42 ± 0.54	157.66 ± 0.24	48.81 ± 0.81	-4.53 ± 0.23	-8.58 ± 0.5	16.74 ± 0.18
39.06	413.41 ± 0.61	-39.13 ± 0.18	-40.6 ± 0.5	152.99 ± 0.31	64.03 ± 0.68	-7.84 ± 0.18	-12.94 ± 0.64	22.91 ± 0.25
48.83	421.06 ± 0.84	-38.9 ± 0.35	-45.05 ± 0.61	152.8 ± 0.4	78.21 ± 0.54	-12.46 ± 0.31	-16.18 ± 0.62	30.47 ± 0.47
58.59	424.08 ± 0.68	-37.65 ± 0.42	-45.33 ± 0.49	151.81 ± 0.57	92.32 ± 0.64	-13.2 ± 0.59	-21.78 ± 0.47	38.51 ± 0.54
68.36	424.72 ± 0.64	-34.71 ± 0.84	-48.39 ± 0.22	153.92 ± 0.23	103.84 ± 0.39	-15.93 ± 0.06	-26.27 ± 0.44	43.48 ± 0.57
78.13	428.62 ± 0.24	-28.65 ± 0.22	-42.33 ± 0.64	153.18 ± 0.43	115.64 ± 1.46	-17.79 ± 0.19	-30.54 ± 0.32	53.06 ± 0.65
87.89	434.49 ± 2.67	-30.68 ± 0.82	-41.42 ± 1.06	153.8 ± 0.78	113.21 ± 2.86	-22.44 ± 0.94	-27.88 ± 2.15	55.46 ± 0.74
97.66	438.08 ± 4.59	-28.26 ± 1.37	-49.11 ± 1.44	158.57 ± 0.94	140.81 ± 5.02	-28.36 ± 1.96	-34.78 ± 1.38	70.44 ± 0.4
107.42	435.33 ± 1.71	-27.08 ± 1.32	-48.25 ± 1.32	159.42 ± 0.5	154 ± 1.79	-31.73 ± 0.31	-34.88 ± 0.99	77.51 ± 0.51
117.19	439.07 ± 0.65	-25.15 ± 0.37	-47.88 ± 0.53	162.76 ± 0.26	168.31 ± 0.45	-38.04 ± 0.46	-39.12 ± 0.35	84.67 ± 0.27
126.95	448.71 ± 0.97	-25.18 ± 0.49	-49.04 ± 0.8	164.3 ± 0.2	183.25 ± 1.27	-43.3 ± 0.27	-42.75 ± 0.59	89.26 ± 0.18
136.72	449.22 ± 1.15	-24.74 ± 0.24	-37.05 ± 0.52	165.42 ± 0.22	178.49 ± 0.87	-45.22 ± 0.28	-31.51 ± 0.83	97 ± 0.39
146.48	455.29 ± 0.57	-27.58 ± 0.38	-36.43 ± 0.29	171.06 ± 0.19	191.17 ± 0.78	-47.83 ± 0.16	-37.31 ± 0.39	104.87 ± 0.27
156.25	448.38 ± 0.31	-19.99 ± 0.11	-30.15 ± 0.26	172.21 ± 0.14	206.72 ± 0.12	-53.01 ± 0.15	-40.22 ± 0.18	107.37 ± 0.1
166.02	451.7 ± 0.89	-24.58 ± 0.49	-32.07 ± 0.44	175.52 ± 0.33	221.01 ± 0.5	-58.92 ± 0.21	-46.66 ± 0.57	120.28 ± 0.16
175.78	468.15 ± 1.8	-25.85 ± 0.49	-28.46 ± 0.95	177.53 ± 0.31	218.22 ± 1	-61.24 ± 0.53	-35.57 ± 0.8	123.3 ± 0.3
185.55	463.51 ± 1.57	-20.45 ± 0.39	-30.69 ± 1.3	182.61 ± 0.39	253.06 ± 1.45	-67.5 ± 1.28	-50.9 ± 0.54	137.34 ± 0.33
195.31	465.37 ± 8.66	-14.6 ± 0.93	-38.61 ± 1.64	181.51 ± 0.63	296.47 ± 1.76	-71.24 ± 1.7	-65.13 ± 3.76	143.64 ± 0.47
205.08	469.4 ± 4.05	-20.99 ± 1.02	-16.5 ± 0.82	189.58 ± 1.36	264.19 ± 1.44	-74.41 ± 2.95	-46.13 ± 1.34	144.48 ± 0.69
214.84	472.48 ± 1.09	-18.21 ± 0.22	-10.62 ± 0.79	191.8 ± 0.42	278.26 ± 0.85	-75.52 ± 0.6	-49.8 ± 0.72	153.08 ± 0.35
224.61	486.96 ± 0.37	-13.25 ± 0.38	-11.94 ± 0.51	206.3 ± 0.25	289.38 ± 0.94	-75.93 ± 0.47	-50.8 ± 0.92	123.58 ± 0.17
234.38	501.01 ± 0.79	-22.89 ± 0.58	-17.46 ± 0.52	201.77 ± 0.4	303.42 ± 1.08	-83.9 ± 0.23	-59.39 ± 0.72	171.86 ± 0.31
244.14	497.93 ± 0.94	-21.01 ± 0.4	-8.75 ± 0.73	201.36 ± 0.51	315.22 ± 0.89	-80.3 ± 0.74	-58.69 ± 0.62	170.1 ± 0.31
253.91	505.67 ± 0.71	-15.46 ± 0.42	-6.97 ± 0.48	202.98 ± 0.42	317.85 ± 0.82	-86.56 ± 0.36	-54.09 ± 0.66	186.42 ± 0.45
263.67	501.32 ± 1.51	-15.8 ± 0.25	-2.73 ± 0.39	218.88 ± 0.39	332.15 ± 1.26	-86.38 ± 0.47	-54.14 ± 1.36	191.11 ± 0.36
273.44	517.29 ± 0.43	-11.22 ± 0.49	-2.39 ± 0.62	207.69 ± 0.46	340.3 ± 0.17	-87 ± 0.37	-54.86 ± 0.51	146.55 ± 0.2
283.20	521.95 ± 1.01	-13.58 ± 0.77	0.82 ± 0.83	258.05 ± 0.59	361.48 ± 0.69	-99.41 ± 0.33	-66.73 ± 0.77	211.19 ± 0.32
292.97	535.35 ± 0.75	-13.13 ± 0.43	10.72 ± 0.33	213.3 ± 0.23	361.1 ± 0.61	-86.76 ± 0.49	-48.89 ± 1.07	194.08 ± 0.3

Table D. 36. Measured dynamic-stiffness real and imaginary parts at 9,000 rpm and 172 kPa for t_p=11.5 mm.

Freq. [Hz.]	Re (H_{xx}) [MN/m]	Re (H_{xy}) [MN/m]	Re (H_{yx}) [MN/m]	Re (H_{yy}) [MN/m]	Im (H_{xx}) [MN/m]	Im (H_{xy}) [MN/m]	Im (H_{yx}) [MN/m]	Im (H_{yy}) [MN/m]
9.77	193.54 ± 0.44	-17.25 ± 0.61	-21.08 ± 0.35	143.93 ± 0.44	14.8 ± 0.23	-2.09 ± 0.47	-3.85 ± 0.43	10.67 ± 0.64
19.53	195.04 ± 0.49	-16.52 ± 0.62	-23.38 ± 0.31	145.43 ± 0.17	27.88 ± 0.4	-4.58 ± 0.45	-7.13 ± 0.54	22.43 ± 0.56
29.30	196.57 ± 0.68	-17.28 ± 0.32	-20.7 ± 0.59	144.87 ± 0.5	38.37 ± 0.42	-5.23 ± 0.41	-5.37 ± 0.36	31.98 ± 0.31
39.06	198.02 ± 0.66	-16.28 ± 0.68	-23.17 ± 0.35	149.5 ± 0.41	51.08 ± 0.8	-8.04 ± 0.52	-11.44 ± 0.6	38.68 ± 0.52
48.83	201.14 ± 0.99	-17.69 ± 0.56	-26.5 ± 0.48	147.58 ± 0.58	61.26 ± 1.94	-9.35 ± 0.57	-13.55 ± 1.41	46.86 ± 0.26
58.59	199.61 ± 0.94	-15.18 ± 0.77	-28.08 ± 1.19	153.13 ± 0.79	75.4 ± 0.78	-7.85 ± 0.57	-10.49 ± 0.82	58.94 ± 0.8
68.36	207.48 ± 1.37	-13.09 ± 0.61	-13.11 ± 0.59	153.61 ± 0.77	83.25 ± 1.46	-13.67 ± 1.16	-15.1 ± 0.55	68.4 ± 0.45
78.13	205.12 ± 0.49	-11.43 ± 0.91	-15.6 ± 1.13	158.46 ± 0.53	91.42 ± 1.7	-16.8 ± 0.47	-21.13 ± 0.48	86.02 ± 0.51
87.89	210.87 ± 0.87	-13.87 ± 0.38	-19.86 ± 3.67	155.43 ± 0.74	110.86 ± 0.87	-16.99 ± 1.53	-16.59 ± 3.24	82.36 ± 0.43
97.66	206.54 ± 0.84	-11.06 ± 1.06	-22.1 ± 1.83	165.37 ± 0.8	114.81 ± 0.5	-19.06 ± 0.65	-20.82 ± 2.1	90.41 ± 1.04
107.42	208.43 ± 0.73	-10.17 ± 0.63	-17.85 ± 0.7	165.26 ± 0.49	125.9 ± 1.07	-18.69 ± 0.36	-24.97 ± 0.89	100.25 ± 0.47
117.19	209.69 ± 1.35	-6.47 ± 0.86	-14.93 ± 0.71	168.57 ± 0.83	136.43 ± 0.84	-20.94 ± 0.19	-29.07 ± 0.91	105.86 ± 0.46
126.95	209.76 ± 0.96	-4.34 ± 0.52	-16.3 ± 0.53	168.91 ± 0.33	149.87 ± 1.13	-20.14 ± 0.3	-32.69 ± 1.17	115.4 ± 0.41
136.72	212.31 ± 0.99	1.21 ± 0.43	-14.19 ± 0.61	172.96 ± 0.25	158.52 ± 0.58	-23.55 ± 0.85	-20.48 ± 0.62	128.95 ± 0.17
146.48	213.82 ± 1.03	1.23 ± 0.56	-8.65 ± 1.81	170.1 ± 0.96	167.58 ± 1.91	-23.08 ± 0.68	-29.95 ± 1.06	135.6 ± 0.62
156.25	209.34 ± 1.75	9.67 ± 0.86	-12.44 ± 1.5	186.17 ± 0.69	182.92 ± 1.8	-28.39 ± 0.67	-28.97 ± 0.63	159.5 ± 0.5
166.02	213.2 ± 1.82	7.33 ± 0.42	-8.85 ± 1.93	195.81 ± 0.45	194.76 ± 1.15	-32.83 ± 0.63	-29.25 ± 1.17	160.6 ± 0.48
175.78	218.19 ± 1.18	12.87 ± 0.8	-4.69 ± 1.38	190.36 ± 0.41	207.24 ± 1.73	-31.96 ± 0.39	-27.37 ± 1.46	172.43 ± 0.48
185.55	213.45 ± 1.7	16.72 ± 0.62	-10.12 ± 1.2	206.22 ± 0.19	222.33 ± 1.61	-37.22 ± 0.43	-23.87 ± 0.69	168.17 ± 0.74
195.31	222.05 ± 2.75	25.52 ± 0.9	-16.71 ± 2.32	201.05 ± 0.71	243.3 ± 1.96	-33.17 ± 0.86	-20.15 ± 1.17	197.73 ± 0.91
205.08	222.23 ± 0.52	29.09 ± 0.96	6.81 ± 0.57	207.85 ± 0.6	251.46 ± 0.73	-42.09 ± 0.94	2.5 ± 0.9	197.29 ± 0.63
214.84	231.69 ± 1.8	43.44 ± 0.43	26.42 ± 1.4	210.65 ± 0.76	274.04 ± 0.73	-39.49 ± 0.43	14.49 ± 1.11	234.63 ± 0.51
224.61	251.63 ± 0.23	48.01 ± 0.69	23.01 ± 0.91	297.34 ± 0.52	286.34 ± 0.76	-67.21 ± 0.77	-1.61 ± 1.37	207.22 ± 0.98
234.38	279.6 ± 3.02	47.94 ± 1.11	179.58 ± 4.98	260.15 ± 1.01	290.8 ± 2.51	-57.54 ± 0.7	66.77 ± 3.94	264.02 ± 1.04
244.14	281.39 ± 3.33	36.38 ± 0.62	133.25 ± 6.94	213.38 ± 1.57	297.04 ± 1.42	-44.15 ± 1.27	54.82 ± 3.29	255.66 ± 1.32
253.91	298.75 ± 7.87	58.7 ± 0.87	140.55 ± 21.18	249.47 ± 2.25	212.24 ± 2.7	-61.16 ± 1.35	-275.28 ± 8.28	246.78 ± 3.55
263.67	311.32 ± 3.95	63.06 ± 1.43	96.76 ± 2.38	242.77 ± 1.31	318.14 ± 2.81	-68.86 ± 1.54	43.56 ± 4.13	271.31 ± 1.62
273.44	249.72 ± 2.18	79.26 ± 1.28	175.84 ± 5.19	411.45 ± 4.27	254.23 ± 2.08	-137.56 ± 3.1	-114.02 ± 4.54	317.01 ± 3.24
283.20	316.85 ± 3.16	32.35 ± 2.99	379.74 ± 7.8	340.26 ± 3.52	247.98 ± 3.37	-125.92 ± 1.49	-50.09 ± 7.08	129.11 ± 3.33
292.97	265.85 ± 1.4	40.55 ± 1.31	85.6 ± 2.43	272.8 ± 1.35	300.53 ± 1.32	-80.17 ± 0.99	-62.66 ± 1.65	268.96 ± 3.2

Table D. 37. Measured dynamic-stiffness real and imaginary parts at 9,000 rpm and 345 kPa for t_p=11.5 mm.

Freq. [Hz.]	Re (H_{xx}) [MN/m]	Re (H_{xy}) [MN/m]	Re (H_{yx}) [MN/m]	Re (H_{yy}) [MN/m]	Im (H_{xx}) [MN/m]	Im (H_{xy}) [MN/m]	Im (H_{yx}) [MN/m]	Im (H_{yy}) [MN/m]
9.77	209.28 ± 0.76	-17.86 ± 0.53	-17.95 ± 0.26	133.92 ± 0.31	14.28 ± 0.53	-2.15 ± 0.21	-1.4 ± 0.13	11.22 ± 0.3
19.53	210.76 ± 0.47	-18.32 ± 0.44	-18.16 ± 0.42	135.11 ± 0.46	27.19 ± 0.88	-3.86 ± 0.28	-6.34 ± 0.34	21.81 ± 0.3
29.30	214.79 ± 0.44	-17.51 ± 0.42	-18.32 ± 0.41	132.77 ± 0.26	39.41 ± 0.77	-6.68 ± 0.28	-9.83 ± 0.57	30.67 ± 0.36
39.06	217.1 ± 0.84	-16.75 ± 0.56	-20.09 ± 1.02	139.53 ± 0.22	52.96 ± 0.46	-8.14 ± 0.13	-13.02 ± 0.72	38.04 ± 0.27
48.83	217.06 ± 1.52	-17.64 ± 0.19	-21.12 ± 0.35	140.73 ± 0.12	65.71 ± 0.98	-9.88 ± 0.93	-16.15 ± 1.13	44.51 ± 0.85
58.59	220.91 ± 0.43	-18.31 ± 0.38	-24.42 ± 0.77	141.53 ± 0.15	74.77 ± 0.85	-12 ± 0.2	-19.72 ± 0.46	55.96 ± 0.59
68.36	223.14 ± 1.54	-13.15 ± 0.13	-17.79 ± 0.36	145.35 ± 0.56	88.64 ± 0.54	-12.34 ± 0.65	-21.3 ± 0.61	68.47 ± 0.23
78.13	228.33 ± 1.21	-13.2 ± 0.52	-11.01 ± 0.57	143.57 ± 0.4	95.26 ± 1.44	-15.72 ± 0.55	-24.42 ± 0.68	77.38 ± 0.13
87.89	236.19 ± 3.54	-16 ± 0.59	-34.47 ± 5.13	147.31 ± 0.6	112.23 ± 4.74	-19.03 ± 0.85	-18.98 ± 2.27	84.19 ± 1.01
97.66	226.54 ± 0.69	-12.81 ± 0.93	-19.76 ± 0.55	154.43 ± 0.53	116.94 ± 0.54	-19.1 ± 0.56	-25.78 ± 1.2	91.01 ± 0.4
107.42	226.6 ± 0.55	-11.98 ± 0.28	-17.54 ± 0.6	153.29 ± 0.43	125.37 ± 0.66	-19.4 ± 0.72	-29.01 ± 1.13	98.88 ± 0.46
117.19	227.91 ± 1.12	-8.26 ± 0.49	-18.03 ± 0.94	156.25 ± 0.63	137.65 ± 1.28	-20.96 ± 0.48	-35.53 ± 0.56	105.68 ± 0.18
126.95	227.88 ± 0.84	-5.8 ± 0.19	-18.1 ± 1.13	159.35 ± 0.44	148.4 ± 0.44	-23.44 ± 0.18	-39.25 ± 0.69	114.6 ± 0.23
136.72	230.34 ± 1.73	-2.69 ± 0.29	-16.59 ± 1.03	161.62 ± 0.19	157.38 ± 0.85	-24.28 ± 0.6	-25.87 ± 0.57	126.34 ± 0.34
146.48	233.8 ± 3.02	-1.26 ± 0.46	-13 ± 1.64	161.19 ± 0.3	166.73 ± 0.53	-26.01 ± 0.5	-34.62 ± 2.06	133.9 ± 0.44
156.25	228.71 ± 1.57	7.15 ± 0.5	-13.56 ± 1.26	167.44 ± 0.47	183.75 ± 1.01	-28.93 ± 0.59	-38.43 ± 1.6	148.07 ± 0.29
166.02	231.43 ± 0.55	3.82 ± 0.37	-12.51 ± 1	176.97 ± 0.45	193.24 ± 1.34	-33.65 ± 0.24	-40.78 ± 1.15	155.12 ± 0.34
175.78	235.68 ± 0.74	7.86 ± 0.23	-10.92 ± 0.54	178.98 ± 0.73	206.26 ± 1.14	-36.12 ± 0.45	-30.59 ± 1.37	163.38 ± 0.27
185.55	234.19 ± 1.28	12.62 ± 0.33	-16.81 ± 1.33	187.29 ± 0.63	220.15 ± 1	-38.3 ± 0.59	-38.94 ± 1.14	170.01 ± 0.68
195.31	235.57 ± 2.39	17.86 ± 0.52	-25.75 ± 1.15	190.44 ± 0.5	235.8 ± 2.93	-39.95 ± 0.8	-43.65 ± 1.6	188 ± 0.5
205.08	240.73 ± 0.25	18.6 ± 0.76	-8.69 ± 0.74	193.08 ± 0.76	243.03 ± 0.46	-45.08 ± 1.24	-15.47 ± 0.51	185.8 ± 0.47
214.84	240.74 ± 1.28	24.9 ± 0.55	-0.15 ± 0.79	194.23 ± 0.39	253.84 ± 1.63	-44.74 ± 0.8	-11.64 ± 0.95	197.11 ± 0.36
224.61	244.3 ± 0.89	43.41 ± 0.94	0.73 ± 0.8	222.79 ± 1.43	269.45 ± 0.87	-59.92 ± 1.06	-21.13 ± 1.48	242.14 ± 0.77
234.38	251.47 ± 0.16	25.47 ± 0.73	6.11 ± 0.38	218.93 ± 0.71	278.73 ± 0.63	-55.15 ± 0.88	-4 ± 0.78	221.63 ± 0.54
244.14	256.09 ± 1.67	28.17 ± 0.28	8.52 ± 1.18	205.69 ± 0.43	298.5 ± 1.15	-54.06 ± 0.64	12.79 ± 1.45	231.99 ± 0.61
253.91	254.14 ± 0.68	35.87 ± 0.36	17.58 ± 0.89	239.83 ± 0.51	310.57 ± 0.78	-56.06 ± 0.96	35.64 ± 0.71	234.34 ± 0.42
263.67	260.26 ± 1.66	43.38 ± 1.31	45.58 ± 2.58	219.68 ± 0.78	325.77 ± 1.82	-53.8 ± 0.51	29.87 ± 3.31	246.67 ± 0.83
273.44	281.58 ± 2.37	58.32 ± 1.12	110.42 ± 1.88	246.58 ± 2.32	341.15 ± 0.96	-81.35 ± 0.86	83.22 ± 2.27	264.21 ± 1.82
283.20	274.23 ± 2.07	57.75 ± 0.98	51.13 ± 2.87	280.53 ± 0.91	363.04 ± 1.73	-64.38 ± 0.59	69.02 ± 2.72	268.65 ± 0.64
292.97	350.44 ± 6.88	29.73 ± 2	89.48 ± 8.03	191.4 ± 1.72	244.35 ± 11.91	-74.89 ± 1.83	-393.66 ± 7.38	297.19 ± 2

Table D. 38. Measured dynamic-stiffness real and imaginary parts at 9,000 rpm and 689 kPa for t_p=11.5 mm.

Freq. [Hz.]	Re (H_{xx}) [MN/m]	Re (H_{xy}) [MN/m]	Re (H_{yx}) [MN/m]	Re (H_{yy}) [MN/m]	Im (H_{xx}) [MN/m]	Im (H_{xy}) [MN/m]	Im (H_{yx}) [MN/m]	Im (H_{yy}) [MN/m]
9.77	244.97 ± 0.8	-21.22 ± 0.24	-17.65 ± 0.32	127.03 ± 0.38	14.48 ± 0.48	-1.6 ± 0.5	2.61 ± 0.59	9.5 ± 0.47
19.53	248.48 ± 0.56	-20.94 ± 0.38	-18.7 ± 0.19	127.04 ± 0.26	29.14 ± 0.22	-4.37 ± 0.2	-4.68 ± 0.45	17.32 ± 0.42
29.30	251.08 ± 0.85	-20.25 ± 0.15	-16.51 ± 0.58	126.62 ± 0.19	41.43 ± 0.77	-5.81 ± 0.33	-8.67 ± 0.86	24.69 ± 0.37
39.06	254.25 ± 1.08	-19.94 ± 0.29	-17.29 ± 0.3	128.94 ± 0.24	55.35 ± 0.88	-9.51 ± 0.18	-14.11 ± 0.87	33.21 ± 0.26
48.83	257.96 ± 0.61	-21.36 ± 0.51	-20.55 ± 1.28	129.07 ± 0.37	67.05 ± 0.18	-12.25 ± 0.29	-16.65 ± 0.39	40 ± 0.31
58.59	260.51 ± 1.02	-21.06 ± 0.45	-19.15 ± 0.5	130.59 ± 0.64	82.06 ± 0.44	-13.83 ± 0.45	-21.08 ± 0.88	49.87 ± 0.27
68.36	264.14 ± 0.69	-17.89 ± 0.59	-18.09 ± 0.64	132.21 ± 0.36	95.81 ± 1.35	-10.82 ± 0.49	-24.34 ± 0.67	65.13 ± 0.41
78.13	265.91 ± 1.7	-16.68 ± 0.57	-18.48 ± 1.52	133.41 ± 0.4	102.82 ± 0.81	-17.5 ± 0.24	-32.93 ± 0.41	73.82 ± 0.32
87.89	268.37 ± 2.18	-19.44 ± 0.53	-17.34 ± 0.39	131.25 ± 0.85	111.17 ± 1.07	-19.7 ± 0.15	-28.19 ± 2.92	75.35 ± 0.45
97.66	272.83 ± 1.66	-16.17 ± 0.84	-24.19 ± 0.68	139.68 ± 0.38	120.46 ± 1.05	-20.22 ± 0.44	-33.89 ± 0.49	85.48 ± 0.46
107.42	272.62 ± 0.54	-16.15 ± 0.43	-22.92 ± 0.42	138.79 ± 0.32	129.83 ± 0.88	-21.04 ± 0.28	-35.76 ± 0.43	92.09 ± 0.5
117.19	273.72 ± 1.56	-12.59 ± 0.21	-24.4 ± 0.81	141.95 ± 0.4	140.29 ± 0.55	-21.98 ± 0.54	-41.8 ± 1.25	100.14 ± 0.51
126.95	274.57 ± 0.58	-9.87 ± 0.36	-26.23 ± 1.07	142.39 ± 0.49	152.94 ± 0.67	-24.22 ± 0.28	-45.66 ± 1.11	107.01 ± 0.39
136.72	276.26 ± 0.79	-6.89 ± 0.28	-22.56 ± 0.42	146.14 ± 0.34	159.54 ± 1.05	-26.62 ± 0.3	-32.59 ± 0.84	118.35 ± 0.26
146.48	276.95 ± 1.69	-5.16 ± 0.92	-21.18 ± 0.54	146.58 ± 0.39	167.97 ± 0.93	-26.78 ± 0.31	-38.97 ± 1.29	125.83 ± 0.69
156.25	275.09 ± 0.79	2.46 ± 0.54	-18.26 ± 0.89	145.99 ± 0.29	183.79 ± 0.95	-29.9 ± 0.42	-43.63 ± 0.67	131.41 ± 0.41
166.02	276.82 ± 0.66	-1.01 ± 0.57	-21.67 ± 1.22	153.95 ± 0.44	196.73 ± 0.97	-35.52 ± 0.42	-42.92 ± 0.85	144.23 ± 0.29
175.78	281.37 ± 1.98	2.57 ± 0.28	-20.12 ± 1.17	156.46 ± 0.35	200.96 ± 1.41	-38.01 ± 0.57	-31.37 ± 1.59	156.72 ± 0.52
185.55	280.82 ± 2.69	5.76 ± 0.38	-22.05 ± 1.05	166.24 ± 0.39	216.96 ± 1.64	-40.6 ± 0.73	-40.73 ± 1.03	162.23 ± 0.42
195.31	278.61 ± 3.56	11.34 ± 0.91	-26.65 ± 2.14	168.8 ± 0.59	230.87 ± 2.48	-44.36 ± 0.69	-46.97 ± 2.01	179.07 ± 0.75
205.08	288.08 ± 0.79	11.75 ± 1.08	-15.54 ± 0.75	171.97 ± 0.68	237.61 ± 1.55	-47.96 ± 0.85	-23.38 ± 0.53	175.22 ± 0.29
214.84	288.42 ± 1.37	14.15 ± 0.9	-6.94 ± 0.58	179.01 ± 0.32	245.86 ± 0.94	-51.21 ± 0.46	-22.94 ± 0.98	186.29 ± 0.54
224.61	293.26 ± 1.16	28.02 ± 0.42	-4.2 ± 0.31	167.8 ± 0.57	258.58 ± 0.8	-49.18 ± 0.48	-22.56 ± 0.98	166.36 ± 0.48
234.38	300.64 ± 1.29	14.36 ± 0.83	-13.44 ± 2.53	194.3 ± 0.59	268.16 ± 2.74	-57.81 ± 0.67	-19.69 ± 1.7	207.89 ± 0.51
244.14	293.76 ± 1.58	18.29 ± 0.28	-5.18 ± 0.88	182.07 ± 0.78	278.85 ± 1.07	-56.64 ± 0.72	-14.03 ± 1.31	216.6 ± 0.83
253.91	299.45 ± 0.98	21.75 ± 0.89	-4.28 ± 0.67	213.81 ± 0.97	286.97 ± 0.83	-66.02 ± 0.88	-4.53 ± 0.97	224.9 ± 0.89
263.67	292.55 ± 0.75	25.57 ± 0.65	3.41 ± 0.89	204.07 ± 0.57	299.03 ± 1.47	-60.98 ± 0.65	4.4 ± 1.4	228.62 ± 0.51
273.44	294.01 ± 0.56	36.69 ± 1.03	8 ± 0.83	164.73 ± 1.05	313.03 ± 0.49	-57.44 ± 0.6	16.14 ± 0.63	200.1 ± 0.57
283.20	289.26 ± 1.06	34.41 ± 1.3	27.2 ± 1.3	243.54 ± 2.04	340.34 ± 1.62	-70.18 ± 0.31	13.85 ± 0.86	236.8 ± 2.08
292.97	296.69 ± 1.62	65.29 ± 1.76	47.54 ± 1.6	185.16 ± 2.24	349.68 ± 1.13	-82.41 ± 2.32	91.38 ± 1.98	349.31 ± 5.19

Table D. 39. Measured dynamic-stiffness real and imaginary parts at 9,000 rpm and 1034 kPa for t_p=11.5 mm.

Freq. [Hz.]	Re (H_{xx}) [MN/m]	Re (H_{xy}) [MN/m]	Re (H_{yx}) [MN/m]	Re (H_{yy}) [MN/m]	Im (H_{xx}) [MN/m]	Im (H_{xy}) [MN/m]	Im (H_{yx}) [MN/m]	Im (H_{yy}) [MN/m]
9.77	292.93 ± 0.5	-28.81 ± 0.39	-23.38 ± 0.9	132.4 ± 0.23	15.14 ± 0.43	-0.86 ± 0.38	1.93 ± 0.56	8.45 ± 0.23
19.53	297.48 ± 0.49	-28.21 ± 0.19	-24.22 ± 0.29	130.8 ± 0.16	28.8 ± 0.65	-3.52 ± 0.26	-3.28 ± 0.44	13.63 ± 0.14
29.30	299.03 ± 0.27	-28.15 ± 0.09	-21.84 ± 0.78	133.01 ± 0.23	43.09 ± 1.19	-5.53 ± 0.44	-6.41 ± 0.53	19.09 ± 0.22
39.06	302.94 ± 1.23	-26.58 ± 0.11	-20.53 ± 0.62	131.07 ± 0.33	58.44 ± 1.07	-9.78 ± 0.38	-14.11 ± 0.98	27.47 ± 0.21
48.83	307.02 ± 0.7	-28.43 ± 0.22	-24.51 ± 1.09	131.69 ± 0.4	70.46 ± 1.03	-12.48 ± 0.49	-16.56 ± 1.03	33.92 ± 0.23
58.59	312.09 ± 0.59	-26.41 ± 0.15	-23.74 ± 0.81	131.01 ± 0.42	83.61 ± 1.37	-12.82 ± 0.41	-22.35 ± 0.51	43.31 ± 0.35
68.36	311.83 ± 0.72	-27.72 ± 0.13	-28.83 ± 0.77	127.72 ± 0.57	94.56 ± 1.37	-13.8 ± 0.35	-26.45 ± 0.73	50.77 ± 0.27
78.13	320.12 ± 1.62	-22.95 ± 0.74	-21.91 ± 0.87	130.71 ± 0.39	104.73 ± 1.99	-16.45 ± 0.24	-30.23 ± 1.3	59.47 ± 0.23
87.89	320.43 ± 3.53	-24.55 ± 0.77	-22.49 ± 3.21	130.22 ± 0.81	114.08 ± 1.58	-18.82 ± 0.63	-31 ± 2.33	64.4 ± 0.49
97.66	325.92 ± 1.21	-23.26 ± 0.37	-30.37 ± 1.09	137.94 ± 0.5	124.94 ± 0.51	-21.54 ± 0.54	-36.85 ± 0.78	76.26 ± 0.47
107.42	331.14 ± 1.13	-21.8 ± 0.28	-26.17 ± 1.53	136.43 ± 0.55	130.01 ± 0.39	-21.5 ± 0.36	-35.15 ± 0.67	83.16 ± 0.28
117.19	325.79 ± 1.3	-18.63 ± 0.2	-30.68 ± 0.71	139.74 ± 0.34	142.41 ± 0.98	-24.07 ± 0.43	-44.67 ± 0.54	90.84 ± 0.22
126.95	329.09 ± 0.96	-15.49 ± 0.26	-35.52 ± 0.83	140.66 ± 0.28	154.5 ± 3.05	-26.53 ± 0.4	-48.75 ± 1.14	97.4 ± 0.28
136.72	327.71 ± 0.64	-12.57 ± 0.28	-29.99 ± 1.45	143.48 ± 0.2	157.93 ± 1.72	-29.54 ± 0.32	-36.2 ± 0.65	110.76 ± 0.29
146.48	332.63 ± 2.19	-11.95 ± 0.75	-30.22 ± 0.85	143.76 ± 0.2	165.78 ± 2.34	-29.17 ± 0.67	-42.38 ± 2.15	114.73 ± 0.44
156.25	325.04 ± 2.3	-4.86 ± 0.45	-27.32 ± 0.8	146.77 ± 0.33	182.24 ± 1.4	-33.55 ± 0.37	-45.03 ± 0.89	120.73 ± 0.33
166.02	326.39 ± 0.85	-7.56 ± 0.18	-31.89 ± 1.33	152.23 ± 0.36	191.14 ± 0.6	-39.52 ± 0.23	-43.91 ± 1.45	132.16 ± 0.31
175.78	334.94 ± 1.28	-5.92 ± 0.33	-28.01 ± 1.48	151.98 ± 0.57	194.83 ± 1.15	-42.15 ± 0.32	-30.2 ± 2.09	138.83 ± 0.28
185.55	331.6 ± 1	-1.45 ± 0.23	-29.79 ± 0.5	158.76 ± 0.79	215.93 ± 1.27	-45.27 ± 0.53	-42.7 ± 0.42	150.9 ± 0.19
195.31	336.45 ± 2.39	3.21 ± 0.47	-38.52 ± 1.64	159.03 ± 0.46	231.52 ± 1.08	-47.97 ± 0.36	-48.94 ± 3.09	163.04 ± 0.51
205.08	339.37 ± 0.85	1.75 ± 0.3	-23.73 ± 0.73	166.18 ± 0.63	232.77 ± 0.28	-53.26 ± 0.42	-27.99 ± 0.66	161.54 ± 0.58
214.84	338.54 ± 0.86	5.18 ± 0.49	-18.89 ± 0.5	170.83 ± 0.6	243 ± 1.07	-55.11 ± 0.49	-28 ± 0.99	175.13 ± 0.49
224.61	345.24 ± 1.21	12.73 ± 0.34	-12.7 ± 0.69	172.52 ± 0.14	250.82 ± 0.78	-53.42 ± 0.8	-25.74 ± 1.18	142.7 ± 0.27
234.38	352.1 ± 1.31	3.63 ± 0.69	-22.09 ± 1.67	180.57 ± 0.53	258.45 ± 2.23	-62.17 ± 0.38	-24.73 ± 1.27	194.93 ± 0.71
244.14	344.73 ± 1.56	6.96 ± 0.59	-10.27 ± 1.47	175.32 ± 0.59	273.97 ± 1.6	-60.18 ± 0.59	-23.71 ± 1.43	197.98 ± 0.23
253.91	349.26 ± 2.02	16.46 ± 0.62	-8.9 ± 0.71	179.57 ± 0.35	278.28 ± 1.04	-65.81 ± 0.36	-14.53 ± 0.77	220.78 ± 0.76
263.67	347.13 ± 1.46	12.85 ± 0.46	0.15 ± 1.09	193 ± 0.32	289.07 ± 1.16	-64.65 ± 0.32	-7.19 ± 1.9	212.52 ± 0.33
273.44	345.54 ± 0.66	23.09 ± 0.37	2.3 ± 0.61	168.88 ± 0.46	300.85 ± 0.4	-62.25 ± 0.63	-4.24 ± 0.8	175.47 ± 0.15
283.20	341.78 ± 1.82	19.14 ± 0.33	10.33 ± 1.34	231.39 ± 0.45	323.41 ± 0.9	-73.72 ± 1	-6.62 ± 0.87	228.33 ± 0.31
292.97	343.1 ± 0.76	24.81 ± 0.83	22.61 ± 0.91	170.93 ± 0.88	335.8 ± 0.54	-62.76 ± 0.84	19.79 ± 1.14	231.67 ± 0.2

Table D. 40. Measured dynamic-stiffness real and imaginary parts at 9,000 rpm and 1,724 kPa for t_p=11.5 mm.

Freq. [Hz.]	Re (H_{xx}) [MN/m]	Re (H_{xy}) [MN/m]	Re (H_{yx}) [MN/m]	Re (H_{yy}) [MN/m]	Im (H_{xx}) [MN/m]	Im (H_{xy}) [MN/m]	Im (H_{yx}) [MN/m]	Im (H_{yy}) [MN/m]
9.77	383.96 ± 0.81	-45.3 ± 0.42	-40.91 ± 1.57	154.99 ± 0.37	18.02 ± 0.93	-0.08 ± 0.34	3.18 ± 1.31	7.22 ± 0.4
19.53	386.74 ± 0.44	-44.64 ± 0.31	-40.81 ± 0.8	153.76 ± 0.34	33.7 ± 0.52	-3.54 ± 0.64	-3.92 ± 0.49	10.5 ± 0.31
29.30	392.39 ± 0.94	-46 ± 0.47	-39.33 ± 0.8	158.84 ± 0.44	45.4 ± 0.91	-4.71 ± 0.25	-9.72 ± 0.79	14.68 ± 0.21
39.06	394.66 ± 1.17	-42.63 ± 0.3	-37.6 ± 0.83	154.21 ± 0.38	59.2 ± 0.94	-9.34 ± 0.48	-15.06 ± 0.7	21.73 ± 0.33
48.83	399.33 ± 1.11	-43.56 ± 0.44	-40.79 ± 0.82	155.28 ± 0.34	72.22 ± 1.08	-13.9 ± 0.47	-17.45 ± 0.76	27.18 ± 0.21
58.59	404.78 ± 0.62	-42.97 ± 0.25	-39.68 ± 1.02	152.52 ± 0.45	84.03 ± 0.51	-13.52 ± 0.37	-23.19 ± 0.35	35.24 ± 0.28
68.36	407.43 ± 1.3	-42.23 ± 0.41	-45.16 ± 0.93	153.78 ± 0.35	97.66 ± 0.95	-15.03 ± 0.26	-28.59 ± 0.48	38.75 ± 0.57
78.13	414.23 ± 1.03	-38.54 ± 0.59	-39.19 ± 0.54	152.02 ± 0.48	109.45 ± 0.66	-17.69 ± 0.52	-34.03 ± 1.2	49.27 ± 0.53
87.89	416.91 ± 2.34	-39.89 ± 0.48	-39.33 ± 2.77	151.88 ± 0.65	103.04 ± 1.31	-17.57 ± 0.56	-30 ± 2.85	49.65 ± 0.43
97.66	420.52 ± 0.21	-37.07 ± 0.57	-47.99 ± 1.23	157.59 ± 0.36	128.88 ± 1.43	-23.16 ± 0.69	-41.08 ± 0.48	63.91 ± 0.49
107.42	424.52 ± 0.77	-36.99 ± 0.63	-47.77 ± 1.25	157.3 ± 0.3	133.63 ± 1.2	-23.28 ± 0.18	-42.98 ± 0.86	70.13 ± 0.52
117.19	425.92 ± 1.58	-33.96 ± 0.24	-50.85 ± 0.29	159.66 ± 0.23	145.19 ± 2.04	-27.43 ± 0.41	-48.83 ± 0.59	77.31 ± 0.25
126.95	430.08 ± 2.13	-31.37 ± 0.28	-54.88 ± 1.6	160.03 ± 0.27	158.34 ± 1.24	-31.35 ± 0.35	-51.08 ± 1.49	81.56 ± 0.34
136.72	427.79 ± 2.79	-28.81 ± 0.31	-47.02 ± 1.64	159.72 ± 0.23	154.13 ± 0.69	-32.17 ± 0.46	-42.8 ± 0.31	89.81 ± 0.33
146.48	434.76 ± 4.54	-29.43 ± 0.64	-52.36 ± 0.81	164.5 ± 0.54	160.46 ± 1.45	-33.7 ± 1.46	-46.18 ± 1.86	97.01 ± 0.41
156.25	425.61 ± 1.59	-21.73 ± 0.24	-46.9 ± 0.65	164.01 ± 0.6	175.43 ± 1.18	-39.14 ± 0.76	-44.95 ± 1.05	99.54 ± 0.24
166.02	431.18 ± 1.12	-26.29 ± 0.28	-52.07 ± 0.56	170.15 ± 0.15	185.82 ± 1.23	-46.05 ± 0.49	-49.79 ± 0.95	113.66 ± 0.47
175.78	438.61 ± 0.96	-25.8 ± 0.34	-51.17 ± 0.67	169.01 ± 0.36	181.35 ± 3.03	-47.25 ± 0.61	-35.48 ± 0.98	115.89 ± 0.41
185.55	440.4 ± 2.77	-21.14 ± 0.86	-55.91 ± 0.58	174.29 ± 0.39	210.75 ± 1.54	-53.35 ± 0.31	-44.27 ± 1.16	129.85 ± 0.67
195.31	440.25 ± 9.92	-16.89 ± 1.41	-48.81 ± 3.48	170.5 ± 0.4	249.08 ± 4	-56.46 ± 1.04	-54.72 ± 2.57	136.18 ± 0.47
205.08	435.3 ± 1.5	-19.77 ± 0.51	-37.62 ± 0.55	177.29 ± 0.31	216.02 ± 1.15	-58.21 ± 0.75	-33.52 ± 1.13	137.64 ± 0.39
214.84	440.55 ± 1.81	-17.43 ± 0.27	-33.15 ± 0.24	179.78 ± 0.3	226 ± 1.42	-59.99 ± 0.43	-32.77 ± 0.96	147.75 ± 0.29
224.61	447.08 ± 0.84	-12.05 ± 0.28	-30.63 ± 0.15	192.36 ± 0.31	236.41 ± 1.02	-60.82 ± 0.44	-31.75 ± 1.34	117.79 ± 0.36
234.38	453.42 ± 1.61	-20.06 ± 0.25	-41.07 ± 0.84	187.89 ± 0.6	251.88 ± 1.78	-66.47 ± 0.4	-34.44 ± 0.89	166.92 ± 0.37
244.14	446.49 ± 1.5	-18.12 ± 0.91	-24.62 ± 0.97	182.69 ± 0.44	252.26 ± 1.74	-63.24 ± 0.63	-31.52 ± 1.13	164.39 ± 0.52
253.91	447.61 ± 0.26	-10.47 ± 0.28	-22.36 ± 0.57	188.66 ± 0.39	260.82 ± 0.61	-68.77 ± 0.53	-26.54 ± 1.05	182.56 ± 0.56
263.67	439.08 ± 1.41	-10.35 ± 0.4	-13.48 ± 1.56	197 ± 0.48	271.21 ± 1.84	-67.78 ± 0.29	-21.16 ± 1.36	183.74 ± 0.59
273.44	441.54 ± 0.67	-4.74 ± 0.54	-9.85 ± 0.69	185.35 ± 0.46	280.68 ± 0.29	-68.82 ± 0.61	-23.09 ± 0.6	140.92 ± 0.3
283.20	440.3 ± 1.72	-6.96 ± 0.64	-5.78 ± 1.06	238.36 ± 0.48	301.53 ± 0.69	-77.86 ± 0.48	-28.84 ± 0.95	199.67 ± 0.53
292.97	439.81 ± 0.97	-5.27 ± 0.38	8.7 ± 1.37	191.88 ± 0.21	310.8 ± 1.21	-69.22 ± 0.81	-16.24 ± 1.24	192.7 ± 0.26

Table D. 41. Measured dynamic-stiffness real and imaginary parts at 12,000 rpm and 172 kPa for t_p=11.5 mm.

Freq. [Hz.]	Re (H_{xx}) [MN/m]	Re (H_{xy}) [MN/m]	Re (H_{yx}) [MN/m]	Re (H_{yy}) [MN/m]	Im (H_{xx}) [MN/m]	Im (H_{xy}) [MN/m]	Im (H_{yx}) [MN/m]	Im (H_{yy}) [MN/m]
9.77	235.77 ± 0.69	-29.71 ± 0.77	-39.81 ± 0.95	186.23 ± 0.48	14.75 ± 0.75	0.01 ± 0.57	-1.08 ± 1.18	3.09 ± 1.15
19.53	238.18 ± 1.38	-29.75 ± 0.81	-34.91 ± 0.83	196.64 ± 0.56	26.29 ± 1.54	-2.23 ± 1.68	-6.8 ± 0.98	17.49 ± 0.98
29.30	239.49 ± 1.04	-29.97 ± 0.68	-29.02 ± 0.76	182.92 ± 1.01	37.02 ± 1.18	-3.54 ± 0.73	-2.63 ± 1.33	25.77 ± 1.33
39.06	239.81 ± 1.61	-25.37 ± 1.27	-31.95 ± 2.31	186.54 ± 0.53	50.6 ± 1.5	-8.9 ± 0.88	-14.12 ± 2.07	32.27 ± 0.63
48.83	245.67 ± 0.89	-29.19 ± 0.95	-31.99 ± 1.51	187.65 ± 1.02	64.74 ± 0.67	-9.11 ± 1.01	-10.24 ± 2	43.14 ± 1.61
58.59	245.37 ± 1.92	-29.37 ± 1.38	-38.29 ± 0.35	188.59 ± 1.07	79.43 ± 1.68	-10 ± 1.19	-8.9 ± 1.27	53.95 ± 2.43
68.36	251.07 ± 0.96	-23.5 ± 1.67	-22.39 ± 1.08	193.99 ± 0.97	85.01 ± 0.97	-14.06 ± 0.76	-20.59 ± 0.32	66.15 ± 1.25
78.13	250.48 ± 1.45	-19.85 ± 0.4	-18.39 ± 1.22	200.16 ± 1.42	93.31 ± 2.24	-20.12 ± 0.81	-26.83 ± 1.4	87.03 ± 1.63
87.89	257.11 ± 1.36	-25.61 ± 1.73	-25.63 ± 1.58	197.57 ± 2.52	112.42 ± 5.45	-19.09 ± 1.95	-30.04 ± 5.16	76.42 ± 1.36
97.66	257.52 ± 1.11	-22.83 ± 0.82	-31.06 ± 2.27	203.76 ± 0.79	118.57 ± 3.12	-21.15 ± 1.51	-26.87 ± 1.46	80.89 ± 0.96
107.42	258.17 ± 1.37	-21.15 ± 0.96	-27.78 ± 0.74	205.6 ± 0.79	126.07 ± 0.8	-21.53 ± 0.95	-30.42 ± 0.98	90.48 ± 0.71
117.19	261.84 ± 1.77	-20.04 ± 1.16	-24.94 ± 0.93	210.2 ± 0.34	134.62 ± 1.59	-22.34 ± 0.56	-38.9 ± 1.34	95.16 ± 0.76
126.95	270.11 ± 0.49	-15.49 ± 0.76	-27.09 ± 1.46	213.25 ± 0.49	147.74 ± 0.93	-24.27 ± 0.98	-42.5 ± 1.81	104.11 ± 1.29
136.72	263.21 ± 1.32	-12.35 ± 0.76	-27.31 ± 1.67	215.27 ± 0.49	150.65 ± 2.86	-24.79 ± 0.6	-30.23 ± 1.74	111.7 ± 0.52
146.48	272.12 ± 0.9	-10.79 ± 0.71	-25.38 ± 0.96	211.97 ± 0.88	157.39 ± 0.8	-21.1 ± 0.59	-35.58 ± 0.64	122.56 ± 1.2
156.25	268.82 ± 1.53	-1.67 ± 0.45	-21.64 ± 0.3	234.11 ± 0.66	169.91 ± 0.47	-32.3 ± 0.5	-35.58 ± 1.06	147.42 ± 1.08
166.02	269.43 ± 0.36	-10.19 ± 0.58	-25.59 ± 2.79	235.51 ± 0.86	182.35 ± 2.97	-36.64 ± 0.55	-36.55 ± 1.38	134.19 ± 0.41
175.78	273.52 ± 3.83	4.09 ± 0.77	-18.5 ± 3.32	235.51 ± 1.39	192.6 ± 3.21	-31.12 ± 0.59	-36.15 ± 2.22	152.23 ± 0.82
185.55	273.08 ± 1.2	0.24 ± 1.13	-18.36 ± 1.89	236.14 ± 1.34	207.34 ± 5.51	-41.94 ± 0.98	-31.17 ± 2.89	142.39 ± 1.4
195.31	286.5 ± 9.43	33.32 ± 2.36	-37.22 ± 2.18	239.25 ± 1.8	227.46 ± 2.89	-33.92 ± 2.37	-31.86 ± 7.65	190.93 ± 1.8
205.08	268.65 ± 1.51	9.63 ± 0.46	6.73 ± 2.58	234.11 ± 1.23	222.29 ± 2.07	-44.28 ± 1.97	-18.33 ± 0.78	175.83 ± 1.09
214.84	266.48 ± 2.93	87.84 ± 4.18	31.02 ± 2.41	257.38 ± 6.11	239.74 ± 3.09	-50.64 ± 4.03	-32.98 ± 4.03	297.01 ± 5.44
224.61	301.48 ± 2.47	-7.79 ± 2.55	-24.55 ± 0.93	332.87 ± 3.56	278.39 ± 1.69	-52.77 ± 3.74	-21.44 ± 2.46	127.23 ± 1.53
234.38	308.43 ± 3.54	43.14 ± 3.74	212.58 ± 6.48	311.5 ± 5.03	276.01 ± 4.42	-75.68 ± 3.5	72.39 ± 10.83	263.08 ± 8.58
244.14	349.29 ± 2.83	49.41 ± 1.79	129.74 ± 4.68	277.3 ± 1.49	277.28 ± 4.47	-38.11 ± 1.84	52.54 ± 4.25	293.75 ± 5.05
253.91	225.49 ± 18.26	215.34 ± 22.7	-122.95 ± 31.68	508.58 ± 15.2	133.1 ± 17.09	67.71 ± 14.45	-393.81 ± 38.76	636.87 ± 49.61
263.67	352.28 ± 7.74	142.28 ± 7.83	64.39 ± 13.95	298.24 ± 7.85	280.53 ± 9.71	-23.97 ± 6.23	42.37 ± 9.56	390.66 ± 10.17
273.44	266.86 ± 1.29	-46.76 ± 7.68	104.12 ± 14.87	463.82 ± 35.4	213.69 ± 6.13	-142.93 ± 4.26	-258.17 ± 14.92	-61.83 ± 8.14
283.20	232.33 ± 11.25	-13.5 ± 4.05	41.55 ± 16.37	187.79 ± 2.67	172.49 ± 8.93	-76.29 ± 4.72	-391.47 ± 5.44	150.52 ± 8.65
292.97	298.41 ± 2.76	28.97 ± 2.95	56.98 ± 5.84	306.53 ± 7.93	237.93 ± 3.61	-90.21 ± 1.93	-142.91 ± 9.14	234.66 ± 4.67

Table D. 42. Measured dynamic-stiffness real and imaginary parts at 12,000 rpm and 345 kPa for t_p=11.5 mm.

Freq. [Hz.]	Re (H_{xx}) [MN/m]	Re (H_{xy}) [MN/m]	Re (H_{yx}) [MN/m]	Re (H_{yy}) [MN/m]	Im (H_{xx}) [MN/m]	Im (H_{xy}) [MN/m]	Im (H_{yx}) [MN/m]	Im (H_{yy}) [MN/m]
9.77	247.67 ± 0.48	-30.02 ± 0.56	-24.73 ± 0.77	167.9 ± 0.53	11.78 ± 0.63	0.13 ± 0.68	-3.26 ± 0.5	11.8 ± 0.56
19.53	248.38 ± 0.48	-29.88 ± 1.45	-24.89 ± 0.8	169.45 ± 0.74	27.58 ± 0.94	-3.85 ± 0.66	-7.74 ± 0.7	19.68 ± 0.65
29.30	250.92 ± 0.75	-27.67 ± 0.49	-27.89 ± 1.45	167.32 ± 0.45	38.37 ± 1.1	-4.62 ± 0.62	-10.04 ± 0.75	28.33 ± 1.16
39.06	254.49 ± 1.52	-27.74 ± 0.91	-30.52 ± 1.06	175.09 ± 0.31	49.33 ± 0.99	-6.68 ± 0.67	-13 ± 0.4	35.54 ± 0.46
48.83	254.67 ± 1.61	-28.55 ± 1.13	-29.76 ± 1.27	175.79 ± 0.86	65.83 ± 0.88	-11.07 ± 1	-18.9 ± 0.78	43.24 ± 1.02
58.59	257.77 ± 0.92	-29.07 ± 1.34	-32.44 ± 1.94	176.51 ± 1.24	76 ± 1.47	-10.91 ± 0.66	-19.16 ± 0.56	50.45 ± 0.43
68.36	261.35 ± 1.35	-23.05 ± 1.4	-25.18 ± 0.82	180.55 ± 0.91	92.34 ± 1.76	-13.98 ± 1.48	-23.85 ± 1.44	65.02 ± 0.72
78.13	270.64 ± 1.65	-24.31 ± 1.11	-20.64 ± 1.28	180.16 ± 0.84	97.78 ± 2.13	-15.05 ± 0.8	-32.25 ± 0.64	73.54 ± 0.37
87.89	272.17 ± 3.41	-26.5 ± 0.43	-41.39 ± 3.61	183.47 ± 0.9	112.86 ± 3.15	-20.55 ± 1.03	-27.44 ± 1.91	81.68 ± 1.13
97.66	271.49 ± 1.19	-24.49 ± 0.37	-23.75 ± 1.87	190.04 ± 0.58	117.93 ± 2.99	-20.03 ± 0.89	-29.31 ± 2.44	83.99 ± 1.01
107.42	274.73 ± 2.95	-22.3 ± 0.62	-25.22 ± 1.27	190.65 ± 0.9	124.01 ± 0.7	-20.61 ± 0.61	-35.49 ± 0.84	91.16 ± 0.81
117.19	275.14 ± 0.94	-20.13 ± 0.49	-27.95 ± 1.24	194.77 ± 1.06	138.2 ± 1.21	-22.81 ± 0.62	-43.36 ± 0.61	97.38 ± 0.75
126.95	275.08 ± 2.38	-17.94 ± 0.23	-28.74 ± 0.79	195.39 ± 0.52	148.7 ± 1.11	-24.24 ± 0.58	-45.55 ± 1.58	105.12 ± 0.62
136.72	280.48 ± 1.55	-15.2 ± 0.54	-23.58 ± 0.98	199.18 ± 0.44	151.93 ± 0.93	-24.07 ± 0.4	-33.38 ± 1.43	112.51 ± 0.57
146.48	285.29 ± 1.08	-16.34 ± 0.55	-23.99 ± 1.12	200.31 ± 0.53	157.92 ± 0.73	-25.06 ± 0.82	-38.86 ± 0.76	119.12 ± 0.39
156.25	282.73 ± 0.72	-7.13 ± 0.66	-24.65 ± 0.66	210.29 ± 0.85	169.33 ± 1.51	-29.91 ± 0.61	-44.41 ± 1.71	137.63 ± 0.41
166.02	283.64 ± 1.83	-10.87 ± 0.36	-26.12 ± 0.87	214.53 ± 0.78	179.51 ± 2.11	-31.75 ± 0.69	-43.34 ± 1.44	137.54 ± 0.24
175.78	286.75 ± 2.53	-6.06 ± 0.94	-22.72 ± 0.91	212.15 ± 1.06	186.39 ± 2.72	-30.43 ± 0.79	-40.28 ± 0.71	146.95 ± 0.78
185.55	281.75 ± 1.95	-0.45 ± 1.06	-32.61 ± 0.72	221.79 ± 0.8	204.05 ± 2.45	-35.78 ± 0.98	-46.92 ± 1.77	152.12 ± 0.98
195.31	267.9 ± 4.63	7.2 ± 1.87	-49.35 ± 8.37	222.29 ± 1.32	225.99 ± 10.06	-34.58 ± 1.2	-40.79 ± 2.88	169.3 ± 1.48
205.08	285.5 ± 2.72	8.34 ± 1.41	-16.13 ± 0.74	221.6 ± 0.52	220.93 ± 2.45	-39.91 ± 0.45	-21.71 ± 2.27	167.69 ± 0.96
214.84	282.99 ± 1.17	12.79 ± 1.02	-3.36 ± 2.17	225.21 ± 0.75	239.04 ± 2.19	-41.34 ± 1.19	-14.94 ± 1.94	181.19 ± 0.82
224.61	286.89 ± 1.09	23.91 ± 0.94	-14.1 ± 1.5	258.8 ± 1.13	247.44 ± 1.32	-49.65 ± 1.2	-30.52 ± 2.16	194.62 ± 1.11
234.38	296.33 ± 3.56	14.37 ± 1.7	2.97 ± 1.56	248.34 ± 1.3	252.07 ± 2.14	-43.12 ± 2.66	-11.04 ± 1.08	207 ± 0.91
244.14	320.05 ± 3.3	18 ± 1.77	2.18 ± 2.21	235.26 ± 1.03	276.29 ± 3.54	-45.52 ± 1.84	11.4 ± 3.5	213.44 ± 1.4
253.91	305.8 ± 2.23	36.28 ± 1.04	27.02 ± 1.87	276.83 ± 1.81	286.05 ± 1.78	-46.6 ± 2	25.67 ± 0.69	218.73 ± 1.43
263.67	313.3 ± 7.12	43.19 ± 1.4	17.26 ± 1.87	255.31 ± 0.95	313.14 ± 4.02	-48.05 ± 2.69	11.69 ± 2.8	223.29 ± 0.66
273.44	369.39 ± 2.65	64.29 ± 1.04	147.85 ± 5.24	275.73 ± 0.6	315.51 ± 2.99	-75.97 ± 1.85	22.61 ± 2.53	212.94 ± 1.24
283.20	356.03 ± 8.06	62.81 ± 1.77	53.8 ± 2.95	326.48 ± 1.32	348.37 ± 4.18	-74.86 ± 1.86	70.53 ± 6.04	237.77 ± 1.96
292.97	328.32 ± 3.91	36 ± 1.5	-115.56 ± 5.33	274 ± 2.17	256.51 ± 3.11	-73.84 ± 1.38	-113.5 ± 7.34	291.4 ± 1.42

Table D. 43. Measured dynamic-stiffness real and imaginary parts at 12,000 rpm and 689 kPa for t_p=11.5 mm.

Freq. [Hz.]	Re (H_{xx}) [MN/m]	Re (H_{xy}) [MN/m]	Re (H_{yx}) [MN/m]	Re (H_{yy}) [MN/m]	Im (H_{xx}) [MN/m]	Im (H_{xy}) [MN/m]	Im (H_{yx}) [MN/m]	Im (H_{yy}) [MN/m]
9.77	274.37 ± 1.86	-29.67 ± 0.5	-22.64 ± 0.69	157.13 ± 0.48	14.05 ± 0.59	-2.13 ± 0.25	1.5 ± 0.52	9.88 ± 0.68
19.53	275.37 ± 0.77	-30.67 ± 0.45	-24.51 ± 0.61	158.23 ± 0.36	27.68 ± 1.07	-5.06 ± 0.68	-4.21 ± 0.9	17.89 ± 0.38
29.30	276.94 ± 0.66	-28.57 ± 0.44	-22.77 ± 0.84	157.07 ± 0.75	40.22 ± 1.47	-6.5 ± 0.47	-9.09 ± 0.77	25.34 ± 0.44
39.06	281.9 ± 0.73	-27.98 ± 0.34	-23.91 ± 1.05	161.97 ± 0.29	52.27 ± 1.26	-7.72 ± 0.63	-13.58 ± 1.49	32.33 ± 0.45
48.83	284.34 ± 1.88	-28.42 ± 0.68	-26.57 ± 1.17	161.85 ± 0.45	63.13 ± 1.19	-12.85 ± 0.8	-15.95 ± 1.14	37.43 ± 0.73
58.59	283.54 ± 1.38	-29.56 ± 0.8	-23.95 ± 1.21	162.8 ± 0.57	80.18 ± 1.3	-14.38 ± 0.35	-22.68 ± 1.08	47.72 ± 0.65
68.36	290.56 ± 1.22	-23.46 ± 1.62	-20.47 ± 1.15	165.4 ± 0.43	93.07 ± 0.83	-12.42 ± 0.88	-23.18 ± 0.76	60.62 ± 0.73
78.13	290.69 ± 2.56	-24.4 ± 1.02	-18.02 ± 0.71	162.24 ± 0.71	105.27 ± 0.98	-18.67 ± 0.81	-35.41 ± 2.34	69.42 ± 0.85
87.89	283.59 ± 1	-25.92 ± 0.73	-19.65 ± 2.1	165.38 ± 0.54	111.22 ± 6.39	-20.82 ± 0.94	-29.79 ± 5.35	71.53 ± 0.67
97.66	301.05 ± 1.42	-25.39 ± 0.58	-26.73 ± 1.88	172.1 ± 0.73	120.05 ± 0.98	-22.07 ± 0.64	-38.24 ± 1.47	79 ± 0.73
107.42	304.52 ± 0.74	-26.46 ± 0.18	-26.95 ± 1.85	172.44 ± 0.7	126.93 ± 2.11	-23.28 ± 0.55	-37.48 ± 0.51	87.35 ± 0.62
117.19	305.79 ± 2.03	-24.2 ± 0.94	-29.43 ± 1.21	177.52 ± 0.69	141.72 ± 1.69	-24.36 ± 0.56	-45.07 ± 0.97	93.4 ± 0.49
126.95	307.06 ± 0.64	-22.04 ± 0.6	-32.87 ± 1.8	177.7 ± 0.44	145.67 ± 1.47	-26.11 ± 0.52	-48.82 ± 0.76	99.78 ± 0.53
136.72	311.27 ± 1.57	-20.25 ± 0.19	-25.77 ± 1.37	180.35 ± 0.33	149.98 ± 0.81	-26.58 ± 0.49	-37.76 ± 1.36	109.12 ± 0.57
146.48	315.19 ± 1.33	-18.51 ± 0.36	-28.4 ± 0.6	180.16 ± 0.39	155.09 ± 0.69	-24.44 ± 0.23	-43.85 ± 1.15	115.94 ± 0.24
156.25	310.71 ± 1.32	-11.75 ± 0.54	-23.76 ± 0.46	180.14 ± 0.29	167.75 ± 0.8	-27.92 ± 0.4	-49.42 ± 1.67	120.11 ± 0.25
166.02	311.65 ± 2.21	-13.71 ± 0.56	-24.47 ± 1.99	184.74 ± 0.57	176.47 ± 1.63	-31.83 ± 0.58	-50.52 ± 1.23	131.03 ± 0.9
175.78	315.19 ± 1.42	-10.54 ± 0.48	-29.97 ± 2.23	187.84 ± 0.47	182.23 ± 1.71	-32.17 ± 0.65	-40.97 ± 3.08	142.87 ± 0.46
185.55	311.28 ± 3.42	-4.35 ± 0.71	-30.87 ± 2.47	196.89 ± 1.29	199.57 ± 2.2	-34.78 ± 1.11	-48.91 ± 1.67	147.95 ± 0.45
195.31	318.5 ± 7.75	-0.7 ± 2.34	-39.87 ± 7.32	200.46 ± 1.6	216.25 ± 12.28	-39.11 ± 1.89	-61.45 ± 5.48	164.36 ± 2.08
205.08	317.32 ± 2.53	0.29 ± 0.94	-26.99 ± 1.4	198.77 ± 1.04	211.74 ± 1.5	-40.2 ± 1.66	-36.15 ± 1.14	164.08 ± 1.01
214.84	318.48 ± 3.05	4.88 ± 1.19	-22.21 ± 2.55	207.15 ± 0.67	226.74 ± 2.64	-42.86 ± 0.82	-31.9 ± 1.7	172.72 ± 0.54
224.61	320.26 ± 1.57	19.61 ± 1.22	-16.83 ± 1.68	201.07 ± 0.46	237.81 ± 1.25	-39.82 ± 0.65	-33.55 ± 1.83	160.58 ± 0.72
234.38	328.61 ± 1.36	6.69 ± 0.97	-21.81 ± 1.9	224.43 ± 0.92	246.03 ± 4.26	-46.31 ± 0.97	-27.15 ± 1.38	195.26 ± 0.33
244.14	319.74 ± 1.13	13.41 ± 0.58	-20.15 ± 2.51	214.8 ± 0.89	253.81 ± 2.37	-43.29 ± 0.63	-25.3 ± 1.96	206.34 ± 0.6
253.91	328.31 ± 1.19	20.84 ± 1.71	-19.01 ± 1.4	249.2 ± 1.49	266.73 ± 1.33	-53.08 ± 1.73	-8.08 ± 1.5	212.26 ± 1.29
263.67	319.26 ± 1.78	26.44 ± 1.31	-14.48 ± 2.11	236.91 ± 1.99	284.13 ± 2.66	-48.84 ± 2.06	0.35 ± 1.73	219.43 ± 1.02
273.44	329.61 ± 0.58	44.68 ± 0.8	-8.11 ± 0.72	200.87 ± 1.48	292.01 ± 0.47	-51.66 ± 1.46	12.65 ± 0.8	189.83 ± 0.77
283.20	324.19 ± 2.92	37.8 ± 1.42	9.9 ± 2.05	276.88 ± 0.59	317.07 ± 1.16	-60.13 ± 1.55	10.43 ± 1.79	227.97 ± 1.48
292.97	342.34 ± 1.78	70.7 ± 1.59	29.22 ± 2.13	214.38 ± 1.42	325.11 ± 1.34	-75.41 ± 1.52	106.36 ± 1.32	330.36 ± 0.81

Table D. 44. Measured dynamic-stiffness real and imaginary parts at 12,000 rpm and 1034 kPa for t_p=11.5 mm.

Freq. [Hz.]	Re (H_{xx}) [MN/m]	Re (H_{xy}) [MN/m]	Re (H_{yx}) [MN/m]	Re (H_{yy}) [MN/m]	Im (H_{xx}) [MN/m]	Im (H_{xy}) [MN/m]	Im (H_{yx}) [MN/m]	Im (H_{yy}) [MN/m]
9.77	307.8 ± 1.24	-32.44 ± 0.69	-28.15 ± 1.8	155.9 ± 0.48	13.62 ± 0.78	-0.32 ± 0.85	2.22 ± 0.6	9 ± 0.6
19.53	309.26 ± 0.8	-32.67 ± 0.27	-26.87 ± 1.48	154.89 ± 0.46	29.46 ± 1.59	-3.87 ± 0.42	-4.71 ± 0.96	14.84 ± 0.62
29.30	309.94 ± 1.41	-32.01 ± 0.72	-25.51 ± 1.14	156.12 ± 0.47	40.45 ± 1.99	-5.6 ± 0.72	-10.45 ± 1.1	20.37 ± 0.52
39.06	313.67 ± 1.73	-31.06 ± 0.7	-24.4 ± 1.78	157.97 ± 0.53	55.77 ± 0.5	-12.12 ± 0.76	-11.56 ± 0.77	27.89 ± 0.62
48.83	318.24 ± 1.41	-32.02 ± 1.05	-28.05 ± 0.98	158.63 ± 0.57	70.16 ± 1.95	-13.51 ± 0.66	-19.67 ± 1.95	34.15 ± 0.65
58.59	320.29 ± 1.32	-32.19 ± 0.13	-26.47 ± 0.82	158.72 ± 0.54	78.97 ± 1.24	-12.9 ± 0.53	-22.31 ± 1.84	41.9 ± 0.44
68.36	322.52 ± 1.19	-33.94 ± 0.28	-32.76 ± 0.97	153.92 ± 0.82	90.64 ± 1.79	-16.24 ± 0.74	-21.85 ± 1.22	51.35 ± 0.74
78.13	327.35 ± 0.93	-28.29 ± 0.16	-22.02 ± 0.89	158.7 ± 0.87	102.89 ± 1.81	-19.18 ± 0.48	-31.3 ± 1.39	58.11 ± 0.67
87.89	335.81 ± 1.94	-31.35 ± 0.59	-25.99 ± 5.34	159.44 ± 0.74	108.24 ± 5.02	-21.43 ± 0.9	-30.35 ± 0.65	61.69 ± 0.38
97.66	342.6 ± 2.01	-30.19 ± 0.22	-30.99 ± 3.31	165.44 ± 0.76	121.98 ± 2.67	-23.11 ± 0.65	-38.33 ± 0.98	73.48 ± 0.93
107.42	341.65 ± 3.38	-30.3 ± 0.77	-29.43 ± 0.45	165.46 ± 0.94	128.68 ± 0.85	-22.91 ± 0.83	-40.48 ± 1.83	79.65 ± 0.52
117.19	344.95 ± 2.09	-28.61 ± 0.41	-33.09 ± 0.9	168.16 ± 0.43	138.66 ± 0.18	-25.14 ± 0.29	-44.9 ± 2.1	85.02 ± 0.65
126.95	345.38 ± 2.15	-26.64 ± 0.5	-33.23 ± 1.96	167.81 ± 0.3	151.62 ± 1.94	-27.45 ± 0.38	-51.92 ± 1.08	92.25 ± 0.47
136.72	346.42 ± 0.7	-24.96 ± 0.31	-30.31 ± 0.58	170.17 ± 0.55	150.31 ± 0.85	-28.08 ± 0.69	-42.9 ± 2.39	104.31 ± 0.29
146.48	351.04 ± 0.63	-23.04 ± 0.27	-31.97 ± 0.52	170.89 ± 0.49	155.6 ± 1.02	-26.09 ± 0.37	-49.26 ± 1.11	108.25 ± 0.44
156.25	346.63 ± 0.88	-16.3 ± 0.16	-27.39 ± 1.22	173.96 ± 0.22	169.17 ± 0.41	-29.23 ± 0.21	-54.87 ± 1.67	112.97 ± 0.38
166.02	346.91 ± 1.45	-18.78 ± 0.25	-32.5 ± 1.42	176.01 ± 0.39	177.44 ± 1.08	-33.28 ± 0.46	-54.76 ± 2.36	123.02 ± 0.48
175.78	349.95 ± 2.09	-14.81 ± 0.4	-33.2 ± 1.54	175.56 ± 0.51	178.85 ± 1.98	-33.84 ± 0.41	-44.63 ± 2.47	131.95 ± 0.95
185.55	350.21 ± 3.22	-11.48 ± 0.61	-36.03 ± 0.74	182.41 ± 0.74	192.09 ± 2.54	-35.12 ± 1.05	-48.76 ± 1.82	138.65 ± 1.07
195.31	359.08 ± 6.1	-7.55 ± 1.23	-50.38 ± 3.78	187.86 ± 2.55	207.4 ± 6.65	-38.5 ± 1.71	-50.26 ± 10.16	156.8 ± 1.21
205.08	355.8 ± 1.43	-5.49 ± 0.49	-37.98 ± 0.98	188.9 ± 1.34	210.25 ± 2.01	-42.3 ± 1.57	-37.39 ± 1.14	157.87 ± 0.79
214.84	355.86 ± 2.11	-0.6 ± 0.77	-33.29 ± 3.33	195.77 ± 0.67	223.83 ± 4.44	-43.29 ± 0.79	-34.36 ± 2.15	168.26 ± 1.29
224.61	358.95 ± 1.5	9.3 ± 0.65	-26.63 ± 1.37	197.7 ± 0.48	233.25 ± 1.08	-42.13 ± 0.95	-36.25 ± 2.36	139.89 ± 0.31
234.38	365.01 ± 2.3	4.99 ± 1.04	-32.21 ± 3.13	207.73 ± 1.29	241.23 ± 4.15	-47.89 ± 1.04	-37.06 ± 1.95	190.14 ± 1.33
244.14	361.15 ± 3.12	9.7 ± 0.81	-25.14 ± 2.19	203.9 ± 1.2	251.75 ± 5.1	-45.02 ± 1.71	-34.21 ± 4.04	195.44 ± 1.46
253.91	363.64 ± 2.43	17.44 ± 0.19	-26.87 ± 2.8	211.68 ± 1.05	259.64 ± 1.61	-50.93 ± 0.87	-18.95 ± 1.73	211.95 ± 1.02
263.67	362.76 ± 1.95	19.16 ± 1.28	-22.28 ± 1.51	224.86 ± 0.67	267.65 ± 4.24	-53.36 ± 0.88	-13.96 ± 1.79	207.33 ± 0.98
273.44	367.33 ± 0.71	32.4 ± 0.78	-17.84 ± 1.21	200.72 ± 1.1	279.79 ± 1.01	-56.85 ± 1.61	-9.02 ± 1.11	170.92 ± 0.67
283.20	359.91 ± 3	29.81 ± 0.84	-16.03 ± 3.5	263.66 ± 1.34	298.11 ± 1.97	-66.61 ± 1.43	-12.38 ± 3.1	219.08 ± 0.61
292.97	366.58 ± 0.47	32.28 ± 1.33	0.01 ± 0.97	205.37 ± 0.52	307.99 ± 0.66	-58.38 ± 0.66	18.39 ± 1.84	224.39 ± 1.31

Table D. 45. Measured dynamic-stiffness real and imaginary parts at 12,000 rpm and 1,724 kPa for t_p=11.5 mm.

Freq. [Hz.]	Re (H_{xx}) [MN/m]	Re (H_{xy}) [MN/m]	Re (H_{yx}) [MN/m]	Re (H_{yy}) [MN/m]	Im (H_{xx}) [MN/m]	Im (H_{xy}) [MN/m]	Im (H_{yx}) [MN/m]	Im (H_{yy}) [MN/m]
9.77	376.94 ± 1.92	-45.44 ± 0.49	-39.23 ± 0.83	175.36 ± 0.33	15.99 ± 0.71	-1.12 ± 0.91	8.57 ± 1.37	6.9 ± 0.62
19.53	379.03 ± 1.15	-45.85 ± 0.21	-41.85 ± 1.38	175.59 ± 0.32	27.17 ± 0.48	-3.67 ± 0.31	-2.73 ± 0.58	11.19 ± 0.26
29.30	383.97 ± 1.27	-45.22 ± 0.34	-40.61 ± 1.3	177.38 ± 1	42.02 ± 0.75	-6.53 ± 0.9	-10.94 ± 1.09	15.38 ± 0.43
39.06	385.4 ± 1.98	-42.63 ± 0.89	-34.93 ± 0.67	177.39 ± 0.78	54.19 ± 1.56	-10.18 ± 0.67	-15.57 ± 0.54	20.2 ± 0.63
48.83	389.37 ± 1.04	-46.48 ± 0.75	-38.9 ± 1.58	175.21 ± 1.15	67.43 ± 1.76	-13.63 ± 1.05	-16.94 ± 0.91	25.24 ± 1.14
58.59	394.58 ± 1.02	-45.91 ± 0.89	-39.35 ± 1.33	175.08 ± 1.02	81.46 ± 2.1	-16.62 ± 0.57	-22.24 ± 1.03	31.43 ± 1.45
68.36	395.98 ± 0.69	-44.06 ± 0.77	-43 ± 0.74	172.21 ± 1.19	91.06 ± 1.82	-15.73 ± 0.7	-25.69 ± 1.43	34.34 ± 1.09
78.13	404.81 ± 0.94	-41.6 ± 1.42	-37.79 ± 1.01	175.28 ± 1.2	103.98 ± 1.07	-18.37 ± 0.51	-33.34 ± 1.58	42.66 ± 0.34
87.89	405.12 ± 1.02	-44.1 ± 1.51	-38.83 ± 0.43	171.1 ± 1.01	106.31 ± 2.51	-20.47 ± 0.69	-36.9 ± 2.91	45.93 ± 0.86
97.66	412.74 ± 3.11	-43.41 ± 0.72	-43.48 ± 0.73	177.77 ± 0.63	123.62 ± 2.28	-24.48 ± 0.68	-40.25 ± 1.54	56.22 ± 0.7
107.42	415.56 ± 1.32	-43.63 ± 1.23	-44.19 ± 0.64	175.8 ± 0.53	129.67 ± 0.51	-22.93 ± 0.77	-44.67 ± 0.82	63.55 ± 0.75
117.19	419.65 ± 0.88	-41 ± 0.23	-45.77 ± 1.44	178.07 ± 0.7	142.47 ± 0.88	-26.07 ± 0.84	-49.71 ± 1.25	68.81 ± 0.72
126.95	424.94 ± 2.11	-41.72 ± 0.69	-48.71 ± 1.75	177.14 ± 0.61	145.58 ± 1.71	-26.16 ± 0.3	-58.3 ± 0.64	73.2 ± 0.21
136.72	416.72 ± 1.3	-36.82 ± 0.55	-42.97 ± 1.5	176.02 ± 0.63	143.91 ± 1.06	-25.74 ± 0.42	-45.66 ± 1.33	81.5 ± 0.39
146.48	426.71 ± 0.84	-37.59 ± 0.63	-48.5 ± 0.53	180.45 ± 0.72	150.21 ± 1.3	-24.72 ± 0.42	-51.57 ± 0.66	89.15 ± 0.47
156.25	423.25 ± 0.81	-30.09 ± 0.36	-45.11 ± 1.33	181.07 ± 0.22	166.77 ± 1.32	-29.39 ± 0.38	-56.76 ± 0.72	90.66 ± 0.78
166.02	422.4 ± 0.88	-31.87 ± 0.34	-50.48 ± 1.75	181.67 ± 1.06	176.09 ± 1.06	-34.21 ± 0.41	-61.06 ± 1.23	102.82 ± 0.64
175.78	435.84 ± 1.53	-28.89 ± 0.7	-51.27 ± 2.03	180.26 ± 0.56	172.13 ± 1.73	-34.11 ± 0.7	-47.41 ± 2.14	109.91 ± 0.6
185.55	431.78 ± 1.6	-25.52 ± 1.07	-56.06 ± 2.51	183.34 ± 1.01	197.25 ± 2.12	-40.03 ± 0.38	-58.75 ± 2.14	120.54 ± 0.82
195.31	436.9 ± 5.11	-16.72 ± 2.51	-77.12 ± 9.33	184.6 ± 1.27	233.81 ± 9.15	-42.14 ± 2.35	-72.15 ± 8.39	130.79 ± 1.54
205.08	424.4 ± 1.43	-17.67 ± 0.72	-49.41 ± 2.78	189.26 ± 1.45	206.72 ± 2.62	-44.09 ± 1.34	-46.4 ± 1.71	134.79 ± 1.42
214.84	433.3 ± 1.36	-15.01 ± 1.32	-46.95 ± 1.39	191.04 ± 1.72	221.62 ± 1.27	-45.66 ± 1.31	-43.1 ± 0.86	145.92 ± 0.89
224.61	441.99 ± 1.18	-6.12 ± 0.24	-47.11 ± 1.47	208.54 ± 1.19	225.48 ± 1.69	-44.92 ± 0.84	-40.16 ± 2.07	113.17 ± 0.69
234.38	449.03 ± 6.89	-13.82 ± 1.21	-64.52 ± 2.52	205.33 ± 1.29	239.26 ± 4.31	-50.24 ± 2.99	-48.47 ± 4.83	165.98 ± 1.05
244.14	437.46 ± 2.64	-7.34 ± 1.01	-49.95 ± 4.37	199.68 ± 1.08	242.22 ± 4.16	-48.44 ± 1.08	-40.26 ± 2.52	167.06 ± 1.31
253.91	445.29 ± 2.65	1.49 ± 1.6	-42.38 ± 1.79	206.58 ± 1.92	241.44 ± 1.08	-57.69 ± 1.06	-34.48 ± 1.61	179.63 ± 0.99
263.67	441.46 ± 1.85	-0.01 ± 1.36	-33.41 ± 1.73	220.38 ± 1.79	254.93 ± 3.1	-63.63 ± 2.2	-25.71 ± 2.77	188.31 ± 2.62
273.44	444.84 ± 1.02	4.34 ± 2.05	-36.08 ± 0.76	207.48 ± 0.79	263.92 ± 0.49	-63.08 ± 1.27	-24.26 ± 1.24	142.03 ± 1.18
283.20	446.06 ± 2.57	1.34 ± 1.35	-31.86 ± 2.66	253.34 ± 2.12	279.26 ± 2.18	-73.85 ± 1.34	-27.49 ± 2.64	201.75 ± 1.27
292.97	446.92 ± 1.72	4.11 ± 1.49	-18.49 ± 0.74	206.37 ± 0.62	287.07 ± 0.32	-64.62 ± 1.05	-11.17 ± 1.08	189.83 ± 1.02

APPENDIX E:

WFR CALCULATION

The procedure reported in this section to calculate the WFR was taken from Modern Lubrication Theory is taught by Dr. Luis San Andrés, offered by the Mechanical Engineering Department at Texas A&M University [36].

1) Non-dimensionalize the measured rotordynamic coefficients

$$k_{ij} = K_{ij}\frac{C_b}{F_s} \quad \text{and} \quad c_{ij} = C_{ij}\frac{C_b\Omega}{F_s} \tag{1}$$

2) Calculate the equivalent stiffness, k_{eq}

$$k_{eq} = \frac{k_{xx}c_{yy} + k_{yy}c_{xx} - c_{yx}k_{xy} - c_{xy}k_{yx}}{c_{xx} + c_{yy}} \tag{2}$$

3) Calculate the whirl frequency ratio, WFR

$$\text{WFR} = \sqrt{\frac{(k_{eq} - k_{xx})(k_{eq} - k_{yy}) - k_{xy}k_{yx}}{c_{xx}c_{yy} - c_{xy}c_{yx}}} \tag{3}$$